

VOLUME 83 NO. ST6

NOVEMBER 1957

PART 1

**JOURNAL of the**

***Structural***

***Division***

---

**PROCEEDINGS OF THE**



**AMERICAN SOCIETY**

**OF CIVIL ENGINEERS**

## BASIC REQUIREMENTS FOR MANUSCRIPTS

This Journal represents an effort by the Society to deliver information to the reader with the greatest possible speed. To this end the material herein has none of the usual editing required in more formal publications.

Original papers and discussions of current papers should be submitted to the Manager of Technical Publications, ASCE. The final date on which a discussion should reach the Society is given as a footnote with each paper. Those who are planning to submit material will expedite the review and publication procedures by complying with the following basic requirements:

1. Titles should have a length not exceeding 50 characters and spaces.
2. A 50-word summary should accompany the paper.
3. The manuscript (a ribbon copy and two copies) should be double-spaced on one side of 8½-in. by 11-in. paper. Papers that were originally prepared for oral presentation must be rewritten into the third person before being submitted.
4. The author's full name, Society membership grade, and footnote reference stating present employment should appear on the first page of the paper.
5. Mathematics are reproduced directly from the copy that is submitted. Because of this, it is necessary that capital letters be drawn, in black ink, ⅛-in. high (with all other symbols and characters in the proportions dictated by standard drafting practice) and that no line of mathematics be longer than 6½-in. Ribbon copies of typed equations may be used but they will be proportionately smaller in the printed version.
6. Tables should be typed (ribbon copies) on one side of 8½-in. by 11-in. paper within a 6½-in. by 10½-in. invisible frame. Small tables should be grouped within this frame. Specific reference and explanation should be made in the text for each table.
7. Illustrations should be drawn in black ink on one side of 8½-in. by 11-in. paper within an invisible frame that measures 6½-in. by 10½-in.; the caption should also be included within the frame. Because illustrations will be reduced to 69% of the original size, the capital letters should be ⅛-in. high. Photographs should be submitted as glossy prints in a size that is less than 6½-in. by 10½-in. Explanations and descriptions should be made within the text for each illustration.
8. Papers should average about 12,000 words in length and should be no longer than 18,000 words. As an approximation, each full page of typed text, table, or illustration is the equivalent of 300 words.

Further information concerning the preparation of technical papers is contained in the "Technical Publications Handbook" which can be obtained from the Society.

---

Reprints from this Journal may be made on condition that the full title of the paper, name of author, page reference (or paper number), and date of publication by the Society are given. The Society is not responsible for any statement made or opinion expressed in its publications.

This Journal is published bi-monthly by the American Society of Civil Engineers. Publication office is at 2500 South State Street, Ann Arbor, Michigan. Editorial and General Offices are at 33 West 39 Street, New York 18, New York. \$4.00 of a member's dues are applied as a subscription to this Journal. Second-class mail privileges are authorized at Ann Arbor, Michigan.



---

Journal of the  
STRUCTURAL DIVISION  
Proceedings of the American Society of Civil Engineers

---

STRUCTURAL DIVISION  
EXECUTIVE COMMITTEE

Leo H. Corning, Chairman; Robert D. Dewell; George S. Vincent;  
Elmer K. Timby; Myle J. Holley, Jr., Secretary

COMMITTEE ON PUBLICATIONS

Josef Sorkin, Chairman; Mace H. Bell; Thomas R. Kuesel;  
K. W. Lange; Wayne C. Lewis; Nathan W. Morgan;  
Alfred L. Parme; Kenneth R. White; and David M. Wilson

CONTENTS

November, 1957

Papers

	Number
Torsion Analysis for Suspension Bridges by Nan sze Sih . . . . .	1431
A Simplified Design of Composite Bridge Stringers by Jack C. Hacker . . . . .	1432
Wood Diaphragms Progress Report of a Sub-Committee of the Committee on Timber Structures of the Structural Division . . . . .	1433
The Design of Rigid Frame Bents by Richard Z. Zimmermann, Jr. . . . .	1434
Grit and Shot-Reinforced High Tensile Bolted Joints by R. L. Sanks and C. C. Rampton, Jr. . . . .	1435
Deas Island Tunnel by Per Hall, Troels Brøndum-Nielsen, and H. R. Kivisild . . . . .	1436
Analysis of Helical Beams under Symmetrical Loading by Alan M. C. Holmes . . . . .	1437

(Over)

Effect of Initial Eccentricities on Column Performance and Capacity by John M. Hayes . . . . .	1440
Elastic Structures with Nonlinear Load-Deflection Curves by Benjamin M. Ma . . . . .	1441
Discussion . . . . .	1442

---

Journal of the  
STRUCTURAL DIVISION  
Proceedings of the American Society of Civil Engineers

---

## TORSION ANALYSIS FOR SUSPENSION BRIDGES

Nan sze Sih,\* A.M. ASCE  
(Proc. Paper 1431)

## SYNOPSIS

Equations are derived in this paper to determine the stresses in the stiffening trusses due to torsion, considering cable interaction and the effect of warping.

The torsional load as considered here is a static load. However, equations derived may also be used to determine certain constants for the analysis of dynamic loads.

## INTRODUCTION

Torsion on a bridge may be produced by unsymmetrical live load, or by unsymmetrical dead load during erection. As the bridges become wider and longer, the torsional load as well as the resulting stresses are no longer small, and they should be considered in the design. For other types of bridges this may also be true, except for the cable interaction.

For simplicity the cross section of the bridge is assumed as uniform and symmetric about the center of the section.

## Notations

All notations used in this paper follow conventional practice, or are as shown on figures.

Torsion of Cross Section with Double Lateral System  
and Without Cable Interaction

## Stress Strain Relation:

Note: Discussion open until April 1, 1958. Paper 1431 is part of the copyrighted Journal of the Structural Engineering Division of the American Society of Civil Engineers, Vol. 83, No. ST 6, November, 1957.

\*Structural Engr., Ammann & Whitney Consulting Engrs., New York, N. Y.

$$\Delta l = \Delta \eta \sin \gamma, \quad \epsilon = \frac{\Delta l}{l} = \frac{\Delta \eta}{a} \sin \gamma \cos \gamma$$

$$\text{or } \epsilon = \frac{\partial \eta}{\partial x} \sin \gamma \cos \gamma \quad (1)$$

$$S = \epsilon E A \sin \gamma = E A \frac{\partial \eta}{\partial x} \sin^2 \gamma \cos \gamma$$

$$\text{or } S = E A \mu \frac{\partial \eta}{\partial x} \quad \text{where } \mu = \sin^2 \gamma \cos \gamma \quad (2)$$

similarly due to warping

$$S = E A \mu \frac{\partial \omega}{\partial \delta} \quad (3)$$

for the horizontal system

$$\eta = \frac{b}{2} \phi, \quad \frac{\partial \omega}{\partial \delta} = \frac{2\omega}{b}$$

for the vertical system

$$\gamma = \frac{d}{2} \phi, \quad \frac{\partial \omega}{\partial \delta} = \frac{-2\omega}{d}$$

substitute (4) into (2) & (3) gives;

$$\left. \begin{aligned} S_h &= E A_h \mu_h \left( \frac{d}{2} \frac{d\phi}{dx} + \frac{2\omega}{b} \right) \\ S_v &= E A_v \mu_v \left( \frac{b}{2} \frac{d\phi}{dx} - \frac{2\omega}{d} \right) \end{aligned} \right\} \quad (5)$$

Equilibrium Equations:

shear due to St. Venant torsion;  $T_x = S_v b + S_h d$

by equilibrium,

$$\frac{S_h}{b} = \frac{S_v}{d} = q_0$$

hence,

$$S_h = \frac{T_x}{2d}, \quad S_v = \frac{T_x}{2b} \quad \text{and} \quad q_0 = \frac{T_x}{2bd} \quad (6)$$

shear due to warping;

$$\Delta F = S_h \frac{a}{b} + S_v \frac{a}{d}, \quad \frac{\Delta F}{a} = \frac{S_h}{b} + \frac{S_v}{d} \quad \text{or} \quad \frac{S_h}{b} + \frac{S_v}{d} = \frac{dF}{dx}$$

$$T_x = S_h d - S_v b = 0 \quad \therefore \frac{S_h}{b} = \frac{S_v}{d} = \frac{1}{2} \frac{dF}{dx}$$

$$\text{but } F = EA_o \omega' \quad \text{hence } \frac{S_h}{b} + \frac{S_v}{d} = \frac{1}{2} EA_o \omega'' = q \omega \quad (7)$$

from (6) & (7) gives;

$$\left. \begin{aligned} S_h &= \frac{T_x}{2d} + \frac{b}{2} EA_o \omega'' \\ S_v &= \frac{T_x}{2b} - \frac{d}{2} EA_o \omega'' \end{aligned} \right\} \quad (8)$$

Differential Equation for Torsion:

from (5) gives;

$$b A_v \mu_v S_h - d A_h \mu_h S_v = 4 E A_h A_v \mu_h \mu_v \omega \quad (5a)$$

substitute (8) into (5a) gives;

$$\omega'' - \lambda^2 \omega + \frac{T_x}{EJ} = 0 \quad (9)$$

$$\text{where } \lambda^2 = \frac{8 A_v \mu_v A_h \mu_h}{b d A_o \left( \frac{b}{d} A_v \mu_v + \frac{d}{b} A_h \mu_h \right)}, \quad \frac{1}{J} = \frac{\frac{b}{d} A_v \mu_v - \frac{d}{b} A_h \mu_h}{b d A_o \left( \frac{b}{d} A_v \mu_v + \frac{d}{b} A_h \mu_h \right)}$$

$$\text{solution,} \quad \omega = A \cosh \lambda x + B \sinh \lambda x + \frac{T_x}{\lambda^2 EJ} \quad (10)$$

where A & B are integration constants.

Angle of Twist:

from (5) & (8) gives;

$$\theta = \frac{d\phi}{dx} = \frac{T_x}{kE} + \alpha \omega'' \quad (11)$$

$$\text{where } k = \frac{A_v \mu_v A_h \mu_h}{\frac{b}{d} A_v \mu_v + \frac{d}{b} A_h \mu_h} \cdot 2bd, \quad \alpha = \frac{\frac{b}{d} A_v \mu_v - \frac{d}{b} A_h \mu_h}{A_v \mu_v A_h \mu_h} \cdot \frac{A_o}{2}$$

#### Torsion of Cross Section with Double Lateral System and with Cable Interaction

Torsional Resistance of Cable:

for equilibrium of cable;  $m_x = (H'_\omega + \Delta H) \eta + \Delta H \cdot y$

$$V_x = (H'_\omega + \Delta H) \frac{d\eta}{dx} + \Delta H \frac{dy}{dx}$$

torsion by cable;  $T_{cx} = V_x \cdot b = b \left[ (H'_\omega + \Delta H) \frac{b}{2} \frac{d\phi}{dx} + \Delta H \frac{dy}{dx} \right]$  (12)

Torsion of Truss with Cable Interaction:

torsion by truss;  $T_{tx} = T_x - T_{cx}$

substitute above into (8) gives;

$$\left. \begin{aligned} S_h &= \frac{T_x}{2d} - \frac{1}{2d} b \left[ (H'_\omega + \Delta H) \frac{b}{2} \frac{d\phi}{dx} + \Delta H y' \right] + \frac{b}{2} E A_o \omega'' \\ S_v &= \frac{T_x}{2b} - \frac{1}{2b} b \left[ (H'_\omega + \Delta H) \frac{b}{2} \frac{d\phi}{dx} + \Delta H y' \right] - \frac{d}{2} E A_o \omega'' \end{aligned} \right\} \quad (13)$$

by substitute (13) into (5) and eliminate  $\frac{d\phi}{dx}$  gives;

$$\omega'' - \lambda^2 \omega + \frac{1}{EJ} (T_x - b \Delta H y') \quad (14)$$

where

$$\lambda^2 = \frac{8 A_v \mu_v A_h \mu_h + \frac{(H'_\omega + \Delta H)}{E} 2 \frac{b}{d} \left( \frac{b}{d} A_v \mu_v + \frac{d}{b} A_h \mu_h \right)}{b d A_o \left( \frac{b}{d} A_v \mu_v + \frac{d}{b} A_h \mu_h \right) + b^2 A_o \frac{(H'_\omega + \Delta H)}{E}}$$

$$\frac{1}{J} = \frac{\frac{b}{d} A_v \mu_v - \frac{d}{b} A_h \mu_h}{b d A_o \left( \frac{b}{d} A_v \mu_v + \frac{d}{b} A_h \mu_h \right) + b^2 A_o \frac{(H'_\omega + \Delta H)}{E}}$$

solution,

$$\omega = A \cosh \lambda x + B \sinh \lambda x + \frac{1}{\lambda^2 E J} (T_x - b \Delta H y') \quad (15)$$

Angle of Twist:

from (13) & (5) gives:

$$\theta = \frac{d\phi}{dx} = \frac{T_x - b \Delta H y'}{k E} + \alpha \omega'' \quad (16)$$

where

$$K = \frac{A_v \mu_v A_h \mu_h}{\frac{b}{d} A_v \mu_v + \frac{d}{b} A_h \mu_h} 2 b d + \frac{b^2}{2} \frac{(H'_\omega + \Delta H)}{E}$$

$$\alpha = \frac{\frac{b}{d} A_v \mu_v - \frac{d}{b} A_h \mu_h}{A_v \mu_v A_h \mu_h + \frac{1}{4} \frac{b}{d} \frac{(H'_\omega + \Delta H)}{E} \left( \frac{b}{d} A_v \mu_v + \frac{d}{b} A_h \mu_h \right)} \frac{A_o}{2}$$

Additional Cable Tension  $\Delta H$  :

work done by loads on one cable;

$$W_1 = \sum \int_0^l \frac{t_{cx}}{b} \frac{\eta}{2} dx$$



$$t_{cx} = \frac{dT_{cx}}{dx} = -b \left[ (H'_\omega + \Delta H) \eta'' + \Delta H y'' \right]$$

hence, 
$$W_1 = - \sum \int_0^l \left[ (H'_\omega + \Delta H) \eta'' + \Delta H y'' \right] \frac{\eta}{2} dx \quad (17)$$

where  $\Sigma$  is for sum of all three spans.

strain energy of cable; 
$$W_2 = (H'_\omega + \frac{\Delta H}{2}) \Delta H \frac{L_s}{A_c E} \quad (18)$$

$W_1 = W_2$ , also  $\Delta H \ll H'_\omega$  gives,

$$\Delta H = - \frac{\sum \int_0^l \left( \eta'' + \frac{\Delta H}{H'_\omega} y'' \right) \eta dx}{\frac{L_s}{A_c E}} \quad (19)$$

when warping is neglected, and assume cable curve as parabolic;

$$\begin{aligned} y'' &= -\frac{\theta f}{l^2} \\ \eta'' &= \frac{b}{2} \phi'' = \frac{b}{2} \frac{-t + b \Delta H \frac{\theta f}{l^2}}{KE} \\ \Delta H &= \frac{\sum \left[ \frac{bt}{2KE} + \left( \frac{1}{H'_\omega} - \frac{b^2}{2KE} \right) \Delta H \frac{\theta f}{l^2} \right] \int_0^l \eta dx}{\frac{L_s}{A_c E}} \quad (20) \end{aligned}$$

Shear in Truss Cross Section:

from (13) we may rewrite as follows:

$$q_h = \frac{S_h}{b} = q_o - q_c + q_\omega, \quad q_v = \frac{S_v}{d} = q_o - q_c - q_\omega \quad (13a)$$

where  $q_o = \frac{T_o}{2bd}$ ,  $q_c = \frac{1}{2d} \left[ (H'_\omega + \Delta H) \frac{1}{2} \frac{d^2 b}{dx^2} + \Delta H y' \right]$ ,  $q_\omega = \frac{1}{2} EA_\omega \omega''$

## Examples:

Data;

$l = 2000 \text{ ft.}$

$H_{\omega} = 21500 \text{ kips one cable}$

$f = 195 \text{ ft.}$

$E = 29000 \text{ kips per sq. in.}$

$b = 90 \text{ ft.}$

$t = 32 \text{ ft. kips per ft.}$

$d = 18 \text{ ft.}$

$L_s = 4390$

$A_O = 100 \text{ sq. in. one chord}$

$H_{\omega}^i = 29000 \text{ kips one cable}$

$A_C = 340 \text{ sq. in. one cable}$

$A_h = 34.4 \text{ sq. in. two}$

$A_v = 27.7 \text{ sq. in. one diagonal}$

from above data gives the following constants;

$$\lambda = .0126 \quad \frac{1}{f} = 5.1 \times 10^{-5} \quad k = 11220 \quad KE = 3254 \times 10^5$$

$$\alpha = 12.9 \quad \frac{1}{\lambda f} = 4.06 \times 10^{-4} \quad \frac{1}{2d} \frac{b}{2} H_{\omega}^i = 29000 \quad 2bd = 3240$$

## Example A;

A uniform torque due to live load on one side of bridge is shown in Fig. 4. The solution of the problem for different assumptions of whether additional cable tension or warping are considered are given in Table 1, for the shear at the end of the span. The truss is simply supported at both ends.

constants of integration;

$$A = \frac{1}{\lambda^2 E f} \frac{t}{\lambda} \frac{1 - \cosh \lambda l}{\sinh \lambda l}, \quad B = -\frac{1}{\lambda^2 E f} \frac{t}{\lambda}$$

	$\Delta H$	$E\omega^*$	$\theta \cdot 10^5$	$q_s$	$q_c$	$q_{\omega}$	$q_h$	$q_v$	$S_h$	$S_v$
1	—	—	9.83	9.89	2.85	—	7.04	7.04	634	127
2	—	-.013	9.25	do	2.69	-.65	6.55	7.85	590	141
3	31	—	9.50	do	3.09	—	6.80	6.80	612	122
4	31	-.013	8.92	do	2.93	-.65	6.31	7.61	568	137

Table 1

## Example B;

An asymmetric uniform torque is applied on the bridge as shown in Fig. 5. Under this loading condition the section at the center of the bridge remains fixed with respect to rotation and longitudinal displacement.

The stresses at the center of the span are given as follows:

$$T = 17000 \quad \Delta H = 0 \quad q_o = 5.24 \quad q_c = .4 \quad q_w = -4.33$$

$$q_h = .53 \quad q_v = 9.17 \quad S_h = -48 \quad S_v = 165 \quad \sigma = \pm 5.86 \text{ ksi}$$

## CONCLUSION

The loadings shown in the examples are for illustrative purpose only, and are not necessarily actual design loadings.

For the same example with a live load of 3200 pounds per foot of bridge, calculation by deflection theory gives a maximum shear of 225 kips at the end of the span, and 120 kips at the center of the span. Also, with a wind load of 730 pounds per foot of bridge, which corresponds to a 30 pound wind, the shear in the lateral system calculated by considering cable interaction and effect of dead load, gives a shear of 230 kips at the end of the span, and 65 kips at the center of the span if a partial wind load is considered.

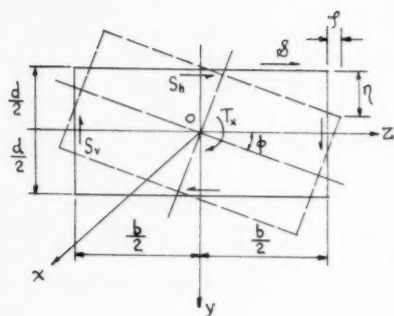


Fig. 1

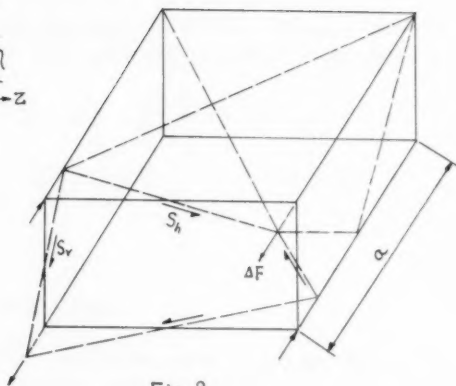


Fig. 2

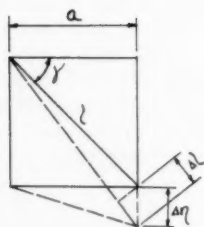


Fig. 3

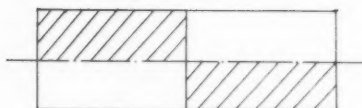
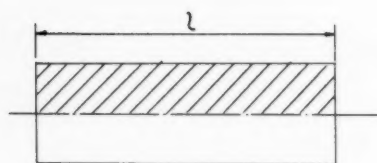
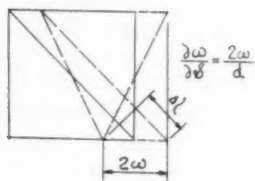


Fig. 5

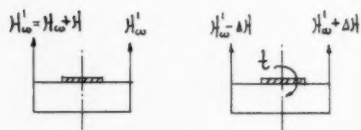


Fig. 4.

---

Journal of the  
STRUCTURAL DIVISION  
Proceedings of the American Society of Civil Engineers

---

A SIMPLIFIED DESIGN OF COMPOSITE BRIDGE STRINGERS

Jack C. Hacker<sup>1</sup>  
(Proc. Paper 1432)

---

SYNOPSIS

Equations for an approximate direct design of balanced composite steel stringers for ordinary highway bridges are presented in this paper. An empirical factor for the ratio of the steel flange areas is used, and the derivation and simplifying assumptions are outlined. Numerical examples for the three basic types of steel stringers (Rolled Section with welded coverplate; welded built-up section and riveted built-up section) are worked out, illustrating practical applications of the equations.

---

INTRODUCTION

In the design of ordinary composite bridge stringers (i.e. steel section composite with concrete deck for live loads only) the most time consuming part is the selection of the first trial section. This is usually followed by the analysis of one or more additional trial sections, the number of which is limited only by the experience of the designer or comparison with a collection of previous designs. Many designers have developed their own short cuts for the various steps involved. A critical evaluation of the problem led to the conclusion that a definite relationship between the top- and bottom-flange areas of the basic steel section exists. The correct mathematical expression for this relationship is involved and dependent upon so many variables that its use in the design office is impractical. However, investigation of a great number of balanced composite stringers with spans from 60 to 140 feet, spacings from 6 to 10 feet and slab thicknesses from 6 to 8 inches, showed that a usable approximation of this relationship would be a proportion, with a proportionality factor  $R$ , which can be expressed in terms of the span. For the above working

---

Note: Discussion open until April 1, 1958. Paper 1432 is part of the copyrighted Journal of the Structural Engineering Division of the American Society of Civil Engineers, Vol. 83, No. ST 6, November, 1957.

1. Senior Structural Engr., Edwards, Kelcey and Beck, Consulting Engrs., Newark, N. J.

range this factor is closely approximated by the expression  $\frac{50}{190-L}$ . Using the factor  $R$  and the approximation that the center of gravity of a flange area coincides with its extreme fibre, it is but a simple algebraic operation to derive expressions for the direct design of the flange areas. For designers with limited experience in composite design, this method will considerably shorten the time required to obtain a satisfactory steel section. In fact, due to compensating errors introduced in the various approximations, the first trial section yields in most cases satisfactory and fairly balanced stress conditions.

### Notation

$A_c$	= Transformed contributory concrete area; sq. in.
$A_{sb}$	= Area of steel in bottom flange; sq. in.
$A_{st}$	= Area of steel in top flange; sq. in.
$d$	= Depth of beam between C.B.'s of flanges; in.
$f_b$	= Allowable steel stress in bending; ksi.
$f_{DL}$	= Dead load stress; ksi.
$f_{LL}$	= Live load stress; ksi.
$I_s$	= Moment of Inertia of Steel Section; in <sup>4</sup> .
$L$	= Design span; ft.
$M_{DL}, M_{LL}$	= Dead Load Moment; Live Load Moment; ftk.
$NAC$	= Neutral Axis of Composite Section.
$NAS$	= Neutral Axis of Steel Section.
$R$	= Empirical Factor for Ratio of Flange areas = $\frac{50}{190-L}$
$s$	= Thickness of contributory concrete; in.
$S_{cb}$	= Section modulus (Composite) of bottom fibre; in <sup>3</sup> .
$S_{sb}$	= Section modulus (Steel) of bottom fibre; in <sup>3</sup> .

### Equations

$$A_{sb} = \frac{12}{f_b} \left[ \frac{M_{DL}}{d} + \frac{M_{LL}}{d+s} \right]$$

$$R = \frac{50}{190-L} \quad (\text{for spans to 140 ft.})$$

$$A_{st} = R A_{sb}$$

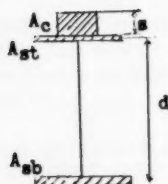


Figure I



## Derivation

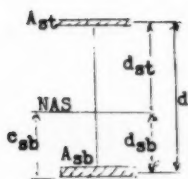


Figure II

$$A_{sb} d_{sb} = A_{st} d_{st} \quad (1)$$

$$I_s = A_{sb} (d_{sb})^2 + A_{st} (d_{st})^2 \quad (\text{approx.})$$

$$\text{Set } c_{sb} = d_{sb} \quad (\text{approximation})$$

$$S_{sb} = A_{sb} d_{sb} + A_{st} \frac{(d_{st})^2}{d_{sb}} \quad (2)$$

From (1)

$$\frac{A_{sb}}{A_{st}} = \frac{d_{st}}{d_{sb}} = \frac{1}{R} \quad (3)$$

Then

$$S_{sb} = A_{sb} d_{sb} \left(1 + \frac{1}{R}\right) \quad (4)$$

From (3)

$$\frac{d_{st}}{d_{sb}} = \frac{1}{R}$$

$$d_{sb} = R d_{st} = R(d - d_{sb})$$

$$d_{sb} = \frac{R d}{R+1} \quad (5)$$

Set (5) into (4)

$$S_{sb} = A_{sb} d \left( \frac{R}{R+1} + \frac{1}{R+1} \right) = A_{sb} d \left( \frac{R+1}{R+1} \right)$$

$$S_{sb} = A_{sb} d \quad (6)$$

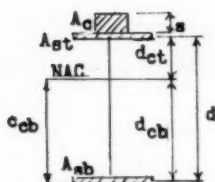


Figure III

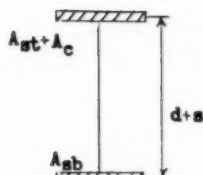


Figure IV

For determination of the section modulus of the composite section, areas and distances shown in Figure III are replaced by those in Figure IV. Another approximation is introduced in this step, namely that the distance from the C.G. of the bottom flange to the C.G. of the combined areas of top flange steel and effective concrete is equal to  $d + s$ .

It can be shown that this approximation contains an error of opposite sign to the error introduced by setting  $c_{cb} = d_{cb}$ .

Using Figure IV, then, to determine the section modulus for the bottom fibre of the composite section by applying equations (1) to (6)

$$S_{cb} = A_{sb} (d + s) \quad (7)$$

With the bottom fibre at the allowable stress  $f_b$

$$\frac{f_b}{12} = \frac{M_{DL}}{S_{sb}} + \frac{M_{LL}}{S_{cb}} \quad (8)$$

Substituting the values for  $S_{sb}$  and  $S_{cb}$  from equ. (6) and (7)

$$\frac{f_b}{12} = \frac{M_{DL}}{A_{sb}d} + \frac{M_{LL}}{A_{sb}(d+s)}$$

or

$$A_{sb} = \frac{12}{f_b} \left[ \frac{M_{DL}}{d} + \frac{M_{LL}}{d+s} \right] \quad (9)$$

From Equation (3)

$$A_{st} = R A_{sb} \quad (10)$$

Comparison of a great number of composite sections used in bridges of ordinary stringer spacing and slab thickness yielded an empirical expression for  $R$  of the form

$$R = \frac{50}{190-L} \text{ for spans up to 140 ft.} \quad (11)$$

#### Example I Rolled Section (A-7 Steel)

Span: 80 ft.

Dead Load:

Stringer Spacing: 8' -0

Slab: 0.756 k/ft

Slab Thickness: 7 1/2"

Steel: Assume 0.200

Load: H20 - S16 - 44

Shear Conn. & Misc.: 0.024

0.98 k/ft

---


$$M_{DL} = 784 \text{ ftk}$$

$$M_{LL} = 1156 \text{ ftk (incl. impact)}$$

---

Assume  $d = 37$  in.

---


$$A_{sb} = \frac{12}{18} \left( \frac{784}{37} + \frac{1156}{44.5} \right) = 31.5 \text{ in}^2$$

$$R = \frac{50}{190-80} = 0.455$$

$$A_{st} = 14.3 \text{ in}^2$$

Try 36 WF 182

with 14 x 1 1/4 Plate

$$A_{st} = 14.24$$

$$A_{PL} = 17.50$$

$$A_{sb} = 31.74$$

Analysis of this section shows the total stresses due to dead load and live load to be as follows:

Bottom steel fibre : 18.26 ksi

Top steel fibre : 16.90 ksi

Top concrete fibre : 0.60 ksi

## Example II Built-up Section

Span: 110 ft.

Dead Load:

Stringer Spacing: 7' -6

Slab: 0.653 k/ft

Slab Thickness: 7"

Steel: Assume 0.300

Load: H20 - S16 - 44

Shear Conn. &amp; Misc.: 0.027

0.98 k/ft

---


$$M_{DL} = 1482 \text{ ftk}$$

$$M_{LL} = 1547 \text{ ftk}$$


---

Assume  $d = 47''$   $d$  can be assumed at  $\frac{L}{25}$  to  $\frac{L}{30}$ ,  
unless clearance considerations dictate a shallower section.

---


$$A_{sb} = \frac{12}{18} \left( \frac{1482}{47} + \frac{1547}{54} \right) = 40.0 \text{ in}^2$$

$$R = \frac{50}{190-110} = 0.625$$

$$A_{st} = 25.0 \text{ in}^2$$


---

## a) Welded Section (A-373 Steel)

(Top Fl. 20 x 1 1/4

Try (Bott. Fl. 20 x 2

(Web 45 x 5/16

Analysis yields these total stresses:

Bottom steel fibre : 18.29 ksi

Top steel fibre : 17.48 ksi

Top concrete fibre : 0.57 ksi

## b) Riveted Section (A-7 Steel)

$$A_{sb} = 40 \text{ in}^2 \text{ (Net)}$$

$$A_{st} = 25 \text{ in}^2 \text{ (Gross)}$$

Try: Top: 2  $\text{I}^{\text{F}}$  8 x 4 x 3/4 Bottom: 2  $\text{I}^{\text{F}}$  8 x 6 x 7/8

1  $\text{H}$  14 x 5/8

1  $\text{H}$  18 x 3/4

1  $\text{E}$  18 x 5/8

Web:  $\text{E}$  50 x 3/8

(For riveted sections the web plate must be deeper than the assumed dimension  $d$ , to account for shift of the C.G. of the flanges due to use of angles.)

Analysis using net areas for bottom & web, gross area for top yields these total stresses:

Bottom steel fibre : 17.69 ksi

Top steel fibre : 17.21 ksi

Top concrete fibre : 0.54 ksi

## ACKNOWLEDGMENT

The writer wishes to acknowledge the suggestions of Mr. John Dalessio,<sup>2</sup> who initially conceived the idea of searching for a simple relation between the flange areas, and the firm of Edwards, Kelcey and Beck for the use of their time and their design records.

2. Chief Struct. Engineer, Edwards, Kelcey and Beck.

---

Journal of the  
STRUCTURAL DIVISION  
Proceedings of the American Society of Civil Engineers

---

WOOD DIAPHRAGMS:  
PROGRESS REPORT OF A SUB-COMMITTEE OF THE COMMITTEE  
ON TIMBER STRUCTURES OF THE STRUCTURAL DIVISION<sup>a</sup>

(Proc. Paper 1433)

INTRODUCTION

The diaphragm is the most prevalent type of structural element used in buildings being far more common than the truss, the rigid frame, and the arch. Wood structural systems are chiefly assemblies of diaphragms in the form of joist floors, raftered roofs, and stud walls. Wood diaphragms are frequently used in conjunction with trusses, rigid frames, and arches, and with collateral masonry, reinforced concrete and steel elements.

Floors, walls, ceilings and roofs may serve as structural diaphragms in conjunction with their ordinary functions. Thus, in addition to supporting loads immediately applied to them, they participate in developing the strength and rigidity of the structural assembly through attachment along their edges to adjacent elements. The effectiveness of a diaphragm is dependent on the adequacy of this attachment particularly with respect to lateral loads.

The modern trend toward elimination of fixed interior walls and reduction of exterior walls by large openings emphasizes the structural importance of diaphragms. In the past, with numerous interior walls and exterior walls and small openings, adequate strength and rigidity were usually attained. Present day problems require accurate engineering analysis and design based on reliable basic data for satisfactory solution. Diaphragm design has become commonplace on the Pacific Coast, where design for horizontal forces is often mandatory. There, experience has proven that it is basically economical to utilize existing walls and roofs to brace a building.

The scope of this chapter is limited to a general consideration of wood diaphragms and their functions, design provisions, and reference to sources of technical data by bibliography.

Terminology

A structural diaphragm may be defined as a relatively thin structural element that usually is flat and of rectangular shape capable of resisting shear

Note: Discussion open until April 1, 1958. Paper 1433 is part of the copyrighted Journal of the Structural Division of the American Society of Civil Engineers, Vol. 83, No. ST 6, November, 1957.

- a. This paper will form the basis for a chapter in a proposed revision to ASCE Manual of Engineering Practice No. 17 entitled "Timber Piles and Construction Timbers."

parallel to its edges, although curved shells and shapes other than rectangular are not uncommon. It is defined by two faces and by four edges and is attached to adjacent elements along two or more edges.

Wood diaphragms are composed of standard, manufactured pieces that are assembled by means of nails, screws, glue, or similar devices. Because diaphragm action resembles that of beams and girders in some respects, similar terms are used to describe the parts. They are classified in accordance with form of assembly as follows:

1. Solid. A solid slab of wood formed by nailing or gluing together pieces of the same cross-section.
2. Sheathed. A rectangular frame-work composed of transverse joists or studs and longitudinal flange members such as sills, headers, and plates to which sheathing that acts as a web is attached on either one or both faces. Kinds of sheathing are:
  - (a) Lumber. Face of standard boards, usually in square edge, shiplap, or tongue-and-groove pattern, which are nailed to the frame-work and placed either (1) Transverse at 0 or 90° to the edges. (2) Diagonal at approximately 45° to the edges.
  - (b) Plywood. Face of plywood panels.
    - (1) Blocked, panel edges nailed to blocking between framing members.
    - (2) Unblocked, panel edges free between framing members.
  - (c) Wall Board. Face of a manufactured wall board such as wood fibre, vegetable fibre, or gypsum.
  - (d) Plaster. Face of either gypsum or cement plaster on a wood, steel, or gypsum lath base.
3. Trussed. The frame-work is either a truss or a rectangular frame with let-in diagonal braces. The faces may be covered by materials of negligible structural properties.
4. Composite. Any combination of 1, 2 (a to d) and 3 above.
  - (a) Double-sheathed. Sheathed both faces by any kind listed in (2) above.
  - (b) Multiple-sheathed. Two or more layers of sheathing on the same face.
  - (c) Sheathed-trussed. Sheathing used in conjunction with trussing or bracing.

It is important to note that a composite diaphragm is not necessarily equal in strength to the sum of the separate parts unless those parts are identical in all respects. Otherwise, each part participates in proportion to its rigidity.

#### Structural Functions

Walls, floors, and roofs, when acting as diaphragms, fulfill two equally important functions as elements of a satisfactory structural system.

- (a) They must participate in the support of regular vertical live and dead loads.



- (b) They must contribute to the rigidity and strength of a structure to withstand sporadic lateral loads due to wind, earthquake and blast that may act in any horizontal direction.

To perform both functions a diaphragm must have sufficient strength and rigidity and be adequately supported. Also, to function properly, the respective elements of an assembly must be so arranged and integrated that all forces imposed on them are conducted to the foundation and ground without excessive stress or deformation.

Diaphragms are in two distinct categories in accordance with their structural functions, (a) and (b) above.

#### 1. Vertical (Wall)

- (a) Takes vertical loads in its plane that come from elements which it supports.
- (b) Provides horizontal support in its plane by rocking action for elements which it supports including other diaphragms which are subjected to horizontal forces due to wind and earthquake.

#### 2. Horizontal or Sloping (Floor, Roof, Ceiling)

- (a) Takes vertical loads transverse to its plane.
- (b) Provides horizontal support for vertical elements and transmits horizontal forces to its supports similar to simple or multispans beam action.

Effective diaphragm action requires sufficient strength to withstand shear and moment in its plane and sufficient rigidity to limit horizontal deflections. It resembles conventional beam and girder action in general concept but differs greatly in behavior because the span-depth ratio is usually less than four and the web thickness is comparatively very small. Consequently, shear stresses and shear deformation or skewing greatly predominate over bending stresses and deflection. Specifically, the properties of solid diaphragms are largely dependent on the nailing of the laminations; the properties of sheathed diaphragms depend principally on the effectiveness of the sheathing; and, the properties of trussed and braced diaphragms depend largely on the diagonals.

### Design Provisions

#### A. Vertical Loads

Present design and construction practices make adequate provisions for the effects of vertical live and dead loads on wood diaphragm roofs, floors, and walls. They have been developed by years of experience and are established standards that are accepted by the architectural and engineering professions and the construction industry. There is an extensive literature on the subject including current building codes, standard specifications, and regulations of government agencies and technical associations and conventional construction practice that assures wood diaphragms with requisite strength and stiffness in this respect. Due to the limited scope of this chapter consideration, this aspect is omitted.

## B. Lateral Loads

Lateral loads are caused mainly by winds and earthquakes. Because of their sporadic nature, their importance is frequently ignored, especially in localities which have not experienced serious damage in recent years. The present trend toward omission of walls which are needed for structural purposes together with the realization that high winds and strong-motion earthquakes can cause great damage emphasizes the need for reliable basic data concerning both the forces involved and the properties of the structural elements which are required to withstand the stresses and deformations that are produced.

In the light of present aerodynamic knowledge, it is known that the specified wind loads are not realistic either in magnitude or pattern of distribution. However, it has been demonstrated that structures which are designed and built for the hypothetical load are adequate for the actual loads. The tendency to disregard wind resistant design in localities where high winds occur infrequently ignores the vagaries of weather and the fact that damage will be determined by the magnitude of one storm rather than a number of lesser storms. Wind loads are conventionally specified in the range of 15 to 40 pounds per square foot of presented area with a permissible increase of one-third of the allowed working stresses.

Strong-motion earthquakes may occur at any place throughout the world but at the present time are considered to be indigenous to the Pacific Coast states, Alaska, and other areas that are presently seismically active. The states of California (1933) and Washington (1955) require by law that certain buildings be designed and constructed to resist earthquakes. All the cities of California and many cities of the Pacific Northwest include earthquake provisions in their building codes. These provisions specify the lateral forces for which the structure shall be designed in the form of inertia force,  $Wa/g$ , where  $W$  is the weight and  $a/g$  is the seismic factor,  $C$ . The value of  $C$  is a matter of engineering judgement based on experience, experiment and theoretical analysis and is in the range 0.02 to 0.20 depending on a wide variety of circumstances. Also, it is usual to permit an increase of one-third in the allowed working stresses because of infrequent occurrence and short duration.

## C. Strength and Stiffness of Diaphragms

In recent years, numerous tests have increased understanding of the factors affecting diaphragm performance. Adequate specifications for lumber and plywood sheathed diaphragms have been incorporated or are under consideration in several regional and municipal building codes.<sup>(29,30)</sup> These specifications include limitations on maximum length-width and height-width ratios for horizontal and vertical diaphragms respectively, with the intention of limiting deflections to reasonable amounts. Also, each diaphragm is required to be connected to its supporting elements in a manner that is adequate to transmit imposed forces. Adequate foundation anchorages are required for vertical diaphragms. Lateral forces may cause rotation, as when a roof diaphragm is supported by wall diaphragms along three edges, that must be considered in the design.

For various constructions, maximum allowable shears in pounds per foot of diaphragm width are specified in these codes, as noted in the following paragraphs. The stress increase normally allotted for short-time loading is included in these values.

Present knowledge concerning the respective types of diaphragms is briefly summarized below.

1. Solid. Laminated floors and walls are frequently used to provide required fire resistance particularly around stair wells and heating plants. They are available for structural purposes including resistance to lateral forces. Properties in this respect depend entirely on the nailing and whether the principal shear is parallel or perpendicular to the direction of the laminations. The allowable lateral loads on nails<sup>(29)</sup> can be used to determine the nailing required for a given diaphragm after the intensity of shear between the laminations has been calculated by fundamental mechanics. Little information is now available on the deformational properties in skewing.<sup>(33)</sup>

2. (a) Lumber Sheathed.

- (1) Transverse. Presently available technical information relating to the properties of transverse sheathing indicates that, for the usual proportions and short spans of small structures, 1" x 6" or 8" sheathing nailed to 2" x 4" or larger studs and joists at 16" centers with 2 8d common nails per joint will probably support shear of not more than 100 pounds per foot of loaded edge with reasonably small deflections.
- (2) Diagonal. Board sheathing placed diagonally at approximately 45° provides greater strength and rigidity than similar material in a transverse direction. From an analytical viewpoint diagonal sheathing acts as a complex combination of a conventional girder web and either a tension or compression field web provided that the boundary members are competent to act as flanges and are securely spliced and tied at the corners. Tests show that diagonal sheathing exerts a normal component of stress on the flange members which may be from 35 to almost 100 percent of the calculated shear stress and for which adequate flange members must be provided.

Experience indicates that a diaphragm which is diagonally sheathed with one layer of 1 x 6 or 1 x 8 boards secured to 2" studs or joists at 16" to 24" centers by 2 8d nails at each crossing and 3 8d nails at the ends of each board is adequate for an allowed shear of 200 pounds per foot of length of edge under ordinary circumstances and, that a value of 300 pounds per foot may be used when the boundary members are incorporated into the assembly. It is good practice to limit the use of these values to horizontal diaphragms with span-width ratios of 3 or less and to vertical diaphragms with a span-width ratio of 4/3 or less. In both cases, it is very important that the members comprising the boundary flanges be capable of taking the localized normal component.

Double diagonal sheathing on one face in which the boards of one layer are mutually perpendicular to the direction of the other layer eliminates the normal component and provides a diaphragm that is susceptible of rational analysis as a latticed beam or girder. The strength and rigidity is limited principally by the nailing pattern and the adequacy of the boundary flange members.

2. (b) Plywood Sheathed. Plywood sheathed diaphragms may be analyzed as flexural elements with fully shear-resistant webs. Flange or chord members must be spliced to transmit tension and compression. The plywood panels exert no important lateral thrust against the chords, so no special corner ties are required. Shear and buckling stresses in the plywood can be computed, although they seldom, if ever, are limiting factors.

The nailing schedule for the plywood, as well as thickness of the plywood and framing, generally determines allowable shears, which range up to 820 plf for common constructions. For maximum strength and rigidity, all four edges of each plywood panel should be nailed, using the same schedule. This normally requires blocking between framing members, but other methods of transmitting the shear have also been worked out. When blocking is omitted, allowable shears are reduced.

Where possible, joints between plywood panels should be staggered. Strength is influenced by the direction of the principal load with respect to unstaggered, or continuous joints, including boundaries of the diaphragm. Under certain conditions such joints and boundaries require additional nailing.(27)

Deflection of blocked horizontal plywood sheathed diaphragms can be calculated by a general formula.(24)

2. (c) Wallboard Sheathed. Technical data on structural properties are not sufficient to indicate proper design values.
2. (d) Plaster Sheathed. No technical data on structural properties are available at this time.
3. Trussed. Trussed diaphragms are analyzed and designed by the conventional methods of elementary mechanics. However, connection details must be adequate and provision for inspection and adjustment is necessary to assure satisfactory performance.
4. Composite. In addition to double-sheathed, multiple-sheathed and sheathed-trussed types of flat elements which are described in part above, the Lamella roof system and other forms of barrel roofs serve as structural diaphragms.(21) They are composed of sheathing on a curved surface attached to a Lamella frame-work, tied arches, or curved chord trusses. The mechanics of such diaphragms is complex and requires careful engineering analysis to utilize the strength and rigidity that are available in thin-shell elements.

#### Research and Tests

The great diversity of diaphragms and the wide variety of circumstances in which they are used delayed systematic, technical study of their structural characteristics until 1929 when the U. S. Forest Products Laboratory published (1) the results of the first quantitative study of the subject. Loads "simulating the effects of wind forces acting on a wall of a building as transmitted from an adjoining wall" were applied to diaphragms with 2 x 4 studs and various types of sheathing in order to determine relative strengths

and deflections. Subsequent tests (5, 9, 14, 15, 16, 17, 20, 26, 27) extended the data to include other types of braces and sheathed walls and demonstrated the importance of boundary conditions that were not considered in the 1929 tests.

The Southern California earthquake of 1933 emphasized the importance of structural diaphragms and provided much reliable evidence of their behaviour when subjected to lateral forces. Study of this evidence and specific problems associated with it has contributed much of the basic information presently available.

In 1933-1934,(6) three 24' x 40' lumber sheathed floor diaphragms were tested for strength and deflection. The joists and framing followed customary practice. Three types of sheathing were used:

(a) One layer of 1" transverse boards, (b) one layer of 1" transverse and one layer of 1" diagonal boards, and (c) two layers of opposed diagonal 1" boards. An analysis of the probable behaviour of these diaphragms in a building with brick walls during an earthquake of 0.1g is included. Supplementary to the above tests, studies of 1/4 scale comparable floor diaphragms including a span-width ratio of 3 were made. A table was developed for the deflections of usual floor diaphragms when subjected to loads of 100# per foot of width.(8)

A series of tests in 1934(4) developed fundamental data on the tensile and shearing strengths of metal joist anchors in masonry walls.

During 1934, comprehensive tests of existing wood diaphragms were made at Los Angeles under the auspices of advisory committees of the California State Division of Architecture.(8) These tests were made on the second floor system of a three-story brick walled school that was condemned after the 1933 earthquake because of foundation conditions. The diaphragms were approximately 18' x 35' and sheathed with two layers of boards in various combinations. Also, lateral deflections and other data on brick walls were studied. As a result of these tests, useful data for the design and checking of earthquake resistance were obtained. They are largely the basis for present earthquake regulations and building code provisions.

In 1948, three tests of one layer diagonally sheathed diaphragms similar to conventional roof construction on 1/4 scale models of 24' x 40' prototypes were made to correlate the scale effect accompanied by incidental tests of the scale effects of nail size.(19) This study includes an analysis in accordance with beam theory, recommendations for the arrangement of sheathing, and for allowable lateral loads for given conditions.

In 1949, a test program of lumber sheathed diaphragms was initiated at the Oregon Forest Products Laboratory for the purpose of obtaining additional fundamental data on the skewing properties of both vertical and horizontal elements. Progress reports have been made and the program is still continuing.(33)

The Douglas Fir Plywood Association has since 1950 tested 10 quarter-scale and 25 full-scale plywood roof and wall diaphragms and cooperated with Oregon Forest Products Laboratory in testing 4 more. Sizes have ranged up to 20' x 60'.(23,24,26,33) Most important variables including seasoning of framing members were covered by the tests, and design procedures have been developed.(23,24,27)

The U. S. Forest Products Laboratory has performed tests on both vertical shear walls and horizontal diaphragms diagonally sheathed with lumber.(18,25,31)

Advancement of knowledge concerning the structural properties of diaphragms, particularly in skewing, has largely depended on the disastrous events of hurricanes, earthquakes, and war and, as a consequence, has been slow and sporadic. Present knowledge is distinctly incomplete and for certain types is practically non-existent. Much investigative research and study are needed to advance this important aspect of structural knowledge in order that structural practice can anticipate the hazards that will cause loss of life and property that might be avoided or minimized.

Respectfully submitted,

Harry Bolin

David Countryman

A. C. Horner

Edward Kuenzi

R. G. Kimbell, Jr.

T. K. May

A. L. Miller, Chairman

Sub-Committee of the Committee  
on Timber Structures

#### BIBLIOGRAPHY

1. The Rigidity and Strength of Frame Walls by G. W. Trayer, Bulletin No. 2896, U. S. Forest Products Laboratory, 1929 (Revised 1947). See also E. N. R., Oct. 24, 1929.
2. Experimental Study of the Dynamic Behavior of Models of Timber Walls Subjected to an Impulsive, Horizontal Ground Vibration by Lydik S. Jacobsen, Stanford University Bulletin of the Seismological Society of America - Sept. 1930.
3. Earthquake Damage Analyzed by Long Beach Officials by C. D. Wailes, Jr. and A. C. Horner, E. N. R., May 25, 1933.
4. Joist Anchors in Masonry Walls Tested for Earthquake Resistance by N. B. Green and A. C. Horner, E. N. R., July 12, 1934.
5. Plywood as a Structural Covering for Frame Walls and Wall Units by G. W. Trayer - Bulletin No. R1025, U. S. Forest Products Laboratory, 1934.
6. Earthquake Resistance of Timber Floors by N. B. Green and A. C. Horner, E. N. R., Feb. 1, 1934.
7. Lateral Loads on Piers by H. C. Whittlesey, Building Standards (Pacific Coast Building Officials Conference - Nov. 1935).
8. Tests Indicate Design Methods for Earthquake-Proof Timber Floors by N. B. Green, A. C. Horner and T. C. Combs, E. N. R., June 20, 1935.
9. Fabricated Wall Panels with Plywood Coverings by R. F. Luxford, U. S. Forest Products Laboratory, The Timberman, Feb. 1936.
10. Earthquake Resistant Design for New School Buildings by Harry W. Bolin, E. N. R., March 18, 1937.



11. The Relative Stiffness of Wall Panels, Research Paper by S. Irwin Crookes, University College, Auckland, N. Z., May 1937.
12. Aseismic Design of Wood Structures: Duration of Stress Considerations by T. C. Combs, Bulletin of the Seismological Society of America, Oct. 1939.
13. A Manual on Sheathing for Buildings, National Lumber Manufacturers' Assn., 1941.
14. The Rigidity and Strength of Braced and Unbraced Walls Covered with Bevel Siding by E. C. O. Erickson, Bulletin R1261 - U. S. Forest Products Laboratory, April 1941.
15. Structural Properties of Prefabricated Plywood Lightweight Constructions for Walls, Partitions, Floors and Roofs by Wexler, Newman, Phelan and Luxford, B. M. S. 104 - U. S. National Bureau of Standards, 1945.
16. Guides to Improved Framed Walls for Houses, Alan D. Freas. E. N. R., October 17, 1946.
17. Tests of Timber Structures from Golden Gate International Exposition - Part IV-Plywood Tests, Transactions ASCE, Vol. 113, 1948, page 1123.
18. Strength of Houses by H. L. Whittemore, J. B. Cotter, A. H. Stand and V. B. Phelan, B. M. S. 109 - U. S. National Bureau of Standards, 1948.
19. Tests Establish Strength of Single Diagonally Sheathed Roof Structure by N. B. Green and A. C. Horner, Western Construction News, Aug. 15, 1949.
20. Expected Resistance to Racking of Douglas Fir Plywood Sheathed Panels, Housing and Home Finance Agency - Technical Bulletin No. 13, 1950.
21. Analysis of the Lamella Roof-Horizontal Forces, Dr. Theodor von Karman. California Institute of Technology.
22. Horizontal Bracing Systems in Buildings Having Masonry or Concrete Walls, Technical Bulletin No. 1 - Structural Engineers Association of Southern California, Feb. 1951. (Reprinted in Building Standards Monthly, June, 1951.)
23. How to Design Plywood Panels by David Countryman, Douglas Fir Plywood Association, E. N. R., Jan. 24, 1952.
24. Lateral Tests on Plywood Sheathed Diaphragms by David Countryman, Douglas Fir Plywood Association Laboratory Report No. 55, 1952.
25. A Study of the Diaphragm Action of 6' x 16' Hayloft Floor Panels by D. V. Doyle, Forest Products Laboratory, 1952.
26. Racking Tests on Wall Sections Sheathed with Texture One-Eleven by David Countryman and Vernon Haskell. Douglas Fir Plywood Association Laboratory Report No. 62, 1953.
27. Summary of 1954 Horizontal Plywood Diaphragm Tests by David Countryman and Paul Colbenson. Douglas Fir Plywood Association Laboratory Report No. 63, 1954.
28. Strength of Stapled Plywood-Lumber Joints by David Countryman and Paul Colbenson. Douglas Fir Plywood Association Laboratory Report No. 68, 1955.

29. Uniform Building Code, Vol. 1, Section 2511, Pacific Coast Building Officials Conference. 1955.
30. California Administrative Code, Title 21. Public Works, State of California. Articles 3 and 6.
31. Diaphragm Action of Full-Scale Diagonally Sheathed Wood Roof or Floor Panels, D. V. Doyle. U. S. Forest Products Laboratory Report TM-94, 1955.
32. Plywood Roofs for Economy, M. C. Conkey. E. N. R., August, 1955.
33. Oregon Forest Products Laboratory Reports. A series of reports on lateral tests on full-scale diaphragms: No. T-2 - 1951, No. T-3 - 1952, Nos. T-5, T-6 - 1953, Nos. T-9, T-10 - 1954, Nos. T-11, T-12, T-14 - 1955.

---

Journal of the  
STRUCTURAL DIVISION  
Proceedings of the American Society of Civil Engineers

---

THE DESIGN OF RIGID FRAME BENTS

Richard Z. Zimmermann, Jr.,\* A.M. ASCE  
(Proc. Paper 1434)

---

SYNOPSIS

This paper is a comparison of three different methods of solution available to the structural designer for the determination of bending moments and shears in an unsymmetrical rigid frame bent subjected to a concentrated vertical load. The same illustrative problem is used throughout, with a brief discussion of the basic theory involved and an explicit and logical development of the actual numerical solution being presented in all three methods. The essential purpose of the article was to demonstrate contemporary design procedure for indeterminate structures and allow the reader to make his own deductions or opinions as to the convenience or amount of labor required for each classical method.

---

INTRODUCTION

The continuous rigid frame structure, whether of reinforced concrete or welded steel, is here to stay. Not only do architects admire the graceful simplicity of a gabled bent, but practical, hard-boiled economics often justify the use of a rigid frame. For relatively short roof spans the conventional truss portal is grossly inefficient in its use of metal since some members may be redundant and many sized for minimum rivet edge distances or least radius of gyration along the unsupported length. Moreover, gusset plates are required for all the joints and the fabricating charges are usually slightly more than those for frames of rolled shapes only. For longer roof spans the rigid frame compares favorably often when the engineer takes full advantage of the available headroom permitted by this type of structure and considers the possible savings in height of the side walls on the building and reduction in interior space which must be heated. Painting and maintenance offer further economies.

---

Note: Discussion open until April 1, 1958. Paper 1434 is part of the copyrighted Journal of the Structural Division of the American Society of Civil Engineers, Vol. 83, No. ST 6, November, 1957.

\*Structural Engr., Day & Zimmermann, Inc., Philadelphia, Pa.

Whether for all the above reasons or a few more not mentioned, the designing engineer may be confronted with a statically indeterminate frame. How he effects the solution to such a problem displays a great deal about that engineer's technical training and comprehension of the theory. Under these circumstances, it is hardly surprising that the gentlemen who compose the State examination questions for professional registration find the inclusion of at least one problem on a rigid frame bent so appealing.

A special difficulty exists for the practical or consulting engineer whose time is limited, however. In the interest of economy in both time and effort this individual must choose the most reliable and expeditious method of solution permitted by the required precision. Unhappily, one standard theoretical approach is seldom efficient or fully satisfactory for all the various types of structures which the designer is apt to encounter. Thus the engineer must overcome the dilemma of which tool to select; and an intelligent choice presupposes some familiarity with the merits and disadvantages of several classical solutions offered by the textbooks. The illustrative problem developed below is intended to afford a ready comparison of three different methods of solution: Moment Distribution, Column Analogy and Slope Deflection.

### Problem

Plot the bending moment diagram and compute all reactions and shears for the frame and concentrated loading shown in Figure 1.

Although the loading is centered, the stiffnesses of the two column members are decidedly not identical; and this non-symmetry of the frame produces a sidesway or lurching movement of the girder which makes the horizontal shear forces unpredictable by ordinary statics. Three possible methods of solution are described below.

### The "Moment Distribution" Method

Typical references are: "Continuous Frames of Reinforced Concrete," Chapter IV, by Hardy Cross and Newlin Morgan as published by John Wiley and Sons or "Structural Analysis by Moment Distribution," Chapter II, by S. Butterworth as published by Longmans, Green and Company of London.

The first step is to apply some propping force "F" horizontally at the juncture of girder and column to prevent sidesway or horizontal displacement of the joints. This force is purely a theoretical fiction of unknown magnitude, as yet; although it helps to create a mental picture of the forces acting to distort the frame. The joints at the supports of the girder are now allowed to rotate to equilibrium under the action of the 1000-pound vertical load. This implies a straight-forward classical distribution of the girder fixed end moments according to the relative stiffnesses of all members.

$$K = \text{Member Stiffness} = \frac{I}{L} \quad (1)$$

$$K_1 = \frac{66.6}{10} = 6.66 \quad K_2 = \frac{66.6}{20} = 3.33 \quad K_3 = \frac{66.6}{15} = 4.44$$

$M_F$  = GIRDER FIXED END MOMENTS UNDER CONCENTRATED LOAD

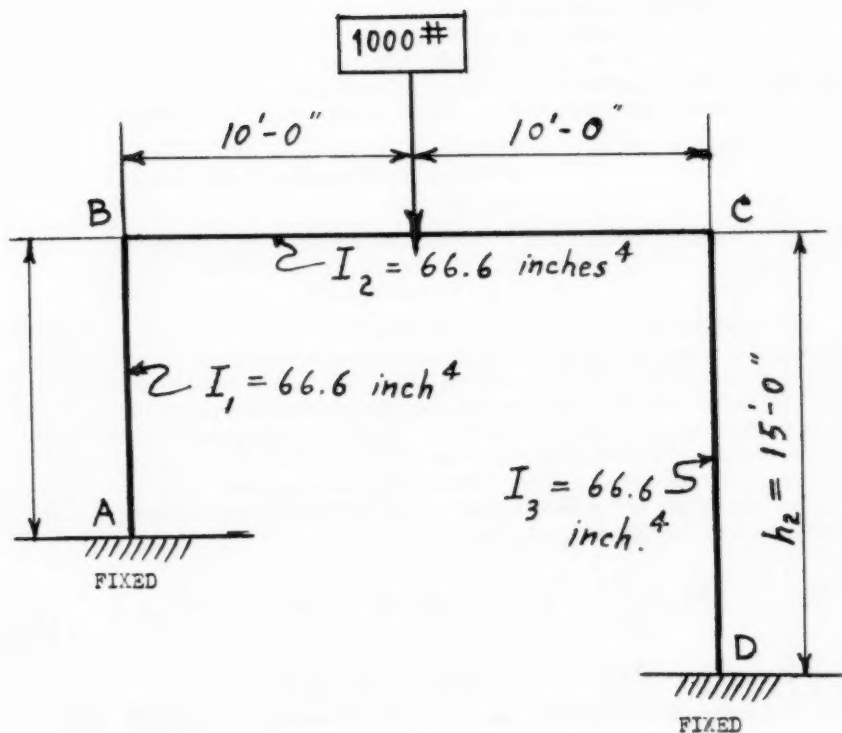


FIGURE 1

$$M_F = \frac{PL}{8} = \frac{1000(20)}{8} = 2500 \text{ foot pounds}$$

Consider the rectangular bent as flattened out in a straight line and perform a standard moment distribution process for the rotation of joints. The result is illustrated in Figure 2.

The final end moments obtained by this first distribution are true only for a frame restrained from sidesway or horizontal displacement of the girder by an arbitrary propping force applied to the top of a column. A bending moment diagram for this condition would appear as shown in Figure 3.

Positive Moment - causes tension stress on the bottom of the girder or righthand side of the columns.

Negative Moment - causes tensile stress from bending on the top of the girder or lefthand side of the columns.

The lateral forces or horizontal shears at the bases of the columns may be determined from the known bending moments on each column by writing the usual equations for static equilibrium. Here it is much more convenient to adopt the more orthodox sign convention that all moments producing a clockwise rotation about a joint are positive. Positive shear forces are assumed acting from right to left at the bottoms of the columns and a negative sign indicates the opposite direction. Admittedly, this business of favorite sign conventions is one of the most troublesome and controversial aspects of any analysis of an indeterminate frame.

$$\text{Since } \sum M_B = 0 \quad H_A h_1 + M_A + M_B = 0 \quad (2)$$

$$H_A = \frac{-M_A - M_B}{h_1} = \frac{-1041 - 2098}{10} = -314 \text{ lbs.}$$

Using the different moments on the righthand column:

$$\text{Since } \sum M_C = 0 \quad H_D h_2 - M_C - M_D = 0 \quad (3)$$

$$H_D = \frac{M_C + M_D}{h_2} = \frac{1723 + 858}{15} = +172 \text{ lbs.}$$

Notice that these horizontal shears are unbalanced, instead of being equal and opposite in direction. Since there were no lateral loads on the bent

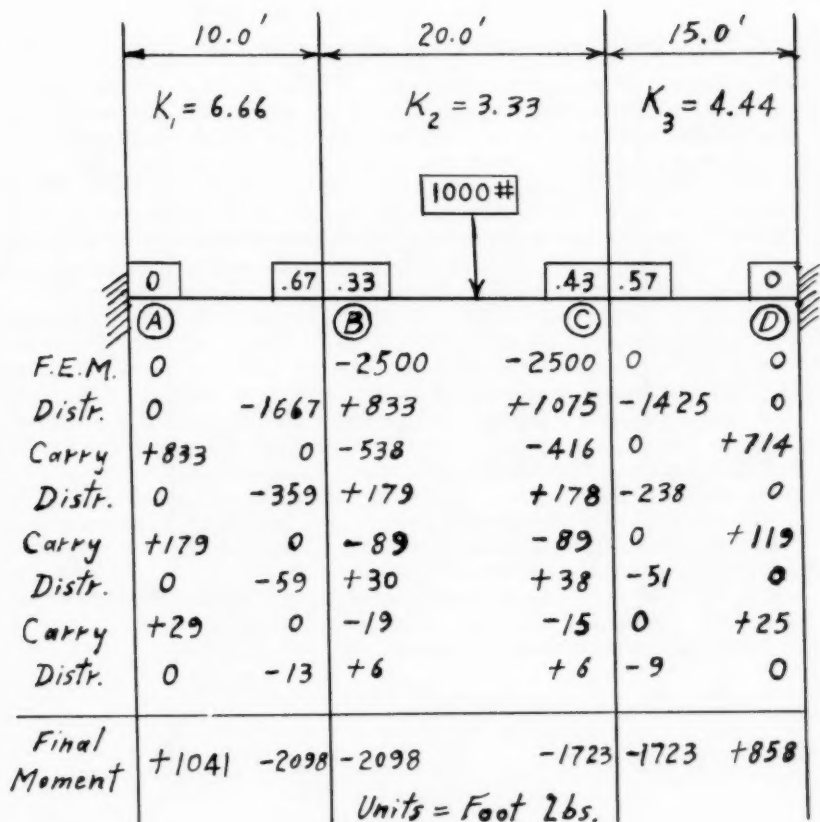


FIGURE 2

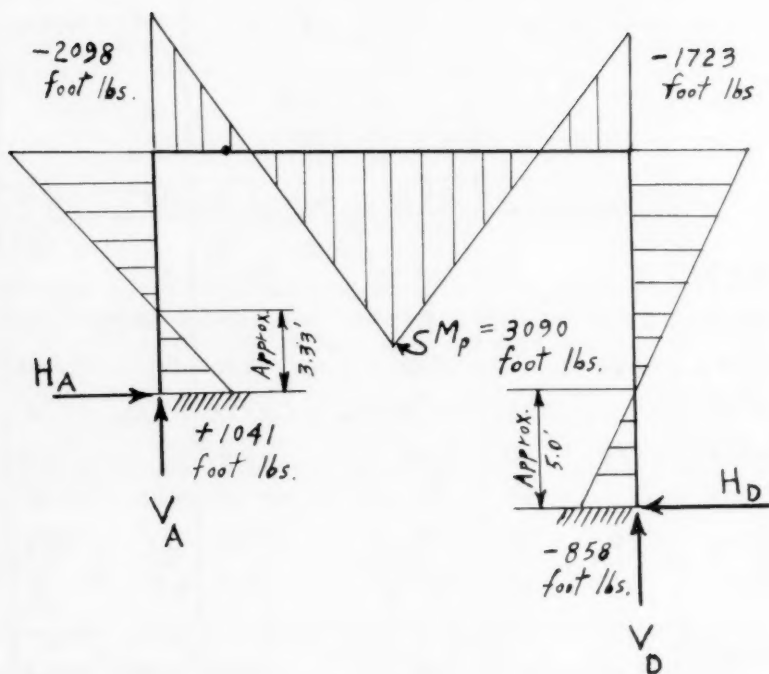


FIGURE 3



originally, such a condition must obviously be in conflict with the truth. This false answer is the consequence of our allowing rotation of the joints only; and the unbalance in shear represents the artificial "propping force" applied horizontally to the top of the frame in order to prevent any lateral displacement of the joints or sideways.

$$\text{Propping Force} = F = -(H_A + H_D)$$

$$F = -(-314 + 172) = +142 \text{ pounds, acting from right to left}$$

The propping force is equal in magnitude, but opposite in direction, to the unbalanced horizontal shear force. The abrupt removal of this force is equivalent to applying a sway force identical to the total unbalanced shear horizontally to the joint "B" of column and girder. This sway force will push the bent over to one side until the resisting tensions in the fibers of the members so induced by this horizontal displacement of the joints constrain the structure from absolute collapse. In the case of a symmetrical vertical loading, the frame will lean towards the column of least stiffness.

Thus we are now confronted with the problem of determining the bending moments produced by the side lurch of a rigid frame under the action of an external lateral force only. This force must exactly neutralize the "propping force." A more scientific and realistic view of the entire process is that the frame must continue to deform in some manner until the horizontal shears at the bases of the columns become equal and opposite, since no lateral force actually existed in the original conditions.

If the joints are now locked, so as to prevent rotation, while the sway force is applied, then each vertical member may be considered as a fixed end beam where one rigid support (the top) moves laterally a small distance with respect to the bottom support. The contraction of the girder under axial compression is regarded as negligible. From slope-deflection equations it may be determined that the bending moments produced at each end of the member by this relative displacement are of equal magnitude. With both ends of the column restrained from rotation, these moments have the following value:

$$\text{F.E.M.} = \frac{6EI \Delta}{L^2}$$

$$\text{Since: Stiffness Factor} = \frac{I}{L} = K$$

$$\text{Then: F.E.M.} = \frac{6EK \Delta}{L}$$

One convenient procedure is to assign some values for the fixed end moments due to horizontal displacement. These moments must bear the proper relationship to each other as dictated by the variables "K" and "L" in the formula. It is then possible to allow rotation of the joints by performing a standard moment distribution; and then from the moments thus obtained calculate the actual sway force necessary to develop them in the particular members under study. The last step is a simple proportion:

$$\frac{\text{True Moments for Actual Sway Force}}{\text{Distributed Moments for Arbitrary Force}} = \frac{\text{Actual Lateral Force}}{\text{Arbitrary Sway Force}}$$

A method for approximating the true moments when assigning initial arbitrary fixed end moments to the bend is to assume a specific joint translation

" $\Delta$ " of some fraction of an inch and then calculate the corresponding column fixed end moments directly. The disadvantage to this direct approach is the probable ignorance of the designer of the real amount of lateral deformation of the frame.

Still another method for estimating the final true moments is to assume inflection points at the midpoints of the columns and distribute the unbalanced

horizontal shear force among the columns in proportion to the  $\frac{I}{L^3}$  or  $\frac{K}{L^2}$  values for each column.

$$\text{Sway Force} = 142 \text{ pounds}$$

$$\text{For left-hand column: } \frac{K_1}{L^2} = \frac{6.66}{100} = 0.067$$

$$\text{For right-hand column: } \frac{K_3}{L^2} = \frac{4.44}{225} = 0.020$$

$$H_A = 142 \left( \frac{.067}{.067 + .020} \right) = 109 \text{ lbs.} \quad (4)$$

$$H_D = 142 \left( \frac{.020}{.067 + .020} \right) = 33 \text{ lbs.}$$

$$\text{Hence: } M_{AB} = M_{BA} = H_A \left( \frac{h}{2} \right) = 109 \left( \frac{10}{2} \right) = 545 \text{ ft.}\#$$

Hence, for the purposes of this problem, we shall arbitrarily select a fixed end moment in column AB of  $\pm 550$  foot pounds representing the strains induced by the relative displacement of the joints.

Since  $E$ ,  $\Delta$  and  $\delta$  are all constants:

$$\frac{M_{DC}}{M_{AB}} = \frac{\left( \frac{K}{L} \right)_{DC}}{\left( \frac{K}{L} \right)_{AB}} \quad \text{or} \quad M_{DC} = \frac{\frac{4.44}{15}}{\frac{6.66}{10}} (550) = 244 \text{ foot lbs.} \quad (5)$$

Actually, it is not important that the initial arbitrary end moments be anywhere near the final true values, except that a close approximation makes the ultimate correction factor approach one and reduces slide rule errors. Using these fixed end moments in the columns due to an unknown hypothetical wind or sway force, we then may perform the standard distribution shown in Figure 4.

The horizontal shears at the bases of the columns in the rigid frame shown in Figure 4 may be determined by writing the equation of static equilibrium for all rotating moments on a column member. Thus:

Equation of moments on column "AB" about joint "B":

$$H_A h_1 - M_{AB} - M_{BA} = 0 \quad \text{or} \quad H_A = \frac{205.1 + 349.1}{10.0} \quad (6)$$

$$H_A = +55.4 \text{ pounds}$$

Equation of moments on column "CD" about joint "C":

$$H_D h_2 - M_{DC} - M_{CD} = 0 \quad \text{or} \quad H_D = \frac{152.3 + 200.6}{15} \quad (6A)$$

$$H_D = +23.6 \text{ pounds}$$

$$\text{Arbitrary Sway Force} = H_A + H_D = -79.0 \text{ lbs.}$$

$$\text{Correction Factor} = X = \frac{142}{79} = 1.80$$

$$\text{True } M_{AB} = X M'_{AB} = 1.8 (-349.1) = -628.0 \text{ ft. lbs.}$$

$$\text{True } M_{BA} = M_{BC} = 1.8 (+205.1) = +369.0 \text{ ft. lbs.}$$

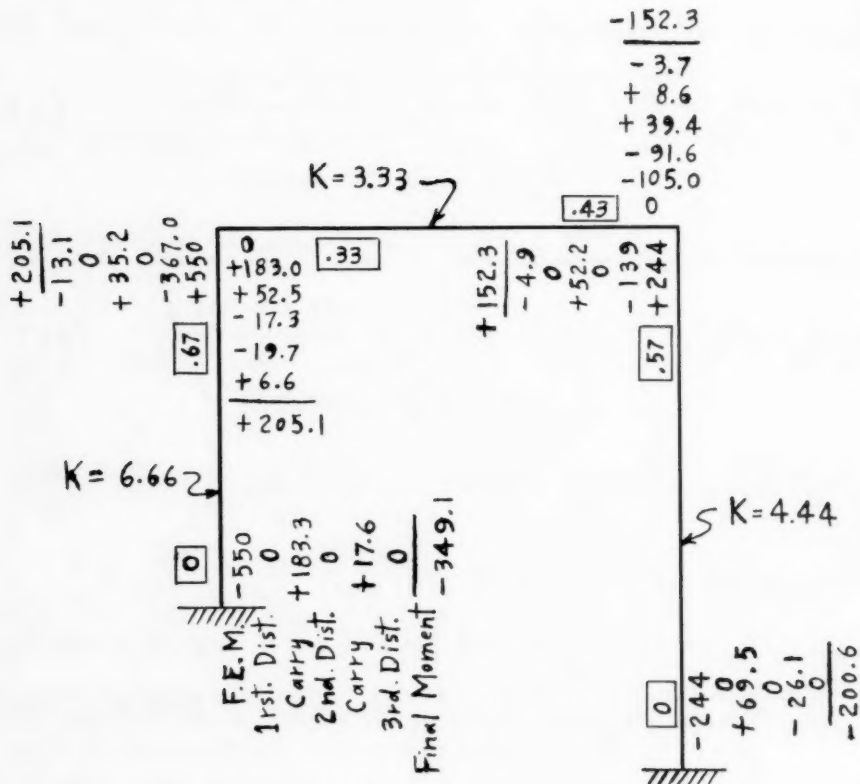
$$\text{True } M_{DC} = X M'_{DC} = 1.8 (-200.6) = -361.0 \text{ ft. lbs.}$$

$$\text{True } M_{CB} = M_{CD} = 1.8 (\pm 152.3) = \pm 274.0 \text{ ft. lbs.}$$

These are the true bending moments which would be produced in the given frame by a horizontal sway force of 142 pounds. See Figure 5.

**.33**

indicates the distribution factor for one side of a joint.



All bending moments shown in foot pounds

FIGURE 4

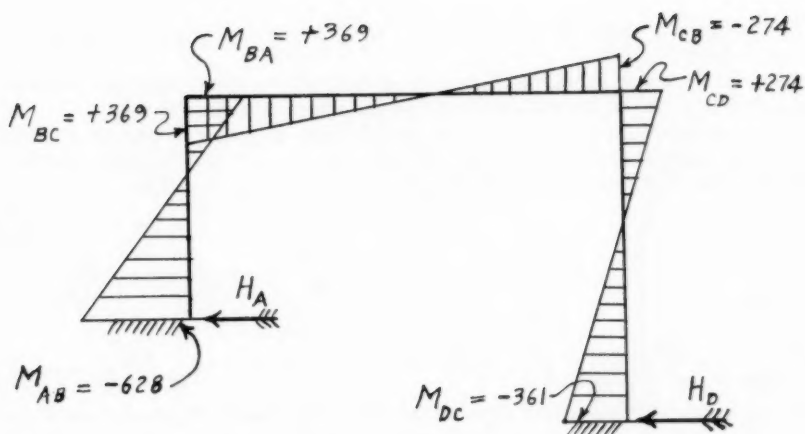


FIGURE 5

Moment equation of lefthand column about the joint "B":

(7)

$$H_A h_1 - M_{AB} - M_{BA} = 0 \quad \text{or} \quad H_A = \frac{628 + 369}{10} = +99.7 \text{ pounds}$$

Moment equation for the righthand column about the joint "C":

(7A)

$$H_D h_2 - M_{DC} - M_{CD} = 0 \quad \text{or} \quad H_D = \frac{274 + 360}{15} = +42.3 \text{ pounds}$$

$$H_A + H_D = 99.7 + 42.3 = 142 = \text{Sway Force}$$

The accuracy of these final sway or side lurch moments may be checked by computing the horizontal shear forces at the column bases.

The complete solution to the original problem may now be obtained merely by adding algebraically the above sidesway moments to the moments due to the vertical load found in the first distribution process on figure 3.

(8)

$$M_{AB} = +1041 - 628 = +413 \text{ foot pounds}$$

$$M_{BA} = -2098 + 369 = -1729 = M_{BC}$$

The moments resulting from this combination represent the actual bending or deformation of the rigid frame bent under an unsymmetrical arrangement of members subjected to a vertical load only. See Figure 6 for the final bending moment diagram.

$$M_{CB} = -1723 - 274 = -1997 \text{ foot pounds}$$

$$M_{CD} = +1723 + 274 = +1997$$

$$M_{DC} = -858 - 361 = -1219 \text{ foot pounds}$$

Moment equation for column "AB" about the joint "B":

(9)

$$H_A h_1 + M_{AB} + M_{BA} = 0 \quad \text{or} \quad H_A = \frac{-413 - 1729}{10} = -215 \text{ lbs.}$$

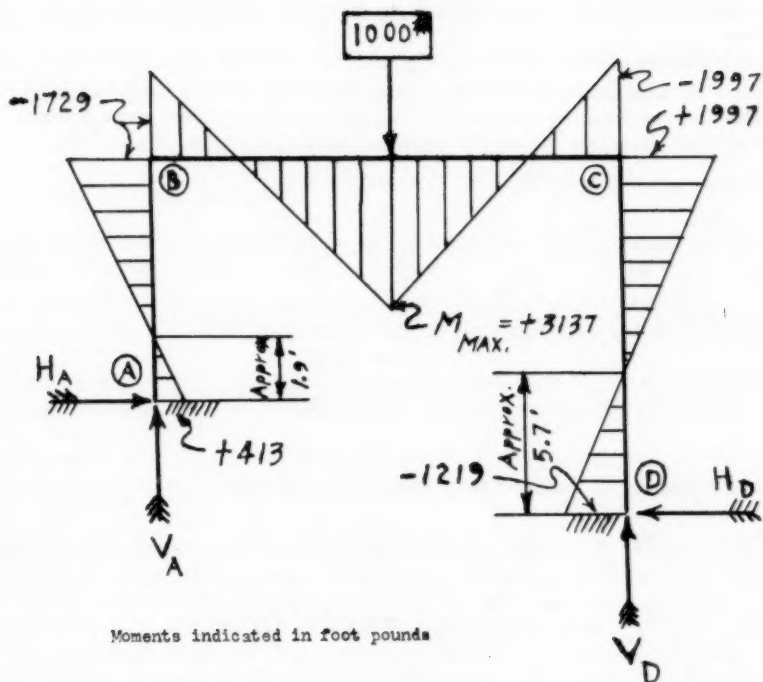


FIGURE 6

Moment equation for the column "CD" about the joint "C" :

$$H_D h_2 + M_{DC} + M_{CD} = 0 \quad \text{or} \quad H_D = \frac{+1219 + 1997}{15} = +215 \text{ lbs.}$$

The fact that the horizontal shears at the bases of the columns cancel out is compatible with the initial conditions in the problem of no lateral loads on the bent.

The vertical column reactions,  $V_A$  and  $V_D$ , may be determined from the external vertical loads and girder end moments by writing an equation of equilibrium for rotating moments in the horizontal member about a joint. Assume that moments causing clockwise rotation are always positive.

Moment equation for girder "BC" about the joint "C" :

$$V_A L - M_{BC} + M_{CB} - P\left(\frac{L}{2}\right) = 0 \quad (10)$$

$$\text{or } 20.0 V_A = 1729 - 1997 + 10,000$$

$$V_A = \frac{+9,743}{20.0} = +487.1 \text{ pounds}$$

Moment equation for girder "BC" about the joint "B" :

$$-V_B L - M_{BC} + M_{CB} + P\left(\frac{L}{2}\right) = 0 \quad (10A)$$

$$\text{or } 20 V_B = -1729 + 1997 + 10,000$$

$$V_B = \frac{+10,257}{20.0} = +512.9 \text{ pounds}$$

$$V_A + V_B = 487.1 + 512.9 = 1000 = P$$

The fact that the sum of the vertical shears equals the original vertical load is a perfect check on the accuracy of the computations. The reliability of the figures for presenting a true picture of stresses in the rigid frame, however, is a function of the practicality of the assumed loading, the justification for the assumed column end conditions and full continuity at the joints and the correlation between the actual shape, size and modulus of elasticity of the various members with the assumed stiffnesses.

Now that the girder reactions are known, the maximum positive bending moment in the girder may be computed by writing the equation for rotating moments about the point of application of the external load at the midspan.



Equation of moments for the girder about its own midspan:

$$V_A \left( \frac{L}{2} \right) - M_{BC} = M_{\text{MIDSPAN}} \quad \text{or} \quad M_M = 487.1(10) - 1729 \quad (11)$$

$$\text{Positive Midspan Moment} = M_M = + 3,142 \text{ foot pounds}$$

### The Column Analogy Method

The same problem may be analyzed by the Hardy Cross method of column analogy. Typical references are:

Chapter III on "Geometry of Deflected Structures" in the textbook "Continuous Frames of Reinforced Concrete" by Hardy Cross and Newlin Morgan. Publishers are John Wiley and Sons.

Chapter 8 on "Arches and Closed Rings" in the book "Theory of Modern Structures" Volume II by Linton Grinter. Publishers are the MacMillan Company of New York.

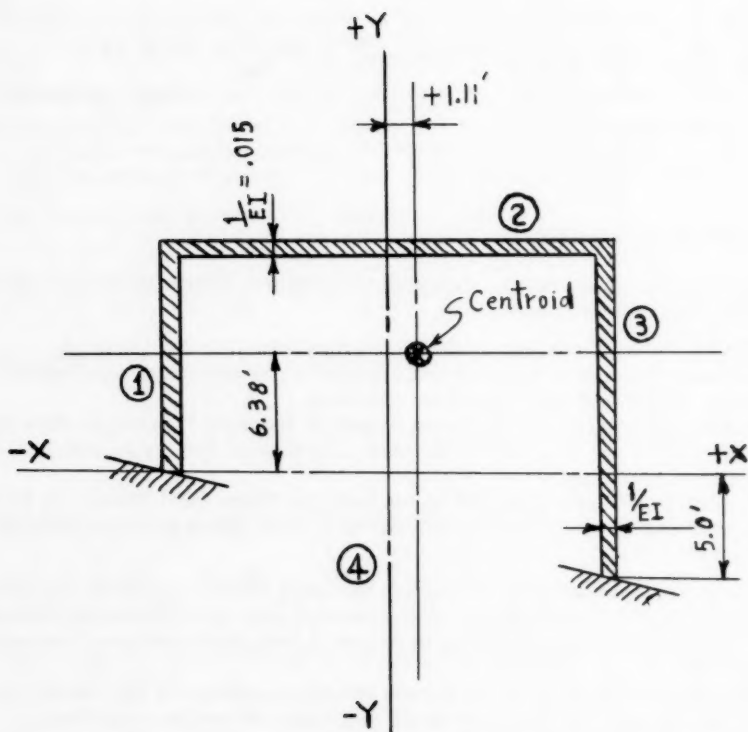
Chapter 8 on "Rigid Frames" in the textbook "Structural Theory by Hale Sutherland and H. L. Bowman as published by John Wiley and Sons, Inc. of New York.

All figures necessary for computing the area, center of gravity and moment of inertia of the analogous column section may be conveniently tabulated. The writer's preference is shown in Figure 8, but other arrangements can be constructed.

The items summed up in the second and third columns of the bottom chart represent the moment of inertia of the analogous column section about the arbitrarily assumed Cartesian axes. For the following calculations, which are similar to finding the extreme fiber stresses on a stubby column section eccentrically loaded, it is necessary to locate the centroid of the analogous column area and correct these moments of inertia to proper values referred to axes passing through this center of area.

$\bar{x}$  = Distance of the centroid of area of the analogous column section from the arbitrary Y axis in feet

$$\bar{X} = \frac{\sum ax}{\sum a} = \frac{+ 0.75}{0.675} = + 1.11 \text{ feet to right}$$



Note : For columns with fixed bases the width of member 4 =  $\frac{1}{\infty} = 0$

ANALOGOUS COLUMN SECTION

FIGURE 7

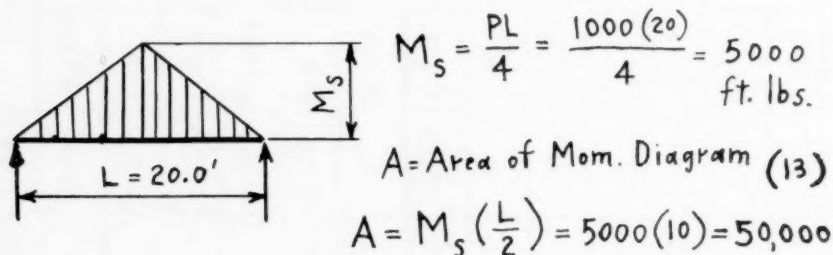
1	2	3	4	5	6	7	8	9	10	11	12
Member	$b = \frac{1}{EI}$	$L$	$a = \frac{L}{EI}$	$y$	$x$	$ax$	$ay$	$i_x$	$i_y$	$ax^2$	$ay^2$
1	0.015	10.0	0.150	+5.0	-10.0	-1.50	+0.75	1.25	Neglect	+15.0	+3.75
2	0.015	20.0	0.300	+10.0	0	0	+3.0	Neglect	10.0	0	+30.0
3	0.015	15.0	0.225	+2.5	+10.0	+2.25	+0.562	4.21	Neglect	+22.5	+1.41
4	0	21.0	0	-2.5	0	0	0	0	Neglect	0	0
Sum $\Sigma$	—	—	0.675	—	—	+0.75	+4.31	—	—	+37.5	+35.16
Member	$i_y + ax^2$	$i_x + ay^2$	$m_s$	$p = m_s a$	$x_i$	$y_i$	$m_x = p y_i$	$m_y = p x_i$			
1	+15.0	+5.0	0	0	-10.0	+5.0	0	0			
2	+10.0	+30.0	+2500	+750	0	+10.0	+7500	0			
3	+22.5	+5.62	0	0	+10.0	+2.5	0	0			
4	0	0	0	0	0	-2.5	0	0			
Sum $\Sigma$	47.5	40.62	—	$P = 750$	—	—	+7500	0			

FIGURE 8

$\bar{y}$  = Distance of the centroid of area of the analogous column section from the arbitrary X axis in feet (12)

$$\bar{y} = \frac{\sum ay}{\sum a} = \frac{+ 4.31}{0.675} = + 6.38 \text{ feet higher}$$

The statically determinate bending moments on each separate member of the bent which are used to evaluate the quantity  $m_s$  in the fourth tabulation column of the bottom chart on Figure 8 are derived from the assumption of pin connections or hinges at the joints of the horizontal girder with the vertical column supports. The first step is to compute the bending moment diagram for this synthetic simple beam.



The item  $m_s$  is regarded as the average bending moment spread out uniformly along the rigid frame member or a hypothetical uniform pressure applied to that portion of the analogous column section.

Since the girder and reactions in this bent are considered as concentric and axial loads on the columns, there are no secondary induced bending moments for these two members in this particular problem. In the case of the girder:

$$m_s = \frac{\text{Area}}{\text{Length}} = \frac{M_s L}{2L} = \frac{M_s}{2} = \frac{5000}{2} = 2500 \text{ foot lbs.} \quad (14)$$

The new coordinates  $x_1$  and  $y_1$  are the distances from the original arbitrary X and Y axes to the centroid of area of the statically determinate moment diagrams being applied as axially parallel column loads on each member area of the analogous stub column representing the actual rigid frame. Thus each pressure loading along a member area may be thought of as having a center of gravity coinciding with the centroid of the simple beam bending moment diagram being applied as a load. With this particular problem the centroid of the pressure loading on the analogous member area representing the girder of the bent lies at the midspan; but this circumstance is due only to the simplicity of the external loads on the frame given in the illustrative problem and is by no means usual.

Corrections to obtain the moments of these loads about the true centroid of area for the analogous column section are made later. This reduces the burden of mental arithmetic while filling in the tabulation charts and allows an almost mechanical process for effecting the final solution.

When using the Column Analogy Method there is one aspect which the designer must be cautious not to overlook. When no axis of symmetry for the actual rigid frame or analogous column section exists whatsoever, then the analysis becomes more complicated. This is very much like the situation where an unsymmetrical bent implies sideways in the solution by moment distribution. It is also perfectly consistent with the determination of extreme fiber stresses in a short column of unsymmetrical cross section subjected to an eccentrically applied axial load. The "Product of Inertia" term is introduced. Refer to any good textbook on strength of materials.

For a completely unsymmetrical column section:

$$f = \frac{P}{A} + \frac{M'_x}{I'_x} y_c + \frac{M'_y}{I'_y} x_c \quad \text{when:} \quad (15)$$

$$M'_x = \frac{M_x I_y - M_y I_{xy}}{I_y} = M_x - \left( \frac{I_{xy}}{I_y} \right) M_y$$

$$\text{and } M'_y = \frac{M_y I_x - M_x I_{xy}}{I_x} = M_y - \left( \frac{I_{xy}}{I_x} \right) M_x$$

$$I'_x = \frac{I_x I_y - I_{xy}^2}{I_y} = I_x - \frac{I_{xy}^2}{I_y} \quad \text{and}$$

$$I'_y = \frac{I_x I_y - I_{xy}^2}{I_x} = I_y - \frac{I_{xy}^2}{I_x}$$

Algebraic substitution in the Formula 15 is equivalent to locating and finding the properties of the column section about some neutral axis inclined to or rotated at an angle with the original assumed axes. The bending moments produced by an eccentrically applied load and the moments of inertia used in

the formulas are all assumed to be related to an axis passing through the actual centroid of area of the analogous column section. It therefore becomes necessary to apply corrections to the moment of inertia values obtained about the initial arbitrary axes and tabulated in Figure 8, since the originally assumed axes would most probably not coincide with the true centroidal axes.

$$\text{Since } I_x = I_o + A y_c^2 = \sum (I_x + a y^2) - A \bar{y}^2$$

$$I_x = 40.62 - 0.675 (6.38)^2 = 13.15 \quad (16)$$

$$\text{Likewise: } I_y = 47.5 - 0.675 (1.11)^2 = 46.67$$

$$M_x = \sum p y_i - P \bar{y} = 7500 - 750 (6.38) = +2720$$

$$M_y = \sum p x_i - P \bar{x} = 0 - 750 (1.11) = -833$$

$I_{xy}$  = Product of Inertia of the column about its centroidal axes

$$I_{xy} = \int_A^B xy \, dA = \sum \bar{I}_{xy} \text{ for components of frame}$$

$$I_{xy} = \sum (I_{xy_o} + a x_c y_c) \quad (17)$$

When a separate member area of a composite column section has at least one axis of symmetry parallel to an axis of the entire column section, then the product of inertia for that particular, individual member area about its own centroid is zero. This means that with a rectangular bent such as used in this problem, which has no sloped members or gabled roof, the product of inertia for the entire gross analogous column reduces to the following expression:

(17A)

$$\text{Hence } I_{yx} = \sum a x_c y_c = \sum a xy - A \bar{x} \bar{y}$$

See the tabulated values for the properties of the analogous column section in Figure 8 for making the appropriate substitutions. The crucial point in the Column Analogy method, for which all the intervening algebra is merely a preparation, is represented by Formula 19.

$$I_{xy} = [(-1.5)(+5.0)(1) + 0(+10) + (2.25)(+2.5)] - .675(1.11)(6.38)$$

$$I_{xy} = (-7.5 + 0 + 5.625) - 4.78 = -6.655$$

By substitution of those values obtained above:

$$M'_x = M_x - \left( \frac{I_{xy}}{I_y} \right) M_y = +2720 - \left( \frac{-6.65}{+46.7} \right) (-833)$$

$$M'_x = +2720 - 118.8 = +2601$$

$$M'_y = M_y - \left( \frac{I_{xy}}{I_x} \right) M_x = -833 - \left( \frac{-6.65}{+13.15} \right) (+2720)$$

$$M'_y = -833 + 1325 = +492$$

$$I'_x = I_x - \frac{I_{xy}^2}{I_y} = 13.15 - \frac{(-6.65)^2}{46.7} = +12.20 \quad (18)$$

$$I'_y = I_y - \frac{I_{xy}^2}{I_x} = 46.67 - \frac{(-6.65)^2}{13.15} = +43.30$$

$m_i$  = Indeterminate moments of continuity in the frame.

$$m_i = \frac{P}{A} + \frac{M'_x}{I'_x} y_c + \frac{M'_y}{I'_y} x_c \quad (19)$$

$y_c$  = Vertical distance from centroid to point on frame.

$x_c$  = Horizontal distance from centroid to point on frame.

$$m_i = \frac{750}{0.675} + \frac{2601}{12.2} y_c + \frac{492}{43.3} x_c$$

$$m_i = 1111 + 214 y_c + 11.37 x_c$$

$m_p$  = Final true rigid frame moment at any desired point.

$m_p$  = Simple moment - Indeterminate moment =  $M_s - m_i$

$H$  = Horizontal shear at the base of a column.

$H = h_s - h_i$  when  $h_i$  = indeterminate expression below:

$$h_i = \frac{M'_x}{I_x}$$

$$\text{Substituting: } H = 0 - \frac{2601}{12.2} = -214 \text{ pounds}$$

#### The Classical Slope Deflection Method

Some typical references are:

"Analysis of Rigid Frames" by A. Amirikian, as published by the United States Government Printing Office.

"Theory of Modern Steel Structures," Volume II, on Statically Indeterminate Structures by Linton E. Grinter, as published by the MacMillan Company of New York.

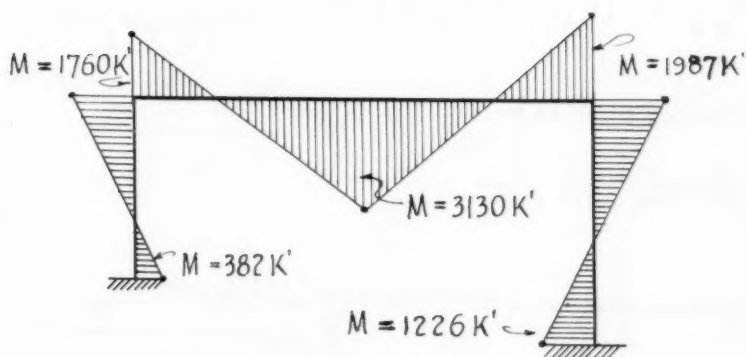
"Analysis of Statically Indeterminate Structures" by Clifford D. Williams, as published by the International Textbook Company of Scranton, Penna.

The illustrative problem remains the same as that described on page 2. All dimensions for member lengths are assumed to be from the intersection points of the neutral axes of the members.

(1) Clockwise angular change is positive. The sign of a deflection angle is determined from the direction of rotation of the tangent to the elastic curve. If rotation with respect to the unstrained position of the member is clockwise, the sign of the angle is considered positive (+); and if the rotation is counter-clockwise, the sign is negative (-).



FACTOR	VARIOUS POINTS ON RIGID FRAME				
$X_c$	- 11.11	- 11.11	- 11.11	+ 8.89	+ 8.89
$y_c$	- 6.38	+ 3.62	+ 3.62	+ 3.62	- 11.38
$M_s$	0	0	5000	0	0
$m_i$	- 382	+ 1760	+ 1870	+ 1987	- 1226
$m_p$	+ 382	- 1760	+ 3130	- 1987	+ 1226



MOMENT DIAGRAM

FIGURE 9

(2) The displacement or deflection of a point on the elastic curve is considered to be positive (+) if the line joining the two points is rotated in a clockwise direction with respect to the original position of the beam before loading. For any columns or cantilevers, if a line drawn from the two ends of the member has rotated in a clockwise direction from the initial unstrained position, the displacement is positive (+).

(3) A bending moment impressed upon a member from the outside or from a system of external loads which causes the neutral axis of the member to rotate clockwise about the point under consideration is called positive (+). From another aspect, if the resisting moment created by the couple of tension and compression in the extreme fibers of the beam militate to cause the external support to rotate in a clockwise direction when the joint is unlocked or unrestrained, that bending moment is positive (+).

This is an unorthodox sign convention which is quite susceptible to erroneous confusion. It is possible at the support of a continuous beam or overhang for a bending moment to be either negative or positive, depending upon whether the left or right side of the support is being studied.

Refer to the elastic deformation picture of the loaded bent in Figure 10. By the requirements of static equilibrium and the summation of all rotating moments about joint "B":

$$M_{AB} + M_{BA} - H_A h_1 = 0 \quad \text{transposing terms:}$$

$$\text{Horizontal shear at "A"} = H_A = \frac{M_{AB} + M_{BA}}{h_1}$$

By the same logic :

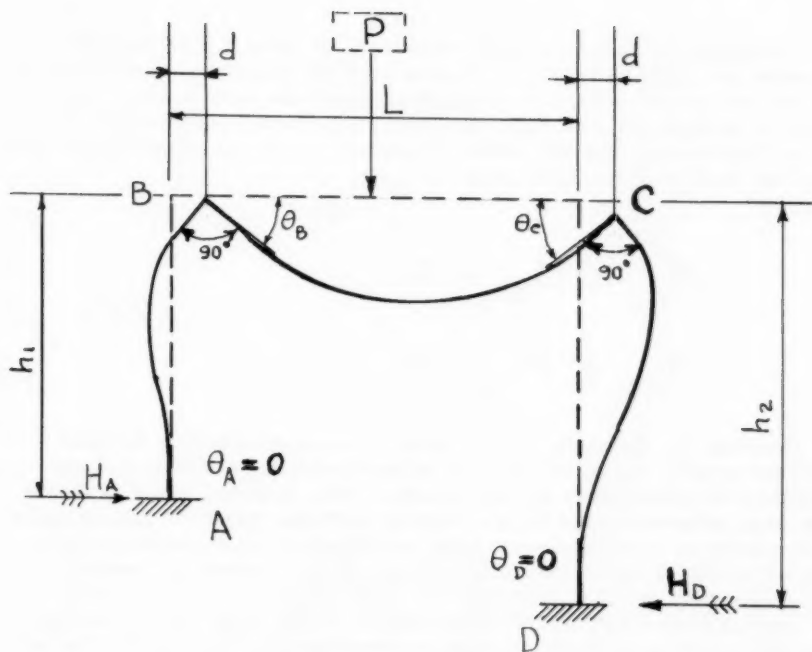
$$\text{Horizontal shear at "D"} = H_D = \frac{M_{DC} + M_{CD}}{h_2}$$

(20)

For static equilibrium the sum of all the horizontal forces on the bent must equal zero; and, since there is no external horizontal thrust on this frame:

$$H_A + H_D = 0$$

Substituting terms :



ELASTIC CURVE OF DEFLECTION

FIGURE 10

$$\frac{M_{AB} + M_{BA}}{h_1} + \frac{M_{DC} + M_{CD}}{h_2} = 0 \quad (21)$$

Continuing to consider simple statics only, we know that for the bent to possess the requisite rigidity to remain erect the angle between the slope of the girder and the slope of a column at a corner joint must remain, theoretically at least, 90 degrees or a right angle. This means that the algebraic sum of the bending moments about any corner joint on the frame of a rectangular bent must be zero. Therefore:

$$\begin{aligned} M_{BA} + M_{BC} &= 0 \\ M_{CD} + M_{CB} &= 0 \end{aligned} \quad (22)$$

Pursuing this application of the rules for static equilibrium, we could proceed to write two more equations by expressing the summation of moments in the girder about its end supports. This, however, would introduce two more unknowns in the form of vertical reactions under the column bases. It is necessary to introduce now some mathematical relationships between the end moments and the modulus of elasticity and relative stiffnesses of all the frame members in order to achieve a solution.

Consider one of the columns of the bent as having fixed ends at both top and bottom; but allow the top to displace horizontally with respect to the bottom support a small distance "d". This will produce two equal and opposite end moments at the faces of the supports. See Figure 11 for the diagram.

Now unlock the end joints and allow the two supports to rotate slightly through angular changes which are not necessarily identical. This will change the values of the end moments in the column member, as illustrated in Figure 12.

From the principles of the Moment-Area or Conjugate Beam methods for computing slopes or deflections in an elastic member, as expounded in any good textbook on Strength of Materials, we may write two algebraic equations.

The difference between the slopes at each end of the member is equal to the area of the  $\frac{M}{EI}$  diagram between the tangent points at the supports.

$$\left(\frac{1}{2}\right)\left(\frac{M_{AB}}{EI}\right)L + \left(\frac{1}{2}\right)\left(\frac{M_{BA}}{EI}\right)L = \theta_B - \theta_A$$

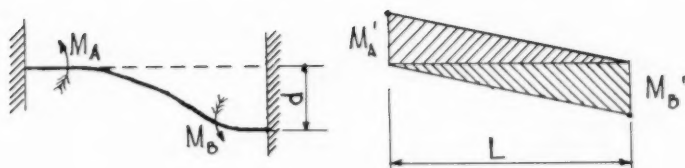


FIGURE 11

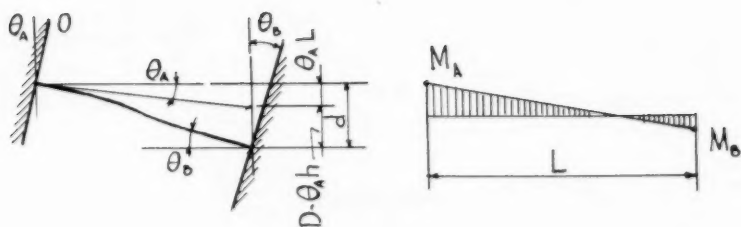


FIGURE 12

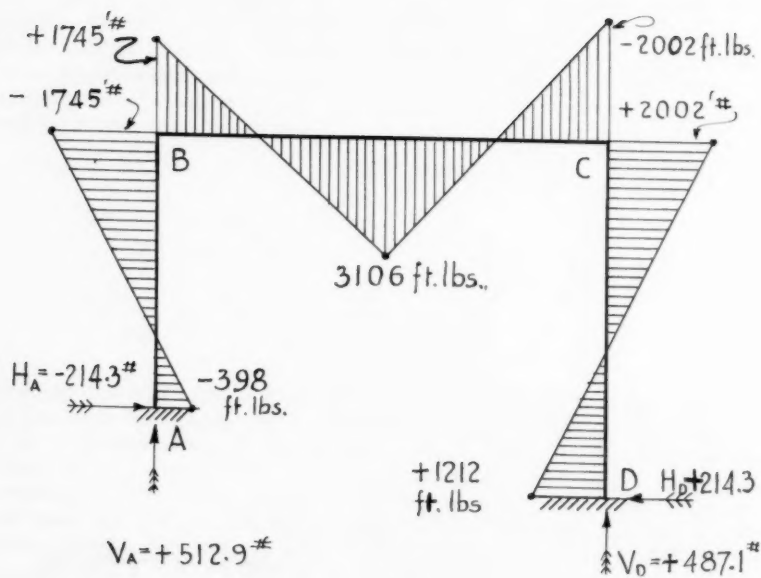


FIGURE 13

The elastic deflection of the support "B" from a line tangent to the strained beam's elastic curve at support "A" is equal to the total moment of the  $\frac{M}{EI}$  areas between points "A" and "B" about point "B".

(23)

$$\frac{M_{AB}}{EI} \left( \frac{L}{2} \right) \left( \frac{2L}{3} \right) + \frac{M_{BA}}{EI} \left( \frac{L}{2} \right) \left( \frac{L}{3} \right) = d - \theta_A L$$

Solve the above two simultaneous algebraic equations for  $M_{AB}$  by eliminating the unknown  $M_{BA}$ . Transposing terms in the equations:

$$2M_{AB}L^2 + M_{BA}L^2 = 6EI(d - \theta_A L)$$

$$\text{and also: } M_{AB}L + M_{BA}L = 2EI(\theta_B - \theta_A)$$

Solving the simultaneous equations:

$$2M_{AB} + M_{BA} = \frac{6EI d}{L^2} - \frac{6EI \theta_A}{L}$$

$$M_{AB} + M_{BA} = \frac{-2EI \theta_A}{L} + \frac{2EI \theta_B}{L}$$

Subtracting:

$$M_{AB} = \frac{6EI d}{L^2} - \frac{4EI \theta_A}{L} + \frac{2EI \theta_B}{L}$$

Factoring:

$$M_{AB} = -\frac{2EI}{L} \left( 2\theta_A + \theta_B - \frac{3d}{L} \right)$$

BY SIMILAR ALGEBRA IT MAY BE PROVEN THAT:

(24)

$$M_{BA} = -\frac{2EI}{L} \left( 2\theta_B + \theta_A - \frac{3d}{L} \right)$$

When the column or member has some kind of external force or loading applied to it between the end supports, the appropriate fixed end moment for the particular load condition is added to the above expressions. We now have the means to write six basic equations about the frame columns alone.

$$\text{Given: } \theta_A = 0 \quad \text{and} \quad \theta_D = 0$$

$$[\text{I}] \quad M_{AB} = \frac{-2EI_1}{h_1} \left( 2\theta_A + \theta_B - \frac{3d}{h_1} \right)$$

$$\text{When } h_1 = 10.0 \text{ feet}$$

$$[\text{II}] \quad M_{BA} = \frac{-2EI_1}{h_1} \left( 2\theta_B + \theta_A - \frac{3d}{h_1} \right)$$

$$[\text{III}] \quad M_{CD} = \frac{-2EI_3}{h_2} \left( 2\theta_C + \theta_D - \frac{3d}{h_2} \right)$$

$$\text{When } h_2 = 15.0 \text{ feet}$$

$$I_1 = I_3 = 66.6 \text{ inches}^4$$

$$[\text{IV}] \quad M_{DC} = \frac{-2EI_3}{h_2} \left( 2\theta_D + \theta_C - \frac{3d}{h_2} \right)$$



$$[\text{V}] \quad M_{BA} + M_{BC} = 0 \quad \text{and} \quad M_{CD} + M_{CB} = 0$$

$$[\text{VI}] \quad \frac{M_{AB} + M_{BA}}{h_1} + \frac{M_{DC} + M_{CD}}{h_2} = 0$$

It may be noted here that the moment of inertia and modulus of elasticity for all the members in the frame remain identical in all the equations for the end moments (an intentional simplification of the sample problem). Substituting numerical values for the actual dimensions of the members or lengths:

(25)

$$[\text{I}] \quad M_{AB} = \frac{-2EI}{10} \left( \theta_B - \frac{3d}{10} \right) = \frac{(3d - 10\theta_B)EI}{50}$$

$$[\text{II}] \quad M_{BA} = \frac{-2EI}{10} \left( 2\theta_B - \frac{3d}{10} \right) = \frac{(3d - 20\theta_B)EI}{50}$$

$$[\text{III}] \quad M_{CD} = \frac{-2EI}{15} \left( 2\theta_C - \frac{3d}{15} \right) = \frac{(2d - 20\theta_C)EI}{75}$$

$$[\text{IV}] \quad M_{DC} = \frac{-2EI}{15} \left( \theta_C - \frac{3d}{15} \right) = \frac{(2d - 10\theta_C)EI}{75}$$

By now it is apparent that expressions for end moments contain a minimum of three unknowns in each equation and that a mathematical expression for some new facts must be introduced in the form of additional equations before a solution may be effected. It now becomes necessary to write the slope-deflection equations for the bending moments in the extreme ends of the horizontal girder, taking into proper consideration the effects of the 1000-pound concentrated load in the center of the beam.

$$M_{Bc} = (\text{F.E.M.})_B - \frac{2E_2I_2}{L} \left( 2\theta_B + \theta_c - \frac{3d}{L} \right)$$

$$\text{Since } (\text{F.E.M.})_B = \frac{PL}{8} = + \frac{1000(20)}{8} = +2500 \text{ ft. lbs.}$$

Algebraic signs here become extremely important.

Substituting:  $d=0$  and  $E_2I_2 = EI$

$$M_{Bc} = +2500 - \frac{2EI}{20} (2\theta_B + \theta_c - 0) \quad (26)$$

$$[\text{VII}] \quad M_{Bc} = \frac{+25,000 - (2\theta_B + \theta_c)EI}{10}$$

Likewise:

$$M_{cB} = (\text{F.E.M.})_c - \frac{2E_2I_2}{L} \left( 2\theta_c + \theta_B - \frac{3d}{L} \right)$$

$$M_{cB} = -2500 - \frac{2EI}{20} (2\theta_c + \theta_B)$$

$$[\text{VIII}] \quad M_{cB} = \frac{-25,000 - (2\theta_c + \theta_B)EI}{10}$$

By equation V:

$$M_{BA} = -M_{Bc} \text{ or } \frac{(3d - 20\theta_B)EI}{50} = \frac{-25,000 + (2\theta_B + \theta_c)EI}{10}$$

$$\text{thus: } (3d - 20\theta_B)EI = -125,000 + 5(2\theta_B + \theta_C)EI$$

$$(3d - 30\theta_B - 5\theta_C)EI = -125,000 \quad (a)$$

$$\text{Also by equation V: } -M_{CB} = +M_{CD}$$

$$\frac{+25,000 + (2\theta_C + \theta_B)EI}{10} = \frac{(2d - 20\theta_C)EI}{75}$$

$$+1,875,000 + (150\theta_C + 75\theta_B)EI = (20d - 200\theta_C)EI$$

$$\text{or } 20d - 350\theta_C - 75\theta_B = \frac{+1,875,000}{EI}$$

$$4d - 70\theta_C - 15\theta_B = \frac{+375,000}{EI} \quad (b)$$

By equation VI :

$$\frac{M_{AB} + M_{BA}}{10} + \frac{M_{CD} + M_{DC}}{15} = 0$$

Clearing fractions with a common denominator of 30:

$$3M_{AB} + 3M_{BA} + 2M_{CD} + 2M_{DC} = 0$$

Substituting equations I through IV:

$$3EI\left(\frac{3d - 10\theta_B}{50}\right) + 3EI\left(\frac{3d - 20\theta_B}{50}\right)$$

$$+ 2EI \left( \frac{2d - 20\theta_c}{75} \right) + 2EI \left( \frac{2d - 10\theta_c}{75} \right) = 0$$

Simplifying by using a common denominator of 150:

$$27d - 90\theta_B + 27d - 180\theta_B + 8d - 80\theta_c + 8d - 40\theta_c = 0$$

$$\text{Hence: } 70d - 270\theta_B - 120\theta_c = 0$$

Dividing through by 10:

$$7d - 27\theta_B - 12\theta_c = 0 \left( \frac{1}{EI} \right) = 0 \quad (C)$$

WE FINALLY HAVE OBTAINED THREE SIMPLE EQUATIONS CONTAINING ONLY THREE UNKNOWN:  $\theta_B$ ,  $\theta_c$  and  $d$

Grouping equations (a) and (b) and eliminating "d":

$$\begin{aligned} 12d - 120\theta_B - 20\theta_c &= -500,000 \left( \frac{1}{EI} \right) \\ - [12d - 45\theta_B - 210\theta_c &= +1,125,000 \left( \frac{1}{EI} \right)] \end{aligned}$$

$$\text{Subtracting: } -75\theta_B + 190\theta_c = -1,625,000 \left( \frac{1}{EI} \right)$$

$$\text{or } -15\theta_B + 38\theta_c = -325,000 \left( \frac{1}{EI} \right)$$

Grouping equations (a) and (C) and eliminating "d":

$$\begin{aligned} 21d - 210\theta_B - 35\theta_c &= -875,000 \left( \frac{1}{EI} \right) \\ - [21d - 81\theta_B - 36\theta_c &= 0] \end{aligned}$$

subtracting:

$$-129 \theta_B + \theta_C = -875,000 \left( \frac{1}{EI} \right)$$

$$0 + 129 \theta_B - \theta_C = +875,000 \left( \frac{1}{EI} \right)$$

Multiply the last equation by 38 throughout:

$$4902 \theta_B - 38 \theta_C = +33,250,000 \left( \frac{1}{EI} \right)$$

By a routine solution of simultaneous equations:

$$-15 \theta_B + 38 \theta_C = -325,000 \left( \frac{1}{EI} \right)$$

Adding:

$$+4902 \theta_B - 38 \theta_C = +33,250,000 \left( \frac{1}{EI} \right)$$

---


$$-4887 \theta_B = +32,925,000 \left( \frac{1}{EI} \right)$$

Therefore:  $\theta_B = + \frac{6,737}{EI}$  (27)

Since  $\theta_C = \frac{-875,000}{EI} + 129 \theta_B$

$$\theta_C = \frac{-875,000}{EI} + \frac{129(6737)}{EI} = \frac{+869,073 - 875,000}{EI}$$

Therefore:  $\theta_C = - \frac{5927}{EI}$  (28)

Since:  $d = \frac{27\theta_B + 12\theta_C}{7}$  by equation (C)

$$\text{then: } d = \frac{27 \left( \frac{6737}{EI} \right) + 12 \left( \frac{-5927}{EI} \right)}{7}$$

$$d = \frac{+181,899 - 71,124}{7EI} = \frac{+15,825}{EI}$$

Check the solution by substituting in equation (a).

$$(3d - 30\theta_B - 5\theta_C)EI = -125,000$$

$$3(+15,825) - 30(+6737) - 5(-5927) = -125,000$$

$$+47,475 - 202,110 + 29,635 = -125,000$$

$$-125,000 = -125,000 \quad \boxed{\text{CHECKS}}$$

The substitution of these values for  $d$ ,  $\theta_B$  and  $\theta_C$  in the original slope-deflection expressions for the bending moments should yield the final results.

$$M_{AB} = \frac{(3d - 10\theta_B)EI}{50} = \frac{\left[ 3 \left( \frac{15,825}{EI} \right) - 10 \left( \frac{6737}{EI} \right) \right] EI}{50}$$

$$M_{AB} = \frac{+47,475 - 67,370}{50} = -398 \text{ foot lbs.}$$

$$M_{CD} = \frac{(2d - 20\theta_C)EI}{75} = \frac{\left[ 2 \left( \frac{15,825}{EI} \right) - 20 \left( \frac{-5,927}{EI} \right) \right] EI}{75}$$

$$M_{CD} = \frac{+31,650 + 118,540}{75} = +2002 \text{ foot lbs.}$$

$$M_{BA} = \frac{(3d - 20\theta_B)EI}{50} = \frac{\left[3\left(\frac{+15,825}{EI}\right) - 20\left(\frac{+6,737}{EI}\right)\right]EI}{50}$$

$$M_{BA} = \frac{+47,475 - 134,740}{50} = -1745.3 \text{ ft. lbs.}$$

$$M_{DC} = \frac{(2d - 10\theta_C)EI}{75} = \frac{\left[2\left(\frac{+15,825}{EI}\right) - 10\left(\frac{-5,927}{EI}\right)\right]EI}{75}$$

$$M_{DC} = \frac{+31,650 + 59,270}{75} = +1212.3 \text{ ft. lbs.}$$

Checking the horizontal shears at the column bases:

$$10(H_A) = M_{AB} + M_{BA} = -398 - 1745$$

$$\therefore H_A = -214.3 \text{ lbs.}$$

$$15(H_D) = M_{CD} + M_{DC} = +2002 + 1212$$

$$\therefore H_D = +214.3 \text{ lbs.}$$

Since no lateral sidesway forces were imposed upon the bent, the horizontal shears should be equal and opposite in direction, as the above computations indicate.

The results may be further checked by:

$$M_{BC} = \frac{+25,000 - (2\theta_B + \theta_C)EI}{10}$$

$$M_{BC} = \frac{+25,000 - \left[2\left(\frac{+6737}{EI}\right) + \left(\frac{-5927}{EI}\right)\right]EI}{10}$$

$$M_{BC} = \frac{+17,453}{10} = +1745.3 = -M_{BA}$$

$$\text{Likewise: } M_{CB} = -M_{CD} = -(+2002) = -2002 \text{ ft. lbs.}$$

$$20V_A + M_{BC} = 10P + M_{CB}$$

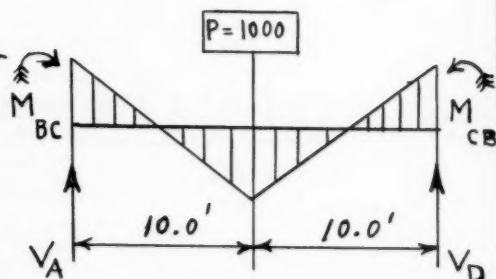
$$V_A = \frac{10(1000) + 2002 - 1745}{20}$$

$$V_A = +512.9 \text{ pounds}$$

$$20V_D + M_{CB} = 10P + M_{BC} \quad \text{or} \quad V_D = \frac{10(1000) + 1745 - 2002}{20}$$

$$V_D = +487.1 \text{ pounds}$$

$$V_A + V_D = 512.9 + 487.1 = 1000 \text{ lbs.} = P \quad \text{CHECKS}$$



The vertical reactions of the girder on the two individual columns may be found by the usual equations for static equilibrium of all rotating moments.

Compare the final bending moment diagram shown in Figure 13 with the results by the other two methods of solution. (Figures 6 and 9).

Anyone who has attempted a similar problem by the slope deflection method, if he is subject to ordinary human fallibility, knows that one small error in the arithmetic or algebraic signs will hopelessly spoil the end solution. Moreover, these oversights will probably escape detection until the last stage of checking horizontal or vertical shears is reached. This is the chief and most serious criticism of the method - the other objection being that with more complicated or gabled bents there may be a large number of simultaneous equations to solve.



---

Journal of the  
STRUCTURAL DIVISION  
Proceedings of the American Society of Civil Engineers

---

GRIT AND SHOT-REINFORCED HIGH TENSILE BOLTED JOINTS

R. L. Sanks,<sup>1</sup> M. ASCE and C. C. Rampton, Jr.,<sup>2</sup> J.M. ASCE  
(Proc. Paper 1435)

---

ABSTRACT

Paint in high tensile bolted joints drastically reduces frictional resistance to slip. Grit and shot placed between painted contact surfaces increases frictional resistance. Shot-reinforced painted joints are, in static tests, equal to or somewhat better than clean mill-scale joints and much superior to riveted joints.

---

SYNOPSIS

This report summarizes procedures and results of exploratory tests designed to determine the effectiveness of reinforcement in increasing the frictional resistance of painted structural steel joints. The reinforcement consisted of particles of angular white cast iron grit, rounded white cast iron shot, and polished steel balls. The particles were held in place by adherence to wet red lead paint or by spot welding to thin steel washers. Each joint consisted of three structural steel plates held by a single 5/8-inch or 7/8-inch high tensile bolt acting in double shear.

Controls for evaluating reinforced joints were provided by identical tests performed on unreinforced joints with painted and with clean mill-scale surfaces. A few tests were made of joints fastened with 7/8-inch rivets for comparison.

Although the ultimate strength is probably unaffected, the frictional resistance of joints with mill-scale surfaces is drastically reduced by paint but

Note: Discussion open until April 1, 1958. Paper 1435 is part of the copyrighted Journal of the Structural Division of the American Society of Civil Engineers, Vol. 83, No. ST 6, November, 1957.

1. Associate Prof. of Civ. Eng., Univ. of Utah, Salt Lake City, Utah.
2. Special Detailer in Design Engineering Dept., Columbia-Geneva Steel Division, U. S. Steel Corp., Geneva, Utah.

can be restored by reinforcement. Reinforced, painted joints are superior to mill-scale joints fastened with 5/8-inch bolts. Reinforced, painted joints are superior in some respects and inferior in others to mill-scale joints fastened with 7/8-inch bolts. Reinforced, bolted joints are considerably superior to unreinforced, riveted joints with mill-scale surfaces. The best reinforcement appears to be polished balls somewhat less than 1/16-inches in diameter. Rounded shot is nearly as effective as polished balls, and far superior to angular grit.

## INTRODUCTION

Specifications<sup>(1)</sup> for the assembly of high tensile bolted joints state: "Contact surfaces of joints subject to stress reversal, impact or vibration, or where stress redistribution due to joint slippage would be undesirable, shall be free of paint or lacquer." After the research program herein described was begun, the Research Council published an appendix<sup>(2)</sup> to the specifications stating that even when slip occurs, the ultimate shear and bearing capacity of high tensile bolts is greater than that of rivets. Therefore, the prohibition against paint is intended to apply only to joints where complete stress reversal occurs, where dynamic loads might cause stress concentration, and to some joints in rigid frames. Otherwise, the painting of most joints in building frames is sanctioned. Bridge engineers, following more conservative practice, may prefer to specify no shop paint in many bridge joints.

To leave contact surfaces of joints free of paint requires layout and marking the outlines of the joint, adds to the labor, and may add considerably to the cost.<sup>(3)</sup> But if particles of a sufficiently hard and strong substance could be applied to the shearing plane of a painted joint, the high tensile force of the bolt would force the particles into the steel, thereby increasing the friction in the joint. If such reinforced joints could be made as slip-resistant as unreinforced joints of clean mill scale, the steel could be painted all over, thereby saving labor and expense in layout. If reinforced joints could be made superior to unreinforced joints, there would be an added advantage of greater safety or a saving in the number of bolts.

### Purpose

The purpose of this research was to explore the possibilities of the effectiveness of grit or shot in increasing the slip resistance of painted joints and to find the optimum particle size and distribution for several sizes of bolts.

### Scope

The program was intended to be exploratory only; so the budget was limited. No repeated loads, reversed loads, nor impact loads were contemplated. Joints were to be as simple as possible. To obtain broad coverage, only one test of each specific type was contemplated and a series of tests was to be carried only far enough to indicate a trend. Statistical confirmation and conclusive finds would be reserved for possible future tests.

Midway through the program it became apparent that more important results could be obtained by broadening the testing program for 7/8-inch and 5/8-inch bolts; so tests on other sizes of bolts were deleted.

## ACKNOWLEDGMENTS

The tests described herein were sponsored by the Committee on Steel Structures Research of the American Institute of Steel Construction. Mr. Byron E. Bushnell, Bushnell Industries, was chairman of the committee. Mr. R. G. Derrick, President of Western Steel Company, represented the committee locally. Additional financial assistance was obtained from the University of Utah Research Fund.

Most of the tests were made by Charles C. Rampton, Jr., graduate student. LeGrand R. Lamb and Clarence R. Skoubye, undergraduate students, assisted in some of the tests. Dr. S. S. Kistler, Dean of the College of Engineering, and Dr. George R. Hill, Head of the Department of Fuel Technology, were advisors. R. L. Sanks, Associate Professor of Civil Engineering, supervised the research and made some of the tests.

The authors are indebted to Mr. C. R. Davis for preparing the drawings and to Mr. T. R. Higgins for comments on the manuscript.

Bolts, washers, and nuts were furnished by Russell, Burdsall and Ward Bolt and Nut Company; grit and shot were furnished by American Steel Abrasives Company; and some apparatus was made by both Eimco Company and Western Steel Company.

## Equipment, Apparatus, and Materials

## Testing Machines

Two testing machines were used, one of 60,000 pounds capacity and one of 200,000 pounds capacity. Both are Southwark Tate-Emery machines in good condition.

## Strain Measurements

All strains were detected by SR-4 gages; some were type A-8, a paper gage which was cemented with Armstrong A-1 epoxy resin glue, and some were type AB-11, a bakelite gage which was cemented with hard deKhotinsky cement. The gage length of both was 1/8 inches. Both were reliable and accurate, but the bakelite gages showed less tendency to creep.

Strains were measured with a Baldwin Type K Strain Indicator or with an Ellis BAM-1 bridge amplifier and meter. The BAM-1 is continuously adjustable over a wide range of sensitivities. Because it can be calibrated directly in terms of load, torque, or displacement, as well as in terms of stress, conversion factors are eliminated; it is particularly well suited for use with the torque wrench and the clip gages.

## Torque Wrench

A T-shaped torque wrench was made of S.A.E. 1040 steel bar one inch square hardened to an elastic limit of about 150,000 psi. Heavy duty sockets were fitted to the stem, or drive shaft. Extension handles of pipe made the wrench eight feet long. SR-4 gages were mounted on the drive shaft in such a way that only pure torsion was measured and the effects of unintentional bending were cancelled.

Torque was read directly in foot-pounds on the BAM-1.

## Vise

A special vise was made to hold the joints while the nuts were tightened.

## Load Cells

Various methods to measure bolt tension were considered. Neither torque nor turns-of-the-nut was considered sufficiently reliable for this research. Elongation of the bolt would not be reliable and accurate unless the bolts were known to be uniform in material and heat treatment, and even if they were, stresses at the root of the threads are well beyond the elastic limit; so creep occurs to complicate calibration.

The load cells shown in Fig. 1 proved to be both accurate and reliable. They were made of S.A.E. 1035 steel hardened to Rockwell C 52, and they behaved elastically within the specified minimum bolt tensile loads. The peculiar shape at the top of the load cell was made to concentrate the stress on the two strain gages (increasing their sensitivity) and to cause limited plastic flow of the bolt head to ensure uniformity in seating.

The load cells were calibrated by applying a tensile load to the end of the bolt. The load cell was squeezed between the bolt head and a standard hardened washer supported by a specially made plate. Tests were made with the plate parallel to the bolt head and also tipped as much as one degree in various directions to produce eccentricities greater than those expected in tests of the joints. Even under eccentric loading, deviations were usually less than 2 per cent and never exceeded 4 per cent in any test except for two load cells which, for that reason, were not used. More extensive testing might have disclosed greater errors, but used bolts gave less reliable results, and since the supply of bolts was limited, the tests were also limited. Nevertheless, it was apparent that the load cells were indeed accurate.

The single disadvantage of the load cell is that the grip of the bolt is increased and its elastic characteristics thereby altered somewhat. This would appear to be of no practical importance, although there is no experimental evidence to support this contention.

## Clip Gages

Clip gages<sup>(4)</sup> instead of dial gages were used to measure the average slip of the joints. Dial gages are awkward to mount and inconvenient to read. In contrast, the clip gages were easy and quick to mount and to read.

The two clip gages were made of phosphor bronze to the dimensions shown in Fig. 2A. SR-4 gages were mounted on both sides and connected to the BAM-1. They were calibrated together by means of a micrometer caliper in two different ranges. Low range permitted a slip of 0.020 inches with a least reading of 0.0001 inches, and high range permitted a slip of 0.200 inches with a least reading of 0.001 inches. From the calibration tests, it appeared that errors were not often greater than one least reading; the maximum error measured did not exceed two times the least reading. The low, sensitive range was always used for the first portion of every test.

In the first series of tests, one end of the gage rested on a pin fastened in the center plate; the other end rested on the bed of the testing machine. Thus the gage measured, in addition to slip, a considerable portion of the elastic deformation of the plate plus any local deformation due to imperfect bearing between the machined edge of the plate and the bed of the testing machine.

These tests are identified in Table 3 by an asterisk.

In all other tests, the slip of the joint was measured by hanging the harness of Fig. 2B on three pins and setting the clip gage between the harness and the center pin as shown in Figs. 3 and 4. The two clip gages, connected in series to the BAM-1, measured the average movement of the inside plate with respect to the two outside plates. Since the pins were set in a straight line, the effects of plate distortion were reduced to a minimum.

### Steel

All structural steel was ASTM designation A-7 supplied as flat bar or plate with surfaces of well-bonded mill scale. The surfaces were cleaned with carbon tetrachloride.

### Bolts

The bolts were of ASTM designation A-325 steel, the washers were carburized steel, and the nuts were ASA heavy nuts of mild steel. The bolts, nuts and washers were used exactly as received except that surfaces bearing against the load cells were wiped clean.

### Grit and Shot

Aluminum oxide, silicon carbide and tungsten carbide grits were too brittle and either cracked or powdered when forced into mild steel. Grit of crushed chilled white iron shot was much better, but a considerable percentage of particles cracked.

The grit used in the tests reported herein was "Malleabrasive." Made of crushed chilled white iron shot processed by a method similar to malleablizing, it was tough and strong and yet possessed a hardness of 375 to 400 Vickers. Only a few particles were ever discovered to be cracked when forced into the mild steel plates.

The shot was chilled white iron. As supplied in commercially screened sizes there was a considerable proportion of malformed particles and a wide variation of size in each grade. Although it possessed a hardness of 750 to 850 Vickers, no particles were ever found cracked.

After a few tests were made with grit and shot, the shot was carefully sieved into much more uniform grades. At the same time the shot was sorted by hand and the badly malformed particles discarded.

After several tests of sieved shot had shown the superiority of round, uniform particles, polished chrome steel balls from 1/8 inches to 1/32 inches in diameter were obtained in small quantity to see whether their polished surfaces would lessen the force required for penetration. Only enough tests with steel balls were made to establish a definite trend and to provide comparison with other particles.

## Testing Procedure

### Load-Penetration Tests

These tests were made to determine the force required to press the particles into mild steel. Each test specimen consisted of a weighed quantity of particles placed between two plates approximately 2 x 1/4 x 2 inches in size.

All burrs were filed off the plates. Plates which were not flat to within 0.001 inches were discarded. All plates were completely covered with mill scale. The hardness of these plates as well as the hardness of the plates used for shear tests were compared on a Rockwell Hardness Tester. The hardness was found to vary from B-66 to B-72. This variation was so small that it was neglected; that is, no corrections for hardness were attempted.

The specimen was placed on an anvil under a specially made ram which permitted the corners to protrude as shown in Fig. 5. The over-all thickness of the specimen was obtained by averaging the thicknesses measured with a micrometer caliper at the four corners.

### Shear Tests

Each specimen consisted of three plates, the outer ones were  $4 \times 3/8 \times 4-1/2$  inches, and the inner one was  $4 \times 1/2 \times 4-1/2$  inches. Each plate projected  $1/2$  inch, leaving faying surfaces 4 inches square. The true area in solid bearing was much less; it averaged approximately 2 inches in diameter for  $5/8$ -inch bolts and about  $2-1/4$  inches in diameter for  $7/8$ -inch bolts. There was considerable variation probably due to the plates being slightly warped. Apparently, the bearing stresses spread at an angle of about 45 degrees from the outer edge of the nut or bolt head; so the surface in actual contact is more a function of the plate thickness than of faying area. Except for a few tests made of plates with punched holes, holes were subpunched and drilled. All burrs were removed, except in tests of plates with punched holes. Holes were of standard size,  $1/16$  inches larger in diameter than the nominal size of the bolt.

Reinforced joints were brushed with red lead primer, and the particles were dropped into the fresh paint. The paint was allowed to dry two days before the joint was assembled and tested. Except for the smaller sizes of particles, the particles were arranged in a definite pattern. Some joints were reinforced with washers made of 0.002-inch steel shim stock to which SS 14 shot<sup>3</sup> were spot-welded. One joint was painstakingly assembled with shot lying on clean mill-scale surfaces, and in one test the shot was dropped into the paint and later covered with strips of transparent scotch tape to simulate a washer made with steel shot enclosed in a plastic envelope.

The plates were assembled in such a way as to permit nearly  $1/8$  inches of slip to occur before there was bearing on the bolt. The load cell was placed under the bolt head with washers under the load cell and the nut. The joint was placed in the vise, and the nut was tightened to produce the minimum specified tension in the bolt—32,400 pounds for a  $7/8$ -inch bolt and 17,300 pounds for a  $5/8$ -inch bolt. There was always some creep present, even with unreinforced and unpainted joints. So after a delay of one to two minutes the bolt was again tightened to minimum specified tension. Creep was always low after the second tightening. The torque and turns-of-the-nut were recorded.

Both ends of the specimen were then machined for uniform bearing against the bed of the testing machine. Holes were drilled in each plate on each side by means of a drilling jig, and tight-fitting pins were driven into the holes. The harness was hung on these pins and the clip gages set in place as shown in Fig. 3. The joint was centered in the testing machine, the load cell was

3. See Table 2 for characteristics of SS 14 shot.



connected to the Baldwin Strain Indicator, and the clip gages were connected to the BAM-1 as shown in Fig. 4.

Loads were applied in increments of 2,500 pounds and, in some tests, in smaller increments. Whenever detectable slip occurred, slip and loads were recorded. The joint slip was noted as soon as the desired load was attained, and that load was maintained until the rate of slip or creep was reduced to 0.002 inches per minute. Since creep was rapid at first, a rate of 0.002 inches per minute represented a very low rate of creep. It was not unusual for a test to require two hours for completion. Except for a very few tests, the tests were stopped whenever it became evident that the bolt came into bearing.

Tension in the bolt was recorded at frequent intervals during the shear test. It was also recorded immediately before and after disassembly of the joint.

### Corrosion Tests

The compressive stresses set up between the shot and the steel plates were thought to be possible foci for corrosion. In order to determine experimentally the magnitude of any stress corrosion, several joints were assembled without load cells. The bolts were tightened by applying a torque of 490 foot-pounds<sup>4</sup> to the nut. These joints were immersed for three months in a normal salt solution well aerated with pure oxygen. Thus, conditions were adjusted to maximize any possible corrosion in these accelerated corrosion tests.

### Rivet Tests

Four riveted joints were tested for comparison. Each joint consisted of a single rivet and three plates with mill-scale surfaces and deburred, drilled holes. Two rivets were driven with a hydraulic press and two rivets were driven with a pneumatic riveting hammer under conditions simulating field practice.

### Shot-Washers

Although applying grit or shot by embedding in wet paint is satisfactory for laboratory tests, it is by no means suitable for practical application in the field. Because steel members are subject to rough handling, the shot must be applied so firmly that it cannot be easily dislodged.

One way to apply the shot is to spot-weld them directly to the steel member. A machine (similar to a stud welder) which would weld a complete pattern of shot all at once is required, because welding them one by one certainly is not practical. The development of such a machine would undoubtedly be costly.

Another way to apply the shot is to fasten the shot first to a washer, then glue the washer to the steel member. The commercial possibilities of this method are feasible. The shot might be enclosed in a thin plastic envelope or between two thin sheets of steel, or the shot might be held in a wafer-like matrix of some collapsible material. Adhesive on one surface can be protected by an easily removed covering.

4. The approximate average torque measured prior to this time was about 490 foot-pounds.

About 20 shot-washers were laboriously hand made of 0.002-inch steel shim stock to which a normal weight of size SS 14 shot were spot-welded one by one. In laboratory tests, the washers were placed in the joint without any adhesive.

To determine the practicability of the washers under actual field conditions, ten of the washers were supplied with a gummed surface by sticking a pressure-sensitive adhesive transfer tape<sup>5</sup> to the back of the washer as shown in Fig. 11. When the tape was peeled off, the adhesive transferred itself to the washer. The washers stuck firmly to painted surfaces; they could be peeled off, but they would not slip nor slide. It was judged that under field conditions they could not easily be dislodged. Eight shot-washers were applied to a steel beam in a small building by the erection foreman. They were nearly as easy to apply as postage stamps; the care required to center them over the holes took but little extra time. It is estimated that six to ten washers could be applied per minute under ordinary field conditions.

On the basis of the limited number of washers applied, it is possible only to speculate concerning the use of the washers in the field. On an actual construction job, the washers would not, in all probability, be applied by the mechanics while climbing, because the extra task would almost certainly slow up the entire erection procedure. However, the washers could quickly and easily be applied to the steel members while they are lying on the ground. At worst, this would require an extra workman; at best, the task could be handled by the regular crew, since the application of the washers would be much less than a full-time job.

The use of the washers in the shop offers no particular problems. However, the washers are not necessary in unpainted joints; so the need for shop applications would be limited.

#### Code Numbers

In order to avoid lengthy descriptions and yet have a meaningful title, each test was assigned a descriptive code number. The code numbers proved so convenient that shortened versions are used in the tables and figures in preference to lengthy descriptions. For example, test RL/SS 14/100%/1 is interpreted: red lead paint, sieved shot number 14, 100 per cent of a normal weight of particles, test number 1. Code numbers are defined as follows:

#### Surface Condition

- MS - Clean mill-scale surfaces. Holes were drilled, burrs removed; and plates were fairly flat unless followed by the symbol, PH.
- PH - Punched hole. Burrs were not removed nor were plates flattened. Two plates were always assembled with burred sides touching; the burred side of the third plate was turned to the outside.<sup>6</sup>
- RL - Surfaces painted with red lead.
- ZC - Surfaces painted with zinc chromate.
- ZCIO - Surfaces painted with a zinc chromatic-iron oxide mixture.
- 2 Day, 7 Day, 14 Day - Indicate drying time of paint before testing. Unless otherwise stated, drying time was two days.

5. Tape No. 466, Minnesota Mining and Manufacturing Co., Saint Paul 6, Minn.

6. It is believed that this assembly would produce the least possible frictional resistance.



### Fasteners

Unless otherwise noted, fasteners were high tensile bolts with hardened washers and ASA heavy nuts.

F Rivet - Field rivet. A rivet driven with a pneumatic hammer under circumstances approximating field conditions.

S Rivet - Shop rivet. A rivet driven by a hydraulic press.

### Reinforcement

- G 18 - Grit number 18. This was the only size tested in shear.
- S 390 to S 230 - Unsieved chilled white iron shot used as supplied in standard grades.
- SS 12 to SS 25 - Chilled white iron shot sieved in successive U. S. Standard sieves. The number indicates the sieve number upon which the shot was retained.
- B 1-8 to B 1-32 - Polished chrome steel balls of the diameter in inches as indicated.
- SW - Single shot-washer. A shot-washer made of one piece of 0.002-inch steel shim stock to which a normal weight of SS 14 shot was spot-welded.
- DW - Double shot-washer. Same as a single shot-washer except the shot was held between two pieces of the shim stock.
- ST - Scotch tape. Transparent scotch tape laid over a normal weight of SS 14 shot.
- 100% (etc.) - 100 per cent (or any percentage indicated) of normal weight of shot required for normal penetration.

### Miscellaneous

- Rust - Corrosion test. Immersion in normal saline solution aerated with pure oxygen for three months.

## Results

### Load-Penetration Tests

The appearance of the plates after testing is pictured in Fig. 6. Note the tendency for grit to crack, for the balls and shot to penetrate halfway into each plate, and for a tiny area around each particle to protrude slightly as the particles were pressed into the plate (especially evident in Fig. 6C).

Typical load-penetration curves are shown in Fig. 7. As the separation approached zero, the load usually began to increase rapidly, due probably to the contact between the protuberances around each shot. This increase in load at near-contact of plates was most pronounced with larger shot and balls.

The thickness of paint films was found to vary from about 0.001 to 0.002 inches; therefore the total paint thickness between two plates could be as much as 0.004 inches. Because the force required for complete penetration could not be determined accurately from the curves, the force required for a plate separation of 0.004 inches was used as a base or reference. "Normal" force is herein defined as the force in kips per gram of particles required to produce a plate separation of 0.004 inches. "Normal" weight is herein defined as the weight of particles required to yield a plate separation of 0.004

inches for any specified force (such as 32,400 pounds for 7/8-inch bolts or 17,300 pounds for 5/8-inch bolts). The amount of particles used in the shear tests is expressed in terms of a percentage of the "normal" weight.

The "normal" force per gram of particles (determined from the kind of curves shown in Fig. 7) is plotted against equivalent diameter in Fig. 8. Equivalent diameter was computed from the formula,

$$d = 0.246 \sqrt[3]{\frac{W}{N}}$$

where  $d$  is the diameter of an equivalent sphere,  $W$  is the weight in grams, and  $N$  is the number of particles. The unit weight of the shot was assumed to be 484 pounds per cubic foot or 127 grams per cubic inch. The diameter of the balls was measured—not computed. The characteristics of grit and shot are given in Table 1 and of sieved shot and balls in Table 2.

From an examination of Fig. 8, grit is the least efficient reinforcement. The most efficient reinforcement is balls, particularly in the smaller sizes. Sieved shot in the larger sizes is nearly as efficient as balls. However, these comparisons are not conclusive, because a polished ball that can be pressed into a plate with less force than a shot might also plow laterally through the plate with less force than shot so that the net efficiency of each as reinforcement might be the same.

### Shear Tests

The appearance of typical faying surfaces before and after testing the joint are shown in Figs. 9 and 10. During the first stage (up to a slip of about 0.001 inches) of nearly every test of reinforced joints, the joint behaved "elastically"; that is, load was proportional to slip. In the second stage (from a slip of about 0.001 to 0.002 inches), slip began to increase more rapidly than load. In the last stage (beyond a slip of about 0.003 inches), the load increased slowly but steadily with slip. The reason for this steady increase in slip is apparent from an examination of the joints after testing; a ridge of metal was formed in front of each particle as it plowed through the plate. (See Figs. 10A and 10B). After a slip of about two particle diameters, the ridge nearly enveloped the particle. So effective was the reinforcement at this stage that there was no break in the load-slip curve when the bolt came into bearing. However, it should be noted that the holes and the bolt were seldom perfectly aligned; so the bolt seldom came into bearing squarely. Moreover, the threaded portion of the shank of 7/8-inch bolts extended nearly through two plates and the threaded portion of the shank of 5/8-inch bolts extended nearly through one plate. Nevertheless, it was evident that the reinforcement was remarkably effective at large slips.

A typical shot-washer after testing is shown in Fig. 12. Again, the characteristic ridges were formed in front of each particle with the washer conforming to the shape of the ridge.

Load-slip curves for typical joints are shown in Figs. 13, 14, 15, and 16. The upper curve in each diagram is plotted to the abscissa scale shown at the bottom of the page; the lower curve is plotted from the same data to an abscissa scale amplified 10 times. Each lower curve is terminated at 0.005 inches slip; and each upper curve is terminated at 0.06 inches slip; so, of course, neither curve indicates the ultimate strength. Attention is called to the fact that the ordinate scale reads total load on the joints in kips. Shearing

stress, of itself, has no meaning here, but as used by structural engineers it can be calculated as total load divided by the product of number of shearing planes (two) and cross-sectional area of the bolt. For tests with 7/8-inch bolts, divide the ordinate by 1.2026 to obtain shearing stress in kips per square inch; and for tests with 5/8-inch bolts, divide the ordinate by 0.6136 to obtain shearing stress in kips per square inch. To invite comparison between 5/8-inch and 7/8-inch bolts, the ordinates for tests of 5/8-inch bolts are plotted to twice the scale of the ordinates for tests of 7/8-inch bolts; since the nominal cross-section area of a 7/8-inch bolt is about twice that of a 5/8-inch bolt, the scale of shearing stress is very nearly equal for all tests.

Comparisons of the best load-slip curves obtained with 7/8-inch fasteners are shown in Fig. 16. Note that the best reinforced joint is superior to the best mill-scale (unreinforced) joint except below a total load of 23 kips and that it is superior to the best riveted joint except between total loads of 26 to 39 kips. Unfortunately the superiority of reinforced joints over mill-scale joints is not clearly defined, because the crucial load is the design load of 18.02 kips; therefore the superiority of one over the other is a matter of opinion. All things considered, it seems clear that the reinforced joints are at least the equal of the mill-scale joints. The superiority of reinforced joints over riveted joints is, however, clearly established.

Comparison of the best load-slip curves obtained with 5/8-inch bolts is shown in Fig. 17. The reinforced joint is superior at every point to the best mill-scale (unreinforced) joint.

In a limited program, the best size and distribution of balls and shot would not be tested except by chance; so it is likely that further tests would disclose even better combinations of reinforcement. Tests of shot-washers, in particular, were limited; no variations of shot size or distribution were made. For this reason, the apparent loss of efficiency of shot-washers as compared with shot is not necessarily indicative.

Load-slip characteristics for all the tests are given in Tables 3, 4 and 5. Although the figures for modulus and elastic limit are subject to personal interpretation, they do give an approximate idea of the slope and extent, respectively, of the first stage of the load-slip curve. The loads at slips of 0.002, 0.005, 0.030, and 0.060 inches are known within narrow limits of error, and provide a more exact basis for comparison.

### Corrosion Tests

Because no load cells were used in these tests, the tension in the bolts is not known exactly. Within the limits of error in bolt tension, the specimens tested after three months of immersion appear to behave no differently than those tested immediately after assembly.

Examination of the external and the faying surfaces demonstrated that corrosion did occur on the external surfaces (as would be expected) but did not occur on the faying surfaces close to the bolt. When the joints were disassembled, the faying surfaces were slightly damp but they dried almost immediately. The shot had been embedded sufficiently so that practically no water nor air was available to form electrochemical stress corrosion circuits. It is most probable that as long as the joints are snug, very little long-term difficulty would arise with regard to corrosion of the particles of shot or of the steel sockets formed around them.

## Bolt Tension

Torque and turns-of-the-nut as well as tension in the bolts before and during the tests are given in Tables 6 and 7. As the tables show, the torque required to obtain minimum specified tension<sup>(5)</sup> varied from 390 to 820 foot-pounds for 7/8-inch nuts and from 170 to 430 foot-pounds for 5/8-inch nuts. Wide variations can be expected because torque is not an accurate measure of tension. Nevertheless, it seems significant that more than 50% of 7/8-inch nuts and more than 80% of the 5/8-inch nuts required greater torques than those specified.

In all tests of mill-scale joints, full bolt tension was achieved with less than one full turn on the nut after turning the nut finger-tight. The turn-of-the-nut method<sup>(6)</sup> of tensioning bolts would, then, appear to insure at least the minimum specified bolt tension.

The number of turns-of-the-nut to develop full tension in bolts in reinforced joints varied depending on the size of the grit or shot. For joints reinforced with shot approximately 1/16 inches in diameter, the maximum number of turns-of-the-nut was 1-7/12. For field construction practice, then, two turns-of-the-nut could be relied upon to produce minimum specified tension.

The tension in the bolt invariably decreased during the test. It might seem that in a joint subjected to a compressive force to produce shear, the tension in the bolt would increase because the plates increase in thickness due to poisson's ratio. Evidently, as the plates begin to slip, tiny protuberances are scraped off permitting the plates to grind closer together, thus effecting an over-all decrease in thickness in spite of any expected increase due to poisson's ratio. The decrease in tension was more pronounced with reinforced joints than with unreinforced joints. Inspection of many reinforced joints showed that the shot appeared to dig slightly deeper into the plates as slip increased.

## CONCLUSIONS

The following conclusions are limited to results of tests in which slowly varying loads were applied in one direction only.

1. Mill-scale joints slipped at approximately the design load.<sup>7</sup> At a slip of 0.002 inches, the load on 7/8-inch bolts varied from 100 per cent to 128 per cent of the design load, and the load on 5/8-inch bolts varied from 87 per cent to 109 per cent of the design load.
2. At a slip of 0.002 inches, 7/8-inch rivets developed only 28 per cent to 89 per cent of the design load. Slips of 0.004 to 0.010 inches were required to develop the full design load. Shop rivets (driven by a press) were superior to field rivets (driven by a riveting hammer).
3. Paint reduced the slip resistance of the joints drastically. Loads at 0.002 inches slip varied from 11 per cent to 67 per cent of the design load depending upon the kind and age of paint. Red lead was the paint most detrimental to slip resistance.
4. Joints, painted with red lead and reinforced with grit, shot, or balls
7. The design load for one 7/8-inch bolt or rivet in double shear is 18.02 kips; for one 5/8-inch bolt, in double shear, the design load is 9.20 kips.

developed (with one exception) 55 per cent to 130 per cent of the design load at a slip of 0.002 inches. The performance of reinforced joints was more reliable than the performance of other joints.

5. Comparing joints with 7/8-inch bolts, the best reinforced, painted joint was markedly superior to the best unreinforced (mill-scale) joint above a slip of 0.004 inches; below a slip of 0.004 inches the mill-scale joint was somewhat superior. The best reinforced, painted joint was superior or equal in all respects to the poorest mill-scale joint.

6. Comparing joints with 5/8-inch bolts, the best reinforced painted joint was superior or equal in all respects to the best mill-scale, unreinforced joint.

7. Reinforced, painted, bolted joints were superior to riveted, mill-scale joints.

8. Punching the hole appears to lessen the slip resistance of unreinforced joints. The single unreinforced (mill-scale) joint with a punched hole developed only 83 per cent of the design load at a slip of 0.002 inches. In comparison, note that only one of the four riveted joints developed more than 45% of the design load at a slip of 0.002 inches. Reinforced joints with punched holes were about as slip resistant as those with drilled holes.

9. Shot-washers were not as effective as shot alone, but as no attempt was made to improve the shot-washers, this is probably not significant.

10. Although some moisture penetrated the joints in the corrosion tests, no rust in any joint was found in that portion of the faying surface near the bolt. Immersion in oxygenated, saturated salt solution for three months had no effect upon the strength of any joint. It appears unlikely that reinforced joints will rust regardless of exposure to the weather if the plates are not separated.

11. Reinforced mill-scale joints were no stronger than reinforced painted joints.

12. According to load-penetration tests, the effectiveness of the particles in order of best to worst was balls, sieved shot, shot and grit. The shear tests confirmed this conclusion, but the difference between balls and sieved shot was small. The best size appears to range from 1/32 inches to 1/16 inches in diameter. The best amount appears to be somewhat in excess of 100 per cent, but there were too few tests to confirm this.

13. The evidence indicates that greater effectiveness can be obtained with shot or ball reinforcement.

14. It would be premature to draw any final conclusions of the comparison of reinforced joints over mill-scale joints without (a) statistical confirmation of these tests, (b) tests on bolts of other sizes, (c) stress reversal tests, and (d) fatigue tests.

## REFERENCES

1. Specifications for Assembly of Structural Joints Using High Strength Steel Bolts, Section 3c, approved by Research Council on Riveted and Bolted Structural Joints of the Engineering Foundation, February, 1954.
2. Ibid. Appendix B, section 5, approved December 15, 1955.
3. Bell, M. H., High Strength Steel Bolts in Structural Practice, ASCE Proc. Separate 651, Vol. 81, p. 6, March, 1955.

4. Sanks, R. L., Two Useful Gages Measure Bolt Tension and Slip in a Joint, Civil Engineering, Vol. 26, No. 11, pp. 62-3, November, 1956.
5. Research Council . . . op. cit., Section 4 b, December 15, 1955.
6. Drew, F. P., Tightening High-Strength Bolts, ASCE Proc. Paper 786, Vol. 81, August, 1955.

TABLE 1. CHARACTERISTICS OF S. A. E. STANDARD SHOT AND GRIT

Grit or Shot No.	Shape	U. S. Std. Sieve Numbers			Equivalent Sphere diameter inches	Normal Penetration Force, kips per gram of particles
		100% Passing	70% + Retained on	15% + Passing		
G 18	Angular	14	18	25	.049	87
G 25	"	16	25	40	.040	102
G 40	"	18	40	50	.025	116
S 390	Spheroidal	14	18	20	.052	66
S 330	"	16	20	30	.042	88
S 230	"	18	30	40	.029	96
S 170	"	20	40	50	.023	102

TABLE 2. CHARACTERISTICS OF SIEVED SHOT AND STEEL BALLS

Ball or Shot No.	Shape	U. S. Std. Sieve Numbers		Equivalent Sphere diameter inches	Normal Penetration Force, kips per gram of particles
		100% Passing	100% Retained on		
SS 12	Spheroidal	10	12	.072	52
SS 14	"	12	14	.060	61
SS 16	"	14	16	.051	72
SS 18	"	16	18	.043	82
SS 20	"	18	20	.040	84
SS 25	"	20	25	.030	96
B 1-8	Spherical	--	--	.125	29*
B 3-32	"	--	--	.094	37*
B 1-16	"	--	--	.063	54
B 1-32	"	--	--	.031	78

\*Hypothetical values. Excessive distortion around each ball prevents a rational value for normal penetration.



TABLE 3. RESULTS FOR ONE 7/8-INCH BOLT IN DOUBLE SHEAR

Item	Test No.	Apparent Modulus Kips/in.	Total Load in Kips at				
			Elastic Limit	Slip of			
				.002"	.005"	.030"	.060"
1	MS/1*	—	13	18	19	22	25
2	MS/2	24,000	16	23	23	26	26
3	MS/3	30,000	16	23	23	24	28
4	MS/4	16,000	13	18	18	18	18
5	MS/PH/1	34,000	8	15	16	17	17
6	MS/Rust/1	20,000	12	19	22	23	—
7	MS/Rust/2	37,000	12	20	20	23	25
8	RL/2 Day/1*	1,000	1	2	3	4	8
9	RL/7 Day/1	—	—	3	4	4	5
10	RL/14 Day/1	—	1	5	5	7	8
11	ZC/2 Day/1	12,000	4	10	11	11	12
12	ZCIO/2 Day/1	26,000	6	12	13	13	14
13	ZCIO/7 Day/1	—	2	6	7	8	10
14	ZCIO/14 Day/1	—	3	5	5	8	9
15	RL/G 18/100%/1	17,000	6	14	19	25	29
16	RL/G 18/108%/1	12,000	7	13	16	23	26
17	RL/S 390/98%/1*	6,000	15	10	20	28	33
18	RL/S 390/106%/1	10,000	11	17	21	27	32
19	RL/S 390/113%/1*	6,000	13	5	17	32	42
20	RL/S 390/125%/1	9,000	9	12	16	25	30
21	RL/S 330/90%/1	17,000	13	19	23	27	32
22	RL/S 330/103%/1	12,000	10	15	19	27	32
23	RL/S 330/120%/1	18,000	9	18	25	33	40
24	RL/S 230/85%/1	17,000	11	19	23	30	34
25	RL/SS 12/100%/1	13,000	13	19	23	29	31
26	RL/SS 14/98%/1	12,000	13	16	21	28	32
27	RL/SS 14/100%/1	15,000	13	19	23	28	31
28	RL/SS 14/100%/PH/1	24,000	7	19	23	28	40
29	RL/SS 14/100%/Rust/1	11,000	12	17	21	26	30
30	RL/SS 16/100%/1	16,000	10	17	20	27	32
31	RL/SS 16/100%/PH/1	25,000	7	16	20	24	34
32	RL SS 18/100%/1	17,000	14	20	24	30	35
33	RL/SS 18/100%/PH/1	26,000	9	20	23	29	40
34	RL/SS 20/94%/1	20,000	7	15	19	26	32
35	RL/SS 25/90%/1	21,000	8	18	20	27	33



TABLE 3. Cont'd.

Item	Test No.	Apparent Modulus Kips/in.	Elastic Limit	Total Load in Kips at Slip of			
				.002"	.005"	.030"	.060"
36	RL/B 1-8/104%/1	13,000	9	16	22	29	32
37	RL/B 3-32/100%/1	10,000	15	18	22	28	32
38	RL/B 1-16/92%/1	19,000	12	20	24	29	37
39	RL/B 1-32/100%/1	25,000	10	20	25	37	47
40	MS/SS 14/100%/1	13,000	12	17	23	33	38
41	MS/DW/1	21,000	8	16	21	31	35
42	MS/SW/1	22,000	8	18	24	32	36
43	RL/ST/1	14,000	8	14	18	25	33
44	RL/SW/Rust/1	20,000	10	18	22	26	29
45	RL/SW/Rust/2	13,000	12	17	21	26	29

\*Indicates clip gage hangers not used. See p. 7

TABLE 4. RESULTS FOR ONE 7/8-INCH RIVET IN DOUBLE SHEAR

Item	Test No.	Apparent Modulus Kips/in.	Elastic Limit	Total Load in Kips at Slip of			
				.002"	.005"	.030"	.060"
1	MS/S Rivet/1	23,000	7	16	22	38	44
2	MS/S Rivet/2	6,000	23	6	13	35	42
3	MS/F Rivet/1	23,000	5	8	15	34	41
4	MS/F Rivet/2	28,000	4	5	9	34	41

TABLE 5. RESULTS FOR ONE 5/8-INCH BOLT IN DOUBLE SHEAR

Item	Test No.	Apparent Modulus Kips/in.	Elastic Limit	Total Load in Kips at			
				Slip of			
				.002"	.005"	.030"	.060"
1	MS/1	25,000	5	8	8	9	12
2	MS/2	30,000	8	10	10	12	15
3	RL/2 Day/1	—	—	1	5	9	9
4	RL/7 Day/1	—	—	2	2	3	4
5	ZCIO/7 Day/1	25,000	2	6	7	8	10
6	RL/SS 12/100%/1	13,000	3	9	11	15	22
7	RL/SS 14/100%/1	7,000	7	10	12	15	17
8	RL/SS 14/126%/1	35,000	6	12	13	17	23
9	RL/SS 16/100%/1	13,000	3	9	11	17	24
10	RL/SS 18/100%/1	7,000	7	10	13	17	19
11	RL/SS 18/225%/1	8,000	7	9	10	15	17
12	RL/SS 20/93%/1	13,000	5	11	12	15	21

TABLE 6. TURNS-OF-NUT AND TENSION IN 7/8-INCH BOLTS

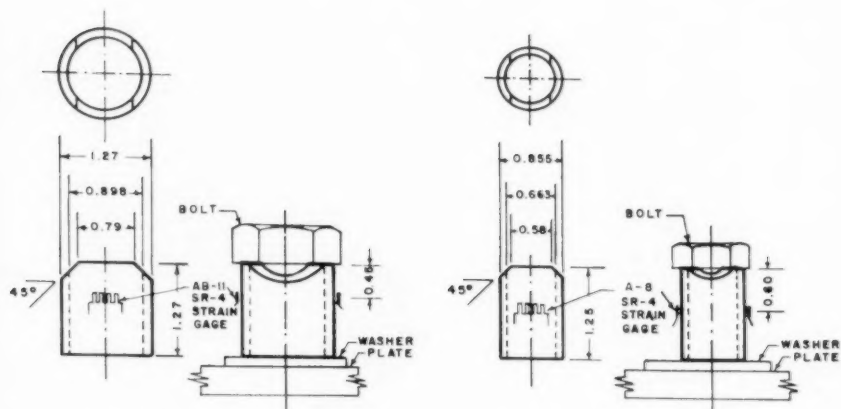
Item	Test No.	Nut		Tension in Bolt, Kips			
		No.	Torque	Start of		At Slip of	
		Turns	Ft. Lbs.	Initial	Load Test	.005"	.060"
1	MS/1	5/12	435	32.4	—	—	—
2	MS/2	5/12	570	32.4	32.0	32.0	31.0
3	MS/3	5/12	450	32.4	31.4	30.0	28.9
4	MS/4	2/3	430	32.4	30.0	—	—
5	MS/PH/1	7/12	430	32.4	31.0	31.0	31.9
6	MS/Rust/1	—	490	—	—	—	—
7	MS/Rust/2	—	490	—	—	—	—
8	RL/2 Day/1	5/12	400	32.4	—	—	—
9	RL/7 Day/1	—	—	—	—	—	—
10	RL/14 Day/1	7/12	430	32.4	31.8	31.9	31.2
11	ZC/2 Day/1	7/12	520	32.4	30.8	30.8	29.0
12	ZCIO/2 Day/1	1/2	520	32.4	31.4	31.2	31.2
13	ZCIO/7 Day/1	—	—	—	—	—	—
14	ZCIO/14 Day/1	2/3	430	32.4	32.4	32.4	32.0
15	RL/G 18/100%/1	1 1/12	510	32.7	30.5	26.7	25.2
16	RL/G 18/108%/1	1	415	32.0	30.1	25.3	22.0
17	RL/S 390/98%/1	1 1/3	460	31.9	—	—	—
18	RL/S 390/106%/1	1 1/6	510	31.4	29.7	25.5	25.0
19	RL/S 390/113%/1	1 1/3	435	31.0	28.7	—	—
20	RL/S 390/125%/1	1	490	31.7	28.6	22.5	19.0
21	RL/S 330/90%/1	1 1/4	470	32.0	30.8	30.1	29.5
22	RL/S 330/103%/1	1 1/12	470	31.4	29.3	23.8	23.6
23	RL/S 330/120%/1	1	495	31.7	—	27.2	27.2
24	RL/S 230/85%/1	11/12	590	32.0	30.6	29.1	27.9
25	RL/SS 12/100%/1	1 5/6	560	32.4	30.5	29.0	28.7
26	RL/SS 14/98%/1	1 1/2	450	32.4	32.0	31.7	32.0
27	RL/SS 14/100%/1	1 7/12	570	32.4	30.6	28.8	29.2
28	RL/SS 14/100%/PH/1	1 7/12	560	32.4	30.4	29.0	26.6
29	RL/SS 14/100%/Rust/1	—	490	—	—	—	—
30	RL/SS 16/100%/1	1 1/4	420	32.7	31.1	28.3	27.3
31	RL/SS 16/100%/PH/1	1 1/6	460	32.8	32.0	30.2	27.5
32	RL/SS 18/100%/1	1 1/4	450	32.6	31.0	30.0	29.1
33	RL/SS 18/100%/PH/1	1 1/4	510	32.4	30.6	28.7	27.1
34	RL/SS 20/94%/1	3/4	390	32.4	30.6	29.0	24.8
35	RL/SS 25/90%/1	5/6	450	32.4	30.3	27.4	25.1

TABLE 6. Cont'd.

Item	Test No.	Nut		Tension in Bolt, Kips			
		No.	Torque	Start of		At Slip of	
		Turns	Ft. Lbs.	Initial	Load Test	.005"	.060"
36	RL/B 1-8/104%/1	2 1/2	600	32.4	31.2	28.2	27.5
37	RL/B 3-32/100%/1	2	560	32.4	29.0	28.0	27.0
38	RL/B 1-16/92%/1	1 5/12	480	32.4	30.0	29.0	28.9
39	RL/B 1-32/100%/1	3/4	820	32.4	31.4	29.7	27.3
40	MS/SS 14/100%/1	1 1/3	430	32.4	30.3	25.6	26.2
41	MS/DW/1	1 5/6	500	—	—	—	—
42	MS/SW/1	1 5/12	480	32.4	30.8	26.8	25.1
43	RL/ST/1	1 5/12	410	32.4	28.0	26.5	24.3
44	RL/SW/Rust/1	—	490	—	—	—	—
45	RL/SW/Rust/2	—	490	—	—	—	—

TABLE 7. TURNS-OF-NUT AND TENSION IN 5/8-INCH BOLTS

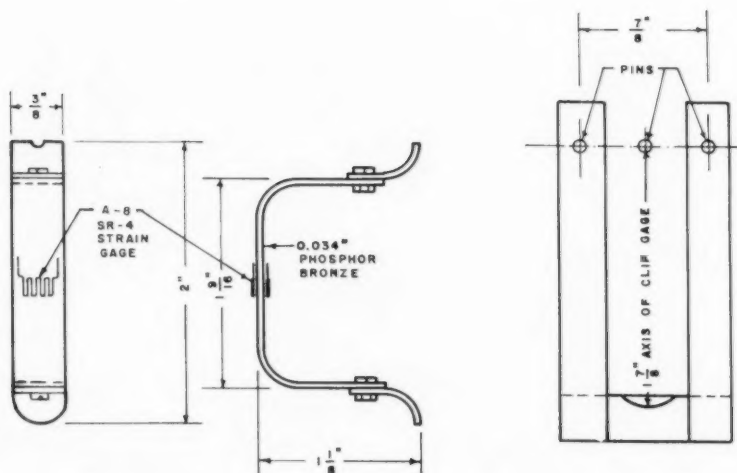
Item	Test No.	Nut		Tension in Bolt, Kips			
		No.	Torque	Start of		At Slip of	
		Turns	Ft. Lbs.	Initial	Load Test	.005"	.060"
1	MS/1	6/12	200	17.3	17.0	17.0	16.9
2	MS/2	6/12	170	17.3	17.0	16.4	15.4
3	RL/2 Day/1	5/6	220	17.3	16.6	16.1	15.2
4	RL/7 Day/1	5/6	420	17.3	16.3	—	15.7
5	ZCIO/7 Day/1	1/2	430	17.3	17.0	17.7	16.6
6	RL/SS 12/100%/1	1 11/12	230	17.3	16.8	15.6	15.1
7	RL/SS 14/100%/1	1 3/4	300	17.3	16.9	15.8	16.1
8	RL/SS 14/126%/1	1 7/12	210	17.3	15.6	14.5	13.5
9	RL/SS 16/100%/1	1 1/2	240	17.3	16.2	15.6	15.8
10	RL/SS 18/100%/1	1 1/2	190	17.3	15.4	14.1	15.0
11	RL/SS 18/225%/1	11/12	260	17.3	16.4	13.6	12.2
12	RL/SS 20/93%/1	1 1/12	180	17.3	15.4	14.6	13.7



(A) 7/8-INCH LOAD CELL

(B) 5/8-INCH LOAD CELL

FIG. 1. LOAD CELLS.



(A) CLIP GAGE

(B) HARNESS

FIG. 2. CLIP GAGE AND HARNESS.

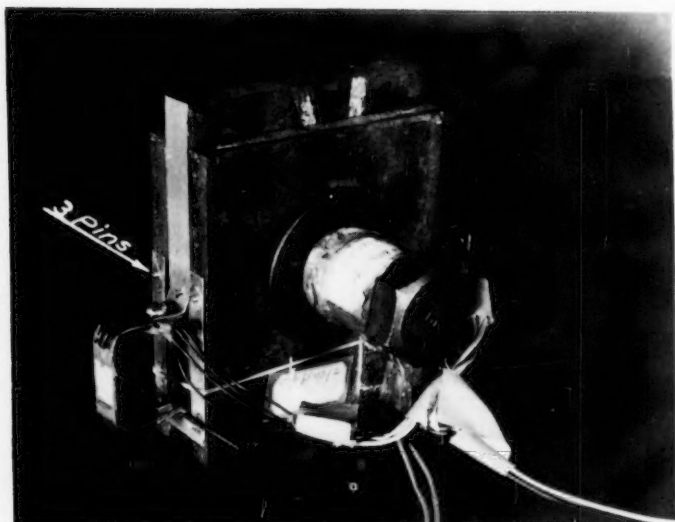


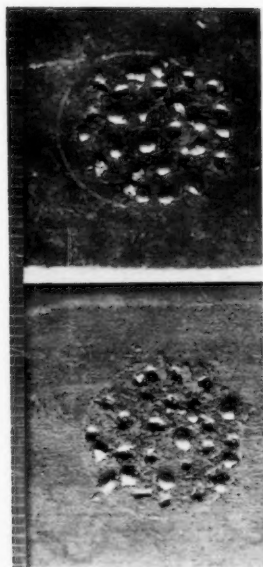
Fig. 3. Joint Ready For Testing.



Fig. 4. Shear Test.



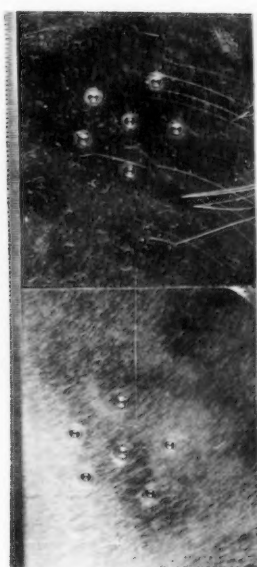
Fig. 5. Load-penetration Test.



(A) Grit (G 18)



(B) Sieved Shot (SS 12)



(C) Balls (B1-16)

Fig. 6. Embedded Reinforcement.

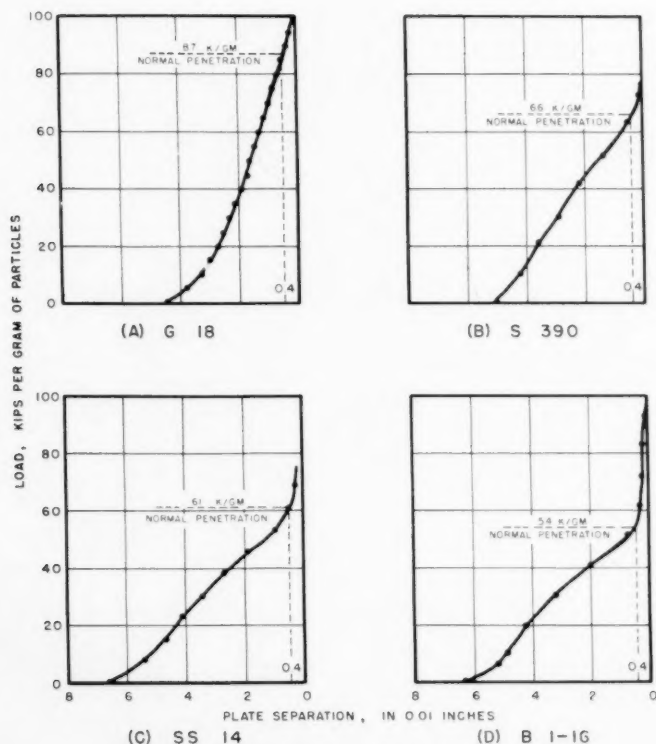


FIG. 7. TYPICAL LOAD-PENETRATION CURVES.

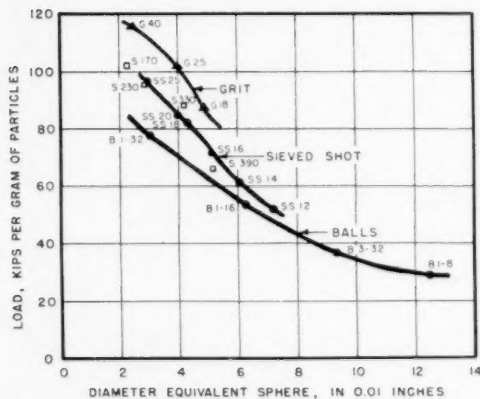
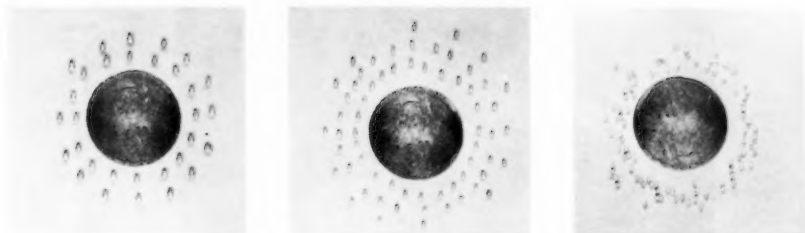


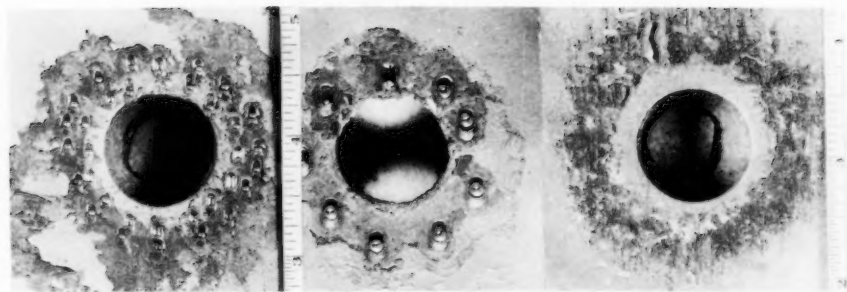
FIG. 8. LOAD VS. DIAMETER FOR NORMAL PENETRATION.





(A) RL/SS 14/100%/1      (B) RL/SS 18/100%/1      (C) RL/SS 20/94%/1

Fig 9. Typical Patterns of Reinforcement.



(A) RL/SS 14/100%/1      (B) RL/B1-8/100%/1      (C) MS/PH/1

Fig. 10. Faying Surfaces After Testing.

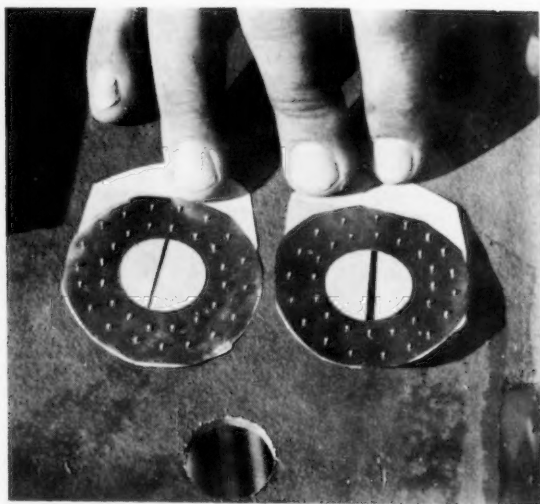


Fig 11. Shot-Washers.

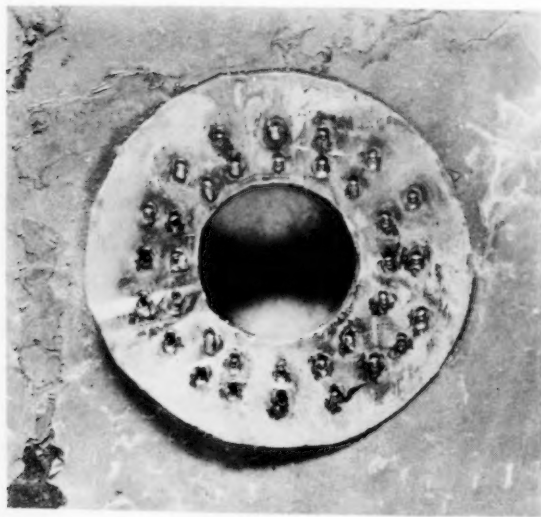


Fig 12. Shot-Washers After Testing.

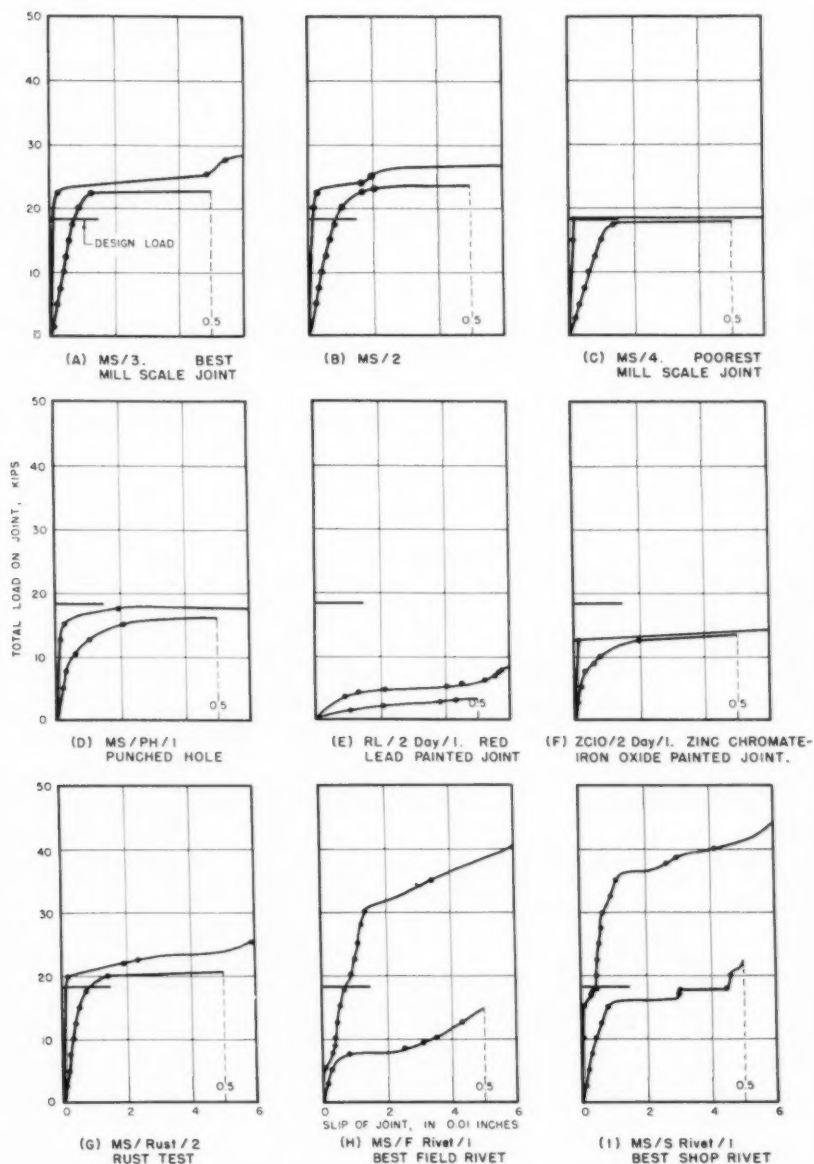


FIG. 13. LOAD-SLIP CURVES. SINGLE 7/8-INCH BOLT OR RIVET IN DOUBLE SHEAR. UNREINFORCED JOINTS.

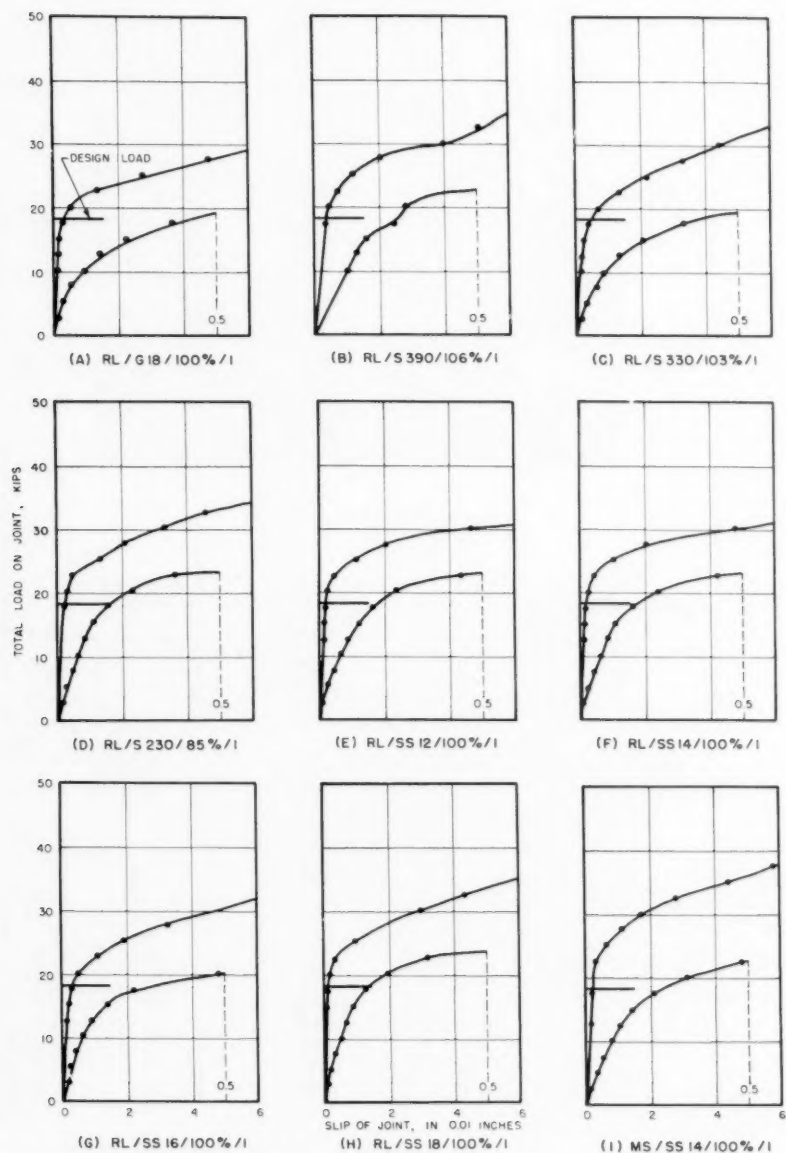


FIG. 14. LOAD-SLIP CURVES. SINGLE 7/8-INCH BOLT IN DOUBLE SHEAR, JOINTS REINFORCED WITH GRIT, SHOT, AND SIEVED SHOT.

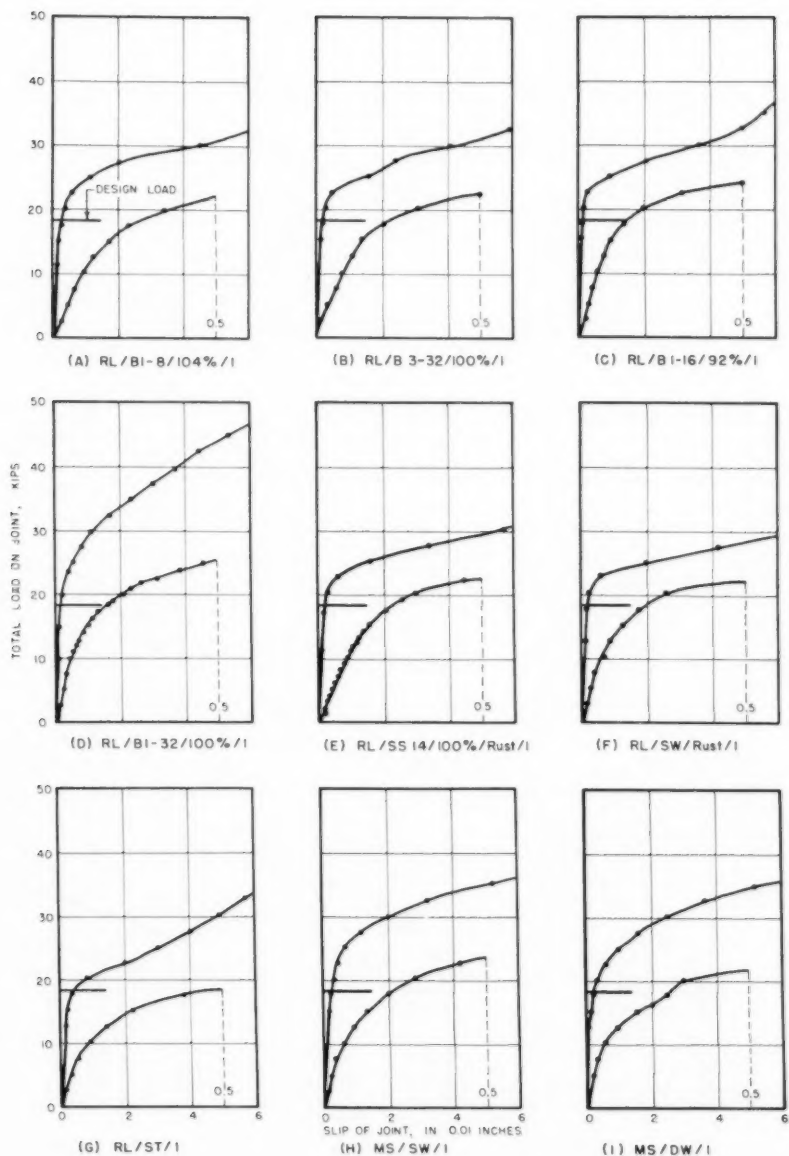


FIG. 15. LOAD-SLIP CURVES. SINGLE 7/8-INCH BOLT IN DOUBLE SHEAR. JOINTS REINFORCED WITH POLISHED BALLS, SIEVED SHOT, AND SHOT-WASHERS.

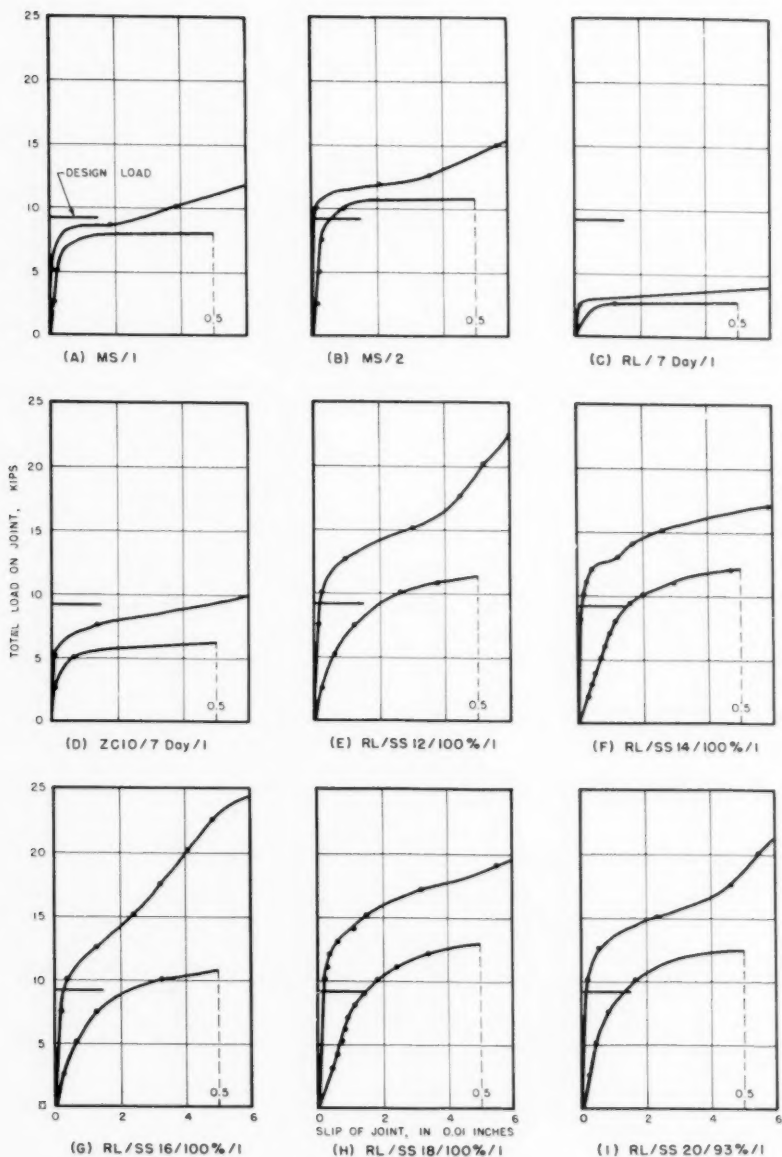


FIG. 16. LOAD-SLIP CURVES. SINGLE 5/8-INCH BOLT IN DOUBLE SHEAR. REINFORCED AND UNREINFORCED JOINTS.

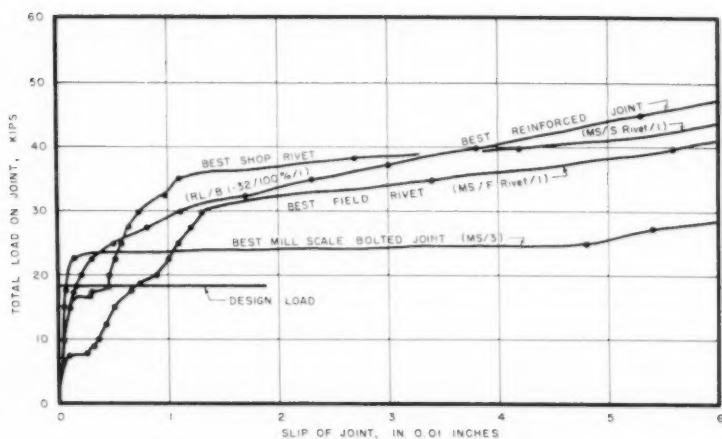


FIG. 17. COMPARISON OF BEST REINFORCED AND UNREINFORCED JOINTS. SINGLE 7/8-INCH BOLT OR RIVET IN DOUBLE SHEAR.

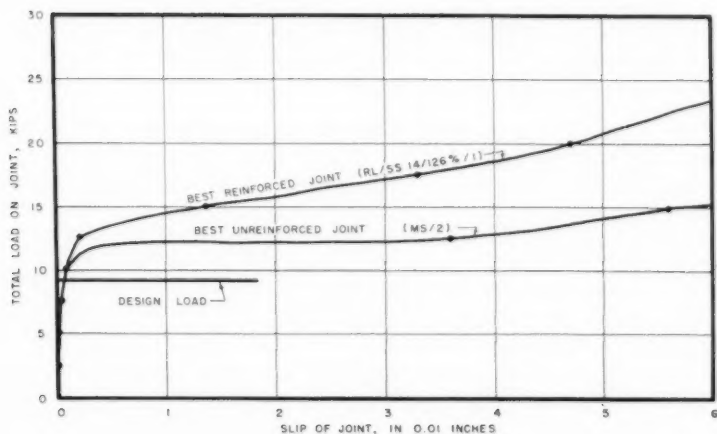
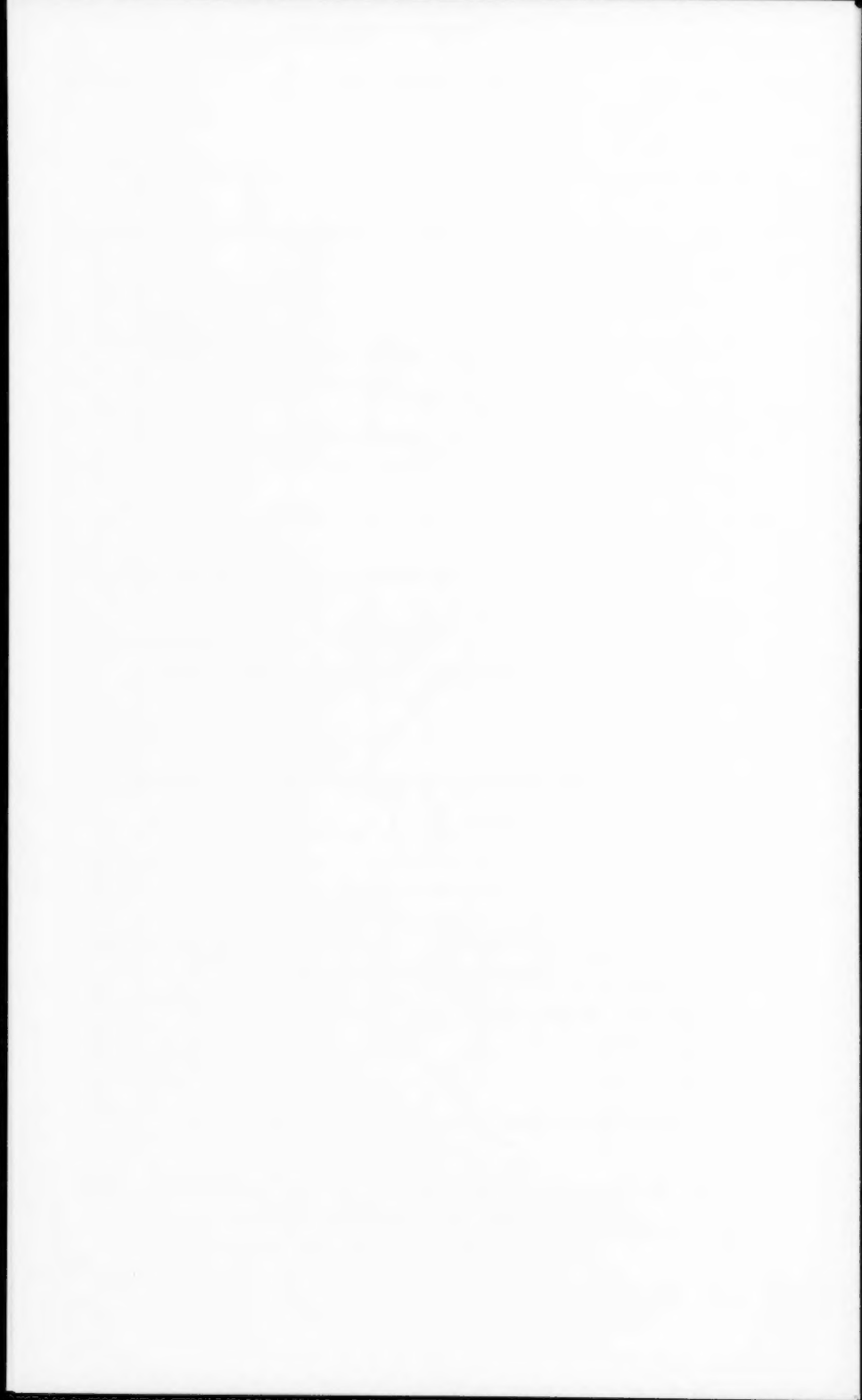


FIG. 18. COMPARISON OF BEST REINFORCED AND UNREINFORCED JOINTS. SINGLE 5/8-INCH BOLT IN DOUBLE SHEAR.





---

Journal of the  
STRUCTURAL DIVISION  
Proceedings of the American Society of Civil Engineers

---

DEAS ISLAND TUNNEL<sup>a</sup>

Per Hall,<sup>1</sup> A.M. ASCE, Troels Brøndum-Nielsen,<sup>2</sup>  
and H. R. Kivisild<sup>3</sup>  
(Proc. Paper 1436)

SYNOPSIS

The Deas Island Tunnel is being built for the British Columbia Toll Highways and Bridges Authority to provide an urgently needed second highway crossing of the Lower Fraser River near Vancouver, B.C. The decision to proceed with a second crossing of the river was based on a report prepared by Provincial Government authorities which indicated that existing facilities were being severely overtaxed and that additional crossings were required to match the growth in commercial, industrial and residential use of land in the greater Vancouver area.

This report, prepared in 1953, was followed by reports by several engineering firms which covered studies of alternative crossings of the river. Consideration of economics and of the development of traffic patterns indicated that the construction of a subaqueous tunnel at Deas Island in the vicinity of Ladner, B.C., was extremely desirable. The tunnel design is such as to provide maximum efficiency in the handling of vehicular traffic and minimum interference with the natural flow of the river and passage of water-borne traffic.

The construction of subaqueous vehicular tunnels by the sinking of shore-built elements is well known, and a number of large tunnels have been built in this manner. The Deas Island Tunnel design is patterned after that of the Maas Tunnel which was the first tunnel of rectangular cross-section to be supported on sand fill jetted under the tunnel elements to form a uniform and reliable support. The major advantage of the rectangular cross-section over the circular cross-section is the fact that shallower tunnels of equal horizontal capacity can be constructed in this way. This reduces the amount of dredging necessary and permits of more gentle gradients in the tunnel profile.

Note: Discussion open until April 1, 1958. Paper 1436 is part of the copyrighted Journal of the Structural Division of the American Society of Civil Engineers, Vol. 83, No. ST 6, November, 1957.

- a. Presented to the joint meeting of the American Society of Civil Engineers and the Engineering Institute of Canada at Buffalo, New York, June 5, 1957.
1. Exec. Vice-Pres., Foundation of Canada Engineering Corp., Ltd., Montreal, Quebec, Canada.
2. Christiani and Nielsen.
3. Foundation of Canada Engineering Corp., Ltd., Montreal, Quebec, Canada.

As a preliminary step in the design of the tunnel detailed site investigations were carried out to obtain information for use in the structural design and in the planning of the construction methods. Fourteen boreholes were made as well as dynamic penetration tests and permeability measurements. Hydraulic investigations consisting of tide recording and measurement of velocities and discharges and determination of salt water intrusion and bed load transport are continuing. Such studies are of major importance in a delta area and in a river effected by tidal movements. In addition to the site investigations, hydraulic model tests were carried out in order to determine the drag forces acting on a tunnel element before and after sinking. The results of these investigations confirmed previous calculations of horizontal forces and supplied further knowledge concerning the vertical forces as well as information on the flow velocity below the tunnel when it is resting on the temporary foundation blocks.

In general, the tunnel consists of an 1800 foot long approach on the Lulu Island or north side, a 2100 foot subaqueous section consisting of precast elements and an 1100 foot approach on the Deas Island or south side. The approach structures are in the form of concrete troughs which retain earth and water so as to keep the roadway free from earth slides and seepage and have cantilevered slabs extending under the earth to provide safety against uplift since the structure is almost wholly below the water table. The approaches have been designed to provide fast, safe transition from the normal highway level to the level of the subaqueous portion of the tunnel and to provide protection against flooding of the tunnel by ground water or by general flooding of the surrounding terrain.

The tunnel proper is built up of six elements each approximately 344 feet long, 76 feet wide, and 25 feet high. The reinforced concrete elements, properly protected by a waterproofing membrane which covers all surfaces, will, when in place, provide four traffic lanes, each 12 feet wide with a vertical clearance of 14 feet. The two 2-lane roadways are separated by a longitudinal partition wall and are flanked by two ventilation ducts which run the entire length of the tunnel.

The subaqueous portion of the tunnel will be founded on sand fill which will be jetted under the elements after they are in place. The river bed and banks in the vicinity of the tunnel will be protected to prevent scour which could result in uncovering of the tunnel and perhaps even in undermining of the structure. The ventilation buildings, the most prominent parts of the whole tunnel, form the joints between approach structures and the subaqueous portion of the tunnel, act as dams against the river, retain both earth and water and in addition are designed to house the main fans for the tunnel and the necessary equipment for the control of the ventilation, lighting and traffic.

Inasmuch as the tunnel is located in a Zone 3 earthquake area it was necessary to base the design on the possible effects of forces generated by earthquakes. Careful investigation and theoretical consideration showed that a limit of 21 per cent of the force of gravity was the maximum which could ever be transmitted by the soil to the structure and this force was used in the design of all portions of the structure. The design of the trough-like approach structures was based on a limit design principal because of the shape of the structure and the nature of the surrounding soil. The design of the ventilation buildings is characterized by the application of the principles of the design of buttresses for dams except that in this case the buttresses are located on the

upstream side of the ventilation building. Detailed studies of the reinforcing of these buttresses permitted great savings in steel and concrete quantities.

The design of the tunnel elements which will form the subaqueous portion of the structure was based on the Hardy Cross moment distribution method for the cross-section and on consideration of the bending moments which would occur in the longitudinal direction of the elements during the sinking operation. The features of this design were the consideration of a sinusoidal loading condition because of the occurrence of dunes which move down the river bed at the rate of about 250 feet a day. These dunes reach an amplitude of 15 feet and a length of 500 feet so that their presence is of major importance to the structural stability of the subaqueous portion of the tunnel.

The construction of the tunnel elements is carried out in a drydock excavated at the bank of the river and kept dry by the use of a wellpoint pumping system. Similarly, the approach structures are constructed in open cut kept dry by wellpoints. On the Lulu Island side the excavation of the approach area was carried out in the dry with draglines, dewatering being done in successive stages as excavation proceeded. On the Deas Island side the excavation is being carried out by means of suction dredges with dewatering planned to follow cofferdamming of the area. The ventilation buildings will also be built in the dewatered open cuts.

When all of the six tunnel elements have been constructed and have been bulkheaded against the entrance of water the drydock will be flooded by opening the channel to the river and the elements will be floated out one at a time to the fitting-out jetty and from there to the site where they will be sunk. While the elements are being equipped with the various equipment to be used in the sinking operation a trench will be dredged in the bottom of the river sufficient to take one element and a carefully laid gravel pads will be placed to receive the temporary foundation blocks which are suspended below the elements. Gentle side slopes on the trench, together with the selection of a period of rather low flow in the river will enable the crew to keep the trench open sufficiently long for the placing of an element.

When the temporary foundation blocks are securely on the bottom the tunnel will be accurately placed by means of cables running to anchors in the river and by means of hydraulic jacks protruding from the element and touching on the foundation blocks.

The ends of the tunnel elements are provided with exterior reinforced concrete collars, rubber gaskets and hydraulically operated hook and eye arrangements which will permit of the sealing of one unit to the one previously placed so that water may be drawn out of the small chamber between bulkheads of adjacent elements and workmen may enter and complete the connection of the two elements by joining waterproofing membrane, reinforcing steel and concrete. When a tunnel element has been placed the sand fill will be jetted underneath it and the entire trench will be back-filled and covered by a protective layer which will prevent scour and increase the safety against uplift.

At the present time construction is proceeding on schedule and no major difficulties are foreseen which may interrupt the work in the future.

## INTRODUCTION

Before discussing the planning and design of the Deas Island Tunnel it seems reasonable to outline the conditions which necessitated the construction of this new highway crossing of the Lower Fraser River.

The Deas Island Tunnel is being built for the British Columbia Toll Highways and Bridges Authority to provide an urgently needed second Highway crossing of the Lower Fraser River.

The City of Vancouver has, at present, a population of about 350,000. The Vancouver-New Westminster metropolitan area, with an annual rate of population growth of nearly 5% in recent years, is one of the fastest growing communities in North America and now has a population of approximately 650,000, more than half the total for the Province as a whole.

As shown on this figure, Vancouver is located in a beautiful natural setting, hemmed in to the north and east by high mountains and to the west by the Strait of Georgia.

To all practical purposes, its location makes Greater Vancouver the west coast Canadian terminal for traffic coming from the east and south. It will be seen on Figure 1(b) that access to Vancouver by land is limited. The geography requires that most traffic must enter and leave the city from the south and southeast sides and therefore, must cross one or more arms of the Fraser River.

## Historical Background

In 1903 the first permanent crossing of the Lower Fraser River was effected by means of a combined highway-railway bridge at New Westminster. This was followed, in 1912, by the introduction of a ferry service at Ladner in place of the bridge asked for by a Delta Municipality citizens' group formed in 1910.

The growth in vehicular traffic channelled over the New Westminster Bridge reached such a stage by 1925 that it was apparent some increased facilities were warranted. In the light of this, steps were taken by the Provincial Government to ensure future development of routes through the efforts of two private bridge companies. However, after preliminary moves toward a crossing at Deas Island, governmental support was withdrawn and in 1933 the project stalled.

Finally, in 1937, the Pattullo Bridge was opened, replacing the highway portion of the New Westminster span and purporting to be capable of handling peak traffic of 3000 vehicles an hour in one direction. By 1953 this route was near saturation and studies were initiated to determine the future need for highways and river crossings. The report resulting from these studies was directed to both immediate and long-range solutions of the problem of highway communication. This report recognized that the overtaking of existing facilities had made it imperative to construct additional crossings over the Lower Fraser River to match the growth in commercial, industrial and residential use of land in the Greater Vancouver area.



Figure 1(a) — Oblique aerial view of Vancouver

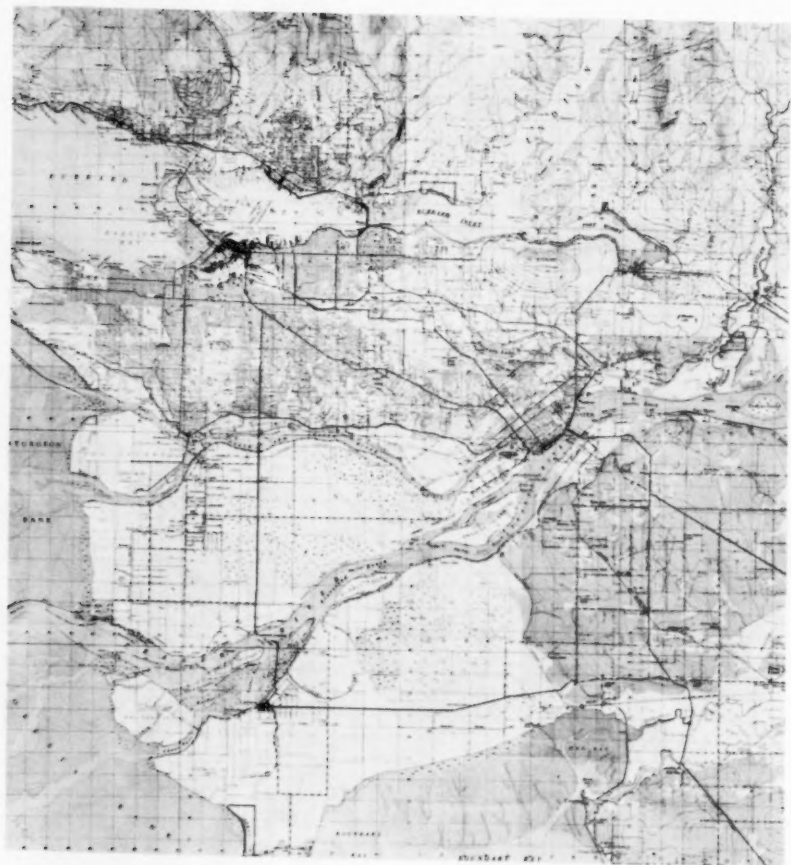


Figure 1(b) -- Topographic map



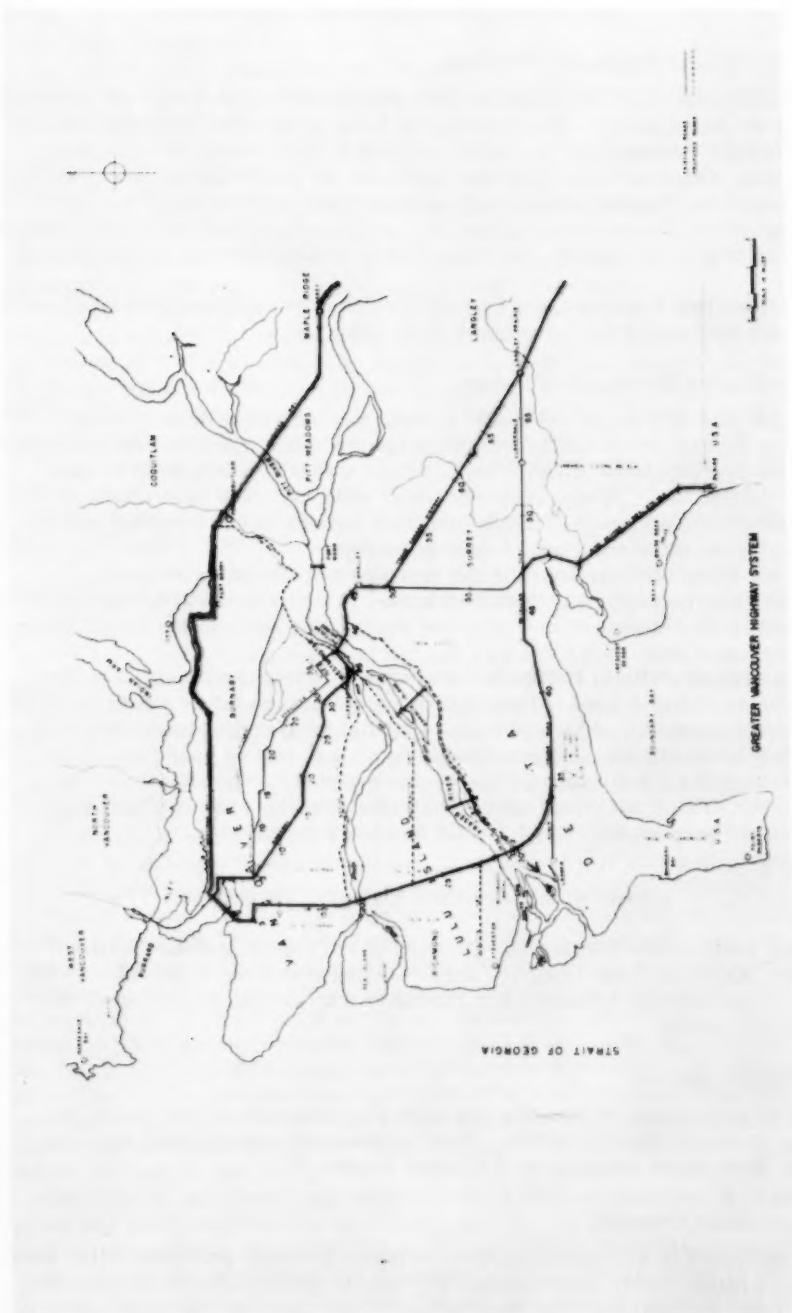


Figure 3 -- Map with superimposed radial highway system

## Present and Future Traffic Requirements

### Present Traffic Routes and Volumes

At this time only two crossings over the Lower Fraser River are provided for north/south traffic. The principal of these is the Pattullo Bridge linking the Burrard Peninsula to the lower mainland at New Westminster. On the peninsula, Kingsway and Granview Highways tie the bridge to downtown Vancouver via Burnaby while the Coquitlam Road leads to the east of New Westminster. The second crossing is a ferry between Ladner and Woodward's Landing on No. 10 Highway, the only highway leading directly south from the city.

Of these two crossings, the Pattullo Bridge carries 96 per cent of the traffic while the Ladner Ferry serves only 4 per cent.

### Future Traffic Routes and Volumes

In the past five years the traffic volume has increased by an average of 12 per cent a year. Forecasts of the increase in vehicle numbers and use, based on predicted population growth, indicate that within 20 years an average of about 100,000 vehicles will cross the river each day. The peak traffic at that time would probably exceed 10,000 vehicles an hour in one direction and require at least three additional 4-lane crossings.

Under these circumstances it has been deemed advisable to develop, through relatively sparsely populated areas, routes which will be capable of handling large volumes of traffic and of redirecting some of the traffic using the existing routes.

The present Pattullo Bridge has encouraged development near it on the south shore of the Fraser. Thus in order to encourage future development to effectively utilize all of the south shore land closest to downtown Vancouver, it is suggested that the next crossing to be built should be considerably removed from the existing one. This would be another step towards providing Vancouver with an additional spoke in a radial highway system which seems to offer the best solution to the traffic problems in this area.

## Crossing Locations and Highway Connections

Four routes were considered, crossing at Port Mann, Annacis Island, Tilbury Island and Deas Island. These crossing points were chosen because they are shorter and probably less expensive than crossings located at intermediate points.

### Port Mann Crossing

There is a practical crossing site near Port Mann about four miles upstream from the Pattullo Bridge. This location has recently been selected for the third major crossing of the Lower Fraser.

### Annacis Island Crossing

Construction of a crossing at Annacis Island presents problems which would make it a rather costly undertaking. A bridge in this location must span the entire river width to keep the Annacis waterfront clear for the establishment of harbor facilities which will be required by industrial developments on the



Island. This would necessitate the adoption of a suspension bridge with a 1,600-foot main span.

A tunnel would be costly because the south approach is from very high ground. This would necessitate long, expensive approaches either up onto the heights or around them.

#### Tilbury Island Crossing

Tilbury Island offers a third possible location for a crossing. Because of the topography of this area, the highway connections to the crossing would run through the peat bogs both in Delta and on Lulu Island. This would make construction of the main roads and access roads expensive.

On such a route, traffic would be hampered by the periodic fogs to which the area is subjected. The fact that vessels often anchor in the deep basin in the Fraser at Tilbury Island when fog rolls in, makes the erection of piers or ventilation towers in the waterway at this point inadvisable. Thus bridge spans and tunnel lengths would have to be great enough to place these parts well outside the channel and consequently construction costs would be high.

The crossings at Annacis and Tilbury Islands were ruled out at this time on account of their relatively high costs and, more important, because the locations were considered to be too close to the existing Pattullo Bridge for the second major crossing.

#### Deas Island Crossing

The fourth possible location is at Deas Island.

This route would form the most westerly spoke of the radial highway system already discussed.

It is felt that this crossing and its connecting arteries will effect a change in the pattern of growth of Greater Vancouver by opening a new area for development. Although the Delta area has been considered as reserved for agricultural use, it is believed that controlled suburban and industrial development should be given serious consideration.

The need for reconsideration of the present ideas on regional planning and land use is indicated by the development presently under way in Richmond which has also been considered as reserved for agricultural purposes.

Figure 3 shows travel time intervals for the existing route via Pattullo Bridge and for the proposed route via Deas Island. These intervals are plotted from a selected centroid in the downtown Vancouver area and represent the distance travelled by a vehicle in successive five-minute intervals. In order to establish these intervals it has been assumed that the average vehicular speed on the Burrard Peninsula, regardless of route, is 20 m.p.h. South of the Pattullo Bridge the average speed is assumed to be 35 m.p.h. while south of the Oak Street span it is assumed to be 40 m.p.h. On the basis of these assumptions, it appears that it would be faster for vehicles travelling between Vancouver and White Rock, the U.S.A., Delta, Cloverdale and Langley, to follow this new route.

Since the route offers rapid access to the Boundary Bay area, it is anticipated that much recreational traffic will use it.

In summary then, the construction of a crossing at Deas Island would be a major step in the development of a highway system ideally suited to the Greater Vancouver area. The route developed in connection with this crossing

will be attractive for a considerable part of the traffic which would otherwise use the Pattullo Bridge and, by opening a new area for development, will re-channel regional development, thus ensuring a more equal distribution of traffic in the future.

### Physical Conditions Governing Design of the Crossing

#### Local Topography

The area in which the Deas Island crossing and its connecting road system will be located is extremely flat, low lying and bare of timber. Dykes along the river from Annacis Island downstream to the mouth prevent flooding of Lulu Island and Delta. These dykes are 6 feet above the land in nearly all places. There are large peat bogs reported to be about 3 feet deep on Lulu Island and about 12 feet deep in Delta. Fortunately the Deas Island system crosses the bog only on Lulu Island, thus avoiding major construction difficulties.

#### Soil Conditions

Boring records available at the time of the preliminary study indicated a heterogeneous soil structure consisting of sand, silt and clay. There appeared to be little uniformity of the strata either in occurrence or in degree of compactness. The sand was loose to very loose. These conditions suggested that considerable settlements might occur.

It was recognized that a tunnel at this site would not impose any significant loads on the foundation material. However, it was felt that during construction the trench dredged for the placing of the tunnel sections might require either rather flat side slopes or small auxiliary trenches on the upstream side to prevent refilling during the work.

On the other hand, the soil conditions were deemed to be less favourable to bridge construction at this location, as heavy piers on a compactible material would be subject to differential settlements. These settlements would result in movement of the superstructure which would have to be anticipated in the design or corrected after erection.

#### River Hydraulics

The site of the proposed crossing is well within the limit of the tidal variation which so markedly affects Fraser River discharge. Information available in the early stages of the study showed the normal tidal range at Ladner Reach to be about 6 to 8 feet and the actual water level range to be about 11 feet because of the effects of variation in fresh water discharge. During the winter months river discharge at Hope, B.C., approximately 60 miles upstream from the site, is small, approximately 21,000 cubic feet a second, with a minimum of 12,000 c.f.s., but during the spring freshet a discharge of 536,000 c.f.s. has been recorded. This discharge is supplemented by outflow from various lakes downstream from Hope, but is again offset by diversion of flow through the Fraser River North and Middle Arms.

Tidal flows superimpose important daily variations on these discharges. Because of the tidal action, the maximum velocity of river flow may be 7 f.p.s., or may be negative by up to 3 f.p.s.

The current in the river, combined with the nature of the bed material,

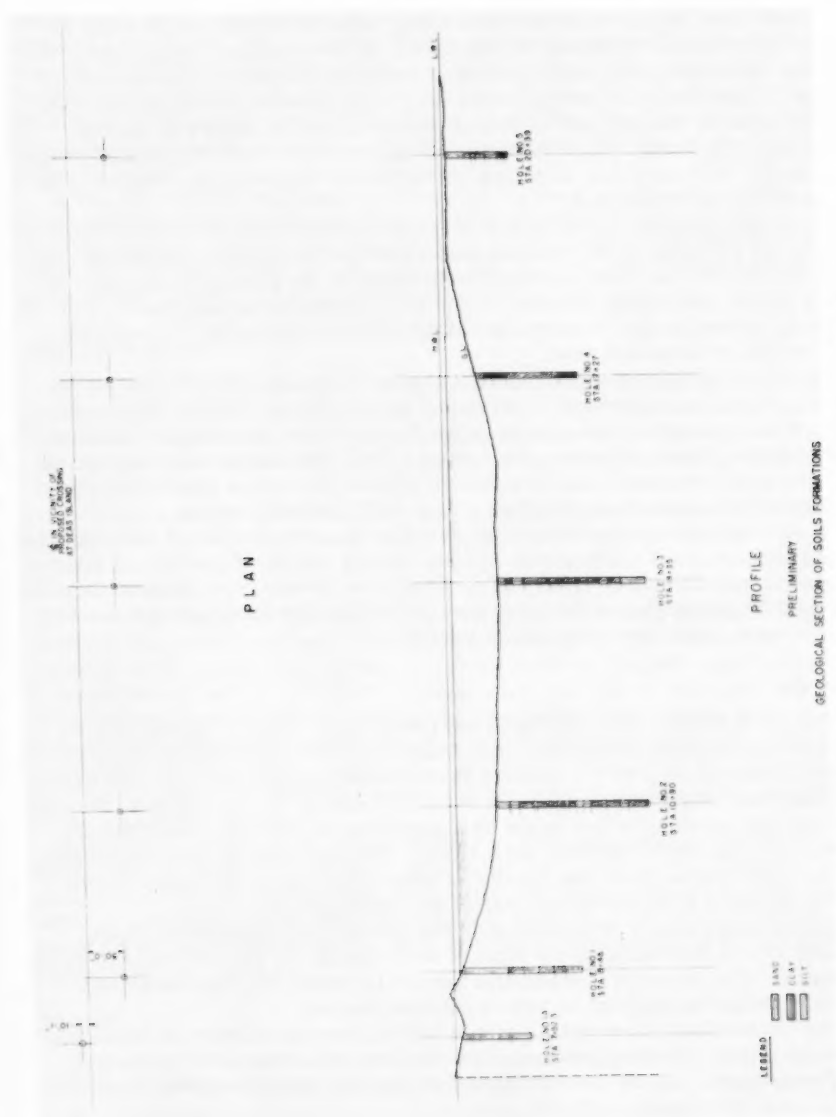


Figure 5.2 – Geological section of soil formations

gives rise to considerable scour and fill action. A portion of the material is transported in suspension while the bed load forms dunes along the channel. These dunes have reached an amplitude of 15 feet with a length of 500 feet and may move downstream at a rate of up to 250 feet a day.

Aside from this general bed movement, there occurs the scour usual in restricted channels at times of high water, at the outsides of bends and downstream of bridge piers, with occasional sedimentation where the channel widens. However, this normal scour may be accentuated in the Fraser estuary because of the extreme discharge variation and the nature of the bed material. Certainly it is to be expected that the river bed will require protection in the vicinity of any structure placed in the current if the adverse effects of scour are to be avoided.

Although the river is not free to meander because it is constrained by dykes and revetments, the erosion pattern alters from season to season. Interference with the river, such as the blocking of the passage at the back of Deas Island, the partial blocking of the Annacis channel around the back of Annacis Island and the construction of the Pattullo Bridge piers, produces significant deviations of flow.

The official hydrographic sounding charts which are available for many years give a good indication of maximum scours during flood with the exception of local scour around islands and extra depth due to passage of high bed dunes during flood. However, the contours show the general maximum scour pattern quite accurately and this pattern follows the course generally to be expected from experience on other rivers and hydraulic models.

It was obvious that any structure placed in the river bottom at this crossing would require special protection. Present plans call for protection of river banks for approximately 1,400 feet upstream and downstream from the tunnel site and for protection of the river bottom for 150 feet upstream and 200 feet downstream from the centre line of the tunnel.

### Climate

The local climate is rather mild and very damp. Over a 38-year period the average extreme maximum temperature was 80°F while the average extreme minimum was 15°F. January is the coldest month, with average daily minimum and maximum temperatures of 32°F and 41°F respectively. Despite the low temperatures which might be experienced during the winter months, there are about 200 frost-free days a year. The mildness of the climate precludes appreciable ice formation on the lower reaches of the Fraser River except during the infrequent periods of low temperature.

The average annual precipitation in the Ladner area amounts to 36.45 inches, 16.4 inches being in the form of snow during the period from November to March. The heaviest precipitation occurs in November, December and January, while the lightest occurs in July and August.

The prevailing wind is from the east with an average maximum velocity of about 10 m.p.h. However, storms from the ocean do occur with winds of hurricane force. These are infrequent, as are periods of complete calm.

### Design Requirements

#### General

Because marine traffic is expected to increase on the South Arm of

the Fraser River, any structure crossing the river must permit unhampered navigation by ocean-going vessels.

While the present navigation channel is only dredged to 22 feet below low water level, it is assumed that this depth might be increased to 26 feet 6 inches in the future. While the navigation channel is presently maintained to a width of only 300 feet, it is economical to allow for some variations in its location from year to year and for this reason it was decided that any structure built at the Deas Island crossing would have to allow for a channel width of not less than 1,200 feet and a vertical clearance of 145 feet above the high water level for the full channel width.

It was not possible to determine from the outset of our investigations whether a high level bridge or a tunnel under the river would provide the most suitable arrangement from the viewpoint of traffic, capital cost and cost of operation. To settle this question, comparative designs for a high level bridge and a tunnel were developed in the early stages of the studies.

### High Level Bridge

As indicated in Figure 6.2, a suspension bridge was developed with a main span of 1,200 feet and flanking spans of 480 feet each. The bridge was designed for four lanes of traffic with a width of roadway of 48 feet from curb to curb and one sidewalk 5 feet wide on the downstream side for pedestrian traffic.

To clear a height of 145 feet over the shipping channel without exceeding a maximum grade of 3.5 per cent, nearly 4,000 feet of approaches were required on each side of the bridge so that the overall length of the bridge would be over 10,000 feet.

For the purposes of this paper it is unnecessary to enter into details of the design of the superstructure of the suspension bridge. The design and construction of the main piers and of the anchor piers on the soft delta formations presented various problems, among which was that of the considerable settlement of these structures which could be anticipated. These settlements, although of a high order, would probably occur rapidly upon the imposition of loads during construction of the pier caissons. The effects of any further settlements would be relatively small and could be compensated by adjustment of the suspender cables.

Notwithstanding the fact that the bridge and its approaches were developed with a definite view to economy, it was found that a high level bridge would cost close to twenty million dollars to build. With the increase in steel prices which has occurred since this investigation, three or four million dollars could safely be added to this figure to present a realistic basis for comparison between the two projects.

### Tunnel

The physical conditions at the Deas Island crossing are favourable for the construction of a tunnel by the trench method.

As illustrated in Figure 6.3, this concrete structure consists of open approach sections, ventilating buildings and a subaqueous tunnel section which is constructed from 6 shore-built elements. Cost estimates indicated that this type of tunnel could be completed and equipped for automatic operation for approximately seventeen million dollars, a saving of 15 per cent over the

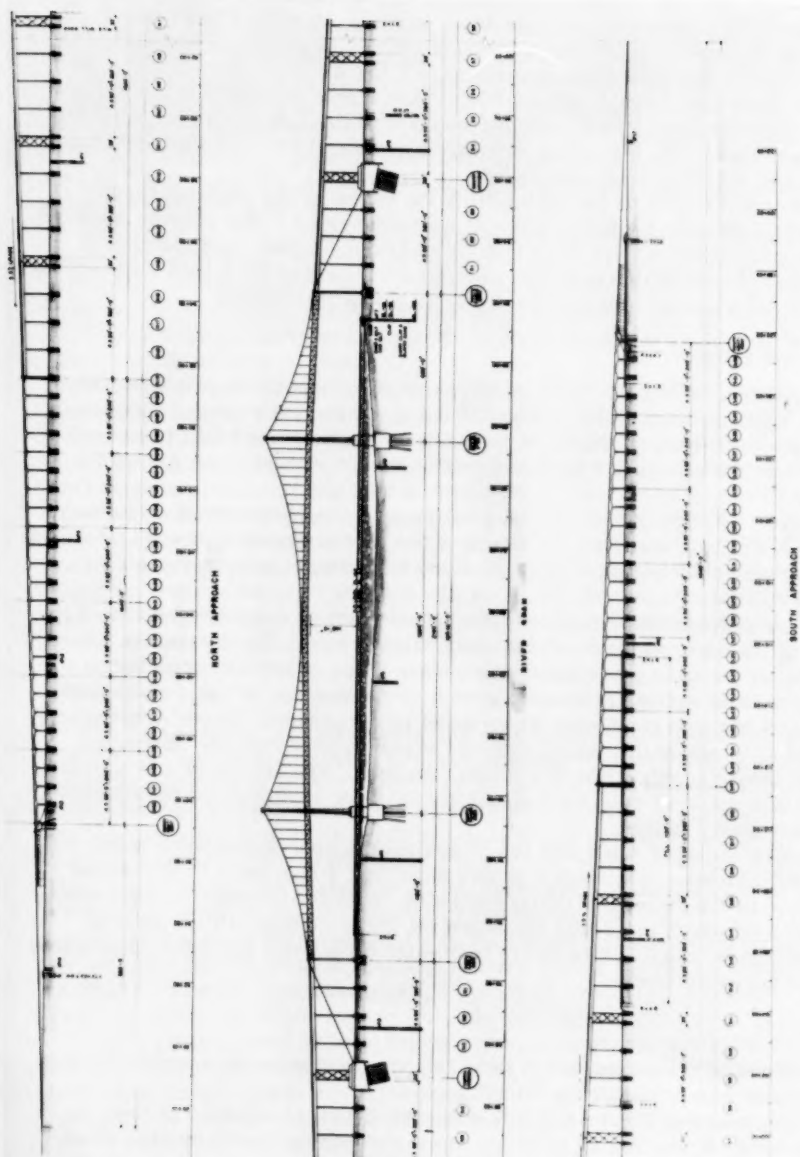


Figure 6.2 — General arrangement, suspension bridge

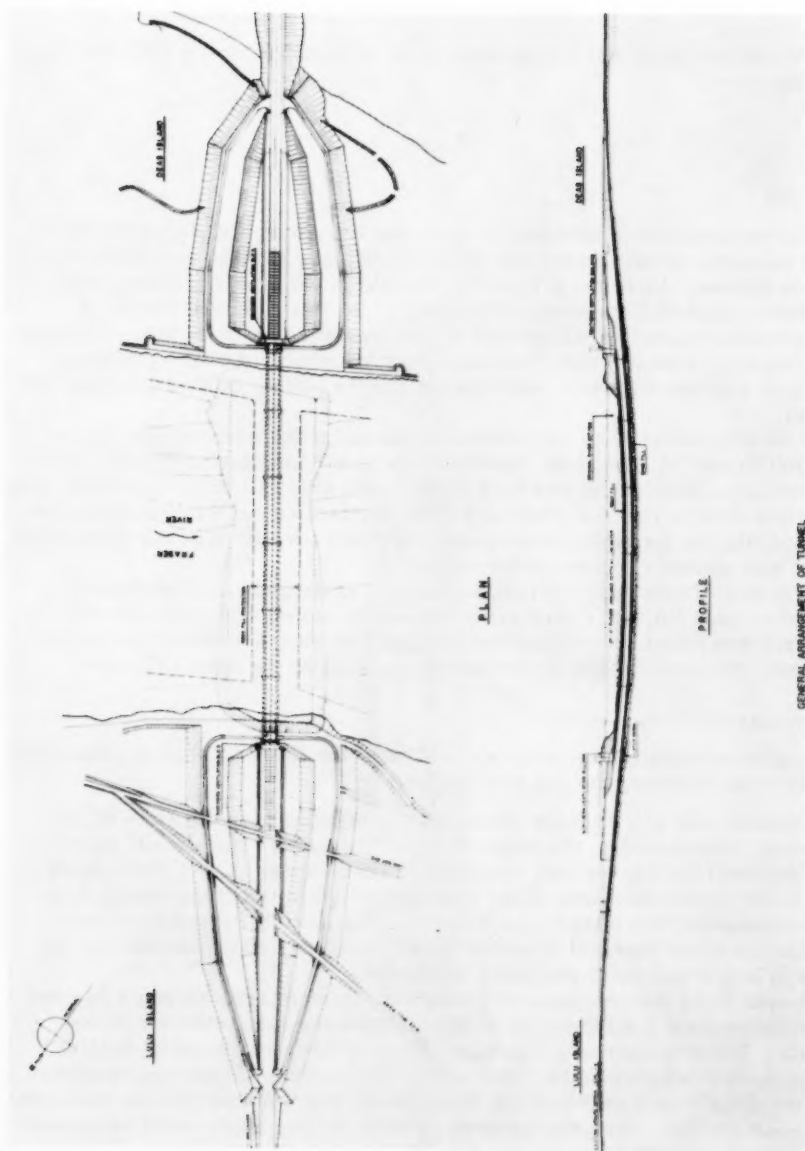


Figure 6.3 — General arrangement of tunnel



cost of a high level bridge. As already mentioned, subsequent increase in steel prices has further widened this cost differential in favour of the concrete tunnel.

Cost of operation and maintenance is of the same order for both the bridge and the tunnel.

## Tunnel

### General

The construction of subaqueous vehicular tunnels by the sinking of shore-built elements is well known, and a number of large tunnels have been built in this manner. Up to the time of the building of the vehicular tunnel under the River Maas at Rotterdam, 1938-1942, which was also constructed of prefabricated elements, all tunnels of this type were designed with a circular or octagonal cross-section. One particular reason for the choice of these sections was that they were well adapted for the placing of sand fill under the tunnel.

A notable exception to circular and octagonal tunnels of this type is the Harlem Tunnel at New York, which is rectangular, measuring 76 feet wide by 25 feet high. This tunnel was built in the years 1913 and 1914 of prefabricated elements sunk in line and connected. The Harlem Tunnel was not supported on sand fill, but the space between the tunnel and the bottom of the trench was filled with concrete, poured under water.

The Maas Tunnel was the first tunnel with rectangular section to be supported on sand fill, and Christiani & Nielsen developed a method whereby the sand fill was jettied under the tunnel elements to form a uniform and reliable support. The Deas Island Tunnel design is based on the same principle.

### Comments on Cross-Section

The rectangular cross-section, see Figure 7.2, has a number of advantages, of which the following are the most important:

The diameter of a circular cross-section depends upon the width of the roadway. Consequently, the height of the cross-section will usually be more than required for the vertical clearance of the roadway. For a given depth of water and a given thickness of the rock protection on top of the tunnel, this necessitates that the level of the roadway in the case of a circular cross-section, be lower than that required for a rectangular cross-section and results in longer and more expensive approaches.

In case more than two lanes are required, these drawbacks would be even more pronounced if all lanes were placed within the same circular cross-section. For this reason, a four-lane tunnel of this type should be designed rather as two independent two-lane tubes. This solution, however, requires a width of the trench considerably in excess of that required for one rectangular cross-section. Also, the distance between the roadways would be greater than for one rectangular cross-section and consequently the width of the approaches would be considerable unless horizontal curves were introduced on the roadways. However, the latter solution is not satisfactory from a traffic point of view.

Furthermore, access doors for emergency escape and maintenance crew



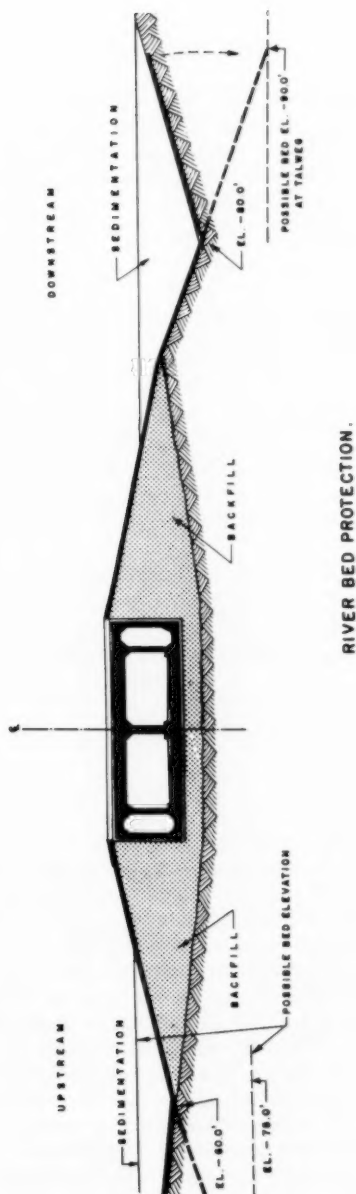


Figure 7.2 - Rectangular cross-section of tunnel in place

interchange travel cannot be provided if the tunnel consists of two separate parallel tubes.

### Site Investigations

Detailed site investigations have been carried out in order to obtain information for use in the structural design as well as for the planning of construction methods. Fourteen boreholes were made, as well as dynamic penetration tests and permeability measurements. Hydraulic investigations consisting of tide recording, measurement of velocities and discharges, and determination of salt water intrusion and bed-load transport are continuing.

### Soil Investigations

The borings were made near the future tunnel line and in the areas of the approaches and the drydock required for the construction of the six tunnel elements and were carried out under the direction of Ripley and Associates, Consultants.

The boreholes were lined with 4-inch casings and samples extracted with thin-walled open samplers with diameters of 2-inches, or 3 inches. The subsoil consists of loose sand and silt layers below ground level. It was, therefore, found necessary to introduce drilling mud, a heavy viscous fluid, into the boreholes in order to prevent the samples from slipping out of the thin-walled open tube samplers.

A pumping test, which is, in fact, a small scale ground water lowering, was carried out in order to determine the permeability of the sand layers. In addition, several field permeability tests were carried out in cased boreholes by raising the water head within the casing and observing the subsequent fall in the water level.

The penetration tests were carried out in accordance with the standard penetration test described by Terzaghi & Peck in "Soil Mechanics in Engineering Practice".

### Hydraulic Investigations

The absence of any detailed prior records of river behaviour at this particular location made it necessary to initiate complete hydraulic investigations on the site. A permanent water level recording station was established adjacent to the proposed site to provide continuous records of water level over at least one full annual cycle. These records, combined with measurements of the velocity of flow, are invaluable in the design of the tunnel and the river bed and bank protection and in the planning of the construction operation.

In order to obtain accurate information on the effects of siltation on the trench which is to be excavated for the placing of the tunnel elements a trial trench was dredged in the river. Periodic soundings provided data on the speed of siltation and indicated the side slopes necessary to ensure the stability of the trench during construction. On the basis of these siltation studies it appears that the trench side slopes will be stable for a sufficient length of time if they are cut to 1:8 upstream and 1:6 downstream.

Measurements of salt water intrusion at the site were made and revealed the existence of a salt water wedge. The presence of salt in the water has necessitated the consideration of possible corrosive action as well as of the influence of the denser water on the sinking of the tunnel elements.

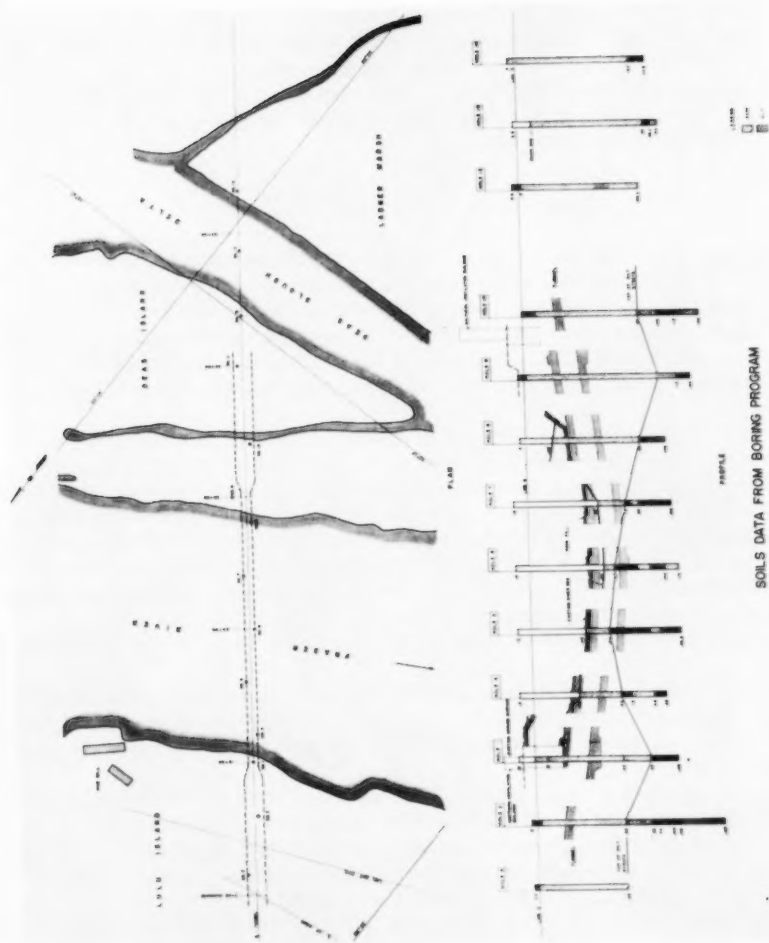


Figure 8.1 -- Boring Plan

## Model Tests

Hydraulic model tests were carried out in order to determine the drag forces acting on a tunnel element before and after sinking. The model testing took place at the Hydraulic Laboratory of the Technical University of Denmark and was carried out in an experimental flume, 50-feet long by 7.2 feet wide.

A plexi-glass model of a tunnel element, in scale 1:70, was placed in the flume and all forces and moments acting on it were measured by spring dynamometers or by strain gauge dynamometers.

The results confirmed the previous calculations of the horizontal forces and supplied further knowledge concerning the vertical forces (downward forces when the element is floating and upward when it is near the bottom), as well as information on the flow velocity below the tunnel when it is resting on the temporary foundation blocks.

## Deas Island Tunnel General Layout

An elevation of the tunnel, including the open approaches, is shown in Figure 6.3. It will be seen from this drawing that the length of the tunnel proper has been reduced to a minimum by extending the approaches at both ends right out to the river banks. This arrangement considerably facilitates the ventilation, lighting and inspection of the tunnel. All horizontal curves have also been avoided purposely to make passage of vehicles and inspection easier.

The tunnel proper is constructed of shore-built elements which are sunk in line into a dredged trench and connected. Once the units are in position, the trench is refilled with sand and covered with a protective layer, which also covers the top of the tunnel, as shown in Figure 7.2. This layer will be so designed and constructed as to provide protection against scour down to 75 feet on the upstream centre line. The purpose of this layer and of the protective works planned for the river banks is to prevent undermining of the tunnel and to reduce the turbulence which might otherwise accompany a change in river cross-section. Design of the protective works is still under study.

The subaqueous tunnel is placed at a level to give the following clearances over the tunnel for a future channel:- 31-feet 6-inches over a width of 1,400 feet, 36-feet 6-inches over a width of 1,000 feet and 40-feet 9-inches over a width of 700 feet.

Figure 9 shows a cross-section of the tunnel. There are four traffic lanes, each 12 feet wide, with a vertical clearance of 14 feet. The two 2-lane roadways are separated by a longitudinal partition wall, the sides of which are sloped to improve acoustics. A bituminous road-surfacing has been chosen because of its smoothness, ease of repair and sound-damping qualities. The two ventilation ducts, which run the entire length of the tunnel, are placed on the outer sides of the roadway tubes.

The tunnel proper is built up of six elements, each approximately 344 feet long. A properly protected waterproofing membrane, covering all surfaces of the subaqueous tunnel is connected to similar water-proofing membranes on the subsoil surfaces of the ventilation buildings and retaining walls.

The waterproofing membrane for the tunnel elements consists of a 3/16" steel plate under the bottom slab and a bituminous membrane of the built-up

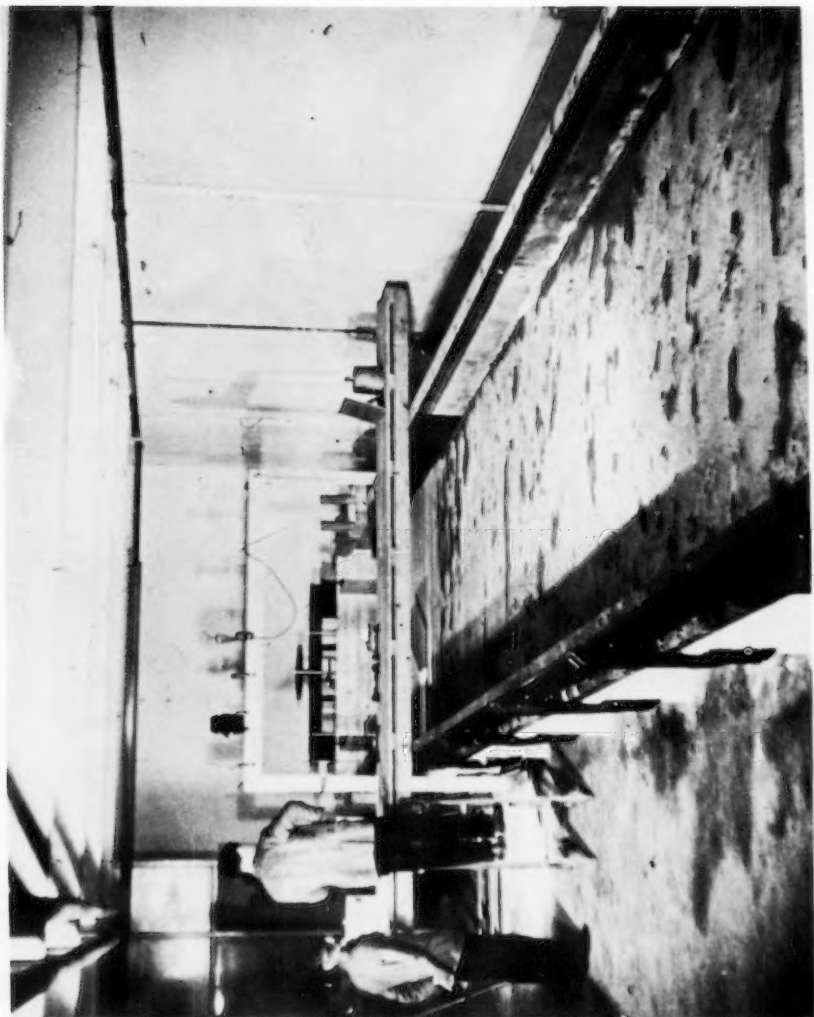


Figure 8.3 (a) — Experimental Flume

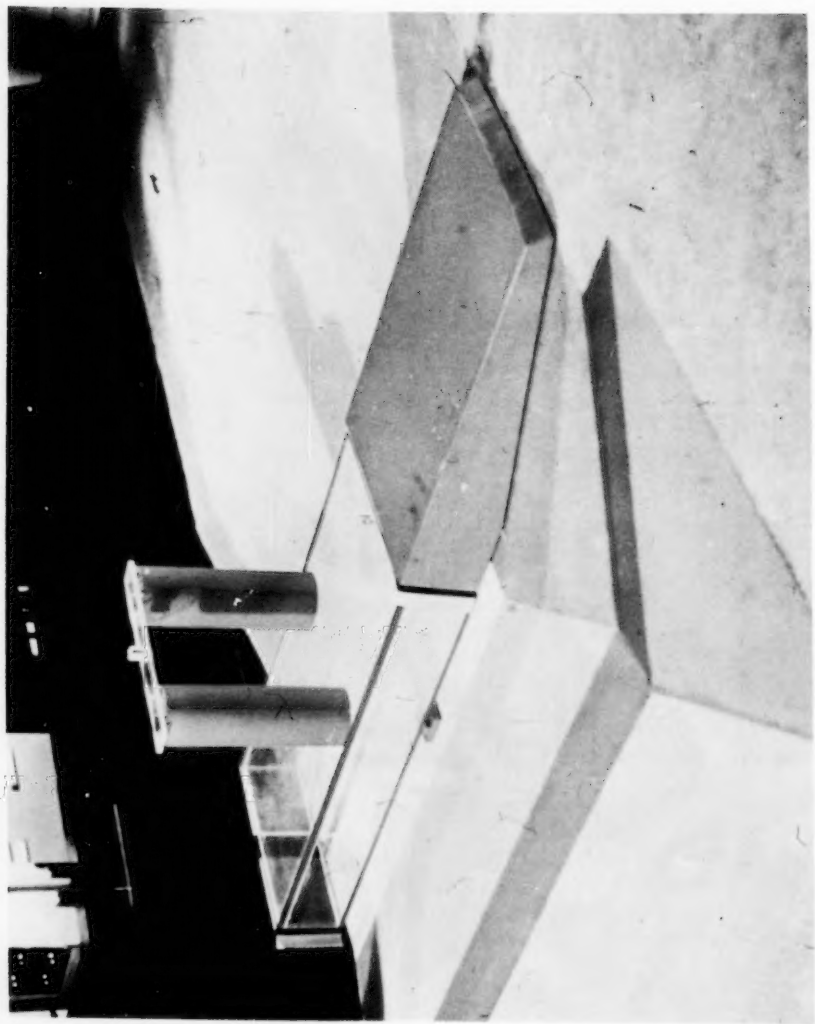


Figure 8.3(b) -- Plexi-glass Model

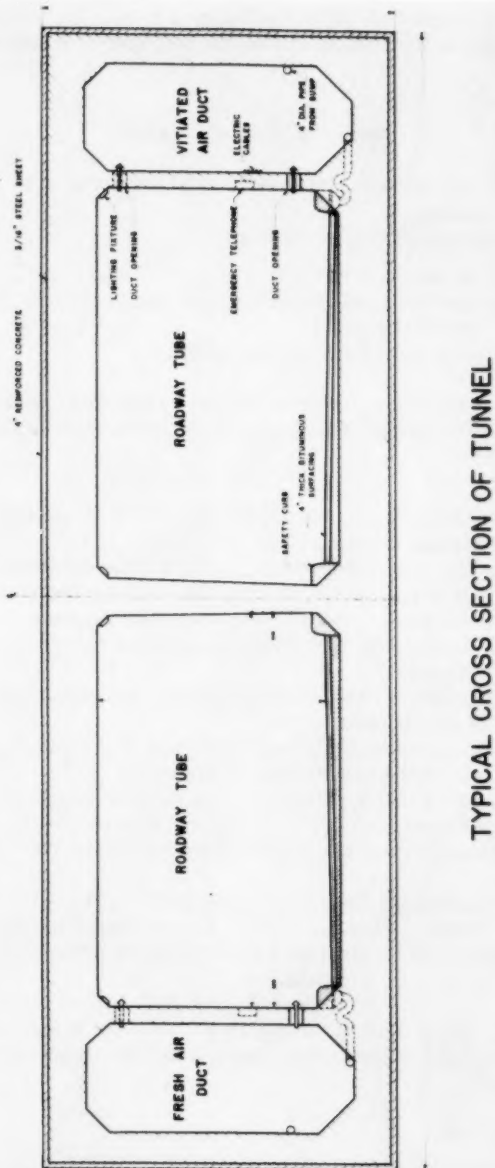


Figure 9 -- Rectangular Cross-Section

type on the major portion of the walls and the roof, which is replaced with 3/16" steel plate for a distance of 11 feet at each end of the tunnel elements. The waterproofing membrane is protected by a 4-inch thick layer of reinforced concrete under the bottom and on the top, and by 4-inch wood planking on the walls.

### Design of Tunnel Sections

The structural calculations were made in accordance with the National Building Code of Canada.

The loads on the tunnel are the following:

- a) Deadweight of tunnel.
- b) Water pressure corresponding to a high water level of 6 feet 0 inches (Geodetic Survey Datum).
- c) Rock fill and sand deposits on the tunnel.
- d) Soil reaction.
- e) Frictional forces, i.e., vertical forces on the outer walls of the tunnel, caused by differential settlements of the ground below and outside the tunnel.
- f) Earthquake loads.

For ordinary loads, items a) to d), the allowable stresses were computed according to the National Building Code of Canada.

A minimum 28-day concrete cylinder compressive strength of 3,750 p.s.i., and an allowable unit tensile stress for the reinforcing steel of 20,000 p.s.i. are specified. The vertical reinforcing in the walls between the roadway tubes and the ventilation ducts is of hard grade steel while all other reinforcing is of intermediate grade steel.

For earthquake loads, a limit design principle was developed, as described in a later section of this paper.

The Hardy Cross Moment-Distribution Method was adopted in the analysis of the cross-sections of the precast tunnel elements.

This analysis proved that a uniform cross-section was appropriate for the entire length of the tunnel, and that even the reinforcement could be the same for all cross-sections, except for a few minor variations near the ends of the tunnel.

Number 11 bars are used for main reinforcement, the minimum spacing being 6 inches as shown on Figure 10(b). The number 7 bars used for longitudinal reinforcement correspond to the minimum requirements of the Code since thermal stresses will be moderate.

In the floating tunnel element, bending moments will occur in the longitudinal direction. These bending moments will be kept within the permissible limits by an appropriate placing of the ballast and so do not necessitate additional reinforcement.

### Differential Settlements

According to the subsoil investigations, the layers which are found directly below the future tunnel bottom consist mainly of compressible silt. The influence of the settlements of these layers was, therefore, investigated in some detail. Undisturbed samples were taken from these silt layers by means of



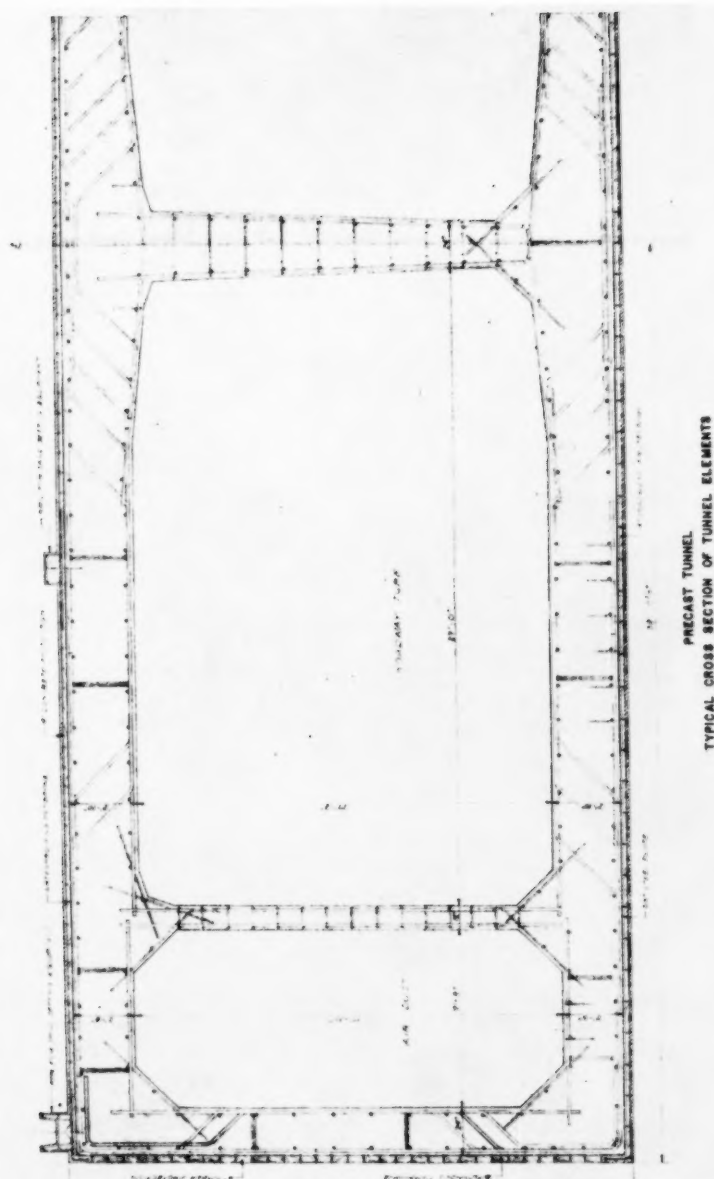


Figure 10(b) -- Reinforcing of tunnel elements

thin-walled tube samplers and Oedometer tests were carried out on the extracted samples as previously mentioned.

As the weight of the tunnel and backfill will be less than the weight of the soil dredged from the trench, the movement of the bottom of the trench will correspond to rebound when the trench is excavated, followed by some re-compression after the tunnel is placed. The anticipated settlements are tolerable.

Soundings have shown that huge sand dunes move down the river bottom and that the river profile at the site is subjected to frequent changes. It is, therefore, expected that the tunnel will be subjected to great load differences in the longitudinal direction which, in turn, will cause differential settlements. From the settlement calculations, it was found that the probable magnitude of the settlements would be 3 to 4 inches.

Considering the tunnel as a beam on elastic foundations, loaded with a sinusoidal load with a maximum corresponding to rock fill plus 20 feet of sand, and a minimum corresponding to rock fill only, the maximum stresses on the uncracked sections will be about  $\pm 300$  p.s.i.

These stresses are fairly high, but due to the fact that the deflection of the tunnel is limited by the settlements of the soil, this loading condition can cause no collapse of the tunnel.

The rather slender tunnel structure as is seen in Figures 6.3 and 9 was designed to be capable of following possible differential settlements without cracking. This called for a shallow cross-section, which was obtained by placing the ventilation ducts within the height occupied by the roadway tubes. The main purpose of this arrangement was, however, to reduce the depths required in the drydock and in the trench.

The backfill on both sides of the tunnel represents a heavier loading on the silt than does the tunnel proper. The corresponding differential settlements result in vertical friction forces between the backfill and the outer walls. These forces were taken into account in the stress analysis and they were calculated by equalizing the elastic deformations of the cross-section and the corresponding settlement of the silt.

### Earthquake Design

The literature on earthquake resistant design of buildings is mainly concerned with structures above ground level. Very little information is available about structures below ground level, and it is generally assumed that these structures are subjected to less damage during earthquakes than structures above ground.

Since the Deas Island Tunnel is located in a Zone 3 area, the effect of earthquakes on tunnels was studied thoroughly. It was concluded that the shear waves resulting from an earthquake would be more serious than the compression waves because the resulting shear forces on the outer surfaces of the tunnel would cause sidesway.

It was found from theoretical consideration that shear waves with an acceleration exceeding 21 per cent of gravity, would cause failure in the soil, consisting, in the present case, of loose saturated sand. This soil would not be capable of transmitting stronger shear waves.

The design was, therefore, based on a maximum acceleration of 21 per cent of gravity. For this acceleration, shear forces equal to 21 per cent of the

over-burden were assumed to be transmitted to the roof of the tunnel. In addition, an increase of the soil pressure on the outer walls of the tunnel to a value corresponding to the pressure from a liquid of the same density as that of the sand, was assumed.

The tunnel was so designed for this loading condition, corresponding to the failure condition in the soil layers, that the stresses exceeded neither the yield point of the steel nor the compressive strength of the concrete.

#### Factor of Safety against Uplift

For the completed tunnel, the factor of safety against uplift, under the most unfavourable conditions, will be 1:16. All loads will be checked during the construction period in order to reveal possible deviations from the design assumptions. If the frictional forces between the backfill and the outer walls were taken into account, the factor of safety against uplift would be 1.28.

### Approach Structures

#### General

While the approaches must be designed to provide fast, safe transition from the normal highway level to the level in the subaqueous portion of the tunnel, they must also provide protection against flooding of the tunnel by ground water or general flooding of the surrounding terrain.

The 1,800-foot long approach on the Lulu Island side shown in Figure 11.1 provides a gentle transition through a drop in the roadway of about 50 feet. The mild vertical curves and the absence of horizontal curves, combined with the wide double roadways and safety curbs, allows traffic speeds up to 80 m.p.h. in extreme cases.

Proper transition from bright sunlight to the lower intensity of lighting in the interior of the tunnel is provided by means of sun screens which extend over both roadways in the lower portions of the approaches. In addition, a central wall running between the roadways for a distance of 420 feet from the portals prevents the passage of vitiated air from one tube of the tunnel to the other.

#### Site Conditions Affecting Design

In the structural design of the approaches, site conditions were studied in order to determine the most advantageous means of meeting the functional requirements. There were three major conditions to be considered. First, the entire area around the approaches is practically level and although it is a few feet above average river stage, it is below high river stages. Second, the soil, as already shown in Figure 8.1, is mainly fine sand and silty sand with a few lenses of silt and clay and results in uneven settlement of structures founded at different elevations as well as rebound after removal of load. Third, quaking of the soil under earthquake shock might cause failure of the structure.

Maximum crown elevation for protection against flooding by the river was established from studies of water level variation. To the maximum flood level of + 9.0 feet Geodetic Datum, which might occur once in 1000 years, was



added 3.0 feet for freeboard and protection against waves and surges. This resulted in the selection of a figure of 12.0 feet as the height to which flood protection must be taken to give maximum protection against the possibility of great loss of life in a flooding of the tunnel.

Observations of ground water level indicated that the amplitude of variations caused by the tide reduced rapidly with increased distance from the river. This condition confirmed the conclusion that an earth dyke of sufficient dimensions would allow the lowering of the crest elevation of the approach walls below maximum water level.

### Structural Design

It was found uneconomical to design the approaches as open cuts in view of the need for cut-off walls of some form and the limit of a 20-degree slope of the sides of an open cut. On the other hand, the continuation of the closed rectangular tunnel section through the approaches to natural ground level would be uneconomical and would increase the problem of ventilation. As a result it was determined that a concrete trough would best satisfy all physical and economic conditions. Typical sections of this structure are shown in Figure 11.3.

In the design evolved, earth dykes are used to retain the river water and thus to decrease the variations of the ground water level at the approach walls. This results in lower pressures on the concrete structures and permits some reduction of the wall sections. The dykes stretch back to the access roads where the roads themselves form the closing link in the system and thus provide complete protection against maximum flood.

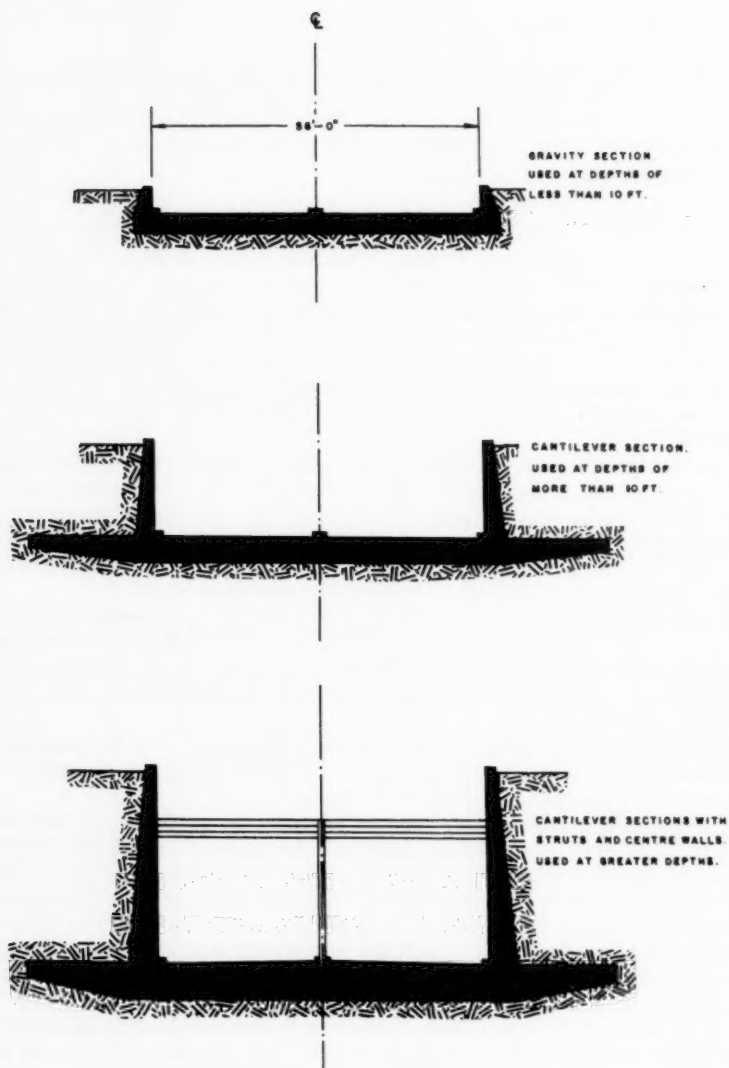
Ground water seepage and rainfall runoff from the area between the dykes and the concrete walls is collected in catch basins on both sides of the ventilation buildings and pumped into the river. Similarly, rainfall on the roadway is collected in catch basins under the ventilation buildings and from them is pumped into the river.

The concrete trough retains earth and water so as to keep the roadway free from earth slides and seepage water. It is also designed to resist the uplift caused by the high water table in the area.

The trough was designed as a reinforced concrete section with cantilevered slabs extending under the earth to provide safety against uplift. At the lower ends of the approaches the retaining wall sides are strutted to support the central partition and to relieve the moments caused by the heavy pressures from soil and water. Two sections of approach structure were evolved, the one being the gravity section used in the shallower parts and the other the section with cantilevered slabs extending into the earth. Both types are shown in Figure 11.3.

Because of the variation in soil conditions it was found advisable to divide the approach structure into units of 46.5 feet in the deeper sections and 30 feet in the shallower gravity sections. All units are connected by keys and the joints are formed as expansion joints to permit some movement. The whole of the outer surface of the structure is waterproofed with an asphalt and fibreglass membrane and the joints are provided with polyvinyl water-stops.

Three loading conditions, two normal and one special, were considered in the design of the main reinforcing. Maximum loading was assumed to be that occurring when the soil at both sides of the approach is retained by a



TYPES OF APPROACH UNITS.

Figure 11.3 -- Cross-sections of approach

rigid structure which will not yield and when the water surface reaches the top of the trough. Reversal of stresses was checked by assuming only active soil pressure and a lowered ground water level. As a third condition, the effects of an earthquake shock were considered. This condition increased soil and water pressures by a horizontal component of 21 per cent of the force of gravity and further increased earth pressures by causing quicking, which was assumed to lower the angle of friction to 15 degrees.

Under the third system of loads a calculation based on ultimate load theory showed an adequate safety factor for the whole structure.

Adequate dimensions have been provided to eliminate the need for shear reinforcing. Secondary reinforcing, always important in a structure of this type, was designed to take care of the forces caused by shrinkage and temperature change as well as to give sufficient longitudinal flexural strength to the slab to distribute loads to the main reinforcing and base.

In the gravity sections the secondary reinforcing was designed on the basis of the subgrade drag theory using a coefficient of friction of one. However, in the heavily reinforced units the greater requirement was imposed by the necessity of distributing cracks, giving sufficient tensile strength and satisfying building codes.

The stability of the approaches was carefully investigated and some basic research was done to estimate the safety of various novel features. Basically, the studies involved the calculation of the lowest friction angle at which movement could occur. This was estimated by calculating the stability of soil segments, which include the approach units. It was determined that approach unit dimensions would be adequate if the angle of friction were 15 degrees or less. The attainment of a lower limit than this could not be justified economically.

### Ventilation Buildings

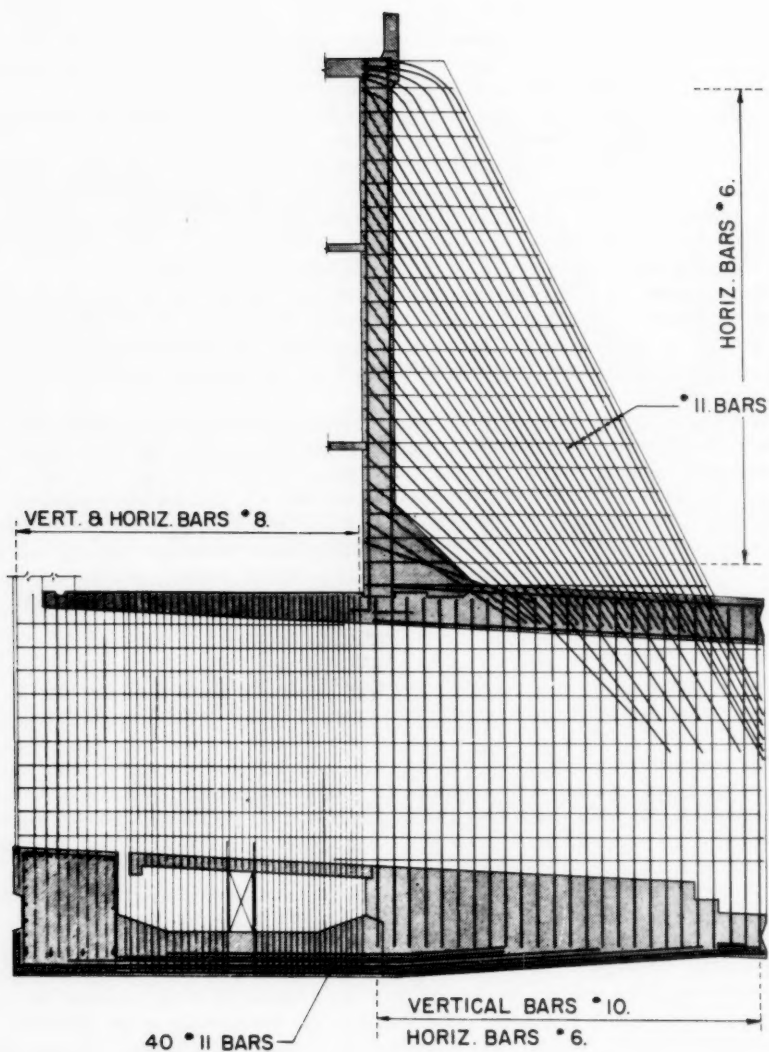
The ventilation buildings are designed to house the main fans for the tunnel and the necessary equipment for the control of the ventilation, lighting and traffic.

The ventilation buildings also act as dams against the river and retain water and earth. As already mentioned, it was considered necessary to divide the approach into relatively short units. Because of the same consideration the ventilation buildings are made self-supporting. As such they act as dams founded on slabs.

The ventilation buildings are the most prominent part of the whole tunnel and the stacks of the buildings are the only parts visible from any distance. Therefore, architectural considerations have played an important part in the design of the exterior. The air intake houses on top of the ventilation buildings have been designed mainly on the basis of the ventilation requirements which determine the area of the open walls and the characteristics of the louvers. The actual shape of the louvers, however, was chosen on the basis of appearance.

In the design of the exhaust air stacks the basic features were determined by the design of the fans but details were worked out to give a pleasing appearance to the structures.

The walls on the river sides of the ventilation buildings retain earth and water and are supported on three longitudinal frames which are in line with the internal partition walls of the tunnel sections. These frames act very



REINFORCEMENT OF VENTILATION BUILDING BUTTRESSES.

Figure 11.3(b) — Cross-section through buttresses of ventilation building



much in the same way as the buttresses of a buttress dam and are designed by similar methods. As in the case of buttress dams, it was more important to determine the direction and magnitude of principal stresses than it was to find moments.

A basic difference between the buttresses of a dam and the supports used here is their location on the upstream side. They act largely in tension. Detailed studies of reinforcing permitted great savings in steel and concrete quantities. High shear causes tensile stresses almost anywhere in the buttresses and, therefore, the reinforcing deviates from standard beam reinforcing, as can be seen in Figure 11.4(b).

### Construction

Figure 12(a) shows an aerial perspective of the tunnel after completion of construction.

In Figure 12(b) may be seen the layout of the construction site showing the temporary locations of railroad and highway and the location of the drydock in which the tunnel elements will be built.

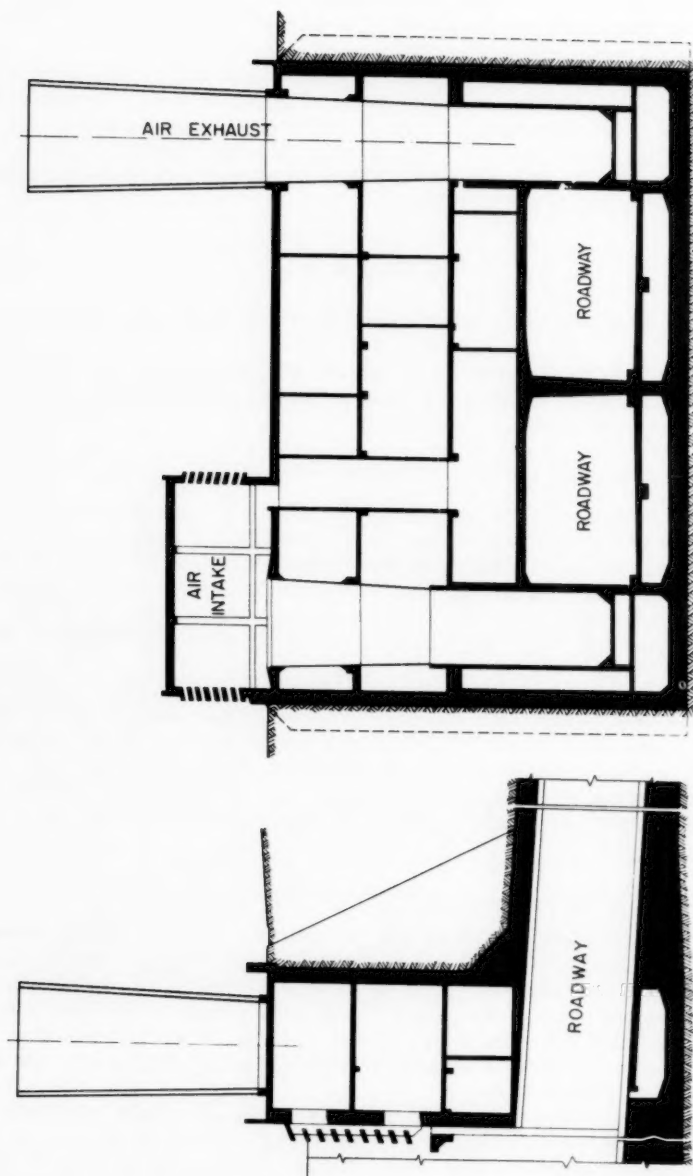
### Construction of Approaches and Ventilation Buildings

It was found advantageous to excavate the pit for the approaches by open cut and to lower the water by wellpoints. This stage of construction has been carried out already as will be seen from Figure 12.1. Our estimates of the ground conditions have proven to be correct and the dewatering operations were completed as planned. After construction of the approaches and the ventilation buildings, the water level will be permitted to rise gradually as the backfilling proceeds. In this way excessive pressures on the ground and dangerous uplifts will be avoided at all stages of construction. This is essential during the placing of the tunnel elements adjacent to the ventilation buildings when the fill will be removed from the river side of the ventilation buildings. In fact at this stage the approach and ventilation building will be flooded to avoid the risk of uplift. When the tunnel is connected to the substructure of the ventilation building and all backfill is in place the structure will be pumped dry again.

### Construction of the Tunnel

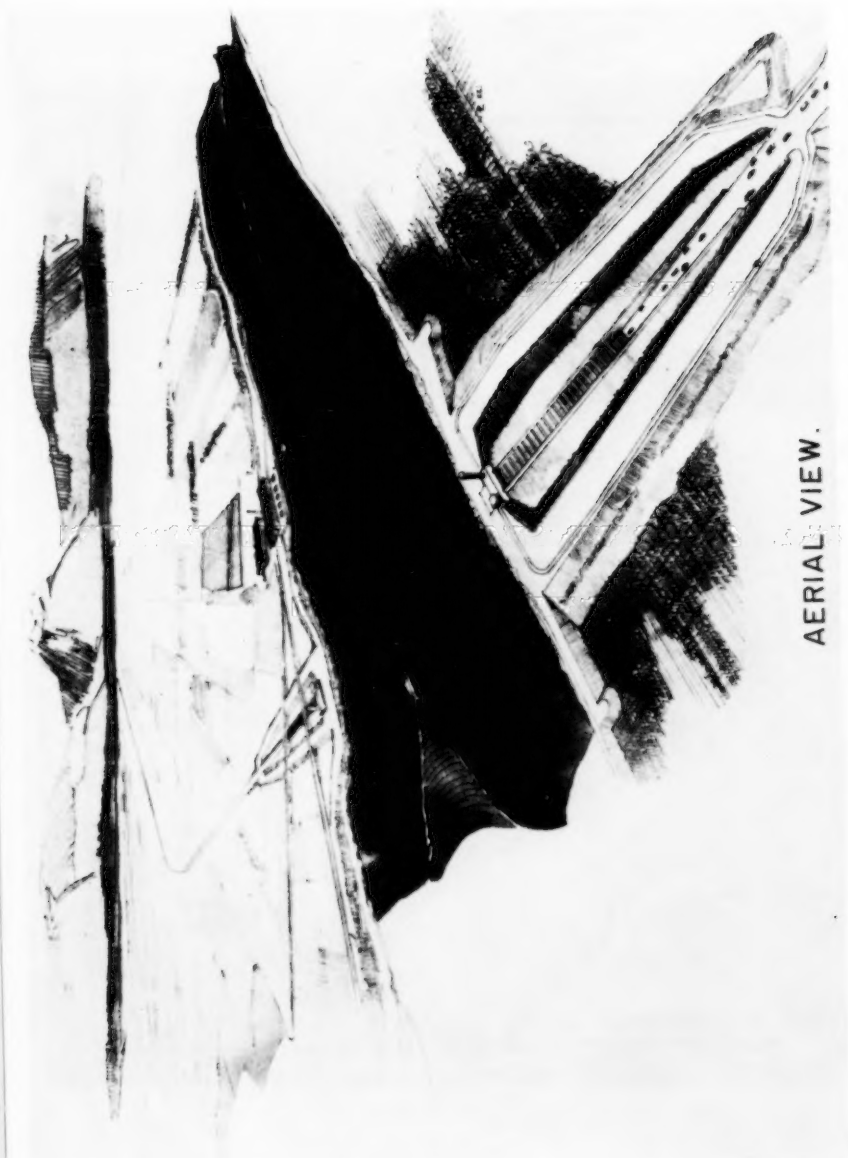
The six precast tunnel elements will be constructed in the drydock situated on the north bank, 1,500 feet west of the tunnel line as shown in Figure 12(b). The drydock was excavated to a depth of 24 feet by means of a suction dredger, and the bottom and banks, which slope 1 in 5, were shaped with graders and drag-lines after the water had been lowered by means of wellpoints. The bottom was covered with a 12-inch thick layer of compacted gravel. The drydock is shown in Figure 12.2(a).

The tunnel elements are provided with temporary watertight bulkheads at both ends and have a freeboard of approximately 12 inches when afloat in the drydock. When all elements have been completed, the wellpoint system will be removed and a channel dredged from the river to the drydock. The elements will then be warped to a fitting-out jetty situated between the drydock and the tunnel centerline. Here, the sinking equipment will be erected on one unit at a time simultaneously with the dredging of a trench at the bottom of



LAYOUT OF VENTILATION BUILDINGS.

Figure 11.4(a) — Section of ventilation building



AERIAL VIEW.

Figure 12(a) - Architectural Perspective

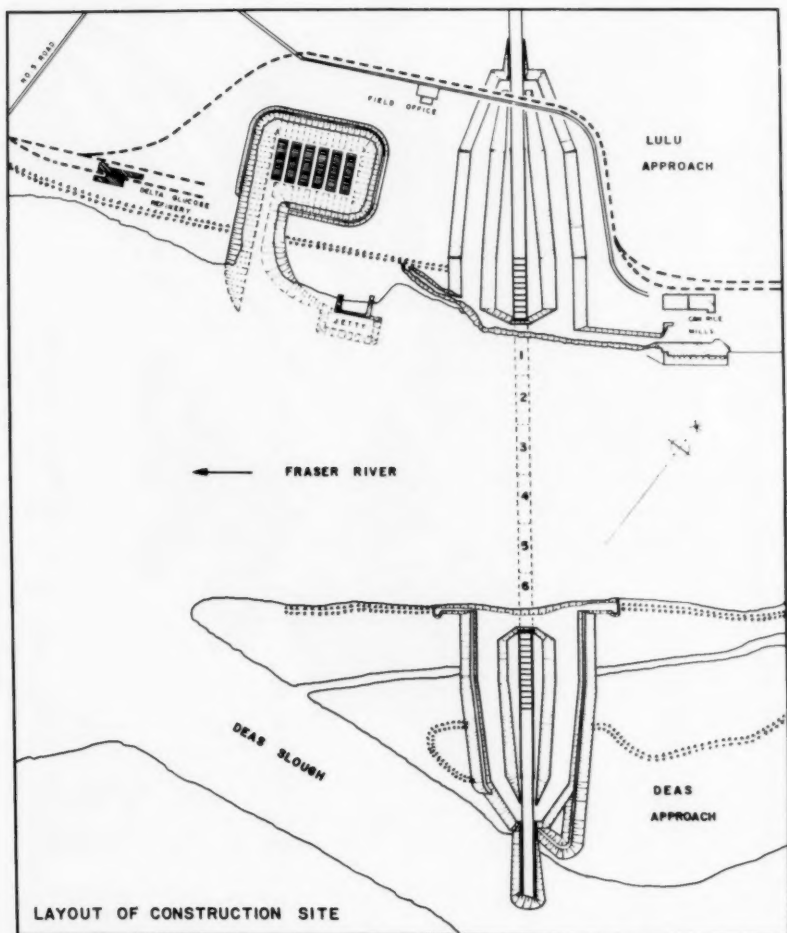


Figure 12(b) -- Layout of Construction Site



Figure 12.1 — Progress Photograph of Work on Lulu Approach



Figure 12.2(a) — Photograph of Drydock

the river. In this trench will be placed four gravel mattresses levelled to about four feet below the finished elevation of the bottom of the tunnel. Each tunnel element will then be floated out and sunk into position in the trench, where it will be supported temporarily on four foundation blocks shown in Figure 12.2(c) which are carried to the trench suspended under the element and are set on the prepared mattresses.

Four hydraulic jacks standing on the foundation blocks will be used then to bring the element into the right position vertically as shown in Figure 12.2(d).

At each end, the tunnel elements are provided with an exterior reinforced concrete collar as shown in Figure 12.2(e). At one side of the joint between two adjacent elements, a rubber gasket is connected to the collar. When the tunnel elements are pressed together by means of a hydraulically operated hook and eye arrangement, the inflated rubber gasket provides water tightness. Subsequently the water is drained from the space between the bulkheads by opening a valve, with the result that the full hydraulic pressure of approximately 4,000 tons acting on the opposite end serves to push the tunnel element firmly into place. The joint between the elements can be constructed inside the collar, with access from the inside of the tunnel elements through doors in the bulkheads.

When a tunnel element has been placed, the sandfilling can start. By means of a frame travelling on reinforced concrete rails on top of the element as shown in Figure 12.2(f), sand is jetted into the space under the tunnel element. When most of the space has been filled with sand, the sinking equipment is disconnected, the sand jetting completed, and backfill placed along both sides of the tunnel. A layer of rockfill is placed on top of the tunnel to protect it and to increase the safety against uplift.

The structural joints at the ventilation buildings will not be constructed until two or three months after the tunnel elements have been placed and backfilled, in order to allow the major part of the differential settlements to take place in advance, under full load.

Figure 12.2(g) shows the site as it looks today with all phases of the work progressing satisfactorily.

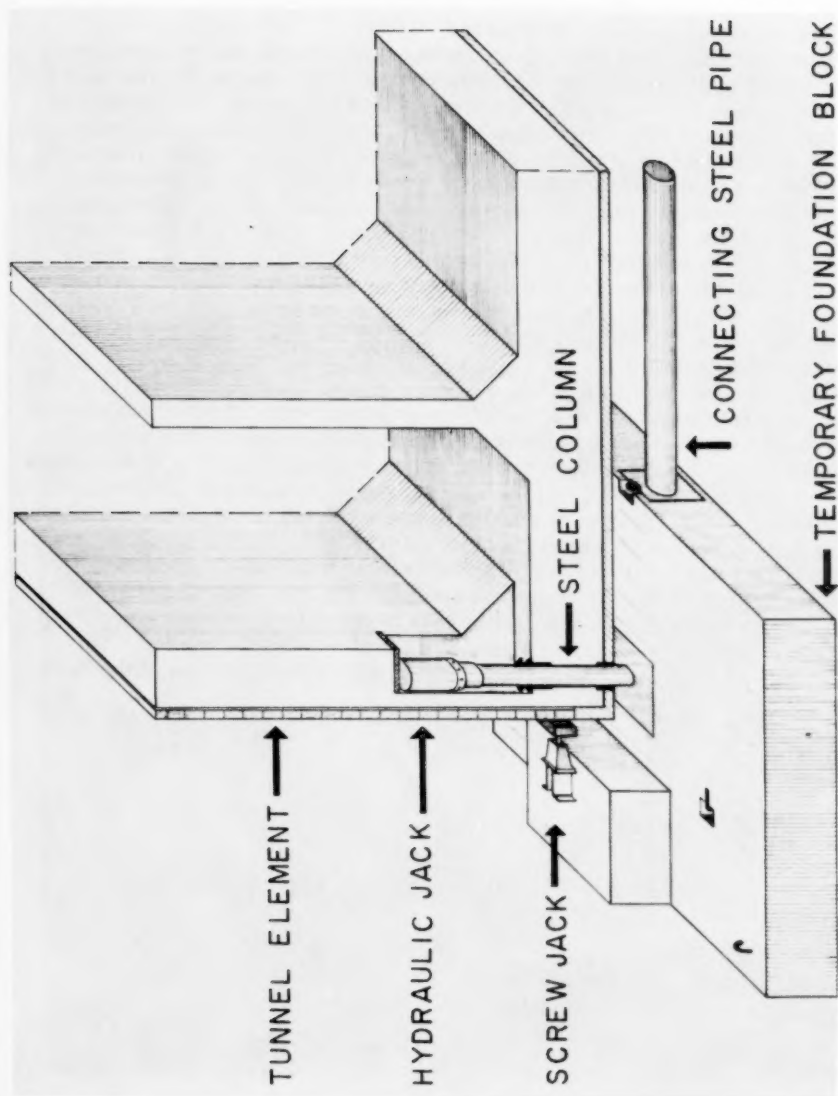


Figure 12.2(c) - Foundation Blocks



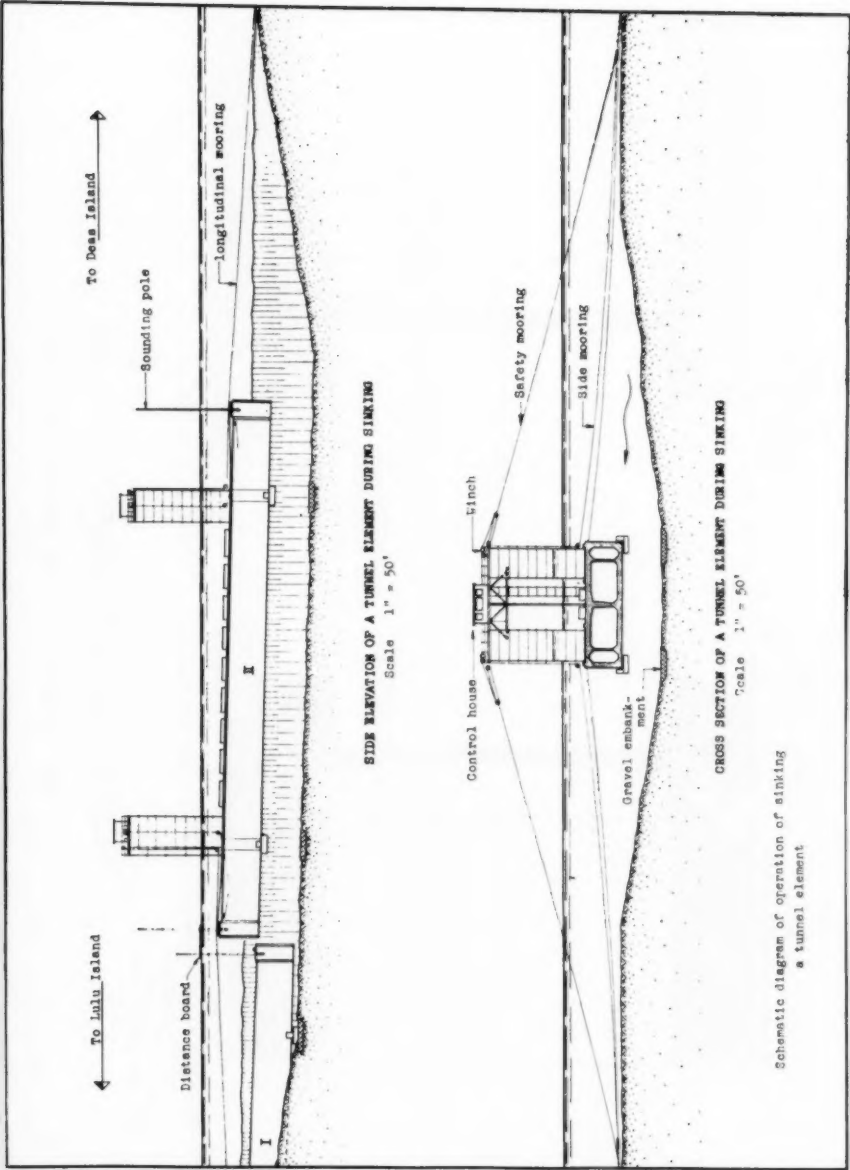
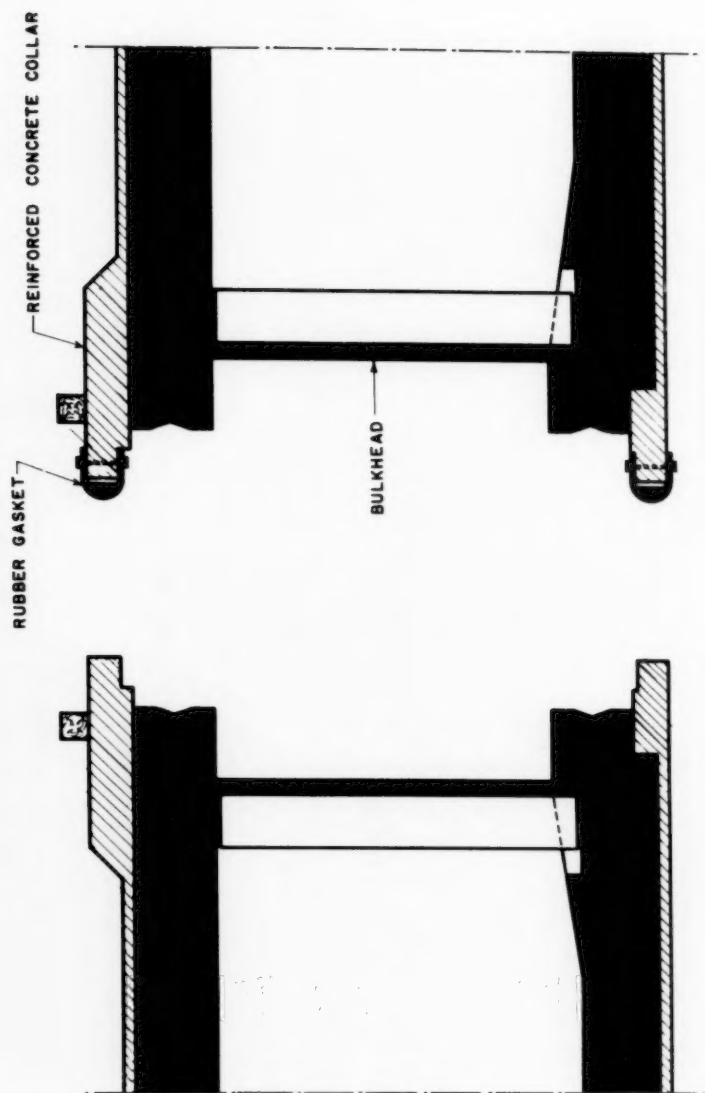


Figure 12.2(d) -- Diagram of Sinking Operation



## REINFORCED CONCRETE COLLAR

Figure 12.2(e) -- Reinforced Concrete Collar

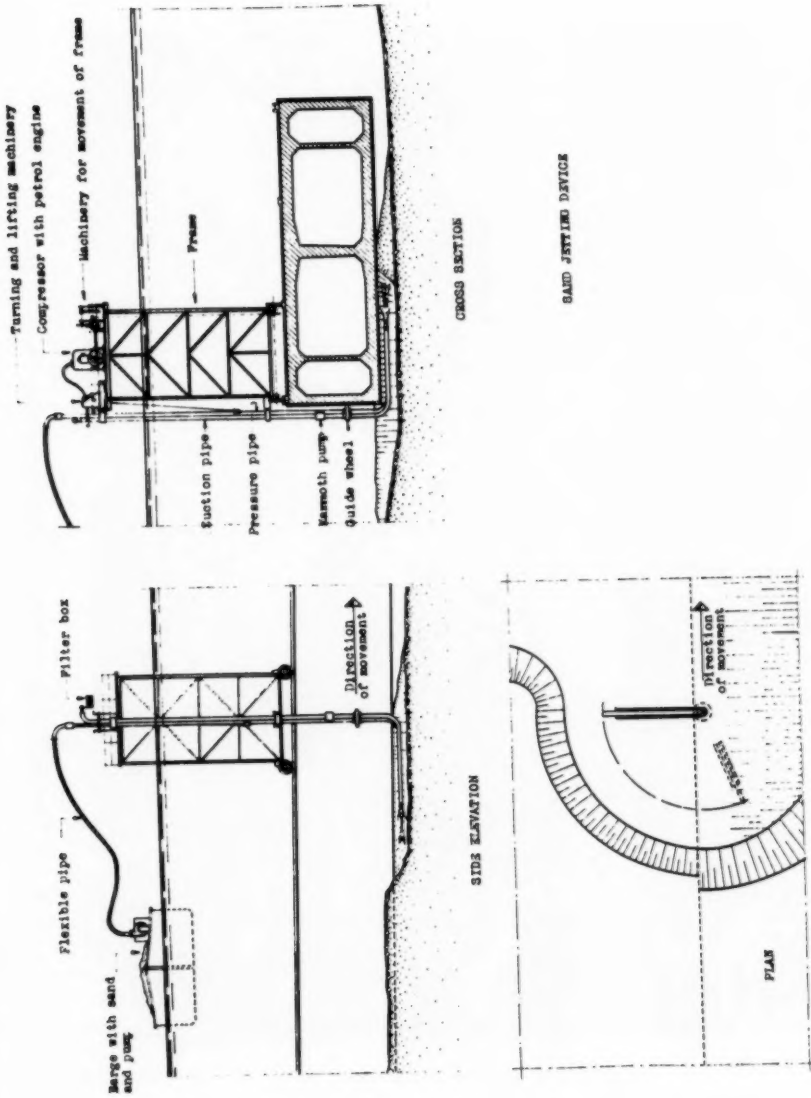


Figure 12.2(f) -- Sand Jetting Device

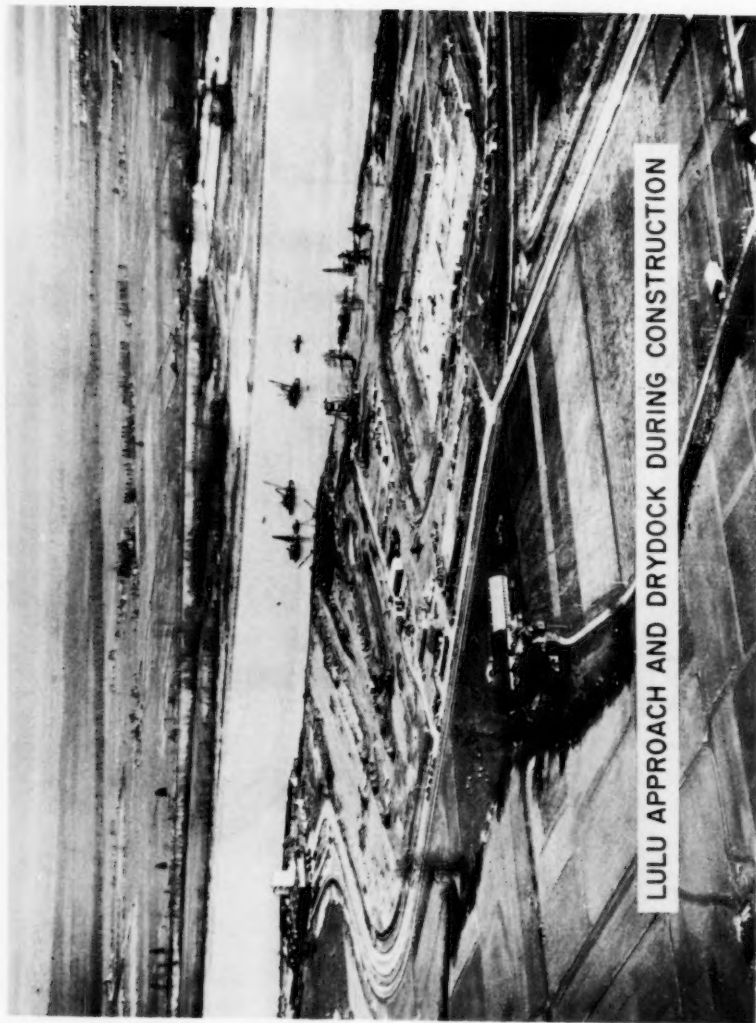


Figure 12.2(g) -- Oblique Aerial Progress Photo of Site

---

Journal of the  
STRUCTURAL DIVISION  
Proceedings of the American Society of Civil Engineers

---

ANALYSIS OF HELICAL BEAMS UNDER SYMMETRICAL LOADING

Alan M. C. Holmes,<sup>1</sup> J.M. ASCE  
(Proc. Paper 1437)

---

SYNOPSIS

Thorough analysis of moments and deflections of a helical beam is simplified by consideration of the symmetrical case, and relationship between design variables and structure's behavior is shown. Tables and curves presented for members of rectangular section, show the greater structural efficiency and smaller deflection of shallower members.

---

INTRODUCTION

The increasing architectural use of "Free-standing spiral stairs" has created a need for a simple but thorough analysis of moments and deflections in helical beams.

A vigorous mathematical analysis in terms general enough to include any unsymmetrical case is available (Reference 5), but the treatment is abstract and becomes so elaborate that it is of little use to the design engineer.

Approximate methods (Reference 10) fail to take into consideration the beneficial structural behaviour of certain types of helical beams that allows more ambitious use of a highly pleasing architectural form.

This paper presents general equations and a solution for a symmetrically loaded helical beam with both ends completely fixed. By considering the symmetrical case, a precise mathematical analysis of the moments is possible without the number of factors and expressions becoming so numerous as to obscure the characteristic behaviour of the structure.

The topics are discussed and developed in this order:

---

Note: Discussion open until April 1, 1958. Paper 1437 is part of the copyrighted Journal of the Structural Division of the American Society of Civil Engineers, Vol. 83, No. ST 6, November, 1957.

1. Structural Designer, Skidmore, Owings & Merrill, Chicago, Ill.

Definition of terms

Derivation of equations for uniform load

Solution for the uniform load case

Derivation and solution for the concentrated load case

Deflection of the midpoint

Particular solutions for  $360^\circ$ ,  $270^\circ$  and  $180^\circ$  helical beams

Characteristic equations and curves

Effect of variations in the torsion stiffness "J"

The first derivations are explained in detail and in simple engineering terms, perhaps too much detail for an engineer used to these problems. But the paper is intended as an introduction for the engineer unaccustomed to problems in curved structures.

The solution for the constants of the general equations involves lengthy equations, but the mathematical operations are those of elementary calculus.

The last part of the paper includes tables of values for these constants and for other important results, so that interpretation of the work is possible without undue labor. The tables are not intended for "handbook design" of helical beams. Although they may be of some value in preliminary designs, their main purpose is to illustrate the comparative behaviour of different cross-section types.

The moments calculated by the method presented in this paper can be mathematically "exact." But since the problem is one in indeterminate structures, the extent to which the actual structure meets the perfection of the mathematical concepts must be considered; the effect of the shortcomings must be evaluated, and the theoretical moments themselves should only serve as guides to judgment.

Because of the complexity of curvature, the moments can not be converted to stress values by any simple formulas such as those used in rectilinear problems. This paper does not attempt to evaluate these stresses.

### Definitions, Symbols and Relations

At any point P on the helix center-line, let the following mutually perpendicular axes be defined:

The NORMAL AXIS (N-N) which is radial and horizontal.

The TANGENTIAL AXIS (T-T) which is tangential to the helix center-line.

The BINORMAL AXIS (B-B) which is at right angles to both the normal and tangential axes.

Two other axes through any point P on the helix center-line are:

The VERTICAL AXIS (Z-Z), parallel to the axis of revolution of the helix and to the direction of gravitational loading.

The HORIZONTAL-TANGENTIAL AXIS ( $T'$  -  $T'$ ) lying in a horizontal plane and in the vertical plane which contains the tangential axis.

The following symbols will be used:

$C_1, C_2$  etc. = the specific constants in the general equations of a particular helix.

E = modulus of elasticity.

$F_{no}$  = a correcting force at the midpoint (in the normal direction).

$F_t$  = the tangential force at any point P.

G = modulus of shear =  $E/2 (1 + \text{Poisson's ratio})$ .

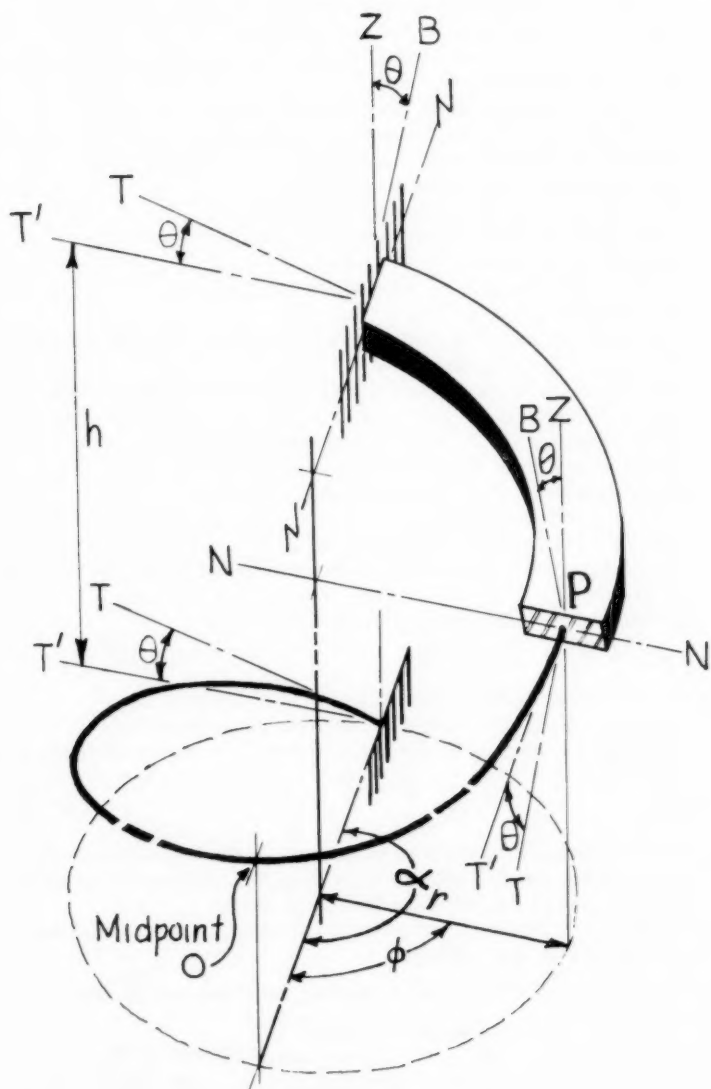


Figure 1  
Perspective Sketch  
Helical Beam with  $\alpha = \pi$  radians

- $h$  = the vertical height between the supported ends of the helix.  
 $I$  = moment of inertia about the normal axis.  
 $J$  = a modified polar moment of inertia, the measure of resistance to torsional deformation.  
 $K$  = moment of inertia about the binormal axis.  
 $K_d$  = the constant in the expression for deflection.  
 $M_n$  = moment at P about a normal axis.  
 $M_t$  = moment at P about a tangential axis.  
 $M_b$  = moment at P about a binormal axis.  
 $M_h$  = moment at P about a horizontal axis.  
 $M_z$  = moment at P about a vertical axis.  
 $M_{no}$  = a correcting normal moment at the midpoint O.  
 $O$  = the midpoint of the helix.  
 $P$  = any point on the helix center-line defined by an arc  $\phi$  (in radians) as seen in the plan view.  
 $r$  = the radius of the helix center-line as seen in the plan view.  
 $s$  = the true length of the helix center-line.  
 $V_n$  = shear at any point P, in the normal direction.  
 $V_b$  = shear at any point P, in the binormal direction.  
 $V_z$  = shear at any point P, in the vertical direction.  
 $W$  = concentrated load at O.  
 $w$  = unit uniform load per unit length of  $s$ .  
 $z$  = the vertical height of any point P above (+) or below (-) the midpoint O.  
 $\alpha$  = half arc of the helix as seen in the plan view.  
 $\delta = \mu \cos^2 \theta + \lambda \sin^2 \theta$   
 $\Delta_{no}$  = the deflection of the midpoint in the normal direction.  
 $\Delta_{zo}$  = the deflection of the midpoint in the vertical direction.  
 $\theta$  = the slope the tangent to the helix center-line makes with any horizontal plane.  
 $\lambda = I/K$ .  
 $\mu = EI/GJ$ .  
 $\phi$  = the arc (in radians) as seen in the plan view which defines the location of any point P with reference to the midpoint O (positive for upper half of helix, negative for lower half).  
 $\psi_{no}$  = the change of slope (or rotation of the elastic curve about the normal axis at the midpoint.

Based on the above definitions, the following relations are stated:

$$\begin{aligned}
 \tan \theta &= h/2r\alpha \\
 s &= 2r\alpha / \cos \theta \\
 z &= r\phi \tan \theta
 \end{aligned}$$

For the sake of clarity, the following points are mentioned:

At any point P, the reference area for stresses (the minimum cross-section of the helical beam), is defined by a plane containing the normal and binormal axes.

The terms  $\delta$ ,  $\lambda$  and  $\mu$  have no significance beyond that of the abbreviations they represent. They are dimensionless quantities which state relationships of the properties for a particular helical beam.

Although the figures show a helix in which  $\alpha = \pi$  radians, the definitions



## CROSS-SECTIONS

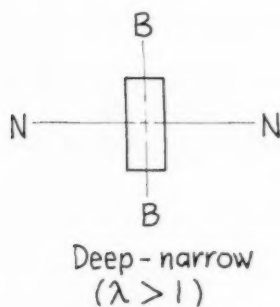
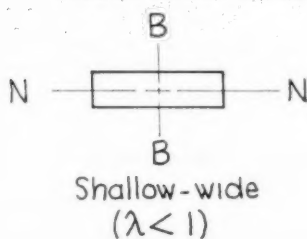
BEAM TYPES

Figure 2

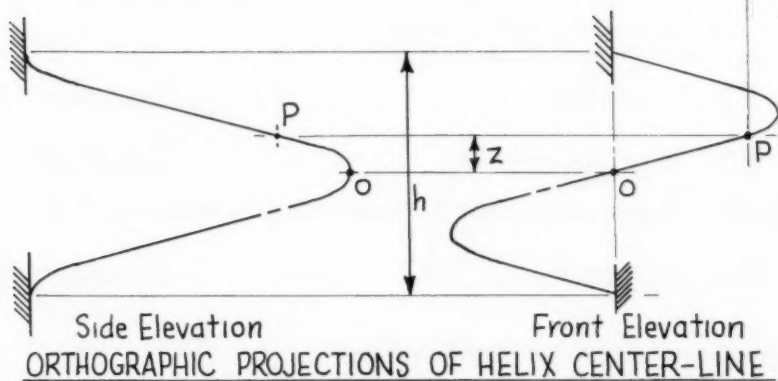
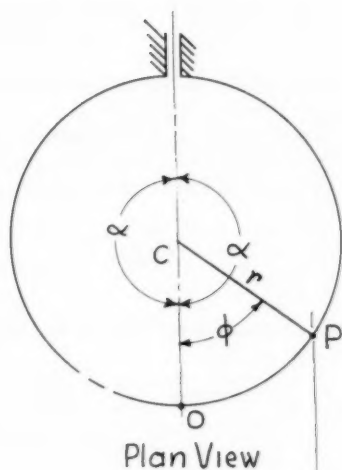
ORTHOGRAPHIC PROJECTIONS OF HELIX CENTER-LINE

Figure 3

made and the derivations which follow apply to the unsupported arc of a symmetrically loaded helix of any reasonable  $\alpha$ , (and with symmetrical end supports).

The terms "Helix" and "Helical beam" are the same, but the term "Helix" will be used to denote the geometrical configuration, and "Helical beam" will be used when reference is being made to some structural aspect.

#### Derivation of Equations for a Uniformly Loaded Helical Beam with Both Ends Fixed

Let the helix be cut at its midpoint (O), and each half act as an independent cantilever supported at A.

Let the shears and moments be considered at the point B (defined by the arc  $\beta$  in the plan view, see figure 4).

Any small element of the uniform load acting at P will have a vertical force of

$$F_z = wds = \frac{wr}{\cos\theta} d\phi \quad \text{Equation 1}$$

The vertical shear at B is the sum of the elements of vertical force over the arc  $\beta$ , or

$$V_z \text{ at B} = \int_0^\beta \frac{wr}{\cos\theta} d\phi' = \beta \frac{wr}{\cos\theta} \quad \text{Equation 2}$$

Any small element of uniform load acting at the point P will have a lever arm PD about the normal axis (N-N) at B, and a lever arm of BD about the horizontal-tangential axis (T'-T') at B.

Reference to Figure 4 shows that

$$PD = r \sin\phi' \quad \text{Equation 3}$$

$$BD = r(1 - \cos\phi') \quad \text{Equation 4}$$

So the element of uniform load at P causes a normal moment at B of

$$M_n = r \sin\phi' \left( \frac{wr}{\cos\theta} d\phi' \right) \quad \text{Equation 5}$$

and a horizontal-tangential moment (at B) of

$$M_{t'} = r(1 - \cos\phi') \left( \frac{wr}{\cos\theta} d\phi' \right) \quad \text{Equation 6}$$

Thus the normal moment at B caused by a uniform load over the arc  $\beta$  is given by

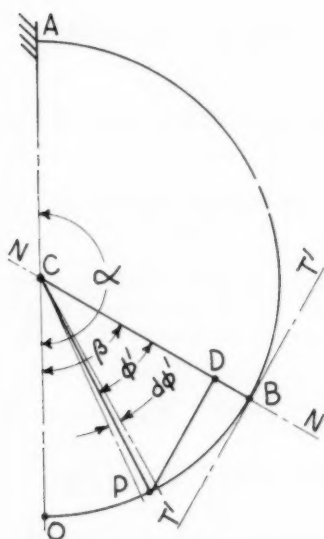


Fig 4: Upper half of helix (Plan view)

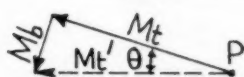
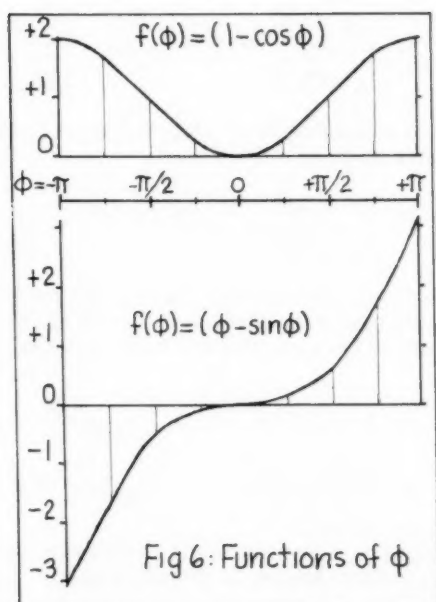


Fig 5: Resolution of  $M_t'$  in a vertical plane

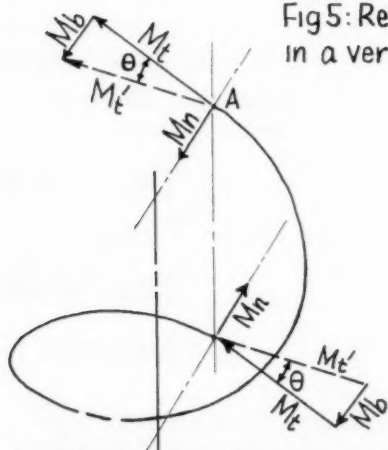


Fig 7: Vectors of End Moments (perspective sketch)

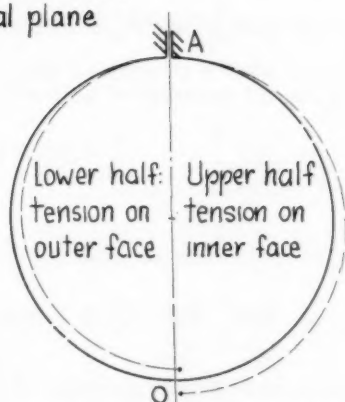


Fig 8: Deflection of elastic curve due to  $M_b$  (Plan view)

$$M_n = \int_0^\beta \frac{wr^2 \sin \phi' d\phi'}{\cos \theta} = \frac{wr^2 (1 - \cos \beta)}{\cos \theta} \quad \text{Equation 7}$$

and the horizontal-tangential moment at B caused by a uniform load over the arc  $\beta$  is given by

$$M_t' = \int_0^\beta \frac{wr^2 (1 - \cos \phi') d\phi'}{\cos \theta} = \frac{wr^2 (\beta - \sin \beta)}{\cos \theta} \quad \text{Equation 8}$$

To obtain the torsional moment and the binormal moment at B, it is necessary to resolve the horizontal-tangential moment into two moments in these directions; the axes of these three moments lie in a vertical plane (see Figure 5).

$$M_t = M_t' \cos \theta = wr^2 (\beta - \sin \beta) \quad \text{Equation 9}$$

$$M_b = M_t' \sin \theta = wr^2 \tan \theta (\beta - \sin \beta) \quad \text{Equation 10}$$

The normal moment is the one already found, so the three moments at B due to uniform loading of the arc  $\beta$  are:

$$M_n = \frac{wr^2}{\cos \theta} (1 - \cos \beta) \quad \text{Equation 11}$$

$$M_t = wr^2 (\beta - \sin \beta) \quad \text{Equation 12}$$

$$M_b = wr^2 \tan \theta (\beta - \sin \beta) \quad \text{Equation 13}$$

But the point B is any point on the cantilever helical beam defined by the arc  $\beta$ , so the moments at any point P defined by the arc  $\phi$  are:

$$M_n = \frac{wr^2}{\cos \theta} (1 - \cos \phi) \quad \text{Equation 14}$$

$$M_t = wr^2 (\phi - \sin \phi) \quad \text{Equation 15}$$

$$M_b = wr^2 \tan \theta (\phi - \sin \phi) \quad \text{Equation 16}$$

The curves of these functions of  $\phi$  are plotted in Figure 6.

Moments that are resolved into component moments, such as  $M_t'$  above, can be represented by vectors. The vector of a moment is drawn along the axis of that moment. The direction of the vector is established by the Right-Hand Rule. If the fingers curl in the direction of the RESISTING MOMENT, the thumb, (which lies along the axis), points in the direction of the vector.

In Figure 7 the vectors are drawn for the end moments of each cantilever

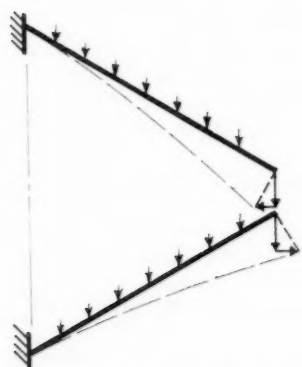


Fig 9: Deflections of sloping cantilevers

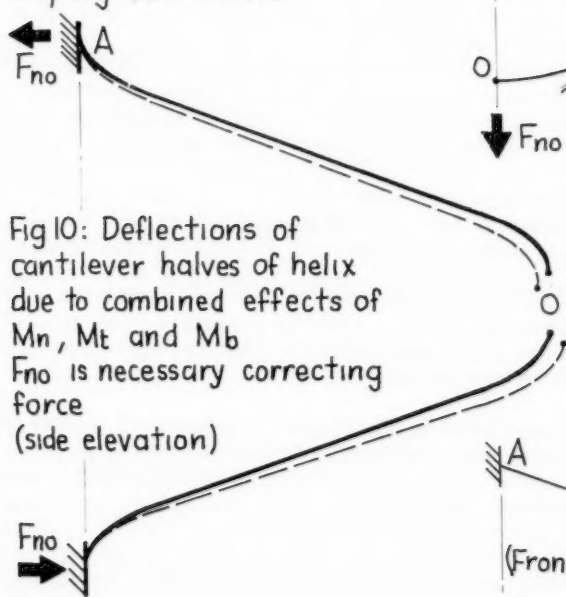


Fig 10: Deflections of cantilever halves of helix due to combined effects of  $M_n$ ,  $M_t$  and  $M_b$   
 $F_{no}$  is necessary correcting force  
(side elevation)

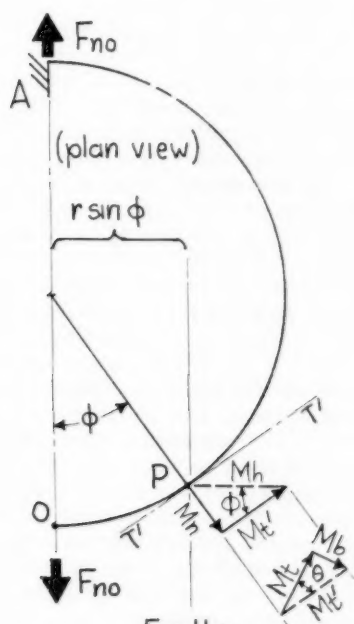


Fig 11 a

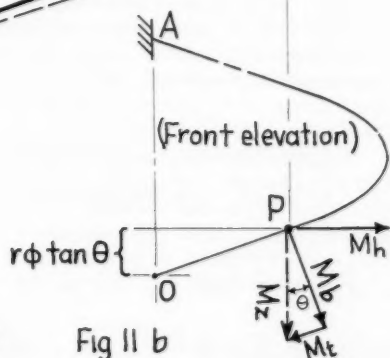


Fig 11 b

Fig 11: (right)  
Vectors of moments  
due to  $F_{no}$  (upper half)

half of the helix. The directions of  $M_n$  and  $M_t$  have been established by the R-H Rule;  $M_t$  and  $M_b$  are shown as component vectors of  $M_t'$ .

For the upper cantilever helix, the R-H Rule indicates that  $M_b$  produces tension on the inner face of the helical beam.  $M_b$  produces tension on the outer face of the lower half. Thus, due to the binormal moment, the free end of the upper half will have an outward deflection, and that of the lower half will have an inward deflection, (see Figure 8).

The deflections of the two halves due to normal and torsional moment are in opposite direction to the deflections due to binormal moment. This can be visualized by considering the deflections of two straight and sloped cantilevers, (Figure 9), in which it is seen that under load, the upper cantilever, which slopes down, will have a component of deflection inward. The lower cantilever will have a component of deflection outward; (and they will both have a component of deflection downward).

For a shallow-wide helical beam, the deflection of the upper half inward due to  $M_n$  and  $M_t$  will exceed the deflection outward due to  $M_b$ . Likewise, for the lower half, the absolute normal deflection (due to  $M_n$ ,  $M_t$  and  $M_b$  combined) will be outward, (Figure 10). Equal and opposite forces in a normal direction must be applied to the free ends of each cantilever so as to make their deflections in the normal direction zero.

Mathematical investigation indicates that for practical structural proportions, the absolute normal deflection of the upper half is always inward, even for beams with deep-narrow cross-sections. This is because these cross-sections have the same low value of torsional stiffness ( $J$ ) as do the shallow-wide cross-sections.

Mathematical investigation is not needed to see that for shallow-wide sections the normal deflection to be corrected will be greater, and that the normal correcting force will have to act against a stiffer binormal moment of inertia ( $K$ ).

This normal shear at the midpoint  $O$ , which becomes greater as the cross-section becomes flatter, does much to decrease the maximum torsional moments of the entire helix. Since torsion stress is usually the criterion, shallow-wide cross-sections will generally be found more practical than deep-narrow ones.

At any point  $P$ , the normal force  $F_{no}$  applied at the free end of cantilever helix will cause two moments about mutually perpendicular axes lying in a plane at right angles to the axis of the force. It is convenient to choose these axes as horizontal and vertical, (Figure 11b).

The lever arms of  $F_{no}$  about these axes at  $P$  are

$$r. \phi. \tan \theta = \text{lever arm about the horizontal axis} \quad \text{Equation 17}$$

$$r. \sin \phi = \text{lever arm about the vertical axis} \quad \text{Equation 18}$$

so the moments about these two axes are

$$M_h = F_{no}.r.\phi \tan \theta \quad \text{Equation 19}$$

$$M_z = F_{no}.r. \sin \phi \quad \text{Equation 20}$$

where  $M_z$  is a moment causing tension on the inner face of the upper cantilever helical beam, and which therefore has a vector pointing down.

$M_h$  is now resolved into two moment vectors still in a horizontal plane, (Figure 11a).

$$M_n = -\sin \phi (M_h) \quad \text{Equation 21}$$

$$M_{t'} = +\cos \phi (M_h) \quad \text{Equation 22}$$

and  $M_{t'}$  is in turn resolved into two moment vectors in a vertical plane.

$$M_t = \cos \theta [\cos \phi (M_h)] \quad \text{Equation 23}$$

$$M_b = \sin \theta [\cos \phi (M_h)] \quad \text{Equation 24}$$

The signs in the above operations are obtained by comparison with the moment vectors of the uniform load.

$M_z$  is resolved directly into  $M_t$  and  $M_b$  (Figure 11b).

$$M_t = -\sin \theta (M_z) \quad \text{Equation 25}$$

$$M_b = +\cos \theta (M_z) \quad \text{Equation 26}$$

The moments at P due to  $F_{no}$  are thus:

$$M_n = -F_{no}.r.\tan \theta.\phi \sin \phi \quad \text{Equation 27}$$

$$M_t = +F_{no}.r.\tan \theta.\cos \theta.\phi \cos \phi - F_{no}.r.\sin \theta.\sin \phi \quad \text{Equation 28}$$

$$M_b = +F_{no}.r.\tan \theta.\sin \theta.\phi \cos \phi + F_{no}.r.\cos \theta.\sin \phi \quad \text{Equation 29}$$

When the vertical and horizontal-tangential deflections ( $\Delta$ ) of the free end of the upper cantilever half are compared to those of the lower half, they are found to be of same magnitude and direction, so that no correcting forces need be applied to make them compatible in this respect, (Figures 12a and 12b).

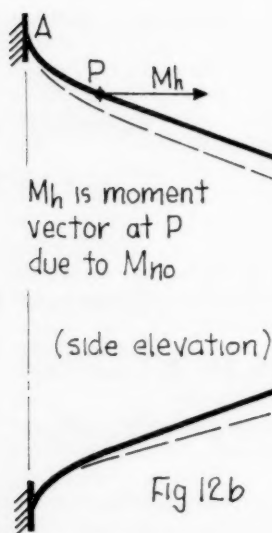
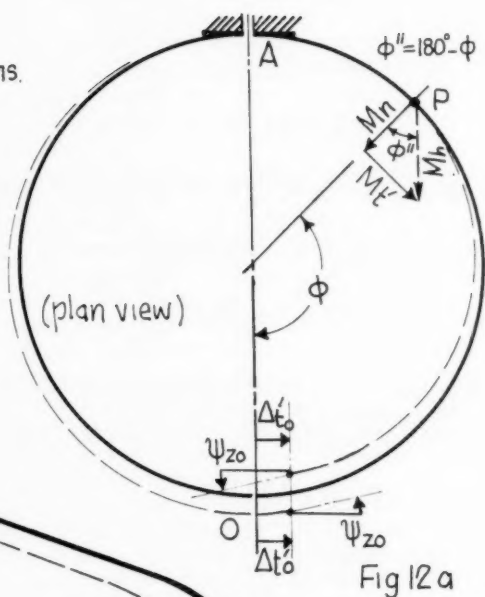
Likewise, angle changes ( $\psi$ ) of the free ends about the vertical and horizontal-tangential axes are compatible without correcting moments. About the normal axis, however, the angle changes of the free ends are equal and opposite, and a correcting moment  $M_{no}$  must be applied to make them compatible, (Figure 12c).

At any point P,  $M_{no}$  causes a moment about a horizontal axis parallel to the radius at the midpoint, (Figures 12a and 12b). This moment is

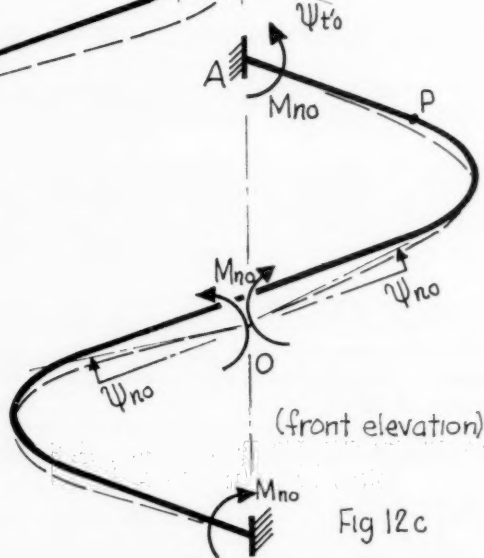
$$M_h = M_{no} \quad \text{Equation 30}$$

$M_h$  is resolved into two vectors still in a horizontal plane, (Figure 12a)

( $\Delta t'_0$  shown is for deep-narrow X-sections. For shallow-wide X-sections  $\Delta t'_0$  is in opposite direction)



$M_{n0}$  is normal moment applied at O to correct for difference in slope ( $\psi_{n0}$ )





$$M_n = -\cos\phi(M_h) \quad \text{Equation 31}$$

$$M_t' = -\sin\phi(M_h) \quad \text{Equation 32}$$

The signs are derived by comparison with the vectors of moment due to uniform load.

$M_t'$  is further resolved into two vectors in a vertical plane:

$$M_t = \cos\theta [-\sin\phi(M_h)] \quad \text{Equation 33}$$

$$M_b = \sin\theta [-\sin\phi(M_h)] \quad \text{Equation 34}$$

The effects of  $M_{no}$  are therefore

$$M_n = -M_{no} \cos\phi \quad \text{Equation 35}$$

$$M_t = -M_{no} \cos\theta \sin\phi \quad \text{Equation 36}$$

$$M_b = -M_{no} \sin\theta \sin\phi \quad \text{Equation 37}$$

The elastic curves of the two cantilever helical beams are colinear at the midpoint after the application of the correcting normal force and correcting normal moment to the free ends. The moments at P due to  $F_{no}$  and  $M_{no}$  are added to those due to the uniform load on the cantilevers. This superposition gives the equations of moments at any point P on the full helix. The values of  $F_{no}$  and  $M_{no}$  in these equations are constants which depend upon the slope and arc of the helix, the properties of its cross-section, and the uniform load  $w$ .

The combined equations for the full helix are:

$$M_n = \frac{wr^2}{\cos\theta} (1 - \cos\phi) - F_{no}.r.\tan\theta.\phi\sin\phi - M_{no}\cos\phi \quad \text{Equation 38}$$

$$M_t = wr^2 (\phi - \sin\phi) + F_{no}.r.\tan\theta.\cos\theta.\phi\cos\phi - M_{no}\cos\theta.\sin\phi - F_{no}.r.\sin\theta.\sin\phi \quad \text{Equation 39}$$

$$M_b = wr^2 \tan\theta (\phi - \sin\phi) + F_{no}.r.\tan\theta.\sin\theta.\phi\cos\phi - M_{no}.\sin\theta.\sin\phi + F_{no}.r.\cos\theta.\sin\phi \quad \text{Equation 40}$$

To make these equations more convenient, let the constants  $C_1'$ ,  $C_1$  and  $C_2$  be chosen so that

$$C_1' wr^2 / \cos \theta = M_{ho} \quad \text{Equation 41}$$

$$C_2 wr / \sin \theta = F_{ho} \quad \text{Equation 42}$$

$$C_1 = (1 + C_1' + C_2) \quad \text{Equation 43}$$

The general moment equations are then written in this final form:

$$M_n = \frac{wr^2}{\cos \theta} \left[ 1 - C_1 \cos \phi - C_2 \phi \sin \phi + C_2 \cos \phi \right] \quad \text{Equation 44}$$

$$M_t = wr^2 \left[ \phi - C_1 \sin \phi + C_2 \phi \cos \phi \right] \quad \text{Equation 45}$$

$$M_b = wr^2 \tan \theta \left[ \phi - C_1 \sin \phi + C_2 \phi \cos \phi + \frac{C_2 (\sin \phi)}{\sin^2 \theta} \right] \quad \text{Equation 46}$$

In the case of a helix with  $h = \text{zero} =$ , (a RING BEAM), the binormal moment is non-existent, the correcting normal force is not needed, so  $C_2$  is zero, and the remaining expressions retain their validity.

The equations for normal shear, tangential thrust and binormal shear at the point P, are obtained by resolving the two forces on the helix in these respective directions.

The two forces at P are

$$V_z = \phi wr / \cos \theta \quad \text{Equation 2}$$

$$F_{no} = C_2 wr / \sin \theta \quad \text{Equation 42}$$

These are resolved into

$$V_n = wr \left[ \quad + \frac{C_2}{\sin \theta} \cdot \cos \phi \right] \quad \text{Equation 47}$$

$$F_t = wr \left[ \phi \cdot \tan \theta + \frac{C_2}{\tan \theta} \cdot \sin \phi \right] \quad \text{Equation 48}$$

$$V_b = wr \left[ \phi - C_2 \cdot \sin \phi \right] \quad \text{Equation 49}$$

## Solution for Constants of the General Equations

The constants  $C_1$  and  $C_2$  in the general equations depend upon the properties of the helix represented by  $\alpha$ ,  $\theta$ ,  $\lambda$  and  $\mu$ .

$C_1$  and  $C_2$  must be such that the angle change about the normal axis ( $\psi_{no}$ ) and displacement in the normal direction ( $\Delta_{no}$ ) are zero at the midpoint of the helix.

Algebraic expressions must be derived for ( $\psi_{no}$ ) and ( $\Delta_{no}$ ). When these equations are set equal to zero and solved simultaneously, they yield specific values of  $C_1$  and  $C_2$  in terms of  $\alpha$ ,  $\theta$ ,  $\lambda$  and  $\mu$ .

The algebraic expressions can be obtained by Castigliano's Theorem, or by the use of the Moment Area Propositions and vectors to represent angle changes and displacements.

If  $M_n$  represents the function for normal moment at any point P,  $M_n(ds)$  is an element of moment area at P, and  $M_n(ds)/EI$  is an angle change in a length ( $ds$ ) at the point P (due to  $M_n$ ). This angle change (per unit length) at P can be represented by a vector lying along the axis of the angle change, and a component of this vector can be taken in the direction of the normal axis at O. In this case, the component makes an angle  $\phi$  with the original vector, so  $M_n(ds)/EI$  is multiplied by  $(\cos \phi)$ .

Thus, the angle change of the elastic curve about the normal axis at O, due to the normal moment only can be given by

$$\psi_{no} = \int_0^{\alpha} \cos \phi \frac{M_n}{EI} ds \quad \text{Equation 50}$$

The vector of angle change (per unit length)  $\frac{M_t}{GJ}(ds)$  at the point P due to torsional moment, makes an angle  $\theta$  with the horizontal plane containing the normal axis at O. In the plan view, the vector makes an angle  $(90^\circ - \phi)$  with the normal axis at O. So the angle change at O about the normal axis, due to torsional moment is

$$\psi_{no} = \int_0^{\alpha} \cos \theta \cdot \sin \phi \cdot \frac{M_t}{GJ} ds \quad \text{Equation 51}$$

In the same way it can be shown that the angle change at O about a normal axis due to binormal moment is

$$\psi_{no} = \int_0^{\alpha} \sin \theta \cdot \sin \phi \cdot \frac{M_b}{EK} ds \quad \text{Equation 52}$$

The total normal angle change at O due to the combined effects of  $M_n$ ,  $M_t$  and  $M_b$  are then

$$\psi_{no} = \frac{r}{EI \cos \theta} \left[ \cos \phi \int_0^\alpha M_n d\phi + \mu \cos \theta \cdot \sin \phi \int_0^\alpha M_t d\phi + \lambda \sin \theta \cdot \sin \phi \int_0^\alpha M_b d\phi \right] \quad \text{Equation 53A}$$

Attention is now drawn to the fact that if the partial derivatives of  $M_n$ ,  $M_t$  and  $M_b$  (as presented in equations 44, 45 and 46) are taken with respect to the normal correcting moment  $C_1 w r^2 / \cos \theta$  ( $= M_{no}$ ), the following expressions are obtained:

$$\frac{\partial M_n}{\partial M_{no}} = -\cos \phi \quad \text{Equation 54}$$

$$\frac{\partial M_t}{\partial M_{no}} = -\cos \theta \cdot \sin \phi \quad \text{Equation 55}$$

$$\frac{\partial M_b}{\partial M_{no}} = -\sin \theta \cdot \sin \phi \quad \text{Equation 56}$$

So that the equation for angle change may be written

$$\psi_{no} = \frac{-r}{EI \cos \theta} \left[ \int_0^\alpha M_n \frac{\partial M_n}{\partial M_{no}} d\phi + \mu \int_0^\alpha M_t \frac{\partial M_t}{\partial M_{no}} d\phi + \lambda \int_0^\alpha M_b \frac{\partial M_b}{\partial M_{no}} d\phi \right] \quad \text{Equation 53B}$$

Here, the negative sign only means that the angle change is in the opposite direction to the original applied correcting moment  $M_{no}$ . Since the equation is eventually set equal to zero, the sign is of no consequence in this solution, and may be omitted.

Equation 53A gives an expression for angle change in terms of the First Moment Area Theorem, and Equation 53B gives it in terms of Castigliano's Theorem. Although the former has the advantage of presenting a less abstract picture of the structure's behaviour (and was presented for this reason), Castigliano's Theorem is a more convenient method for deriving the expression for displacement.

The normal displacement is obtained by taking partial derivatives of  $M_n$ ,  $M_t$  and  $M_b$  (Equations 44, 45 and 46) with respect to the normal correcting

force  $C_2wr/\sin\theta (= F_{no})$ .

$$\frac{\partial M_n}{\partial F_{no}} = r \frac{\sin\theta}{\cos\theta} (\cos\phi - \phi\sin\phi) \quad \text{Equation 57}$$

$$\frac{\partial M_t}{\partial F_{no}} = r \sin\theta (\phi\cos\phi) \quad \text{Equation 58}$$

$$\frac{\partial M_b}{\partial F_{no}} = r \sin\theta \tan\theta \left( \frac{\sin\phi}{\sin^2\theta} + \phi\cos\phi \right) \quad \text{Equation 59}$$

and

$$\begin{aligned} \Delta_{no} = & \int_0^\alpha \frac{M_n}{EI} \frac{\partial M_n}{\partial F_{no}} ds + \int_0^\alpha \frac{M_t}{GJ} \frac{\partial M_t}{\partial F_{no}} ds \\ & + \int_0^\alpha \frac{M_b}{EK} \frac{\partial M_b}{\partial F_{no}} ds \end{aligned} \quad \text{Equation 60}$$

or

$$\begin{aligned} \Delta_{no} = & \frac{r}{EI \cos\theta} \left[ \int_0^\alpha M_n \frac{\partial M_n}{\partial F_{no}} d\phi + \mu \int_0^\alpha M_t \frac{\partial M_t}{\partial F_{no}} d\phi \right. \\ & \left. + \lambda \int_0^\alpha M_b \frac{\partial M_b}{\partial F_{no}} d\phi \right] \end{aligned} \quad \text{Equation 61}$$

Thus, in effect, moments of appropriate vectors for the elements of moment area have been taken about the axis of normal displacement at the midpoint.

Inserting Equations 44, 45, 46 and 54, 55, 56 into Equation 53B gives :

$$\psi_{no} = \frac{wr^3}{EI \cos \theta} \left\{ \frac{1}{\cos \theta} \left[ + \int_0^\alpha \cos \phi d\phi - C_1 \int_0^\alpha \cos^2 \phi d\phi \right. \right. \\ \left. \left. - C_2 \int_0^\alpha \phi \sin \phi \cos \phi d\phi + C_2 \int_0^\alpha \cos^2 \phi d\phi \right] + \right. \\ \left. \mu \cos \theta \left[ + \int_0^\alpha \phi \sin \phi d\phi - C_1 \int_0^\alpha \sin^2 \phi d\phi \right. \right. \\ \left. \left. + C_2 \int_0^\alpha \phi \sin \phi \cos \phi d\phi \right] + \right. \\ \left. \frac{\lambda \sin^2 \theta}{\cos \theta} \left[ + \int_0^\alpha \phi \sin \phi d\phi - C_1 \int_0^\alpha \sin^2 \phi d\phi \right. \right. \\ \left. \left. + C_2 \int_0^\alpha \phi \sin \phi \cos \phi d\phi + C_2 \int_0^\alpha \frac{\sin^2 \theta}{\sin^2 \theta} \sin^2 \phi d\phi \right] \right\} \\ \text{Equation 62}$$

Recalling that  $\gamma = \mu \cos^2 \theta + \lambda \sin^2 \theta$

$$\psi_{no} = \frac{wr^3}{EI \cos^2 \theta} \left\{ + \left[ \gamma \int_0^\alpha \phi \sin \phi d\phi + \int_0^\alpha \cos \phi d\phi \right] \right. \\ \left. - C_1 \left[ \gamma \int_0^\alpha \sin^2 \phi d\phi + \int_0^\alpha \cos^2 \phi d\phi \right] \right. \\ \left. + C_2 \left[ (\gamma - 1) \int_0^\alpha \phi \sin \phi \cos \phi d\phi + \lambda \int_0^\alpha \sin^2 \phi d\phi \right. \right. \\ \left. \left. + \int_0^\alpha \cos^2 \phi d\phi \right] \right\}$$

Equation 63

In a similar way, inserting Equations 44, 45, 46 and 57, 58, 59 into Equation 61 gives

$$\Delta_{no} = \frac{wr^4 \tan \theta}{EI \cos^2 \theta} \left\{ \begin{aligned} & \left[ \gamma \int_0^\alpha \phi^2 \cos \phi d\phi + (\lambda-1) \int_0^\alpha \phi \sin \phi d\phi + \int_0^\alpha \cos \phi d\phi \right] \\ & + C_1 \left[ (1-\gamma) \int_0^\alpha \phi \sin \phi \cos \phi d\phi - \lambda \int_0^\alpha \sin^2 \phi d\phi - \int_0^\alpha \cos^2 \phi d\phi \right] \\ & + C_2 \left[ \gamma \int_0^\alpha \phi^2 \cos^2 \phi d\phi + 2(\lambda-1) \int_0^\alpha \phi \sin \phi \cos \phi d\phi + \right. \\ & \left. \frac{\lambda}{\sin^2 \theta} \int_0^\alpha \sin^2 \phi d\phi + \int_0^\alpha \phi^2 \sin^2 \phi d\phi + \int_0^\alpha \cos^2 \phi d\phi \right] \end{aligned} \right\}$$

Equation 64

Particular solutions of equations 63 and 64 for specific values of  $\alpha$  are presented further in the text.

#### Derivation of Equations for a Helix with a Concentrated Load at its Midpoint and Both Ends Fixed

These equations are derived primarily because they are needed to obtain an expression for the vertical deflection of the helix at its midpoint.

The method of derivation is the same as in the case of the uniform load; the correcting forces and moments to make the deflections and angle changes at the free ends of the cantilever halves compatible have the same character.

The equations of moment for the two cantilevers each supporting half the concentrated load  $W$  at their respective free ends are:

$$M_n = \frac{Wr}{2} (\sin \phi) \quad \text{Equation 65}$$

$$M_t' = \frac{Wr}{2} (1 - \cos \phi) \quad \text{Equation 66}$$

and  $M_t'$  is resolved into

$$M_t = \frac{Wr}{2} \cdot \cos \theta (1 - \cos \phi) \quad \text{Equation 67}$$

$$M_b = \frac{Wr}{2} \cdot \sin \theta (1 - \cos \phi) \quad \text{Equation 68}$$

The normal correcting force is  $C_4.W/2 (\tan \theta)$ , the normal correcting moment  $C_3'.Wr/2$ , and  $C_3 = C_3' + C_4$ . The general equations are obtained in the same way as are those for uniform load; they are:

$$M_n' = \frac{Wr}{2} \left[ \sin \phi - C_3 \cos \phi - C_4 \phi \sin \phi + C_4 \cos \phi \right] \quad \text{Equation 69}$$

$$M_t' = \frac{Wr \cos \theta}{2} \left[ 1 - \cos \phi - C_3 \sin \phi + C_4 \phi \cos \phi \right] \quad \text{Equation 70}$$

$$M_b' = \frac{Wr \sin \theta}{2} \left[ 1 - \cos \phi - C_3 \sin \phi + C_4 \phi \cos \phi + \frac{C_4}{\sin^2 \theta} \sin \phi \right] \quad \text{Equation 71}$$

$$V_n' = \frac{W}{2} \left( \frac{C_4}{\tan \theta} \cdot \cos \phi \right) \quad \text{Equation 72}$$

$$F_t' = \frac{W}{2} \left( \sin \theta + \frac{C_4}{\tan \theta} \cdot \cos \theta \cdot \sin \phi \right) \quad \text{Equation 73}$$

$$V_b' = \frac{W}{2} \left( \cos \theta - \frac{C_4}{\tan \theta} \cdot \sin \theta \cdot \sin \phi \right) \quad \text{Equation 74}$$

The expressions for  $\psi_{no}$  and for  $\Delta_{no}$  are also obtained in the same way as for uniform load; they are:

$$\psi_{no} = \frac{Wr^2}{2EI \cos \theta} \left\{ \begin{aligned} &+ \left[ (1-\gamma) \int_0^\alpha \sin \phi \cos \phi d\phi + \gamma \int_0^\alpha \sin \phi d\phi \right] \\ &- C_3 \left[ \gamma \int_0^\alpha \sin^2 \phi d\phi + \int_0^\alpha \cos^2 \phi d\phi \right] \\ &+ C_4 \left[ (\gamma-1) \int_0^\alpha \phi \sin \phi \cos \phi d\phi + \lambda \int_0^\alpha \sin^2 \phi d\phi \right. \\ &\quad \left. + \int_0^\alpha \cos^2 \phi d\phi \right] \end{aligned} \right\} \quad \text{Equation 75}$$



$$\Delta_{ho} = \frac{Wr^3 \tan \theta}{2EI \cos \theta} \left\{ \begin{aligned} & \left[ \gamma \int_0^\alpha \phi \cos \phi d\phi - \gamma \int_0^\alpha \phi \cos^2 \phi d\phi + \lambda \int_0^\alpha \sin \phi d\phi \right. \\ & \quad \left. - \int_0^\alpha \phi \sin^2 \phi d\phi + (1-\lambda) \int_0^\alpha \sin \phi \cos \phi d\phi \right] \\ & + C_3 \left[ (1-\gamma) \int_0^\alpha \phi \sin \phi \cos \phi d\phi - \lambda \int_0^\alpha \sin^2 \phi d\phi - \int_0^\alpha \cos^2 \phi d\phi \right] \\ & + C_4 \left[ \gamma \int_0^\alpha \phi^2 \cos^2 \phi d\phi + 2(\lambda-1) \int_0^\alpha \phi \sin \phi \cos \phi d\phi + \right. \\ & \quad \left. \frac{\lambda}{\sin^2 \theta} \int_0^\alpha \sin^2 \phi d\phi + \int_0^\alpha \phi^2 \sin^2 \phi d\phi + \int_0^\alpha \cos^2 \phi d\phi \right] \end{aligned} \right\}$$

Equation 76

Particular solutions of equations 75 and 76 for specific values of  $\alpha$  are presented further in the text.

#### Derivation of an Expression for the Vertical Deflection at the Midpoint of a Uniformly Loaded Helix with Both Ends Fixed

To determine the vertical deflection by Castiglano's Theorem, the general equations of moment for a load in the direction of the deflection are established, (Equation 69, 70 and 71). Partial derivatives of  $M'_n$ ,  $M'_t$  and  $M'_b$  are taken with respect to the load  $W$ ; the deflection is then given by

$$\Delta_{zo} = \int_0^\alpha \frac{M_n}{EI} \frac{\partial M'_n}{\partial W} ds + \int_0^\alpha \frac{M_t}{GJ} \frac{\partial M'_t}{\partial W} ds + \int_0^\alpha \frac{M_b}{EK} \frac{\partial M'_b}{\partial W} ds$$

Equation 77

The final expression can be reduced to

$$\Delta_{zo} = \frac{K_d}{2 \cos^2 \theta} \cdot \frac{wr^4}{EI} = K_d' \frac{wr^4}{EI}$$

Equation 78

where  $K_d$  is a constant for any particular helix and is obtained by using Table 1.

In Table 1, the values of the definite integrals in column A are determined for any specific value of  $\alpha$ . For each horizontal line, the value of the integral is multiplied by the constants shown in columns B, C and D respectively. The products of column B are totalled algebraically and multiplied by  $\delta$ , those of column C by  $\lambda$ , and the algebraic totals of column D are multiplied by unity. The algebraic sum of these last three products is  $K_d$ .

For a  $360^\circ$  helix, in which  $\alpha = \pi$ , Table 1 gives the following expression for  $K_d$

$$K_d = \frac{\pi}{4} \left\{ \begin{aligned} &\gamma \left[ \begin{aligned} &+ 8.82 - 2.54 C_1 - 5.68 C_2 - 4 C_3 - 8 C_4 \\ &+ 2 C_1 C_3 + C_1 C_4 + C_2 C_3 + 7.58 C_2 C_4 \end{aligned} \right] \\ &+ \lambda \left[ \begin{aligned} &\phantom{+ 8.82 - 2.54 C_1 - 5.68 C_2 - 4 C_3 - 8 C_4} + 2.54 C_2 \phantom{+ 7.58 C_2 C_4} + 4 C_4 \\ &\phantom{+ 8.82 - 2.54 C_1 - 5.68 C_2 - 4 C_3 - 8 C_4} - 2 C_1 C_4 - 2 C_2 C_3 - 2 C_2 C_4 + 2 \frac{C_2 C_4}{\sin^2 \theta} \end{aligned} \right] \\ &+ 1 \left[ \begin{aligned} &+ 2.54 \phantom{- 5.68 C_2 - 4 C_3 - 8 C_4} - 3.14 C_2 \phantom{+ 7.58 C_2 C_4} - 4 C_4 \\ &+ 2 C_1 C_3 - 3 C_1 C_4 - 3 C_2 C_3 + 9.58 C_2 C_4 \end{aligned} \right] \end{aligned} \right\}$$

Equation 79

In Table 2 values of  $K_d'$  are given for helical beams of various slopes and cross-sections and with  $\alpha = \pi$  radians.

#### Particular Solutions for $\alpha = \pi$

For  $\alpha = \pi$ , Equations 63, 64, 75 and 76 take the forms:

$$\psi_{no} = \frac{w r^3}{E I \cos^2 \theta} \frac{\pi}{4} \left[ 4 \gamma - (2 \gamma + 2) C_1 + (-\gamma + 2 \lambda + 3) C_2 \right]$$

Equation 63A

COLUMN-A	COLUMN-B	COLUMN-C	COLUMN-D
$\int_0^\alpha \phi d\phi$	1	0	0
$\int_0^\alpha \phi \sin \phi d\phi$	$-C_3$	$C_4$	$-C_4$
$\int_0^\alpha \phi \sin^2 \phi d\phi$	0	0	$-C_2$
$\int_0^\alpha \phi \sin \phi \cos \phi d\phi$	$-C_1 C_4 - C_2 C_3$	$2C_2 C_4$	$C_1 C_4 + C_2 C_3 - 2C_2 C_4$
$\int_0^\alpha \phi \cos \phi d\phi$	$C_2 - 1$	0	0
$\int_0^\alpha \phi \cos^2 \phi d\phi$	$-C_2$	0	0
$\int_0^\alpha \phi^2 \sin^2 \phi d\phi$	0	0	$C_2 C_4$
$\int_0^\alpha \phi^2 \cos \phi d\phi$	$C_4$	0	0
$\int_0^\alpha \phi^2 \cos^2 \phi d\phi$	$C_2 C_4$	0	0
$\int_0^\alpha \sin \phi d\phi$	$-C_1$	$C_2$	1
$\int_0^\alpha \sin^2 \phi d\phi$	$C_1 C_3$	$-C_1 C_4 - C_2 C_3 + \frac{C_2 C_4}{\sin^2 \theta}$	0
$\int_0^\alpha \sin \phi \cos \phi d\phi$	$C_1$	$-C_2$	$-C_1 + C_2$
$\int_0^\alpha \cos \phi d\phi$	0	0	$-C_3 + C_4$
$\int_0^\alpha \cos^2 \phi d\phi$	0	0	$C_1 C_3 + C_2 C_4 - C_1 C_4 - C_2 C_3$
	$\Sigma$ to be multiplied by $\gamma$	$\Sigma$ to be multiplied by $\lambda$	$\Sigma$ to be multiplied by 1

TABLE 1 Deflection Constant  $K_d$

$$\Delta_{no} = \frac{Wr^4 \tan \theta}{EI \cos^2 \theta} \cdot \frac{\pi}{4} \left[ \begin{aligned} &-8\gamma + 4\lambda - 4 - (-\gamma + 2\lambda + 3) C_1 \\ &+ (7.65\gamma - 2\lambda + \frac{2\lambda}{\sin^2 \theta} + 9.65) C_2 \end{aligned} \right]$$

Equation 64A

$$\Psi_{no} = \frac{Wr^2}{2EI \cos \theta} \cdot \frac{\pi}{4} \left[ \begin{aligned} &2.54\gamma - (2\gamma + 2) C_3 + (-\gamma + 2\lambda + 3) C_4 \end{aligned} \right]$$

Equation 75A

$$\Delta_{no} = \frac{Wr^3 \tan \theta}{2EI \cos \theta} \cdot \frac{\pi}{4} \left[ \begin{aligned} &-5.68\gamma + 2.54\lambda - 3.14 - (-\gamma + 2\lambda + 3) C_3 \\ &+ (7.65\gamma - 2\lambda + \frac{2\lambda}{\sin^2 \theta} + 9.65) C_4 \end{aligned} \right]$$

Equation 76A

Setting Equations 63A and 64A equal to zero and solving them simultaneously yields:

$$C_1 = \frac{2\gamma}{(\gamma+1)} - \frac{(\gamma-2\lambda-3) C_2}{2(\gamma+1)}$$

Equation 80

$$C_2 = \frac{\gamma(3\gamma+9) - 2(\lambda-1)}{\gamma(3.54\gamma+10.08) - (\lambda+2)^2 + \frac{\lambda(\gamma+1)}{\sin^2 \theta} + 6.54}$$

$$\alpha = \pi$$

Equation 81

Specific values of  $C_1$  and  $C_2$  are given in Table 2.

Setting Equations 75A and 76A equal to zero and solving them simultaneously yields:

$$C_3 = \frac{1.27\gamma}{(\gamma+1)} - \frac{(\gamma-2\lambda-3) C_4}{2(\gamma+1)}$$

Equation 82

$$C_4 = \frac{2}{\pi} \cdot \frac{\gamma(3.47\gamma + 9.94) - 2\lambda + 2.47}{\gamma(3.54\gamma + 10.08) - (\lambda + 2)^2 + \frac{\lambda(\gamma + 1) + 6.54}{\sin^2 \theta}}$$

$$\alpha = \pi$$

Equation 83

Specific values of  $C_3$  and  $C_4$  are given in Table 2.

Table 2 also gives values for maximum moments; for a helix with  $\alpha = \pi$  radians, they occur as follows:

$$M_n(\max) = \frac{wr^2}{\cos \theta} (1 + C_1 - C_2) \quad \text{when } \phi = \pm \pi$$

$$M_t(\max) = \pm wr^2 \cdot \pi (1 - C_2) \quad \text{when } \phi = \pm \pi$$

$$M_b(\max) = \pm wr^2 \cdot \pi \tan \theta (1 - C_2) \quad \text{for } \lambda > 4 \text{ (approx)} \\ \text{when } \phi = \pm \pi$$

OR

$$M_b(\max) = \pm wr^2 \cdot \tan \theta \left( \frac{\pi}{2} - C_1 + \frac{C_2}{\sin^2 \theta} \right) \quad \text{for } \lambda < 4 \\ \text{when } \phi = \pm \frac{\pi}{2}$$

In Table 2 the value of  $\mu$  is taken as  $0.7(1 + \lambda)$ ; this is for rectangular cross-sections only and assumes  $E/G = 2.5$ . This is discussed further in the text.

#### Particular Solutions for $\alpha = 3\pi/4$

With Equations 63 and 64 equal zero and  $\alpha$  in these equations equal  $3\pi/4$ , simultaneous solution yields:

$$C_1 = \frac{2.39\gamma + 0.71}{1.43\gamma + 0.93} - \frac{(0.125\gamma - 1.43\lambda - 1.06)C_2}{1.43\gamma + 0.93}$$

Equation 84

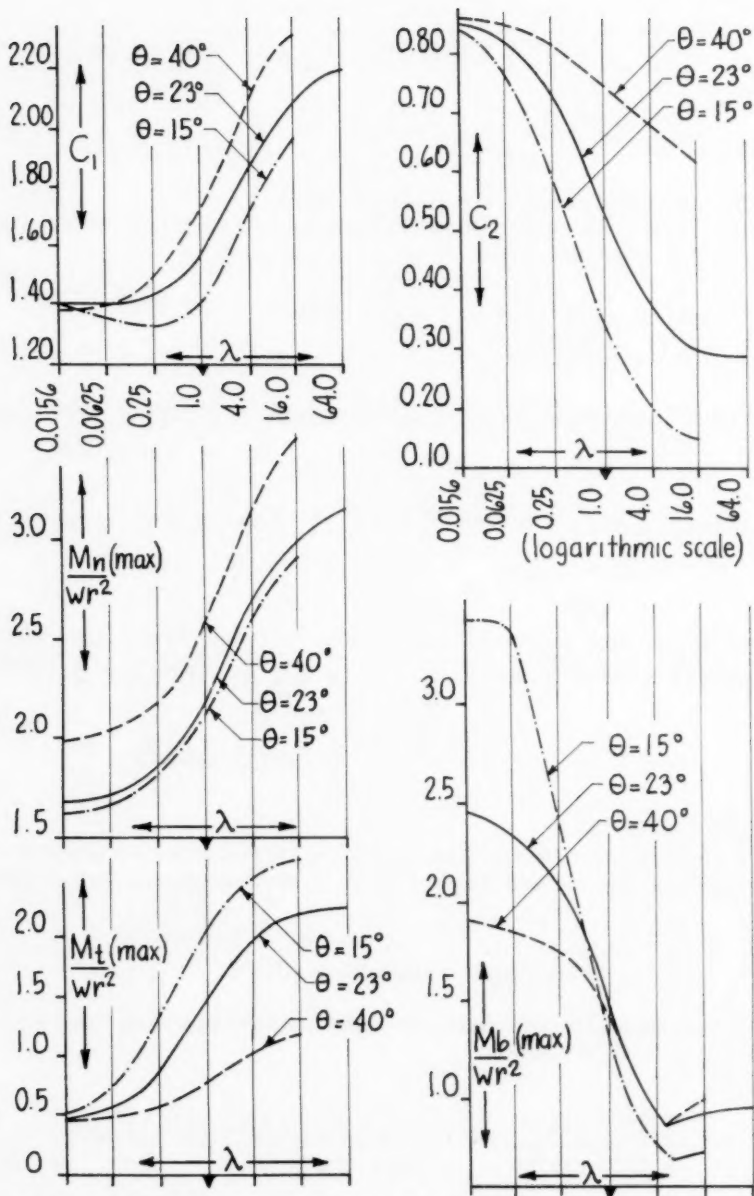


Figure 13 CONSTANTS &amp; MAX. MOMENTS of TABLE 2

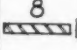

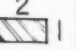

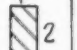
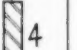
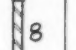
	$\theta$							
$\lambda$		0.0156	0.0625	0.25	1.0	4.0	16.0	64.0
$\mu = 0.7(1+\lambda)$		0.71	0.74	0.88	1.4	3.5	11.9	45.5
$C_1$	40°	1.38	1.40	1.49	1.74	2.10	2.32	2.20
	23°	1.40	1.40	1.43	1.56	1.87	2.10	
	15°	1.40	1.36	1.33	1.40	1.72	1.97	
$C_2$	40°	0.86	0.84	0.82	0.75	0.68	0.62	0.29
	23°	0.85	0.82	0.73	0.53	0.38	0.30	
	15°	0.84	0.76	0.58	0.34	0.20	0.15	
$C_3$	40°	0.96	0.96	1.03	1.17	1.39	1.53	1.43
	23°	0.95	0.94	0.96	1.03	1.22	1.36	
	15°	0.95	0.92	0.89	0.96	1.11	1.27	
$C_4$	40°	0.65	0.62	0.61	0.55	0.50	0.46	0.21
	23°	0.62	0.60	0.53	0.39	0.28	0.23	
	15°	0.61	0.55	0.43	0.24	0.15	0.11	
$K_d'$ in $\frac{\Delta_z}{EI}$ $\Delta_z = K_d' w r^4$	40°		0.17		1.50		12.0	58.5
	23°	0.10	0.23	0.69	2.20	5.85	16.4	
	15°		0.42		2.70		19.7	
$\frac{M_n(\text{MAX})}{w r^2}$	40°	1.98	2.04	2.18	2.60	3.16	3.52	3.16
	23°	1.68	1.72	1.85	2.20	2.71	3.04	
	15°	1.62	1.66	1.81	2.14	2.62	2.92	
$\frac{M_t(\text{MAX})}{w r^2}$	40°	0.47	0.50	0.58	0.79	1.04	1.19	2.23
	23°	0.47	0.57	0.88	1.48	1.98	2.19	
	15°	0.50	0.75	1.32	2.07	2.51	2.67	
$\frac{M_b(\text{MAX})}{w r^2}$	40°	1.90	1.85	1.74	1.38	0.93	1.00	0.95
	23°	2.45	2.34	2.07	1.47	0.92	0.93	
	15°	3.42	3.36	2.39	1.40	0.75	0.72	

TABLE 2  
VALUES OF CONSTANTS AND MAXIMUM MOMENTS

HELICAL BEAMS with  $\left\{ \begin{array}{l} \alpha = \pi \text{ radians} \\ \text{Rectangular cross-section} \\ \text{Both ends completely fixed} \end{array} \right.$

$$C_2 = \frac{0.86\gamma(\gamma+6.51) - 1.21(\lambda-1.92)}{1.30\gamma(\gamma+5.95+1.57\lambda) - 2.04\lambda^2 - 3.26\lambda + 1.33\lambda + 3.18} \frac{\sin^2\theta}{\sin^2\theta}$$

$$\alpha = 3\pi/4$$

Equation 85

Specific values of  $C_1$  and  $C_2$  are given in Table 3.

Table 3 also gives values of maximum moments; for a helix with  $\alpha = 3\pi/4$ , they occur as follows:

$$M_n(\max) = \frac{wr^2(0.707)}{\cos\theta} [1.42 + C_1 - 3.36 C_2]$$

$$\text{when } \phi = \pm 3\pi/4$$

$$M_t(\max) = wr^2(0.707) [2.36(1.42 - C_2) - C_1]$$

$$\text{when } \phi = \pm 3\pi/4$$

$$M_b(\max) = wr^2(0.707) \tan\theta \left[ 2.36(1.42 - C_2) - C_1 + \frac{C_2}{\sin^2\theta} \right]$$

for deep x-sections

$$\text{when } \phi = \pm 3\pi/4$$

OR

$$M_b(\max) = wr^2 \tan\theta \left[ 1.57 - C_1 + \frac{C_2}{\sin^2\theta} \right]$$

for shallow x-sections when  $\phi = \pm \pi/2$

Table 3 is for rectangular cross-sections where  $\mu$  is taken as  $0.7(1 + \lambda)$ .

Particular Solutions for  $\alpha = \pi/2$

With Equations 63 and 64 equal zero and  $\alpha$  in these equations equal  $\pi/2$ , simultaneous solution yields:

$$C_1 = 1.27 + 0.50 C_2 + \frac{\lambda}{(\gamma+1)} C_2$$

Equation 86

$$C_2 = \frac{0.20\gamma^2 + 2.74\gamma + 2.54}{0.28\gamma^2 + 4.62\gamma + (\gamma+1)4\lambda - 4\lambda^2 + 4.34} \frac{\sin^2\theta}{\sin^2\theta}$$

Equation 87



Specific values of  $C_1$  and  $C_2$  are given in Table 3 which also gives the corresponding maximum moments; for a helix with  $\alpha = \pi/2$ , they occur as follows:

$$M_n(\max) = \frac{wr^2}{\cos \theta} \left[ 1 - 1.57 C_2 \right]$$

when  $\phi = \pm \pi/2$

$$M_t(\max) = wr^2 \left[ 1.57 - C_1 \right]$$

when  $\phi = \pm \pi/2$

$$M_b(\max) = wr^2 \tan \theta \left[ 1.57 - C_1 + \frac{C_2}{\sin^2 \theta} \right]$$

when  $\phi = \pm \pi/2$

Table 3 is for rectangular cross-sections where  $\mu = 0.7(1 + \lambda)$ .

#### What the Graphs and Tables Show

For the range of arcs ( $\alpha$ ) considered, the following observations and comments can be made about members of rectangular section:

For the same uniform load carried at the same radius, and for members of constant cross-sectional area, the normal and tangential moments decrease as the depth is decreased. The decrease tapers off after the sections become flatter than 1 to 4. Furthermore, for sections flatter than this, the torsional stress will start rising sharply despite further decreases in torsional moment, because torsional stress varies inversely as the square of the smaller dimension of the rectangle.

As the member becomes flatter, the binormal moment increases, but this is more than offset by the section's increasing ability to carry the binormal moment at low stresses.

If the member's depth is increased, the increase in normal moment is likewise offset by the section's increased moment of inertia. But as the member becomes deeper, the inverse of the square of the smaller dimension is again causing rapid increases in torsion stress, and making matters worse, the torsional moment is now several times greater than that of the flatter member of same rectangular proportions.

The superior structural efficiency of the flatter sections is also apparent when the deflection is considered. If  $K_d'$  is divided by the relative  $I$  for members of constant cross-sectional area, it is seen that a 4 to 1 deep section deflects approximately four times as much as a 1 to 4 flat section of the same radius and under the same uniform load.

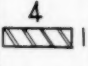
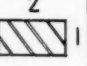
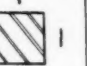
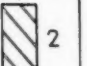
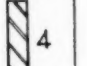
	$\theta$	$\alpha$					
$\lambda$			0.0625	0.25	1.0	4.0	16.0
$\mu = 0.7(1 + \lambda)$			0.74	0.88	1.4	3.5	11.9
$C_1$	$23^\circ$	$3\pi/4$	1.59	1.59	1.61	1.67	1.72
	$23^\circ$	$\pi/2$	1.50	1.43	1.36	1.32	1.28
$C_2$	$23^\circ$	$3\pi/4$	0.65	0.50	0.29	0.13	0.08
	$23^\circ$	$\pi/2$	0.43	0.25	0.10	0.03	0.01
$\frac{M_n (\text{MAX})}{wr^2}$	$23^\circ$	$3\pi/4$	0.62	1.01	1.59	2.03	2.20
	$23^\circ$	$\pi/2$	0.35	0.68	0.91	1.03	1.06
$\frac{M_t (\text{MAX})}{wr^2}$	$23^\circ$	$3\pi/4$	0.15	0.40	0.75	0.96	1.01
	$23^\circ$	$\pi/2$	0.07	0.14	0.21	0.25	0.29
$\frac{M_b (\text{MAX})}{wr^2}$	$23^\circ$	$3\pi/4$	1.79	1.38	0.89	0.66	0.58
	$23^\circ$	$\pi/2$	1.23	0.75	0.36	0.20	0.14

TABLE 3

VALUES OF CONSTANTS AND MAXIMUM MOMENTS

HELICAL BEAMS with  $\left\{ \begin{array}{l} \alpha = 3\pi/4 \text{ or } \pi/2 \\ \text{Rectangular cross-section} \\ \text{Both ends completely fixed} \end{array} \right.$

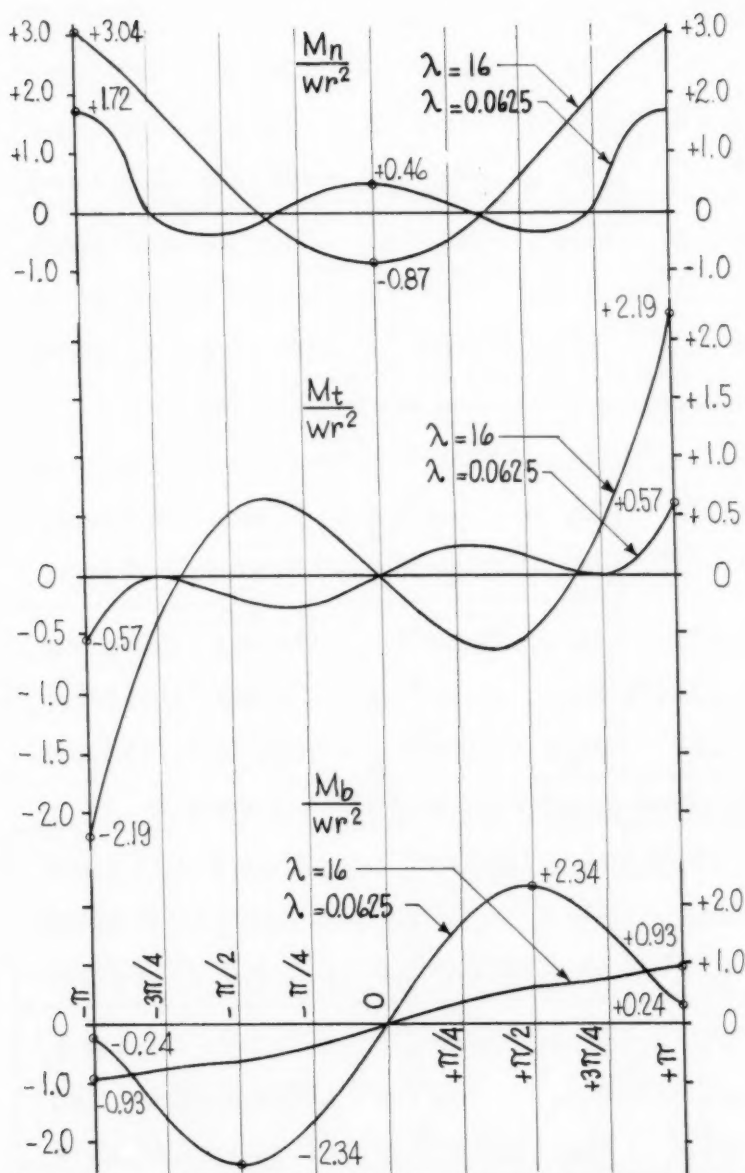


Figure 14 MOMENT CURVES - Helical Beams with  $\theta = 23^\circ$   
 $\alpha = \pi$  radians - rectangular cross-section -  $\lambda$  as shown

# CHARACTERISTIC EQUATIONS (Rectangular Cross-sections)

$\alpha = \pi$	$M_n = 1.086 wr^2 (1 - 1.80 \cos \phi - 0.30 \phi \sin \phi)$
$\lambda = 16$	$M_t = wr^2 (\phi - 2.10 \sin \phi + 0.30 \phi \cos \phi)$
$\theta = 23^\circ$	$M_b = 0.424 wr^2 (\phi - 0.14 \sin \phi + 0.30 \phi \cos \phi)$
$\alpha = \pi$	$M_n = 1.086 wr^2 (1 - 0.58 \cos \phi - 0.82 \phi \sin \phi)$
$\lambda = 0.625$	$M_t = wr^2 (\phi - 1.40 \sin \phi + 0.82 \phi \cos \phi)$
$\theta = 23^\circ$	$M_b = 0.424 wr^2 (\phi + 3.96 \sin \phi + 0.82 \phi \cos \phi)$

The above equations are plotted in Figure 14

$\alpha = 3\pi/4$	$M_n = 1.086 wr^2 (1 - 1.64 \cos \phi - 0.08 \phi \sin \phi)$
$\lambda = 16$	$M_t = wr^2 (\phi - 1.72 \sin \phi + 0.08 \phi \cos \phi)$
$\theta = 23^\circ$	$M_b = 0.424 wr^2 (\phi - 1.20 \sin \phi + 0.08 \phi \cos \phi)$
$\alpha = 3\pi/4$	$M_n = 1.086 wr^2 (1 - 0.94 \cos \phi - 0.65 \phi \sin \phi)$
$\lambda = 0.0625$	$M_t = wr^2 (\phi - 1.59 \sin \phi + 0.65 \phi \cos \phi)$
$\theta = 23^\circ$	$M_b = 0.424 wr^2 (\phi + 2.66 \sin \phi + 0.65 \phi \cos \phi)$

The above equations are plotted in Figure 15

$\alpha = \pi/2$	$M_n = 1.086 wr^2 (1 - 1.27 \cos \phi - 0.01 \phi \sin \phi)$
$\lambda = 16$	$M_t = wr^2 (\phi - 1.28 \sin \phi + 0.01 \phi \cos \phi)$
$\theta = 23^\circ$	$M_b = 0.424 wr^2 (\phi - 1.23 \sin \phi + 0.01 \phi \cos \phi)$
$\alpha = \pi/2$	$M_n = 1.086 wr^2 (1 - 1.07 \cos \phi - 0.43 \phi \sin \phi)$
$\lambda = 0.0625$	$M_t = wr^2 (\phi - 1.50 \sin \phi + 0.43 \phi \cos \phi)$
$\theta = 23^\circ$	$M_b = 0.424 wr^2 (\phi + 1.32 \sin \phi + 0.43 \phi \cos \phi)$

The above equations are plotted in Figure 16

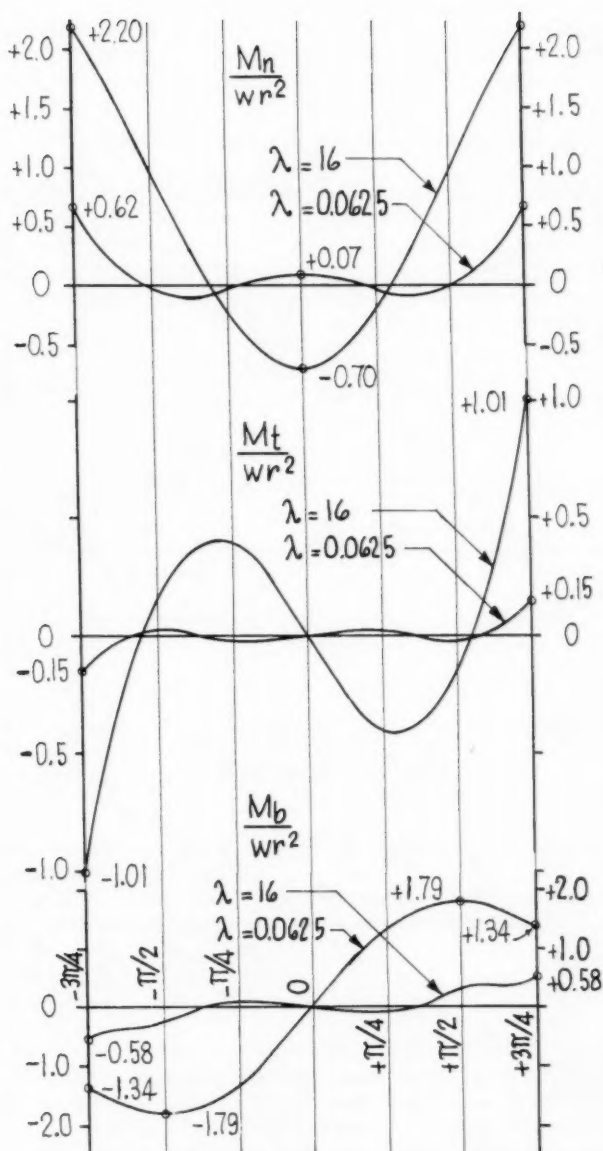


Figure 15 MOMENT CURVES - Helical Beam with  $\theta = 23^\circ$   
 $\alpha = 3\pi/4$  radians - rectangular cross-section -  $\lambda$  as shown

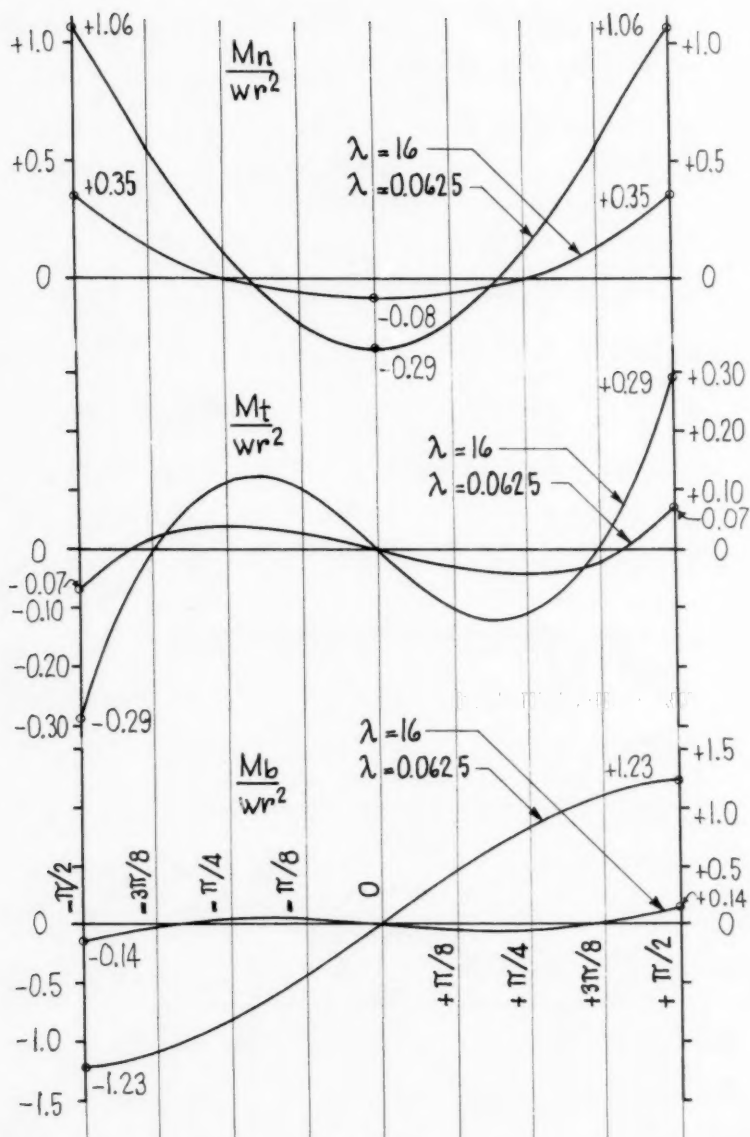


Figure 16 MOMENT CURVES - Helical Beams with  $\theta = 23^\circ$   
 $\alpha = \pi/2$  radians - rectangular cross-section -  $\lambda$  as shown

With caution and some modifications, the statements above can be applied to sections other than rectangular. The criteria is the ratio  $\lambda$  of the moments of inertia and its relation to the structure's behaviour. The torsion factor  $\mu$  plays a lesser part, and this is discussed in the next section.

#### Effect of Variation in J, the Modified Polar Moment of Inertia

The term "J" in the expression  $\mu = EI/GJ$  is the polar moment of inertia of the cross-section if the latter is circular or annular.

For rectangular, oval and other solid sections of simple outline, the value of "J" is not as great as the value indicated by the true polar moment of inertia. For wide-flange sections and other complex shapes, "J" drops off even more sharply from the value of the polar moment of inertia. For instance, the value of "J" for an 18 WF 85 is given as 5.82 inches<sup>(4)</sup> (reference 1) whereas its true polar moment of inertia is 1529 inches<sup>(4)</sup>.

For rectangular cross-sections, "J" has been given by the following expressions:

$$J = \frac{b^3 d^3}{3.58(b^2 + d^2)} \quad \text{Reference 2}$$

$$J = \frac{bd^3}{16} \left[ \frac{16}{3} - 3.36 \frac{d}{b} \left( 1 - \frac{d^4}{12b^4} \right) \right] \quad \text{Reference 3}$$

$$J = \frac{b^4 d^4}{40 I_p} = \frac{b^3 d^3}{3.33(b^2 + d^2)} \quad \text{Reference 4}$$

In each of the above, d is the smaller dimension of the rectangle.  $I_p$  is the True Polar Moment of Inertia.

Recalling that  $\lambda = I/K = d^2/b^2$  (for rectangular cross-section), and assuming that  $E/G = 2.5$  and using the last of the expressions for "J", it can be shown that

$$\frac{EI}{GJ} = \mu = 0.70(1 + \lambda) \quad \text{Equation 88}$$

This value of  $\mu$  has been used throughout the computation of all data presented in this paper. It is emphasized that it applies only to rectangular cross-sections, and that even in this domain it is not an exact expression.

However, it can be shown that the expression  $\mu$  (and consequently  $\delta$ ) can vary considerably without causing large variations in the constants  $C_1$ ,  $C_2$  and the maximum moments. This is shown in Table 4.

$\lambda$	Assumed $\mu$	$C_1$	$C_2$	$M_n(\max)/w r^2$		$M_t(\max)/w r^2$		$M_b(\max)/w r^2$	
0.062	$0.35(1 + \lambda)$	1.34	0.80	1.67	- 3%	0.63	+11%	2.32	- 1%
0.062	$0.70(1 + \lambda)$	1.40	0.82	1.72	0%	0.57	0%	2.34	0%
0.062	$1.40(1 + \lambda)$	1.46	0.84	1.75	+ 2%	0.50	-12%	2.37	+ 1%
1.0	$0.35(1 + \lambda)$	1.41	0.46	2.12	- 5%	1.70	+15%	1.34	- 9%
1.0	$0.70(1 + \lambda)$	1.56	0.53	2.20	0%	1.48	0%	1.47	0%
1.0	$1.40(1 + \lambda)$	1.65	0.61	2.20	0%	1.23	-17%	1.61	+ 9%
16.0	$0.35(1 + \lambda)$	1.46	0.25	2.40	-21%	2.36	-8%	1.00	+ 8%
16.0	$0.70(1 + \lambda)$	2.10	0.30	3.04	0%	2.19	0%	0.93	0%
16.0	$1.40(1 + \lambda)$	2.03	0.40	2.85	- 6%	1.88	-14%	0.91	- 2%

TABLE 4

EFFECT OF VARIATIONS IN ASSUMED VALUE OF  $\mu$   
(For Helical Beams with  $\alpha = \pi$  radians and  $\theta = 23^\circ$ )

## CONCLUSIONS

For shallow-wide cross-sections, a beneficial "Bent Action" occurs which reduces normal and torsional moments. This "Bent Action" can be summarized as follows:

As the member becomes weak in bending about a horizontal-radial axis, the upper and lower halves tend to "lean" on each other. The forces set up by this "leaning" are carried by each half acting as a canted bent which is relatively stiff in bending about an axis roughly perpendicular.

For constant uniform load, radius and cross-sectional area, the midpoint deflection of a helical beam decreases as the depth of the cross-section is decreased. This rather unique behaviour is the result of the "Bent Action" and can also be explained in terms of the moment areas which are smaller at the regions most remote from the midpoint, and so disposed in sign and location as to cancel each other for the shallow-wide sections.

As some of the curves tend to indicate, the maximum deflection does not necessarily occur at the midpoint. Model tests now in progress show that for shallow-wide cross-sections the deflection of the quarter-points of a  $360^\circ$  helix is roughly three times that of the midpoint.

The same model tests tend to show that the beneficial "Bent Action" of shallow-wide sections also reduces torsional moments for cases of unsymmetrical loading.



The properties required for a solution are easily ascertained, except one, the torsional factor  $J$ , and it has been shown that this one has only a small effect on the results.

The solution suggests that thin helical slabs which are architecturally preferable are also structurally more efficient.

#### REFERENCES

1. "Torsional Stresses in Structural Beams," Booklet S-57, Bethlehem Steel Company.
2. Andersen, Paul, "Design of Reinforced Concrete in Torsion," Transaction ASCE V. 103, October, 1938, P. 1503.
3. Roark, R. J., "Formulas for Stresses and Strain," (McGraw Hill).
4. Panayotounakos, E. D., "Circular Beams Loaded Perpendicular to Their Plane," Technica Chronica (Athens), issues 298, 300, 301-302, 304, 305 and 306.
5. Panayotounakos, E. D., "Statically Indeterminate Helical Beams Fixed at Both Ends," Technica Chronica (Athens), issue 313.
6. Soutter, P., "Wendeltreppe in Eisenbeton," Schweizerische Bauzeitung Issue 41, October, 1954.
7. Cohen, J. S., "Design of Helical Staircases," Constructional and Engineering, May, 1955.
8. Kingsbury, R. and Riessauw, F. G., "Construction d'un escalier Helicoidal en Beton Precontraint," Precontrainte-Prestressing, extract 1-1955.
9. Beton Kalendar, Part II, 1955, pp. 177-202.
10. Bergman, Victor, "Helicoidal Staircases of Reinforced Concrete," Journal of the ACI, V. 28, No. 4, October, 1956.

#### ACKNOWLEDGMENTS

The author wishes to acknowledge the assistance and advice in the preparation of this paper of Andrew J. Brown, Dr. Fazlur R. Khan and John A. Sbarounis, Chief Structural Engineer and Structural Engineers, respectively, of Skidmore, Owings & Merrill.



---

Journal of the  
STRUCTURAL DIVISION  
Proceedings of the American Society of Civil Engineers

---

EFFECT OF INITIAL ECCENTRICITIES ON  
COLUMN PERFORMANCE AND CAPACITY

John M. Hayes,<sup>1</sup> Member, ASCE  
(Proc. Paper 1440)

SYNOPSIS

This paper summarizes the results of tests made to study the effect of initial eccentricities upon column performance and capacity. The type of section investigated was the rolled H-section. The eccentricity was created by milling out-of-square about the weak axis the bearing ends at a partially riveted splice. The columns were all fabricated from ASTM A7 structural steel.

This type of eccentricity had only a small effect upon the capacities of the columns tested. It gave greater unit shortening and reduced the stiffness of the column. The capacity of the column may, in general, safely be considered equal to that of an identical unspliced column, provided that the Euler critical load, based on hinged-ends, is greater than the yield point strength of the material, and the ends of the column are, at least, partially restrained.

INTRODUCTION

Columns in buildings are usually spliced at a convenient distance above floor level. The load is considered to be transferred in direct bearing and a partially connected splice is made to hold the abutting ends in line. What is the effect on the column performance and capacity of out-of-squareness at the splice due to poor milling or erection inaccuracies?

This problem is also encountered at column bases and in compression members in trusses with partially connected splices.

The tests described in this paper were made to study the effect of out-of-squareness at a partially riveted splice on the performance and capacity of a column fabricated from a rolled H-section of ASTM A7 structural steel.

Five models were tested with flat ends as shown in Fig. 1. They were fabricated from a 60 ft. stock length of a 6 x 6 light column section at 25 lb. per foot of ASTM A7 structural steel.

Models CO and COL were straight unspliced control columns.

Models C1 and C3 had splices at the bottom quarter point riveted for about

---

Note: Discussion open until April 1, 1958. Paper 1440 is part of the copyrighted Journal of the Structural Division of the American Society of Civil Engineers, Vol. 83, No. ST 6, November, 1957.

1. Associate Prof. of Struct. Eng., Purdue University, Lafayette, Inc.

25% of the working load and an out-of-squareness with respect to the weak axis of 1/16 in. across the 6 in. flange width. The tips of the flanges touched at one extreme fiber and were 1/16 in. apart at the opposite extreme fiber.

Model C2 consisted of the top three-quarters length directly over the bottom one-quarter length with the 1/16 in. out-of-squareness across the 6 in. flange width. A clamp braced the two portions, preventing relative lateral movement, but offering no resistance against longitudinal movement.

### Description of Tests

#### Set-up

All models were tested with flat ends. Models C0, C1, and C2 were tested in a 300,000 pound constant strain mechanical type testing machine. Models COL and C3 were tested in a 600,000 pound constant stress hydraulic testing machine.

Typical locations of SR-4 electrical resistance strain gages for Model C1 are shown in Fig. 2. Lateral deflections of the web with respect to the ends of the models were measured with dial gages attached to a one inch diameter rod supported from the web of the column. Rotations of the elastic curve were also measured.

The overall shortening of a model was determined by suspending a 3/8 in. diameter rod on each side of the column from blocks attached to the middle of the flanges and 3 in. from the upper end of the model. The bottom ends of the rods rested on the pointers of dial gages attached to the flanges 3 in. from the lower end of the model.

The rate of closing of the gap at the splice was measured as well as the relative slip between the main material and the splice plates.

#### Procedure

The models were checked for uniformity of area and initial crookedness. They were aligned in the testing machine to give as uniform a distribution of load as practicable.

The loads were slowly applied in increments of about 2 kips per square inch (ksi) and all measurements were taken. The loadings were continued by strain increments well into the plastic range after the maximum load had been reached.

### Tests of Material Properties

#### Coupons

Compression and tension stress-strain curves for one series of coupons around the cross-section of the material from which the models were fabricated are shown in Fig. 3. The location of the coupons in the cross-section and the variations in the measured moduli of elasticity are shown in Fig. 4. The variations in the measured yield point stresses are shown in Fig. 5.

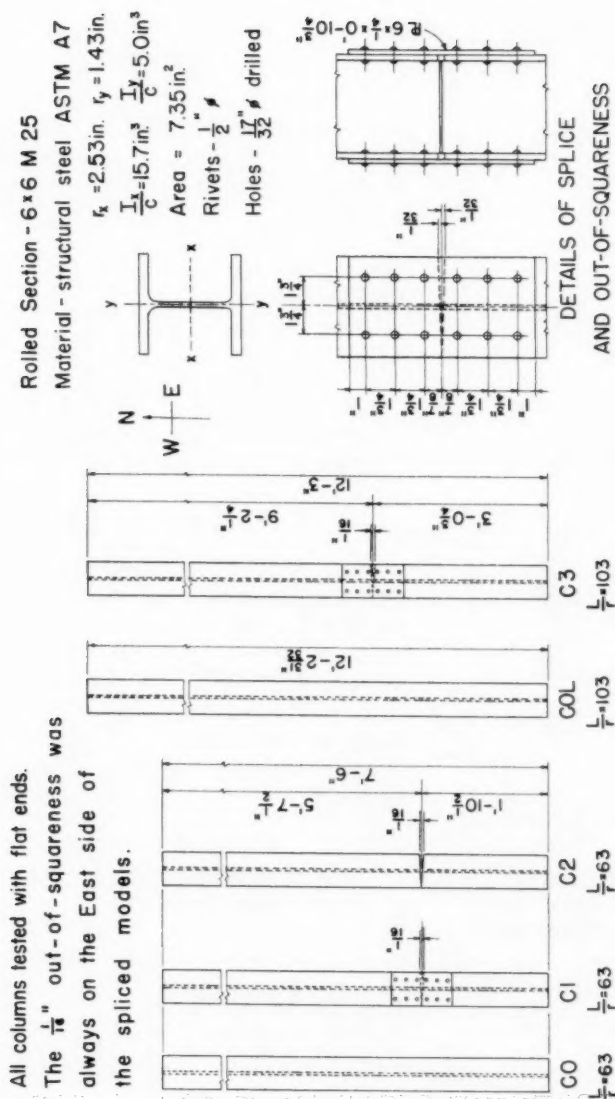
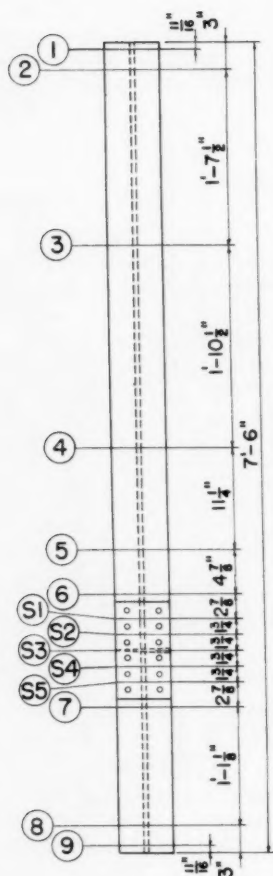


Fig. 1.  
DETAILS OF FIVE COLUMN MODELS TESTED

All columns tested with flat ends.

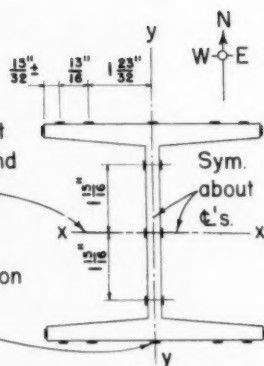
The  $\frac{1}{16} \text{ in.}$  out-of-squareness was always on the East side of the spliced models.



No. SR-4 gages used  
122 Type A-1  
302 Type A-7

Omit web gages at  
sections 3 & 4 and  
on  $\epsilon$  at sections  
1, 5 & 9.

Omit gages here on  
both flanges at  
sections 2 & 8.

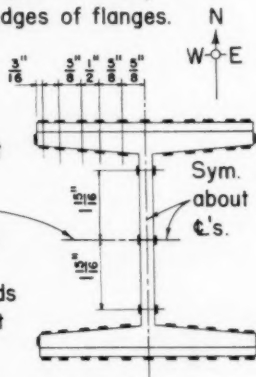


#### SECTIONS 1 TO 9

Showing location of SR-4 electric  
strain gages—Type A-1 except  
Type A-7 on edges of flanges.

Omit web gages at  
sections S1 & S5  
and on  $\epsilon$  at  
sections S2 & S4.

Gages on both ends  
of main material at  
section 3.



#### SECTIONS S1 TO S5

Showing location of SR-4 electric  
strain gages Type A-7.

Fig. 2 COLUMN C1

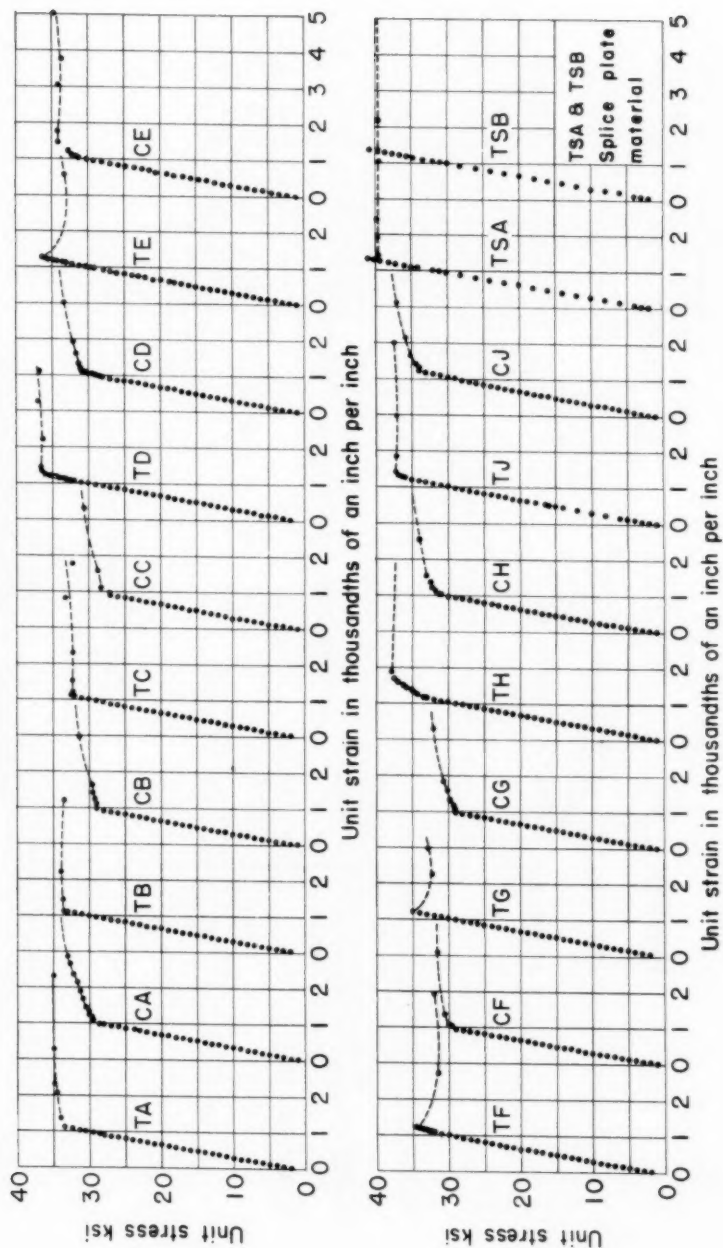
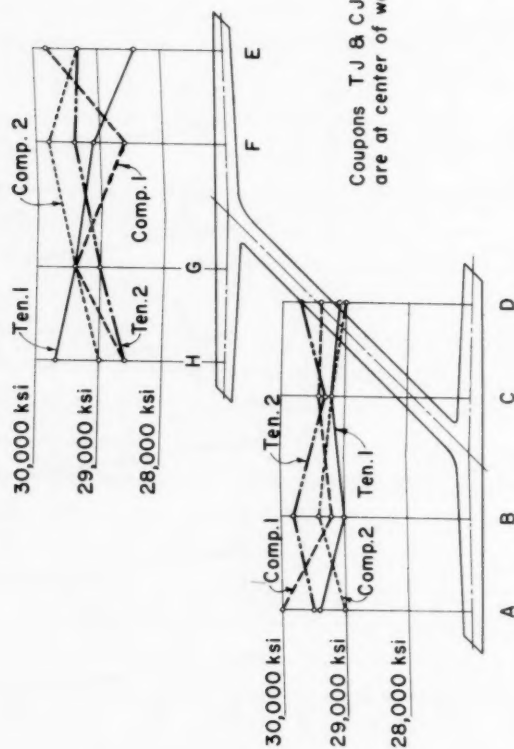


Fig. 3  
COUPON STRESS-STRAIN CURVES — SECOND SERIES

Strains measured with Tuckerman Optical Strain Gages.



Rolled Section 6M25  
A-7 Steel

Fig. 4  
VARIATIONS IN MODULUS OF ELASTICITY

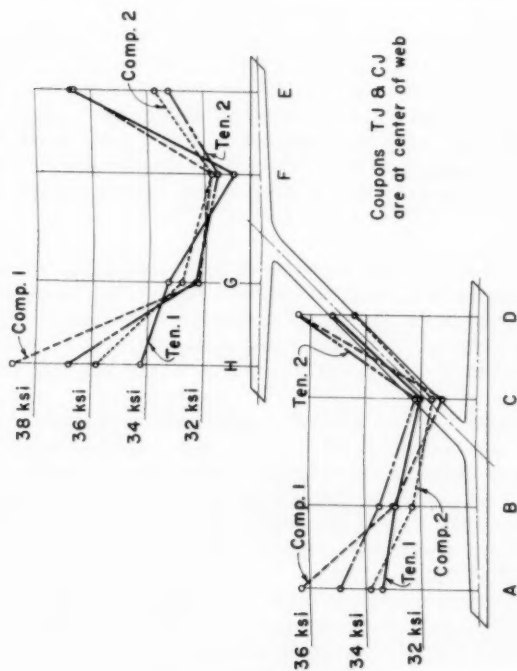
The weighted value of the Modulus of Elasticity was taken as 29,400 ksi.

Two coupon tests on the splice plate material each gave values for the modulus of elasticity of 29,800,000 psi.

Coupon Loc.	MODULUS OF ELASTICITY x 10 <sup>-6</sup> psi			
	1st. Series		2nd. Series	
	Comp.	Ten.	Comp.	Ten.
A	30.0	29.4	29.0	29.5
B	29.2	29.0	29.4	29.8
C	29.4	29.2	29.2	29.3
D	29.4	29.1	29.0	29.7
E	29.8	28.4	29.3	29.3
F	28.6	29.1	29.8	29.4
G	29.4	29.4	29.4	29.0
H	28.6	29.7	29.0	28.6
J	30.0	29.9	29.0	29.4



Strains measured with Tuckerman Optical Strain Gages



Rolled Section 6M25  
A-7 Steel

Fig. 5

VARIATIONS IN YIELD POINT STRESS

The weighted value of the Yield Point Stress was taken as 34.4 ksi

Two coupon tests on the splice plate material each gave values for the yield point stress of 39.6 ksi.

YIELD POINT STRESS					
Coupon Loc.	1st Series		2nd Series		ksi
	Comp.	Ten.	Comp.	Ten.	
A	36.3	33.4	33.8	34.9	
B	33.0	32.9	32.3	33.5	
C	31.2	32.0	31.6	32.2	
D	36.4	35.2	34.4	36.4	
E	36.6	36.7	33.7	33.2	
F	31.7	30.9	31.7	31.5	
G	32.2	33.3	32.8	32.3	
H	38.8	34.2	35.8	36.8	
J	38.2	37.5	38.3	37.1	

Stress at a definite yield of material, or at a unit elongation of .005% if there is no definite yield.

## Residual Stresses

Fig. 6 shows the residual stresses measured at one section of the original 60 ft. stock length.

## Action of Test Models

### Experimental Behavior of Columns

The correlation of the experimental behavior of a flat-ended column in a testing machine with the action of a similar member in a structure is always complicated. The load on the column in the testing machine will fall off after its maximum value is attained. The maximum load on a member in a structure, if applied, would be acting at all times after its first application.

Salmon in his treatise<sup>2</sup> on columns states that the experimental life of a flat-ended specimen is divided into three stages as follows:

"1st. From the initial application of the load until the ends bear all over it will deflect as an eccentrically loaded position-fixed specimen.

"2nd. From the moment of full contact until the maximum load is reached it will behave as a position- and direction-fixed column with an initial curvature.

"3rd. After the maximum load has been passed, it will continue to deflect possibly under a reduced load, until when the deflection attains a certain value it will "swing round" one edge of the end cross section, which will leave the crosshead, and if the experiment be continued, the specimen will go on deflecting under a greatly reduced load as a position-fixed column. "Swing round" may and does occur in certain cases under the maximum load, but does not of necessity occur when that load is reached."

### Test Data

Column stress-strain curves based on overall shortening are shown in Figs. 7 and 8. Pictures of Models C1 and C3, taken from the south looking north, at the end of the tests are shown respectively in Figs. 9 and 10. The lateral deflections for several loadings are shown in Figs. 11 and 12. The closure measurements at the splices are shown in Fig. 13 with notation given in Fig. 14.

The average strains and the internal bending moments were computed at each section in all models where SR-4 strain gage readings were taken. Stress-strain curves based on these average strains for Model C1 are shown in Figs. 15 and 16, and for Model C3 in Figs. 17 and 18. The internal bending moments for Models COL and C3 are shown in Fig. 19. Plots of strain volumes at loads where there were significant changes in strain distribution are shown in Fig. 20 for Model COL.

These average strains and internal bending moments were computed by a process of arithmetical integration as outlined in Fig. 21. Each quadrant of the flange was divided into three areas and the average strains on these areas were determined from the SR-4 gage data at each section. The web was considered as an equivalent rectangle. The yield point strength was assumed to

2. "Columns," by E. H. Salmon, Oxford Technical Publications, London, England, 1921, P. 164.

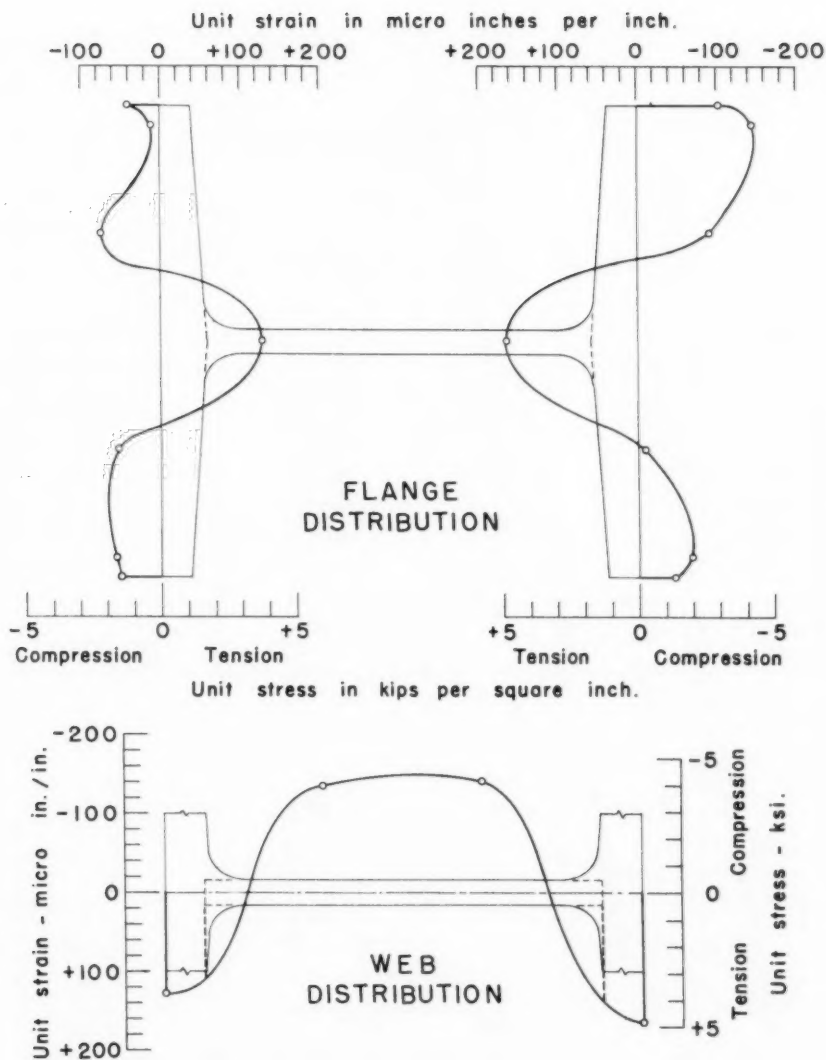


Fig. 6 RESIDUAL STRESS DISTRIBUTION

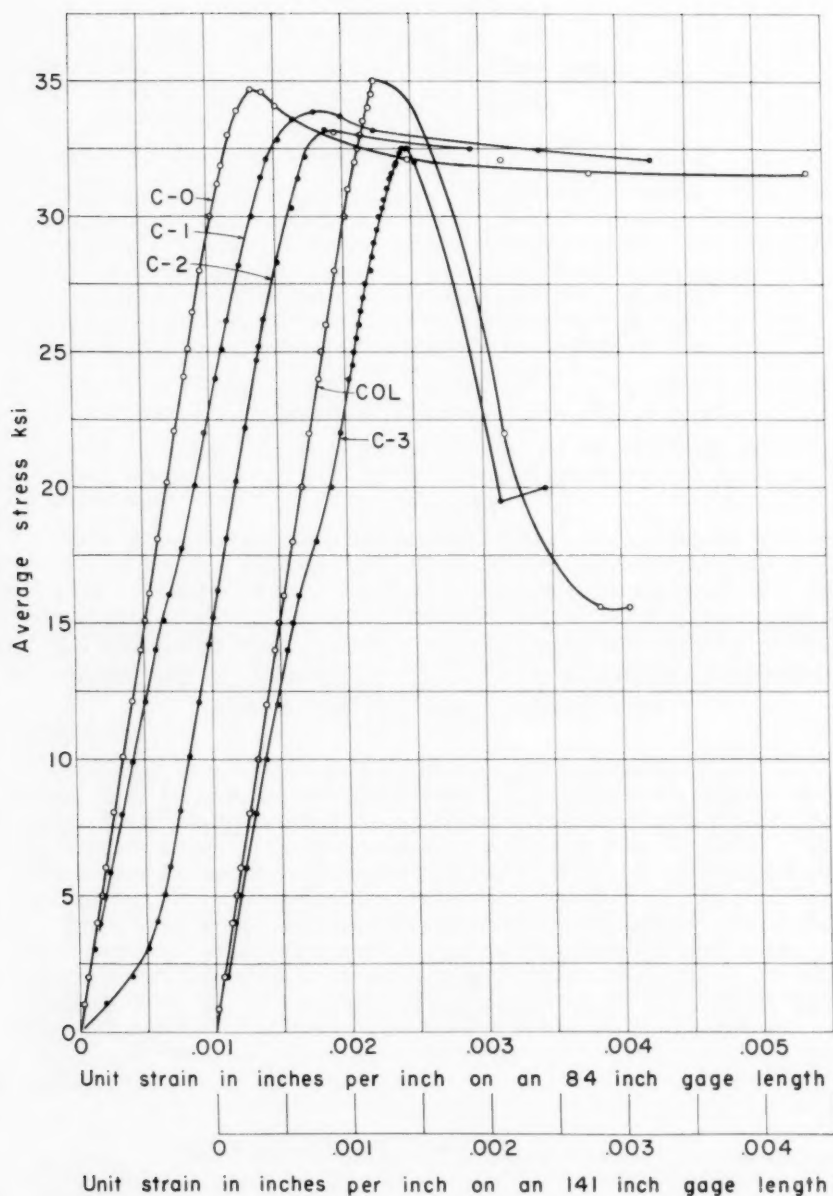


Fig. 7 COLUMN STRESS-STRAIN CURVES

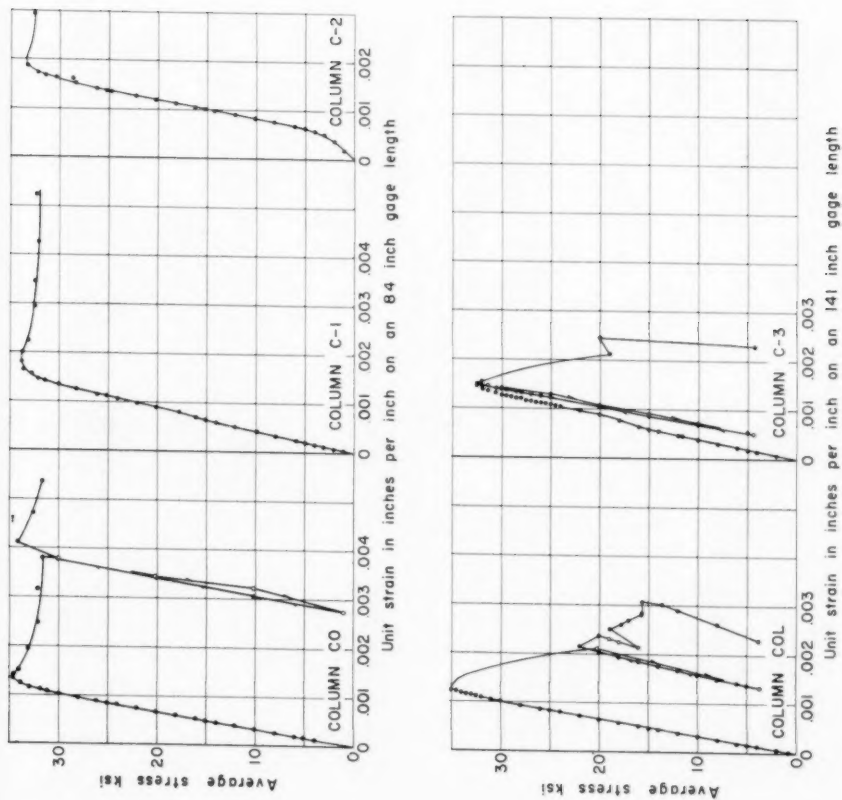


FIG. 8 COLUMN STRESS-STRAIN CURVES

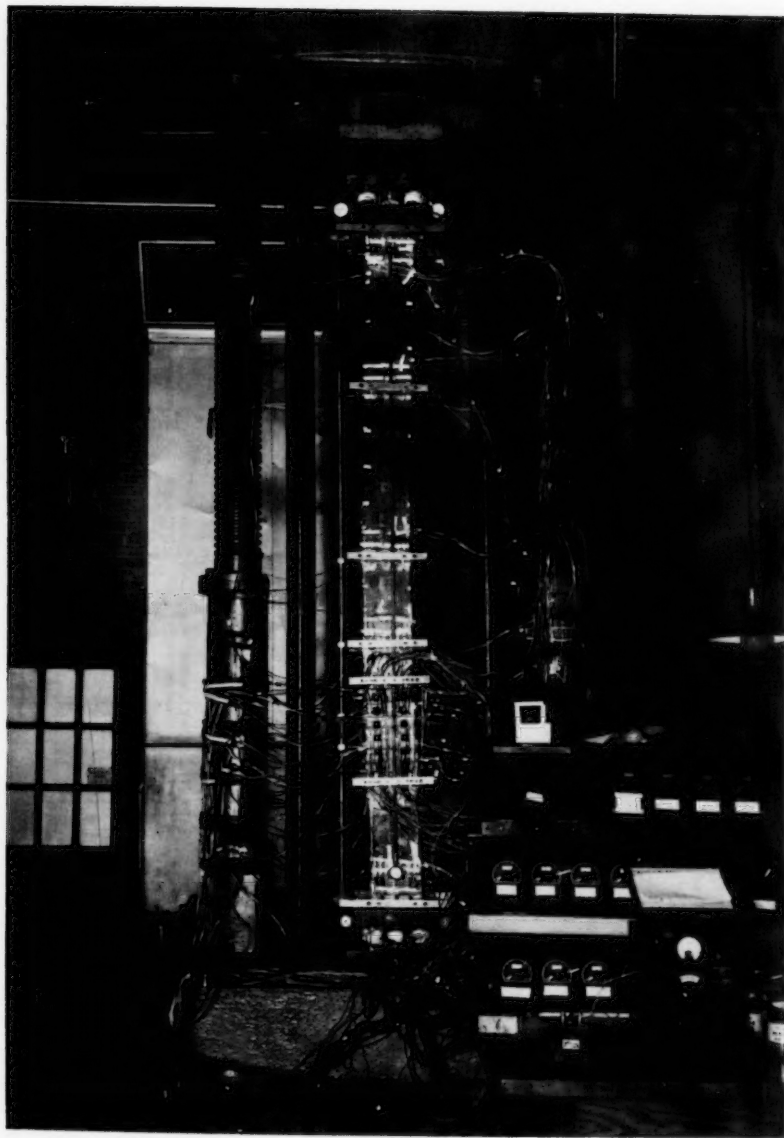


Fig. 9 COLUMN C1--AFTER FAILURE

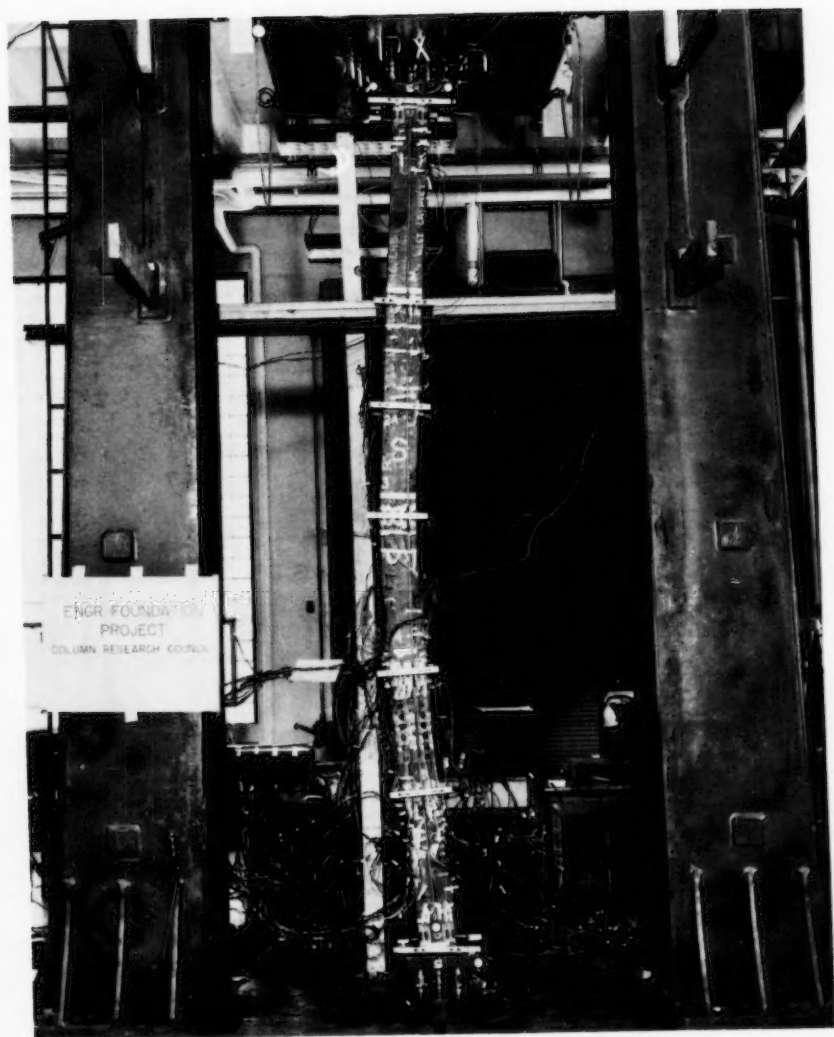


Fig. 10 COLUMN C3--AFTER FAILURE

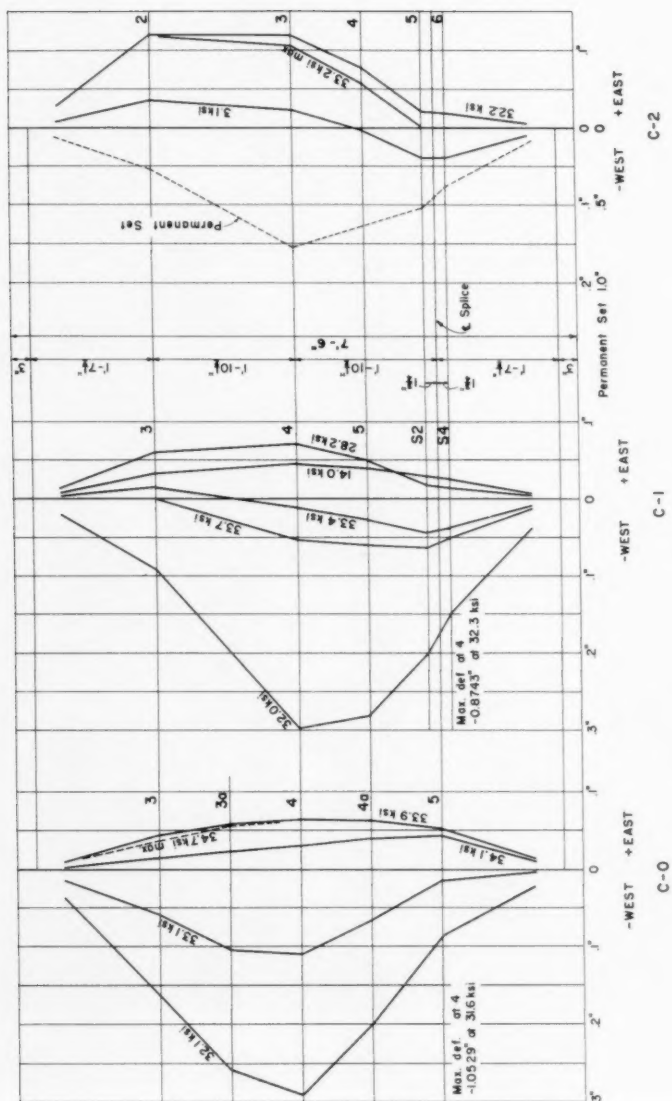


Fig. 11  
LATERAL DEFLECTIONS ABOUT Y-Y AXIS  
COLUMNS TESTED WITH FLAT ENDS  
1-63



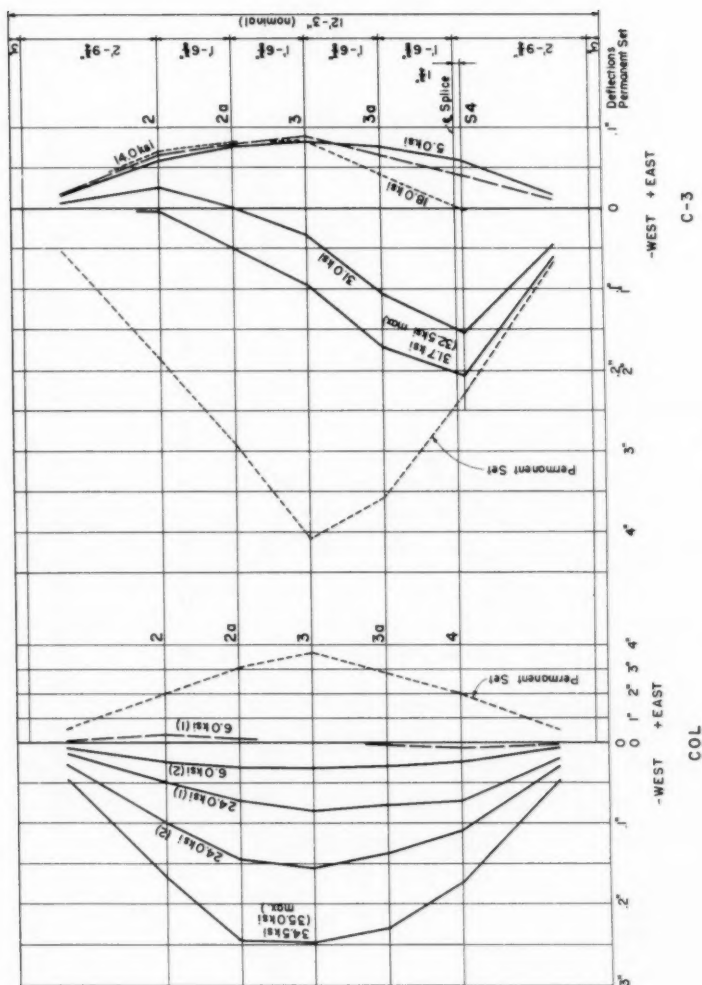


Fig. 12  
LATERAL DEFLECTIONS ABOUT Y-Y AXIS  
COLUMNS TESTED WITH FLAT ENDS  
b=103

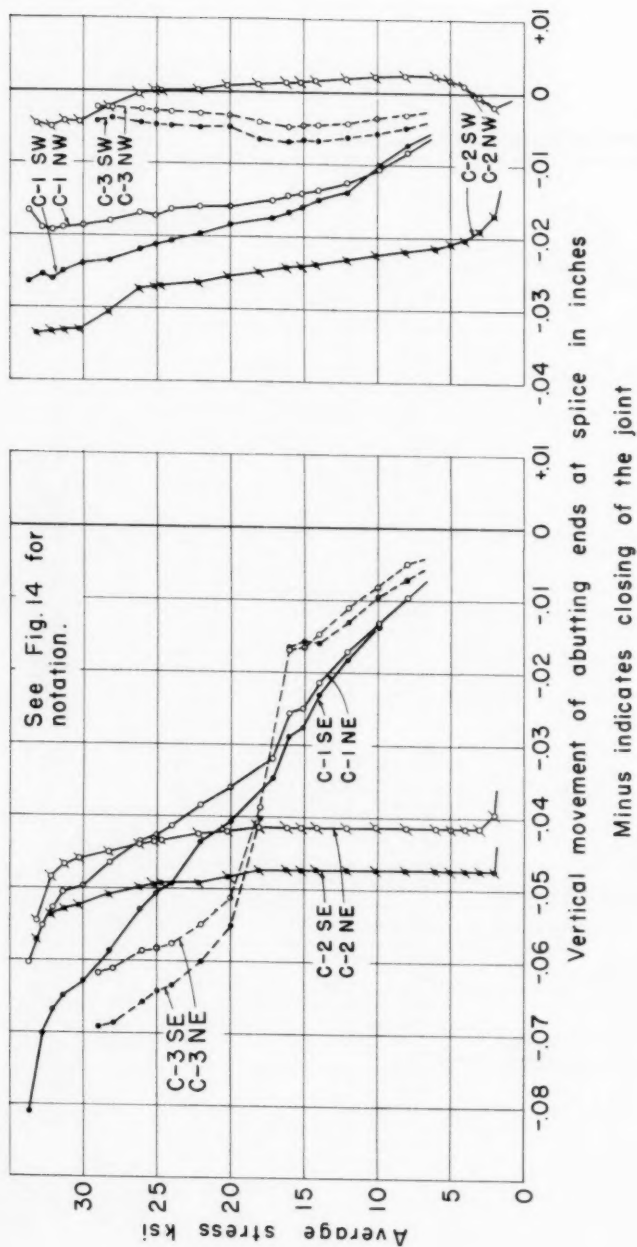
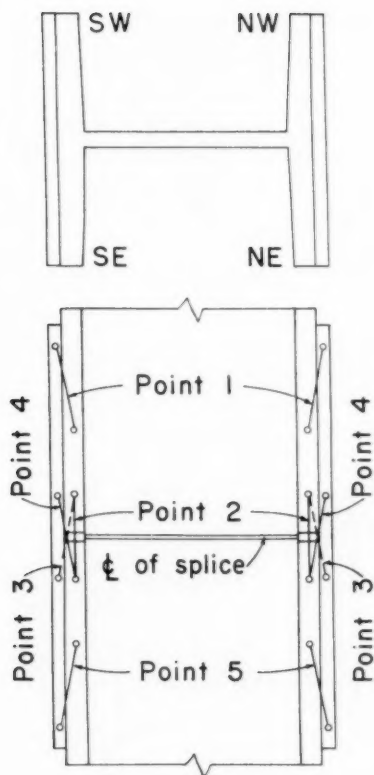


Fig. 13  
VERTICAL MOVEMENT OF ABUTTING ENDS AT SPLICE  
AT POINT 2



LOCATION OF SLIP AND FLOW  
MEASUREMENTS

Fig. 14

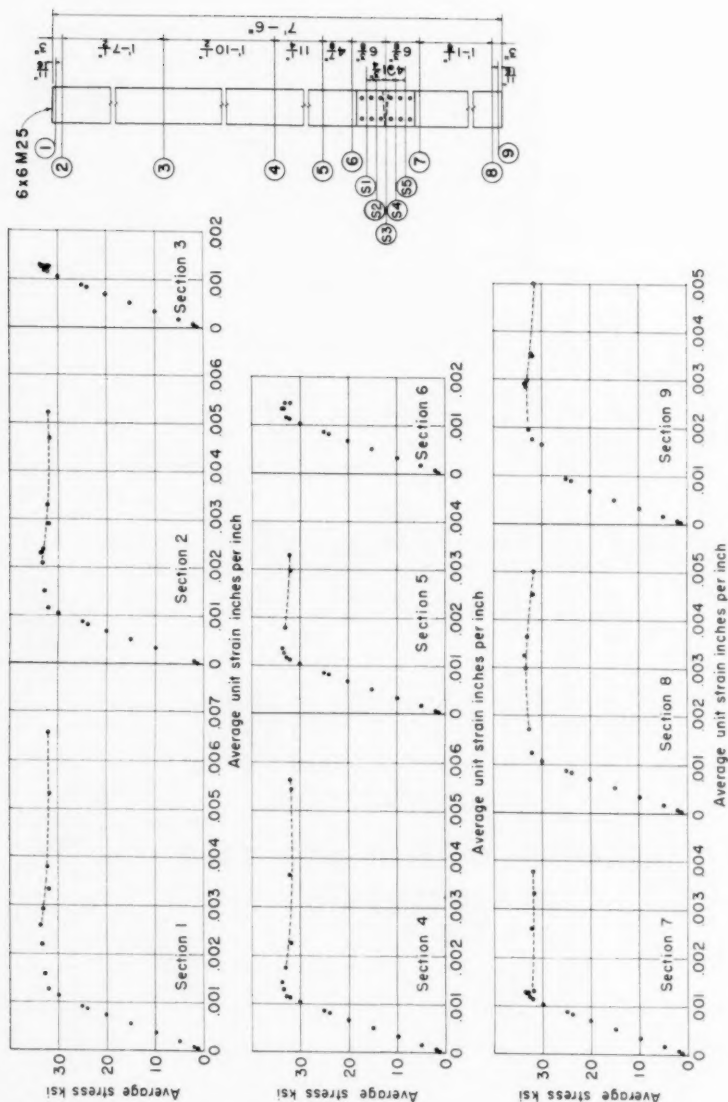


Fig. 15  
COLUMN C-1-AVERAGE STRESS-STRAIN CURVES FROM SR-4 ELECTRIC STRAIN GAGES

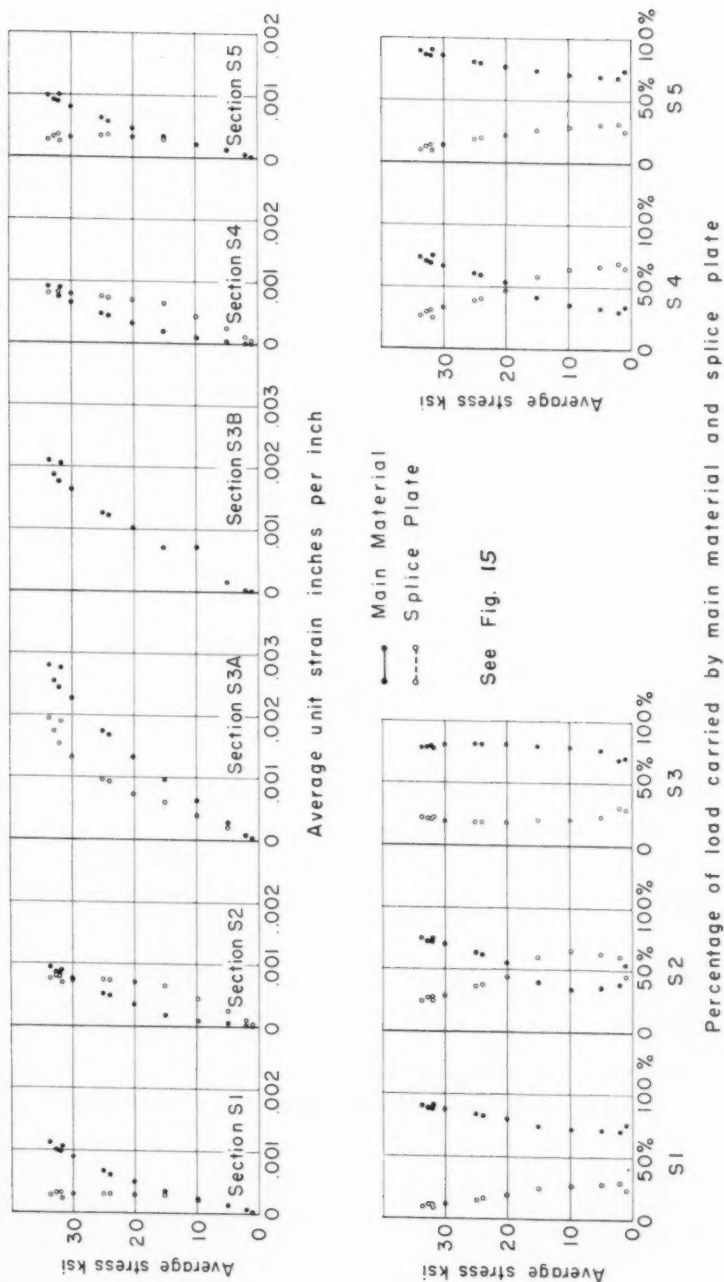


Fig. 16  
 COLUMN C-1—AVERAGE STRESS-STRAIN CURVES FROM SR-4 ELECTRIC STRAIN GAGES

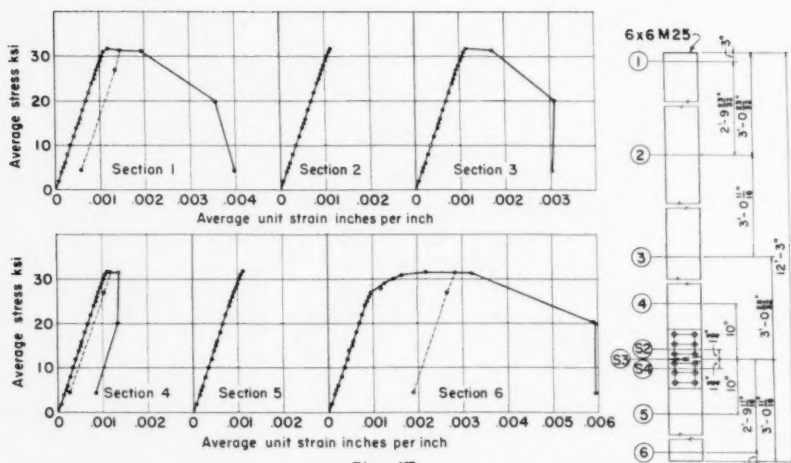
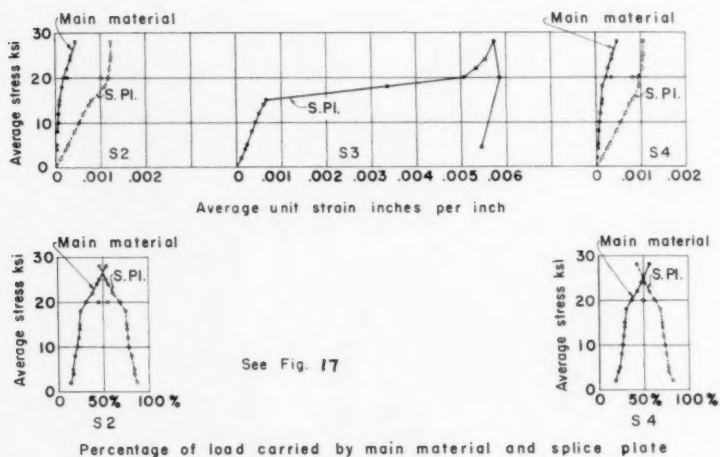


Fig. 17

COLUMN C-3-AVERAGE STRESS-STRAIN CURVES FROM SR-4 ELECTRIC STRAIN GAGES



See Fig. 17

Fig. 18

COLUMN C-3-AVERAGE STRESS-STRAIN CURVES FROM SR-4 ELECTRIC STRAIN GAGES

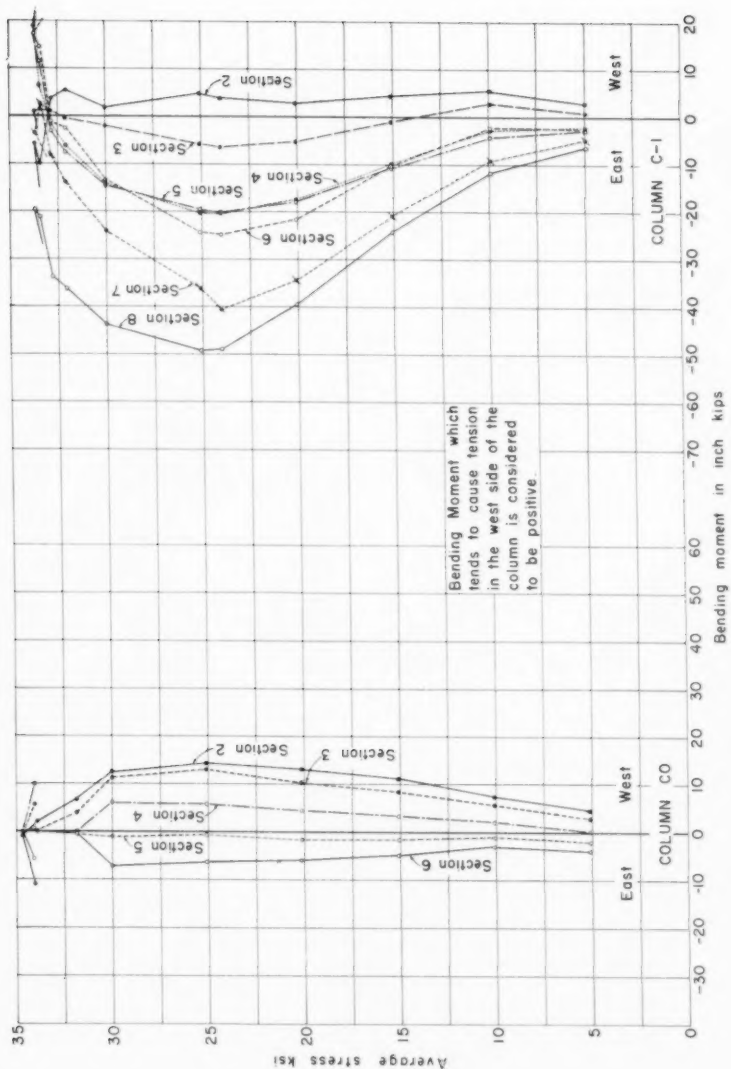


Fig. 19  
BENDING MOMENTS FROM STRAIN VOLUMES

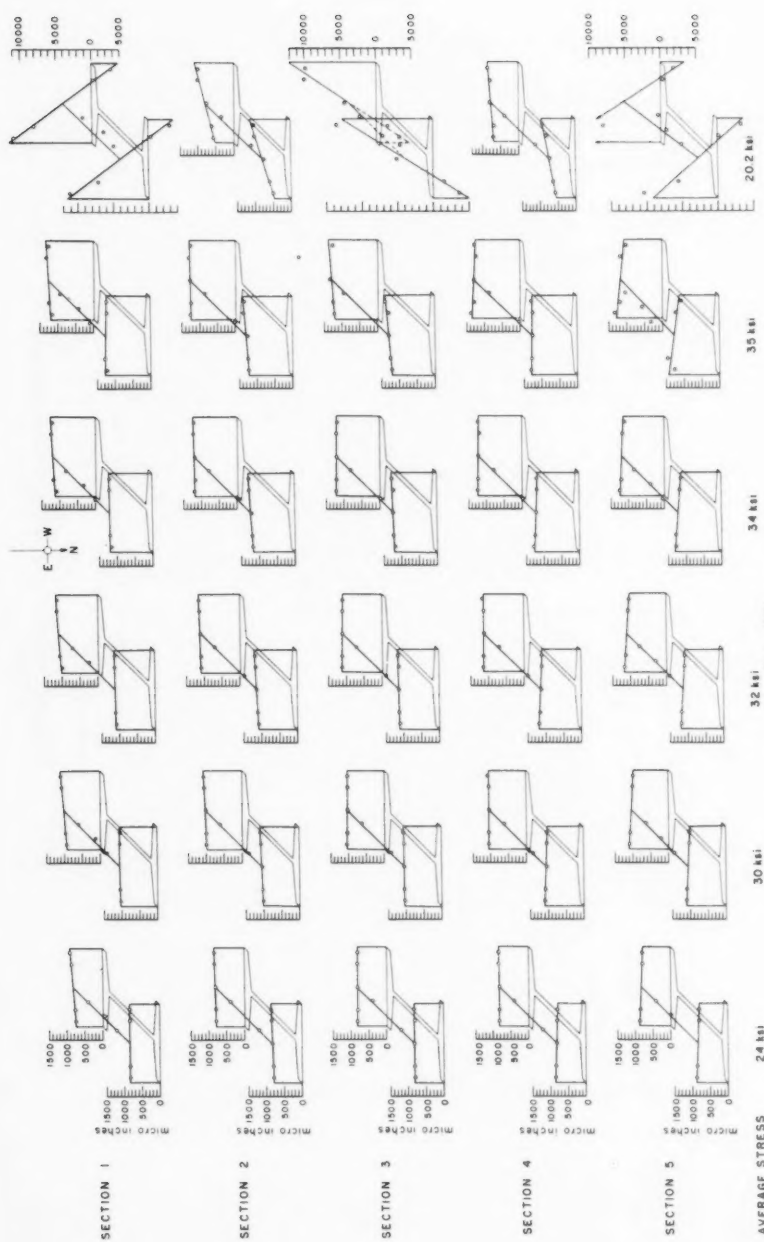
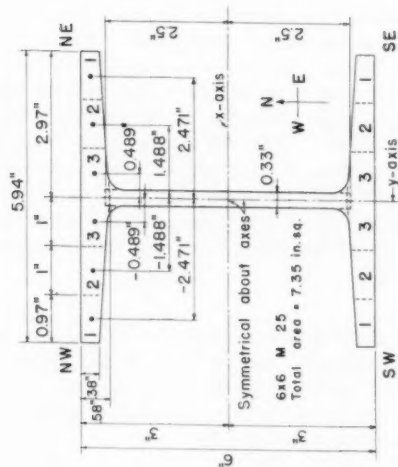


Fig. 20  
COLUMN COL - STRAIN DISTRIBUTION  
12'-3" Control Model

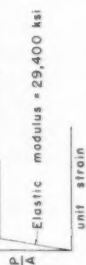


$$(\Sigma \text{Average strain} \times \text{Area} = \text{Strain volume}) \times \text{Arm to y-axis} = \frac{\text{Bending Moment}}{\text{Modulus of Elasticity}}$$



AVERAGE CROSS-SECTION

yield point strength - assumed to be of  
a unit strain of 1100 micro in. per in.



IDEALIZED STRESS-STRAIN CURVE

Pair of elements	Average strains micro in./in.	Area of element sq. in.	Strain volume	Arm y-axis inches	Bending Moment $E$
1SW+1NW	1938	4.01	777	-2.471	-1920
1SE+1NE	1841	4.01	738	2.471	+1825
2SW+2NW	1907	479	914	-1.488	-1360
2SE+2NE	1855	479	889	1.488	+1323
3SW+3NW	1889	5.46	1030	-489	-504
3SE+3NE	1872	5.46	1022	489	+500
Web	928	1.65	1531		

$$\Sigma \text{Strain volumes} = 6901$$

$$\Sigma \text{BM} = -136 \times 29.4$$

$$= -4000 \text{ in.-lbs}$$

$$\text{Average strain} = \frac{\Sigma \text{Strain volumes}}{\text{Total area}} = \frac{6901}{7.35}$$

$$= 940 \text{ micro in./in.}$$

Pair of elements	Average strains micro in./in.	Area of element sq. in.	Strain volume	Arm y-axis inches	Bending Moment $E$
1SW+1NW	2418	4.01	970	-2.471	-2180*
1SE+1NE	1922	4.01	772	2.471	+1905
2SW+2NW	2351	479	1126	-1.488	-1566*
2SE+2NE	2022	479	970	1.488	+1443
3SW+3NW	2243	5.46	1227	-489	-589*
3SE+3NE	2137	5.46	1167	489	+571
Web	1097	1.65	1805		

$$\Sigma \text{Strain volumes} = 8037$$

$$\Sigma \text{BM} = -414 \times 29.4$$

$$= -12,160 \text{ in.-lbs}$$

$$\text{Average strain} = \frac{\Sigma \text{Strain volumes}}{\text{Total area}} = \frac{8037}{7.35}$$

$$= 1094 \text{ micro in./in.}$$

\* Average strains on each element exceeding the assumed yield point strength of the material are not considered effective in resisting additional moment.

Fig. 21  
COMPUTATIONS OF STRAIN VOLUMES

be at 1100 micro-inches per inch of unit strain in using the idealized stress-strain curve. Unloading was assumed to follow the elastic modulus of elasticity.

### Load Capacity

The maximum average load capacities are shown in Table 1. They are

TABLE 1.--Maximum Load Capacity of Models

Model	Type	Slenderness Ratio <sup>a</sup> L/r	Maximum Average Load  ksi	Percentage Maximum Average Load of Control Model	Plastic Strength
CO	Control	63	34.7	100	High
C1	Riveted	63	33.9	97.7	High
C2	Braced	63	33.2	95.7	High
COL	Control	103	35.0	100	Low
C3	Riveted	103	32.5	92.8	Low

<sup>a</sup>Based on full length of models, all tested with flat ends.

also shown in Fig. 22 in relationship to the average yield stress for the material of 34.4 ksi and the critical Euler buckling curves for both fixed-end and hinged-end conditions. The load carrying capacity after the maximum load had been reached, plastic strength, diminished slowly for the short models,  $L/r = 63$ , and rapidly for the long models,  $L/r = 103$ .

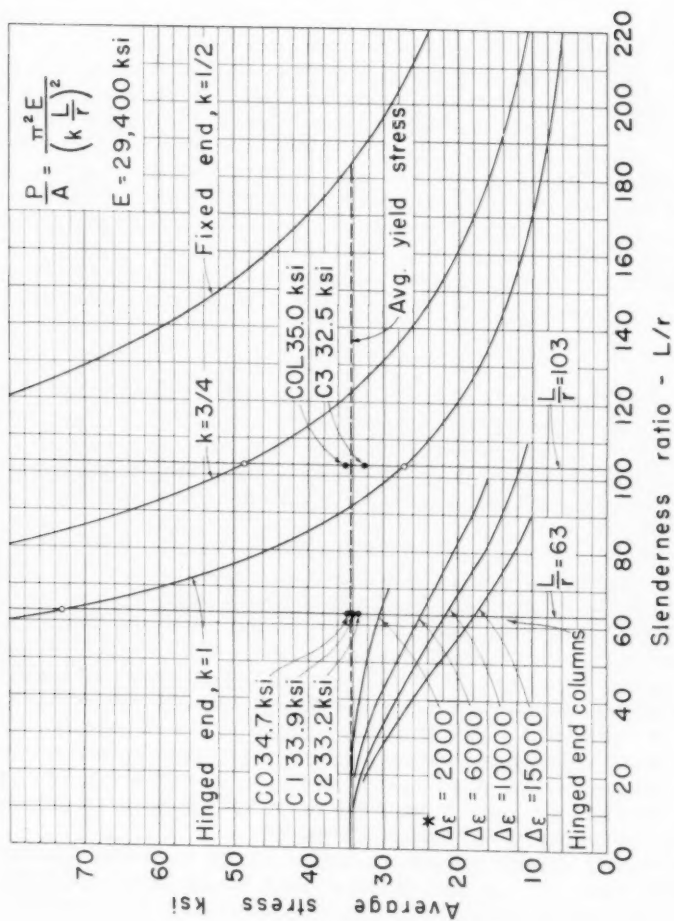
A theoretical treatment of the plastic strength of the 6 x 6 M 25 of ASTM A7 structural steel is given in a later section of this paper. Curves found from this theory showing the relationship between the drop-off in load carrying capacity after the maximum load has been reached, and  $L/r$  for different values of the strain differential,  $\Delta\epsilon$ , across the flange width at the mid-height of a hinged-end column are shown in Fig. 22 and labeled in terms of  $\Delta\epsilon$ . These curves may be used to determine the drop-off in load carrying capacity for any end condition by using the effective length of the column. The effective length for a flat-end column is the same as for a fixed-end column as long as there is direct stress entirely over the end cross-sections.

### Unspliced Control Models

Models CO and COL represent ideal action, except for initial eccentricities and curvatures due to errors in fabrication and/or the test set-up, variations in the modulus of elasticity and yield point strength of the material, and residual stresses. With a perfect set-up they would not start to bend until after the critical tangent modulus loads were reached.

The models were tested with flat ends. This means that during most of the test they behaved like fixed-end columns. Initial eccentricity in the application of the loads would not be effective in flat-end columns with full end fixity in effect.

The lateral deflections and the bending moments computed from the strain volumes were small for both Models CO and COL. The test set-ups seemed to be free from measurable errors. The strains over the entire cross-sections at all points along their lengths were in the plastic region as the



\* Micro-inches per inch

See Figs. 25 &amp; 26

Fig. 22  
MAXIMUM LOADS ON TEST MODELS

maximum loads were reached. Both models followed the experimental life of a flat-end column as outlined by Salmon. "Swing round" occurred after the maximum loads were reached.

Model CO reached its maximum load as the average load reached the yield point strength of the material. It was a crushing-type failure. There was a reversal of strain in one side after the maximum load was reached. This amounted to an elastic unloading and the column began to build-up resistance to moment and was able to carry a reduced load in a state of stable equilibrium. The rate of drop-off in load carrying capacity was small as more strain reversal occurred and the deflections increased. See Figs. 7 and 22.

Model COL reached its maximum load as plastic hinges were developed at the ends. The effective length of the column increased from a value of one-half, for the fixed-end condition, to the full length for the hinged-end condition. The model failed by buckling when the effective length reached the point where the applied average load coincided with the Euler critical load based upon the active effective length. It was a sudden buckling failure. The elastic unloading took place rapidly. The drop-off in load carrying capacity was fast as strain reversal took place. See Figs. 7 and 22.

The maximum load carrying capacity for each model was simply the cross-sectional area multiplied by the yield point strength of the material.

### Spliced Models

The action of a column with an out-of-square partially connected splice depends upon the rate of closure of the gap at the splice. Later sections of this paper develop the theoretical action of columns due to closure at out-of-square partially connected splices and an approximate procedure for determining the maximum load for a column with an out-of-square partially connected splice.

The closing of the gap in a partially riveted out-of-square splice is dependent upon the slip in the splice rivets and flow in the splice material. These two factors are interdependent and slip in rivets will vary with the quality of the rivet driving job. The differences in the closing of the gaps in the riveted spliced Models C1 and C3 are apparent in all of the data obtained. The gap in Model C1 closed gradually and there was considerable slip in the rivets and differential movement between the splice and main materials. The gap in Model C3 closed in a series of abrupt changes in rate of closure. There was not much differential movement between the splice and main materials. See the column stress-strain curves in Fig. 7. Also see Fig. 13. The differences in the rivet slip may be observed in Fig. 23 which shows pictures of sections through the rivets for Models C1 and C3.

During the process of joint closure the action may be determined by the theory presented later in this paper. If full closure should occur before the maximum load has been reached, the column may be treated as an initially curved member, where the initial curvature is given by the deflected position after full closure occurs. As the gap closes the bending moment at the bottom of the column builds up faster than elsewhere—assuming the ends either fixed or partially restrained. This causes the material at the bottom of the column to reach the plastic state over a large part of the cross-section at a lower load than in the unspliced column.

All of the spliced models followed the experimental life of a flat-end column as outlined by Salmon. "Swing round" started before the maximum load was reached.

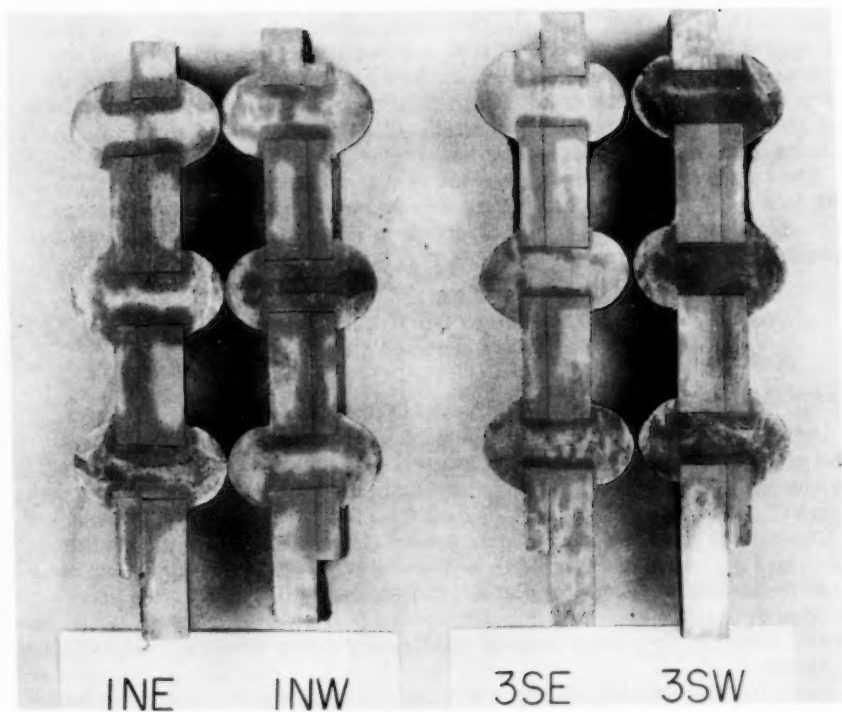


FIG. 23 SECTIONS THROUGH SPLICE RIVETS

Model C2 represents the extreme in a partially connected splice, since there was no resistance to shortening. The joint closed at an average load of about 3 ksi. The maximum load occurred under a crushing-type failure.

The action of Model C1 was between that of Control Model CO and Braced Model C2. See Fig. 7. Its action was dependent upon the rate of closure of the gap at the out-of-square splice. Its maximum load also occurred under a crushing-type failure.

Both Models C1 and C2 had a reversal of strain on one side after the maximum load was reached. The elastic unloading took place slowly. The drop-off in load carrying capacity was slow and the plastic strength was low for each model. The measured plastic strengths were practically the same as those for the unspliced Control Model CO. This indicates that eccentricities and accidental errors have only a minor effect on the plastic strength of a column, if general or local elastic buckling is not involved.

The action of Model C3 was similar to that of the unspliced Model COL with  $L/r = 103$ . This model reached its maximum load suddenly and there was a buckling-type failure. The drop-off in load carrying capacity was fast and the plastic strength was low. See Fig. 7.

#### Theoretical Action of Columns Due to Closure at Out-of-Square Partially Connected Splices

##### Elastic Action

Until closure begins the column acts like any unspliced member. As the joint closes the splice is displaced transversely with respect to the ends of the column. Rotations at the splice also take place. Figure 24 shows this action.

The column may be considered as a two span structure with the notation shown in Fig. 24. It is assumed to be fixed at the top and bottom with a transverse displacement,  $\Delta$ , taking place at the splice with respect to the ends. Rotation  $\theta_{CA}$  takes place at the bottom of the portion of the column above the splice. Rotation  $\theta_{CB}$  takes place at the top of the portion of the column below the splice.

Using the slope deflection procedure the following equations are written:

$$M_{AC} = 2E \frac{I}{L_A} \left[ -C_A \theta_A - C'_A \theta_{CA} - (C_A + C'_A) \frac{\Delta}{L_A} \right]$$

$$M_{CA} = 2E \frac{I}{L_A} \left[ -C_A \theta_{CA} - C'_A \theta_A - (C_A + C'_A) \frac{\Delta}{L_A} \right]$$

$$M_{CB} = 2E \frac{I}{L_B} \left[ -C_B \theta_{CB} - C'_B \theta_B + (C_B + C'_B) \frac{\Delta}{L_B} \right]$$

$$M_{BC} = 2E \frac{I}{L_B} \left[ -C_B \theta_B - C'_B \theta_{CB} + (C_B + C'_B) \frac{\Delta}{L_B} \right]$$

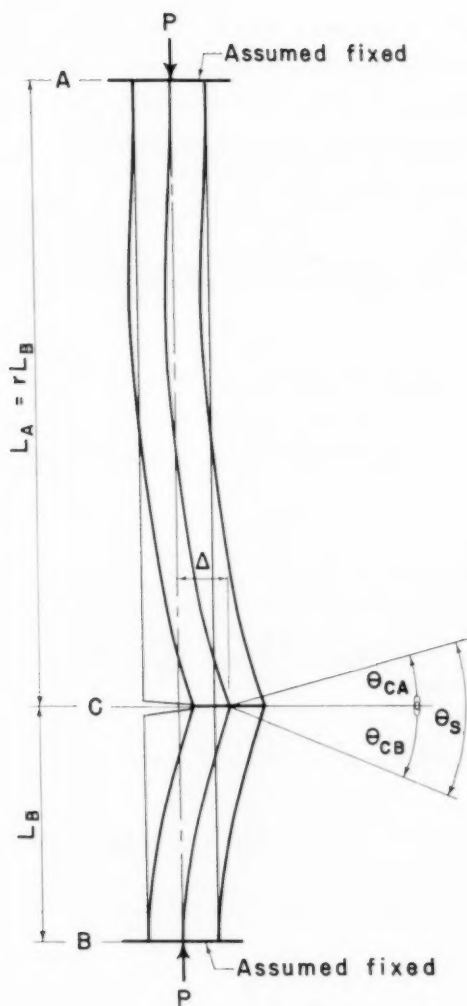


Fig. 24  
THEORETICAL ACTION  
AT PARTIALLY RIVETED SPLICE

where:

$C_A$  is stiffness of portion AC at end A or C,

$C_B$  is stiffness of portion BC at end B or C,

$C'_A$  is stiffness of portion AC times carry over factor for AC,

$C'_B$  is stiffness of portion BC times carry over factor for BC.

Using the following condition equations and notations:

$$1. \quad M_{CA} + M_{CB} = 0$$

$$2. \quad \frac{M_{AC} + M_{CA} + P}{L_A} = \frac{M_{CB} + M_{BC} - P}{L_B}$$

$$3. \quad -\theta_{CA} + \theta_{CB} = \theta_S$$

$$L_A = rL_B$$

$$K = \frac{r+1}{2EI} r^2 L_B^2$$

gives:

$$1. \quad \theta_{CA} - \theta_{CB} + \theta_S = 0$$

$$2. \quad -rC_A\theta_{CA} - r^2C_B\theta_{CB} + \left[ -(C_A + C'_A) + r^2(C_B + C'_B) \right] \frac{\Delta}{L_B} = 0$$

$$3. \quad r(C_A + C'_A)\theta_{CA} - r^3(C_B + C'_B)\theta_{CB} +$$

$$\left[ 2(C_A + C'_A) + 2r^3(C_B + C'_B) - KP \right] \frac{\Delta}{L_B} = 0$$

The solution of these equations gives:

$$\frac{\Delta}{L_B} =$$

$$\left[ \frac{\frac{C_A + C'_A}{C_A + C'_A - r^2(C_B + C'_B)} - \frac{C_A}{C_A + rC_B}}{\frac{-(C_A + C'_A) + r^2(C_B + C'_B)}{rC_A + r^2C_B} + \frac{2(C_A + C'_A) + 2r^3(C_B + C'_B) - KP}{3(C_A + C'_A) - r^3(C_B + C'_B)}} \right] \theta_S$$



$$\theta_{CB} = \left[ \frac{-(C_A + C'_A) + r^2(C_B + C'_B)}{rC_A + r^2C_B} \right] x$$

$$\left[ \frac{\frac{C_A + C'_A}{C_A + C'_A - r^2(C_B + C'_B)} - \frac{C_A}{C_A + rC_B}}{\frac{-(C_A + C'_A) + r^2(C_B + C'_B)}{rC_A + r^2C_B} + \frac{2(C_A + C'_A) + 2r^3(C_B + C'_B) - KP}{r(C_A + C'_A) - r^3(C_B + C'_B)}} + \frac{rC_A}{rC_A + r^2C_B} \right] \theta_S$$

$$\theta_{CA} = \theta_{CB} - \theta_S$$

The stiffnesses  $C_A$  and  $C_B$  and the constants  $C'_A$  and  $C'_B$  may be taken from Table 1 in "Exact Slope Deflection Method for the Calculation of Secondary Stresses and Analysis of Statically Indeterminate Structures," published in 1935 by Walter J. Grabner, by dividing his factors  $A_c$  and  $B_c$  by two; or taken from Appendix D of "Buckling of Trusses and Rigid Frames," by Winter, Hsu, Koo, and Loh, Cornell University, Engineering Experiment Station Bulletin No. 36, April, 1948, by dividing their factors  $\alpha_n$  and  $\alpha_f$  by two. These coefficients take the effect of the axial load into consideration.

The values of  $\Delta$ ,  $\theta_{CB}$ , and  $\theta_{CA}$  are all determined in terms of  $\theta_S$ , the angle of closure. A solution must be made for every value of axial load since the slope deflection constants vary with the load. The resulting bending moments,  $M_{AC}$ ,  $M_{CA}$ ,  $M_{CB}$ , and  $M_{BC}$ , are determined by direct substitution in the slope deflection equations. These bending moments may be evaluated when the magnitude of  $\theta_S$  for any axial load is known.

#### Plastic Action

The above solution is sufficient so long as the yield point strength of the material is not exceeded at any point in the column. When this occurs a plastic hinge begins to develop at this point and its development is accelerated as more of the material at this point becomes plastic. This plastic hinge will usually form first at the bottom of the column.

A plastic hinge will, in general, be developed in the partially riveted column with out-of-square ends at the splice at a lower load than one would develop in an identical unspliced column. This differential in load depends upon the rate of closure of the out-of-square-ness at the partially riveted splice.

# Plastic Strength of Axially Loaded Columns After Reaching the Maximum Load

This is an analysis for the axial load which an ideal hinged-end column can carry in a state of stable equilibrium after the maximum load has been reached and strain reversal has taken place at the mid-height of the column.

It is assumed that the stress-strain curve for the material consists of two straight lines. The elastic portion slopes at a value of the elastic modulus of elasticity,  $E$ , up to the yield point of the material. The yield portion is considered to be a horizontal line.

At the maximum load the average load is at the yield point stress of the material and the stress and strain distributions are uniform at every cross-section in the column. This assumes that elastic buckling has not occurred.

It is assumed that for some reason the column is deflected at mid-height a small amount,  $m$ , and that:

1. Sections plane before bending are plane after bending.
2. The stress from strain reversal on the convex side is in accordance with the elastic modulus of elasticity.
3. There is no additional stress carrying capacity on the concave side where the plastic modulus is zero.
4. The deflected position of the centerline of the column is a cosine curve given by the following equation, with the origin at the mid-height:

$$y = m \cos \pi x / L,$$

where:  $y$  = deflection at any point  $x$  from mid-height,  $m$  = deflection at mid-height, and  $L$  = length of hinged-end column.

The equation of the centerline of the column may also be written as follows:

$$\frac{1}{R} = \frac{\Delta \epsilon}{h} = - \frac{d^2 y}{dx^2},$$

where:  $R$  = radius of curvature at mid-height,  $\Delta \epsilon$  = difference in unit strains in opposite edges of cross-section, and  $h$  = distance in inches between the opposite edges where  $\Delta \epsilon$  is measured.

Using these two equations gives:

$$\frac{\Delta \epsilon}{h} = m \left( \frac{\pi}{L} \right)^2 \cos \pi x / L,$$

which gives for the models tested—6 x 6 light column section at twenty-five pounds per foot:

$$m = \left( \frac{L}{\pi} \right)^2 \frac{\Delta \epsilon \pi^2}{h} = 0.0348 \Delta \epsilon \left( \frac{L}{\pi} \right)^2.$$

The resisting moment at the mid-height of the column,  $RM$ , may be determined by integrating the strain volume reversal at the mid-height cross-

section. This may be done for any specific value of  $\Delta\epsilon$ . Then a relation between the resisting moment, the equilibrium load on the column,  $P_p$ , and the deflection at the mid-height is:

$$RM = P_p m.$$

The plastic strength,  $P_p$ , for any assumed value of  $\Delta\epsilon$ , may be determined for various values of  $L/r$  and any given cross-sectional shape by the use of the two preceding equations.

The values of the strain volume reversal and the resisting moments,  $RM$ , are determined by arithmetical integration similar to the procedure outlined in Fig. 21. These values are determined for different values of  $\Delta\epsilon$  and  $d_r$ , the distance the strain reversals extend into the cross-sectional area from the convex side. The procedure is as follows, see Fig. 25:

1. Determine the value of the strain reversal at the center of gravity of each element into which the flanges of the 6 x 6 M 25 is divided. Use unit strains in micro-inches per inch.
2. Determine the total amount of strain volume reversal by summing the products of the strain reversal at the center of gravity of each element by the area of each element in square inches.
3. Determine the resisting moment of the strain reversal,  $RM$ , by summing the products of the strain volume reversal on each element by the distance of the center of gravity of the element from the y-axis.
4. Determine the plastic strength,  $P_p$ , by subtracting the total strain volume reversal from the total strain volume at the maximum load and multiplying by 29.4—divide this result by 7.35 square inches to get average plastic strength.

Fig. 26 is a plot of these two equations,  $m = 0.0348 \Delta\epsilon (L/r)^2$  and  $m = RM/P_p$ , for assumed values of  $\Delta\epsilon$  and various values of  $d_r$ , which are chosen to coincide with the elements of the cross-sectional area as shown in Fig. 25.

The equation,  $m = 0.0348 \Delta\epsilon (L/r)^2$ , is plotted in Fig. 26 for assumed values of  $\Delta\epsilon$ , with  $m$  as ordinates and  $L/r$  as abscissas. The curves are shown in solid lines and labeled in terms of  $\Delta\epsilon$ .

The equation,  $m = RM/P_p$ , is plotted in Fig. 26 for assumed values of  $\Delta\epsilon$  and various values of  $d_r$ , with  $m$  as ordinates and  $\Delta\epsilon$  as abscissas. The curves are shown in dashed lines and are labeled in terms of  $d_r$ .

Values of  $P_p/A$  as determined for assumed values of  $\Delta\epsilon$  and various values of  $d_r$ , with  $P_p/A$  as ordinates and  $\Delta\epsilon$  as abscissas, are also shown in Fig. 26 in solid lines and labeled in terms of  $d_r$ . These lines intersect at the assumed average maximum load of 34.72 ksi when  $\Delta\epsilon = 0$ —uniform strain distribution. This value was used because it gave an even total strain volume of 8680 micro-inches and the maximum average load on Model CO was 34.7 ksi.

#### Approximation of Maximum Load for Column with Out-of-Square Splice

The decrease in load capacity of the columns with out-of-square splices over that of the unspliced control models is a result of the material at the

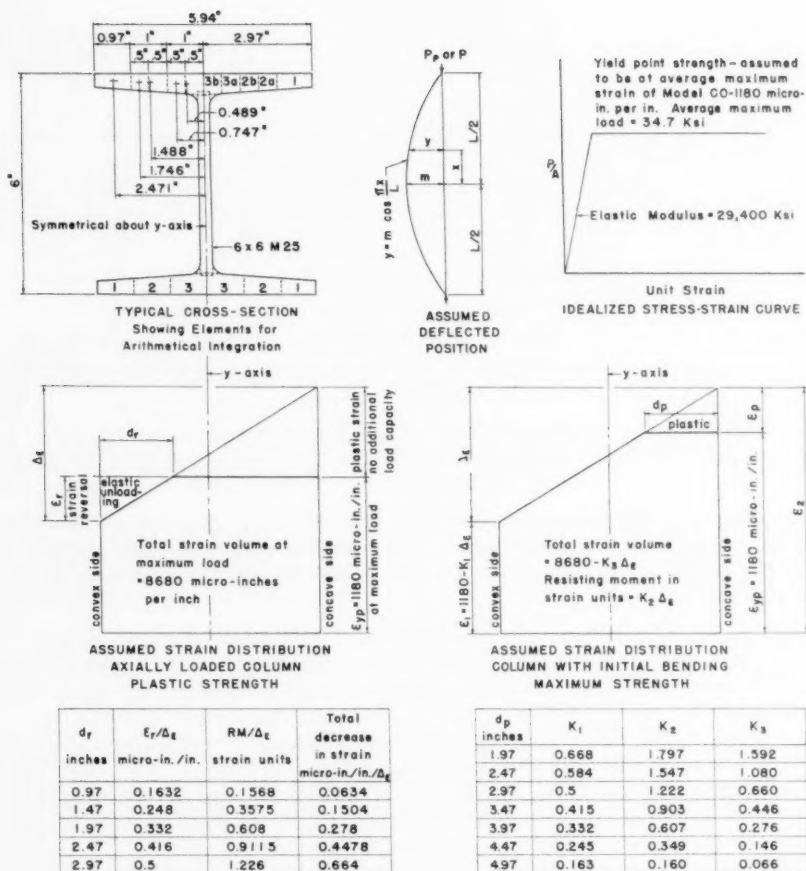


Fig. 25  
PLASTIC AND MAXIMUM STRENGTHS

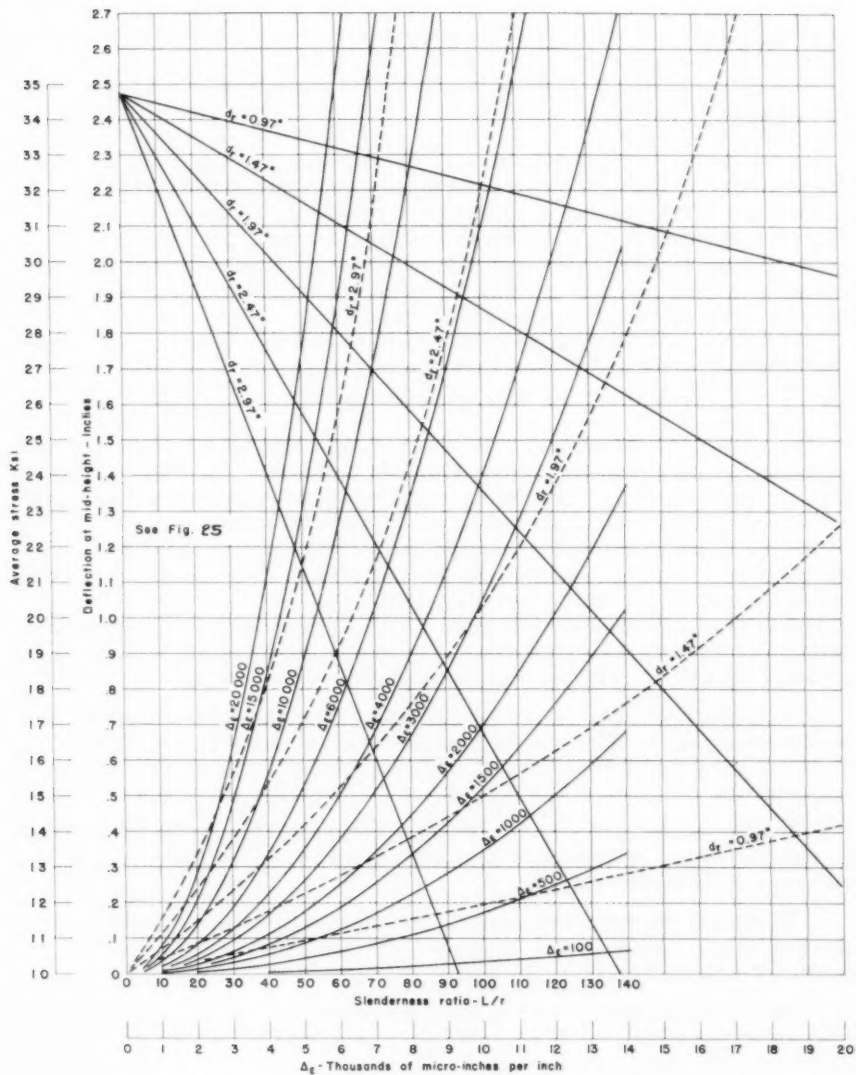


Fig. 26  
PLASTIC STRENGTH CURVES  
Axially Loaded Column  
6x6 M25

bottom of the member reaching the plastic state over a large part of the cross-section at a lower load than in the unspliced model. This is a result of the large bending moments built-up at the bottom of the spliced columns due to joint closure. An approximate method of determining this decrease in load capacity is outlined below.

Consider the ideal hinged-end column which bends from some cause at the first loading. Assume the equation of the deflected centerline as:  $y = m \cos \pi x/L$ . See Fig. 25.

As the load is increased the strains will increase on both the convex and concave sides of the cross-section at mid-height. Sections plane before bending are assumed plane after bending. Finally the strain on the concave side will reach the yield point strength of the material. The portion of the cross-section strained above the yield point strength will offer no resistance to additional load. Denote the distance of the penetration of the plastic state into the cross-sectional area from the concave side as  $d_p$ .

The column will carry more load because the strains on the convex side are increasing elastically. From the assumed shape of the deflected centerline the mid-height deflection may again be written for a 6 x 6 M 25 as:  $m = 0.0348 \Delta \epsilon (L/r)^2$ .

Again the resisting moment, RM, at mid-height may be determined by integrating the strain volume at the mid-height cross-section. This is done for any specific value of  $\Delta \epsilon$ . The relationship between the maximum load on the column, P, and the mid-height deflection, m, is:  $RM = Pm$ .

The maximum load for any assumed value of  $\Delta \epsilon$ , may be determined for various values of  $L/r$  and any given cross-sectional shape by the use of these two equations:  $m = 0.0348 \Delta \epsilon (L/r)^2$  and  $RM = Pm$ .

The values of the resisting moments, RM, are determined by arithmetical integration, as previously described. The values are determined for different values of  $\Delta \epsilon$  and  $d_p$ . The procedure is as follows, see Fig. 25:

1. Determine the value of the total effective strain, that strain below the yield point strain, at the center of gravity of each element into which the flanges of the 6 x 6 M 25 is divided, including the web. Use unit strains in micro-inches.
2. Determine the total effective strain volume by summing the products of the effective strain at the center of gravity of each element by the area of each element in square inches.
3. Determine the resisting moment, RM, by summing the products of the effective strain volume on each element by the distance of the center of gravity of each element from the y-axis.
4. Determine the load capacity, P, of the column by multiplying the total effective strain volume by 29.4—divide this result by 7.35 square inches to get the average load on the column.

The equation  $m = 0.0348 \Delta \epsilon (L/r)^2$  has been plotted in Fig. 26 and may be used for this case.

Fig. 27 is a plot of  $m = RM/P$  for assumed values of  $\Delta \epsilon$  and various values of  $d_p$ , which are chosen to coincide with the elements of the cross-sectional areas as shown in Fig. 26. These curves are plotted, as before, with m as ordinates and  $\Delta \epsilon$  as abscissas and are labeled in terms of  $d_p$ .

Also shown in Fig. 27 are values of  $P/A$  for assumed values of  $\Delta \epsilon$  and

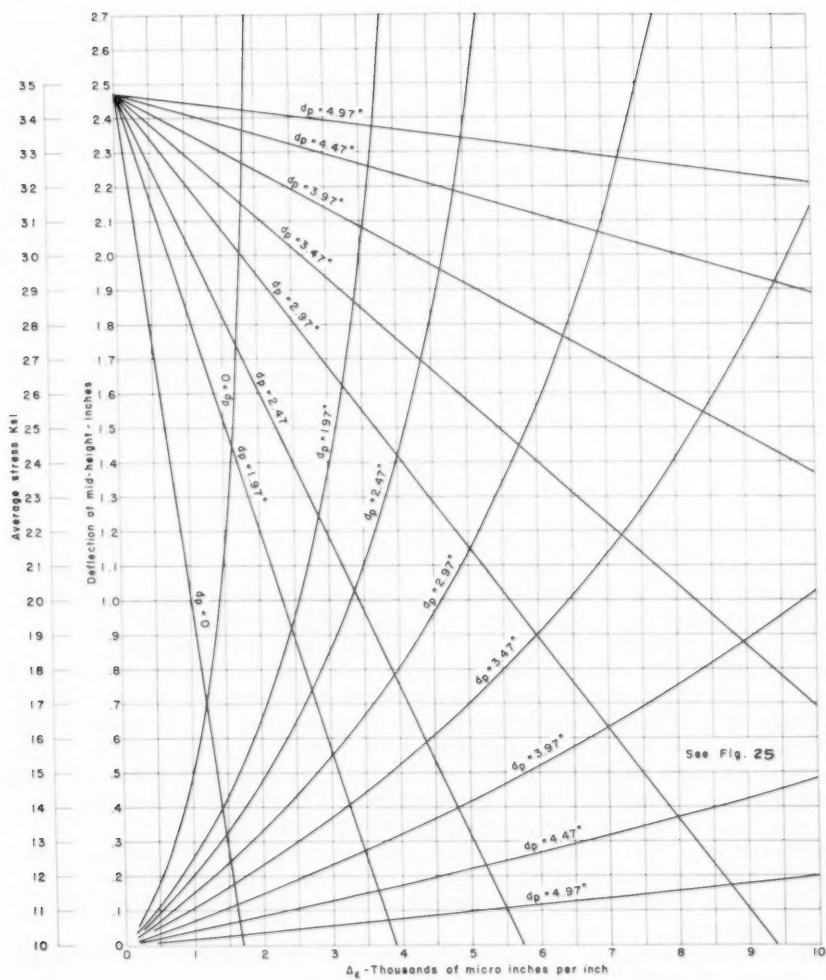


Fig. 27  
MAXIMUM STRENGTH CURVES  
Column With Initial Bending  
6x6 M25



various values of  $d_p$ . These curves intersect at the assumed average maximum load of 34.72 ksi when  $\Delta\epsilon = 0$ —assumed yield point strength, based on the maximum load of Model CO.

The curves shown in Fig. 28 with  $P/A$  as ordinates and  $L/r$  as abscissas and labeled in terms of  $\Delta\epsilon$  are plotted by use of the curves in Figs. 26 and 27. Assume a value of  $L/r$  and obtain the mid-height deflection from curves in Fig. 26 for a specific value of  $\Delta\epsilon$ . Use this value of  $m$  and in Fig. 27 for the specific value of  $\Delta\epsilon$  determine its relationship with the curves labeled in terms of  $d_p$  and converging on zero  $m$ . Use this relationship to obtain the average load from the straight lines labeled in terms of  $d_p$  and converging on 34.72 ksi.

These curves show the decrease in the load carrying capacity of hinged-end columns due to various amounts of mid-height bending as measured in terms of  $\Delta\epsilon$ . They may be used for columns with any degree of end restraint by the use of the proper effective length—one-half for fixed-end columns.

These curves may be used to approximate the maximum load for columns with out-of-square splices by determining the value of the bending moment at the bottom of the column due to joint closure and determining the value of  $\Delta\epsilon$ . Then, assuming a fixed-end condition, the effective length is one-half the full length and the average load,  $P/A$ , may be taken from the curves in Fig. 28.

### CONCLUSIONS

Two types of failure should be considered: (1) ultimate failure and (2) functional failure. Ultimate failure is the total collapse of a structure. Functional failure is the occurrence of permanent set or excessive deflection which prevents the structure from serving its intended purpose.

Columns are designed with a factor of safety based on the loading at which the maximum extreme fiber stress reaches the yield point strength of the material, in which bending due to accidental errors is considered. This is design against a functional-type failure—no permanent set is allowed. The ultimate strength will be that limited by plastic buckling. This is higher than the strength at the loading of first yield in all columns found in practice, since bending due to accidental errors is considered. The margin between these two strengths is variable and depends upon the slenderness ratio of the column and the actual stress-strain curve of the material. This presupposes that general or local elastic buckling does not occur. It is this reserve strength which sometimes holds up structures after the functional strength has been exceeded.

The rational design of a structure depends upon knowing both its functional and ultimate strengths. In general, a smaller factor of safety could be used based on functional strength than that based on ultimate strength. This could mean an increase in working stresses as the margin between the two types of failure increased. This is done in the design of bearing rollers in bending because of the large margin between the elastic and plastic bending strengths of a member with circular section.

The eccentricity created by milling out-of-square about the weak axis the bearing ends at a partially riveted splice in an H-section, 6 x 6 M 25, of ASTM A7 structural steel had only a small effect on the capacities of the columns in the tests described in this paper.

The capacity of spliced Model C1,  $L/r = 63$ , was 2.3% less than that of



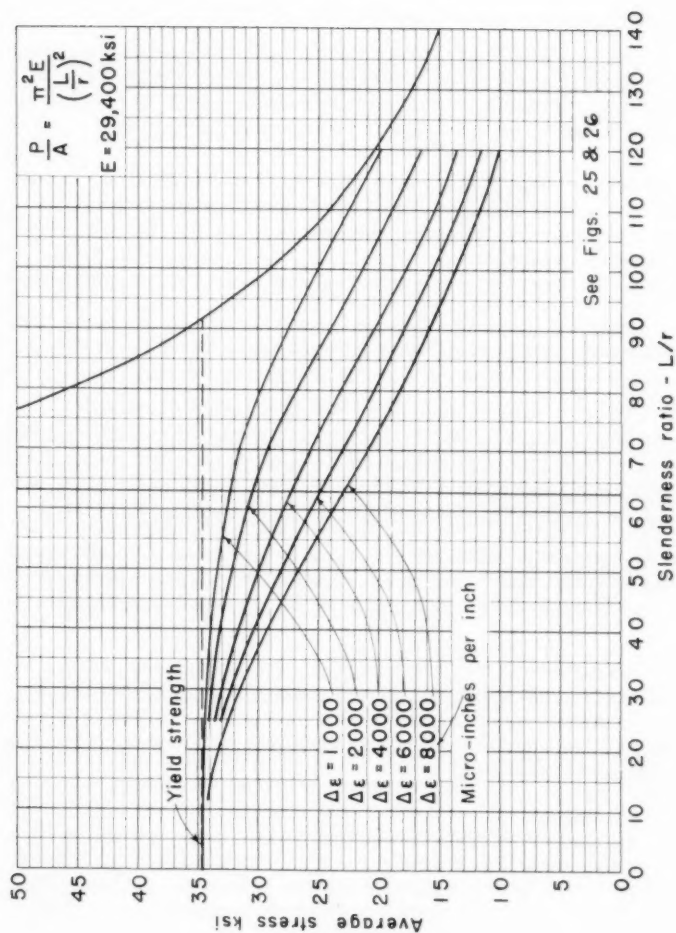


Fig. 28  
 MAXIMUM LOADS FOR COLUMN WITH BENDING  
 6x6 M 25

unsplined Model CO,  $L/r = 63$ . The capacity of braced Model C2,  $L/r = 63$ , was 4.3% less than that of Model CO. All three had a crushing-type failure. The plastic strengths were high and the drop-off in load carrying capacities was slow. Both were practically the same for all three models. The splice in Model C2 gave no resistance to longitudinal movement.

The capacity of spliced Model C3,  $L/r = 103$ , was 7.3% less than that of unsplined Model COL,  $L/r = 103$ . Both models had a buckling-type failure. The plastic strengths were low and the drop-off in load carrying capacities was fast for each model.

There was more reserve strength in the shorter than in the longer models. The fact that the experimental plastic strengths of all three of the shorter models were practically the same indicates that initial errors in eccentricity of load and curvature tend to become less effective on the final plastic action of a column.

The value of the out-of-squareness used in these tests, 1/16 in. across a 6 in. flange width is high. It would probably never be exceeded in practice.

It seems logical to make the following statements, based on the fact that the reserve and plastic strengths were practically the same for the three short models tested, and limited to H-section columns of ASTM A7 structural steel.

1. Out-of-squareness at a partially riveted splice increases the unit shortening and reduces the stiffness of the column in the elastic region.
2. The capacity of an H-section column of ASTM A7 structural steel with out-of-squareness at a partially riveted splice may, in general, safely be considered equal to that of an identical unsplined column, provided that the Euler critical load, based on hinged-ends, is greater than the yield point strength of the material and the ends of the column are, at least, partially restrained.
3. Care must be exercised in the case of a column with out-of-squareness at a partially riveted splice where the hinged-end Euler critical load is less than the yield point strength of the material or where the ends are actually hinged.
4. No values can be given on the permissible magnitudes of out-of-squareness at a partially connected splice as a result of these tests. They will give guidance in the exercise of judgment in the field inspection of out-of-squareness at the abutting ends of a partially connected splice in an H-section column of ASTM A7 structural steel.

#### ACKNOWLEDGMENTS

The columns were tested by the writer at Purdue University in cooperation with Subcommittee B of the Column Research Council, composed of J. E. Goldberg, T. R. Higgins, G. M. Magee, E. J. Ruble, G. S. Vincent, and L. T. Wyly, all Members, ASCE. The following research assistants helped with the work at various times: A. Y. Aragaki and F. E. Koebel, both J. M. ASCE, and A. S. Ryan and J. A. Sbarounis. Professor Vakkas Aykurt, Istanbul Teknik Okulu, Istanbul, Turkey, assisted for about nine months. The American Bridge Company furnished material and fabrication.

---

Journal of the  
STRUCTURAL DIVISION  
Proceedings of the American Society of Civil Engineers

---

ELASTIC STRUCTURES WITH NONLINEAR LOAD-DEFLECTION CURVES

Benjamin M. Ma<sup>1</sup>  
(Proc. Paper 1441)

---

SYNOPSIS

This paper presents the essential characteristics of the action of a simple structure in practical use for which the linear stress-strain relation results in a non-linear load-deflection curve involving a region where the load decreases with increase in deflection.

The behavior of this type of structure is similar to that of a segment of spherical shell under a uniform external pressure or a strip of cylindrical shell under an axial compression. In all these cases, the load-deflection curves are not linear and have an unstable region within the elastic range.

Based on the assumptions of elementary beam theory and the principle of consistent deformations, this simple structure subjected to a concentrated load at the outer end or a uniformly distributed load over the whole span of the bar is analyzed and a concise comparison between these two loading conditions is made. The range of large deflection is also discussed.

---

INTRODUCTION

In the field of structures, one of the most complex problems is the influence of curvature on buckling characteristics.<sup>(1)</sup> Everyone who has contact with this subject will realize that a clear understanding of buckling phenomena even for a simple curved panel is not easy to obtain. Anything that throws light on the matter is of great value even if it applies only to a very simple case.

In the investigations of the buckling of thin spherical shells<sup>(2)</sup> and thin cylindrical shells<sup>(3)</sup> by Theodore Von Karman and H. S. Tsien and of thin curved plates<sup>(4)</sup> by H. L. Cox, the very important common characteristic is brought out that for these curved thin-walled structures the load-deflection

---

Note: Discussion open until April 1, 1958. Paper 1441 is part of the copyrighted Journal of the Structural Division of the American Society of Civil Engineers, Vol. 83, No. ST 6, November, 1957.

1. Associate Prof. of Mech. Eng., South Dakota State College, Brookings, S. Dak.

relations are non-linear. In other words, with these structures the load sustained is not a linear function of the deflection even when the stresses are within the elastic limit and are proportional to the corresponding strains. Experience also shows a systematic discrepancy between the theoretical buckling loads calculated by the linear small deflection theory and the results obtained from experiments. To obtain consistent results between theory and experiments, the large deflection theory is needed. But the mathematical expression of the large deflection theory for these curved thin-walled structures involves two non-linear partial differential equations<sup>(5)</sup> for which an exact solution is very difficult.

In view of the mathematical difficulty of using the large deflection theory to find exact solutions of the problems of thin cylindrical shells and curved plates, experiments have been carried out on columns with non-linear elastic supports.<sup>(1)</sup> These have shown that the essential characteristics of the buckling of thin cylindrical shells and curved plates can be represented by such structures. This is true, because, under axial compression a longitudinal strip of a cylindrical shell or a curved plate may be considered as a column with elastic lateral support.

The simple structure considered in this paper is of interest because it is in common, practical use and shows the same essential buckling characteristics as thin shells, curved plates and columns with non-linear lateral supports. Moreover, an exact solution can be easily obtained for it without any mathematical difficulty, nor complementary energy method<sup>(6)</sup> involved.

It is believed, therefore, that by taking advantage of the essential characteristics of this type of structure, some buckling phenomena of thin shells and curved plates may be further clarified and developed.

### Basic Assumptions

In investigating the problem of the simple structure, Figs. 1 and 9, the following basic assumptions are made:

1. The deflection at the outer end of the bar AB is small as in elementary beam theory.
2. The shortening due to the axial compression and bending of the bar AB can be neglected.
3. For the small deflections of practical interest the change of angle  $\theta$  is negligible.

### Structure Subjected to Concentrated Load

#### 1. General Description of the Structure

The simple structure, Fig. 1, is a statically indeterminate one with one degree of redundancy if the wire AC is supposed to be incapable of carrying bending. The bar AB may be considered as a beam-column subjected to the axial compressive force  $T_h$ , with a restraining moment at the right end and pin-ended at the left. Under the lateral load the left end A, subjected to the restraint offered by the wire AC, is able to deflect in the Y-direction. The right end B is fixed against both rotation and translation. This is one of the common structures in practical use, such as bracket, hoisting crane and externally braced aircraft.

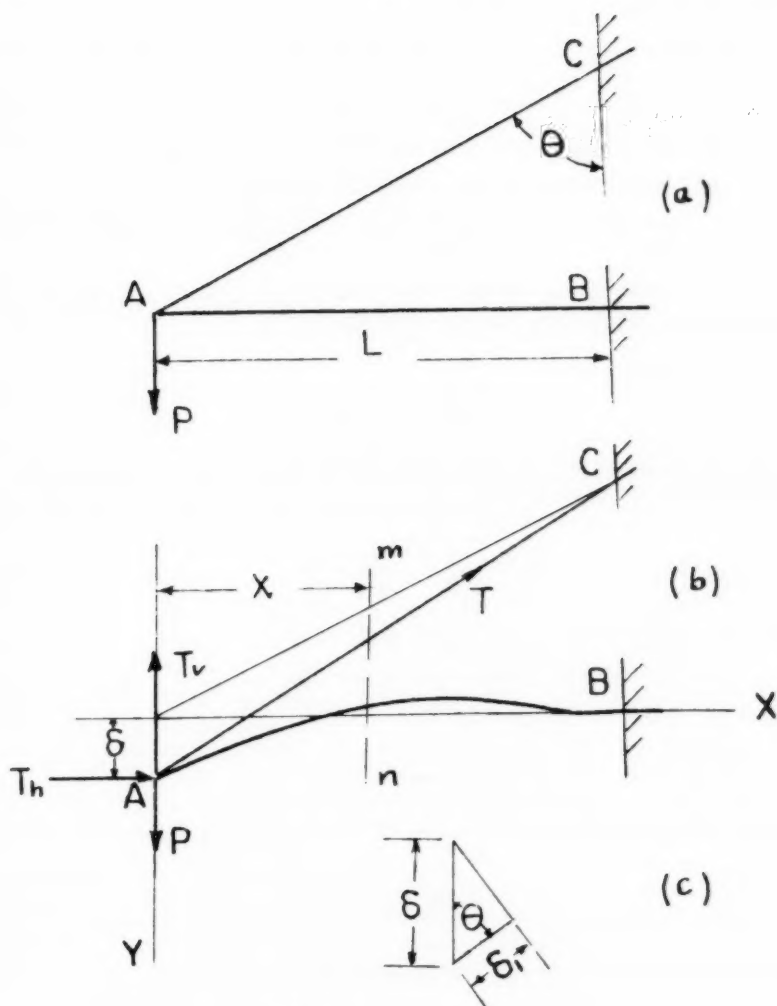


FIG. 1

The vertical and horizontal components of tensile force of the wire AC are

$$T_v = T \cos \theta$$

$$T_h = T \sin \theta$$

whence

$$T_v/T_h = \cot \theta \quad (1)$$

where

$T$  = the tensile force of the wire AC

$\theta$  = the angle of inclination of the wire AC, Fig. 1a.

## 2. Derivation of Bending Moments

The bending moment,  $M$ , at the section  $mn$  of the bar  $AB$ , Fig. 1b, is given

$$\text{by } M = (P - T_v)x + T_h (\delta - y) \quad (2)$$

where  $M$  = the bending moment at any section of the bar  $AB$ .

$S$  = the deflection at the outer end of the bar  $AB$ .

$x$  = the distance between the outer end  $A$  and any section  $mn$  of the bar.

$y$  = the deflection at the section  $mn$ .

Differentiating twice with respect to  $x$ , we obtain

$$\frac{d^2 M}{dx^2} = -T_h \frac{d^2 y}{dx^2} \quad (3)$$

Considering the curvature of the bar  $AB$  due to bending only, from the elementary beam theory, we have

$$\frac{d^2 y}{dx^2} = \frac{M}{EI} \quad (4)$$

Where  $E$  = the modulus of elasticity of the bar  $AB$

$I$  = the moment of inertia of the bar  $AB$

Substituting Eq. 4 in 3 and denoting that

$$\frac{T_h}{EI} = k^2 \quad (5)$$

We obtain the differential equation for the bending moment of the bar.

$$\frac{d^2 M}{dx^2} + k^2 M = 0 \quad (6)$$

The general solution of this equation is given by

$$M = C_1 \sin kx + C_2 \cos kx \quad (7)$$

The end conditions for determining the integration constants  $C_1$  and  $C_2$  are

$$\text{at } x = 0, \quad M = 0; \quad \text{whence } C_2 = 0 \quad (a)$$

$$\text{at } x = L, \quad M = M_b \quad \text{whence } C_1 = M_b / \sin kL$$

Substituting these values in Eq. 7, we have the equation for the bending moment of the bar

$$M = \frac{M_b}{\sin kL} \sin kx \quad (8)$$

Where  $M_b$  = the bending moment at the fixed end B of the bar

$L$  = the length of the bar AB.

The value of  $M_b$  will be determined later.

From Eq. 8, it is obvious that the bending moment is a maximum when the value of  $\sin kx$  is a maximum. Now let

$$\sin kx = 1$$

The maximum moment of the bar is, then

$$M_{\max} = M_b / \sin kL \quad (6)$$

provided that  $M_b$  and  $\sin kL$  have the same sign.

The location of the section of maximum moment may be found by putting

$$kx = (2n + 1) \frac{\pi}{2} \quad n = 0, 1, 2, 3, \dots$$

for  $\sin kx = 1$ .

In this case, the smallest value of  $kx$  and, therefore, of the axial compressive force  $T_h$  (see Eq. 5), is obtained by taking

$$n = 0$$

and

$$kx = \pi/2$$

or

$$x = \pi/2k = \frac{\pi}{2} \sqrt{\frac{EI}{T_h}} \quad (b)$$

It is necessary that this should be less than  $L$ , otherwise the greatest  $M$  which is equal to  $M_b$  is at  $x = L$ .

It is seen that for the given properties of material and cross section of the bar AB (i.e. for the given flexural rigidity  $EI$ ), the location of the section of maximum moment depends only on the axial compressive force  $T_h$ . The relation between  $T_h$  and the lateral load  $P$  will be given later (see Eq. 17).

### 3. Derivation of Load-Deflection Relation

Attention should be called to the load-deflection relations of the structure. From Eqs. 2 and 4, we have the most essential expression

$$EI \frac{d^2 y}{dx^2} = (P - T_v) x + T_h (\delta - y) \quad (10)$$

or

$$\frac{d^2 y}{dx^2} + k^2 y = k^2 \delta + (P - T_v) x / EI$$

The general solution of this differential equation for the deflection curve of the bar is given by

$$y = A \sin kx + B \cos kx + \delta + \frac{P - T_v}{T_h} x \quad (11)$$

and the general equation for the slope of the deflection curve found, by differentiating Eq. 11 with respect to  $x$ , is

$$y' = Ak \cos kx - Bk \sin kx \neq \frac{P-T_v}{T_h} \quad (12)$$

In Eqs. 11 and 12, A and B are constants of integration, which must be determined to satisfy the boundary conditions at the built-in end of the bar:

$$\text{at } x = L \quad y = 0$$

$$A \sin kL \neq B \cos kL \neq \delta \neq \frac{P-T_v}{T_h} L = 0 \quad (c)$$

$$\text{at } x = L \quad y' = 0$$

$$Ak \cos kL - Bk \sin kL \neq \frac{P-T_v}{T_h} = 0 \quad (d)$$

or

$$B = (Ak \cos kL \neq \frac{P-T_v}{T_h}) / k \sin kL$$

Substitution of this expression in (c) gives

$$A = -\frac{P-T_v}{T_h k} (\cos kL \neq kL \sin kL) - \delta \sin kL \quad (e)$$

$$B = \frac{P-T_v}{T_h k} (\sin kL - kL \cos kL) - \delta \cos kL \quad (f)$$

By substituting e and f in Eqs. 11 and 12, the particular solutions for the deflection and the slope of the bar are

$$y = \left[ -\frac{P-T_v}{T_h k} (kL \sin kL \neq \cos kL) - \delta \sin kL \right] \sin kx \\ \neq \left[ \frac{P-T_v}{T_h k} (\sin kL - kL \cos kL) - \delta \cos kL \right] \cos kx \neq \delta \left( \frac{P-T_v}{T_h} \right) x \quad (11a)$$

$$y' = \left[ -\frac{P-T_v}{T_h k} (\cos kL \neq kL \sin kL) - \delta \sin kL \right] k \cos kx \\ \neq \left[ -\frac{P-T_v}{T_h k} (\sin kL - kL \cos kL) \neq \delta \cos kL \right] k \sin kx \neq \frac{P-T_v}{T_h} \quad (12a)$$

From Eqs. 11a and 12a, the deflection and the slope at the outer end of the bar can be easily obtained. Since  $y = S$  at  $x = 0$ , we have

$$\delta = \frac{P-T_v}{T_h} (\sin kL - kL \cos kL) / k \cos kL \\ \text{or } \delta/L = \frac{P-T_v}{T_h} (\sin kL - kL \cos kL) / kL \cos kL \quad (13)$$

$$= (P/T_h - \cot \theta) (\tan kL - kL) / kL$$

$$y'_{x=0} = \frac{P-T_v}{T_h} (1 - \sec kL) \quad (14)$$

$$= (P/T_h - \cot \theta) (1 - \sec kL)$$

Where  $T_v/T_h = \cot \theta$ , as given, Eq. 1, and  $P/T_h$  is the ratio of the lateral load to the axial compressive force of the bar AB.



#### 4. Equation of Consistent Deformations

In order to determine the deflection of the bar from Eq. 11a and 13, an additional equation is needed to express the relation between the axial compressive force  $T_h$  of the bar, and the corresponding tensile force  $T$  of the wire. This equation of consistent deformations can be easily obtained if we assume Hooke's law holds and that the shortening of the bar AB and the change in angle  $\theta$  are small enough to be negligible. Then, the tensile force  $T$  of the wire is, Figs. 1b and 1c.

$$T = A_1 E_1 \delta_1 / L_1 = E_1 A_1 \delta \sin 2\theta / 2L \quad (15)$$

and the corresponding axial compressive force is, from Eq. 1,

$$T_h = E_1 A_1 \delta \sin \theta \sin 2\theta / 2L \quad (15a)$$

Where  $E_1$  = the modulus of elasticity of the wire AC.  
 $A_1$  = the cross-sectional area of the wire AC.  
 $L_1$  = the length of the wire AC.

$$L_1 = L / \sin \theta$$

$\delta_1$  = the total elongation of the wire AC

$$\delta_1 = \delta \cos \theta.$$

Using Eqs. 5, 15, and 15a, the non-dimensional form of deflection at the outer end of the bar can be obtained.

$$\begin{aligned} \delta/L &= 2 T / E_1 A_1 \sin 2\theta \\ \text{or } \delta/L &= \frac{2 EI k^2}{E_1 A_1 \sin \theta \sin 2\theta} = \frac{\beta \cdot 2(kL)^2}{\sin \theta \sin 2\theta} \end{aligned} \quad (16)$$

Where  $\beta = EI / E_1 A_1 L^2$  = a non-dimensional coefficient. (g)

For any given values of  $\beta$  and  $\theta$ ,  $\delta/L$  can be obtained from Eq. 16 corresponding to different values of the parameter  $kL$  so that  $kL$  is one of the essential functions of the deflection  $\delta/L$ . It is noted that there would be no deflection at the outer end of the bar when the coefficient  $\beta$  approaches zero, i.e. when the cross-sectional area  $A_1$  of the wire becomes very great.

#### 5. Relation Between Concentrated Load $P$ and Axial Compressive Force $T_h$

Eliminating  $\delta/L$  from Eqs. 13 and 16, we have

$$\begin{aligned} (P/T_h - \cot \theta) (\tan kL - kL)/kL &= \beta \cdot 2(kL)^2 / \sin \theta \sin 2\theta \\ \text{or } P/T_h &= 2\beta / \sin \theta \sin 2\theta \cdot (kL)^3 / (\tan kL - kL) + \cot \theta \end{aligned} \quad (17)$$

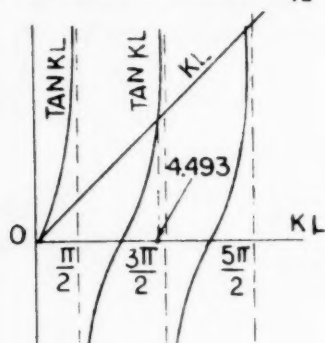
The ratio of the lateral load to the axial compressive force,  $P/T_h$ , can be calculated for various values of  $kL$  provided that the values of  $\beta$  and  $\theta$  are given.

It should be pointed out that in Eq. 17 there are three special cases of interest:

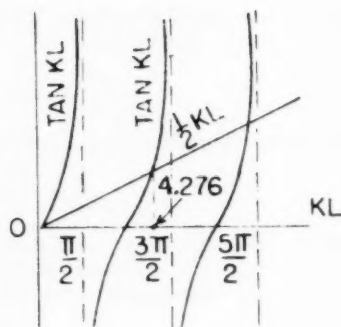
1.  $P/T_h$  is a function of  $\theta$  only when  $kL = \pi/2$  and  $\tan kL$  becomes infinite.

2.  $P/T_h = \infty$ , i.e. the lateral load  $P$  becomes infinite when  $\tan kL - kL = 0$

The graphical method for determining the value  $\tan kL - kL = 0$  is given in Fig. 2a, where  $kL = 4.493 = \frac{103''}{72}$



(a)  $\tan kL - kL = 0$



(b)  $\tan kL - \frac{1}{2} kL = 0$

FIG. 2

3.  $(kL)^3/(\tan kL - kL) = \text{indeterminate form when } kL = 0$ .

In order to determine the value of  $P/T_h$  at the limiting case  $kL = 0$ , it is necessary to find the limit of the term  $(kL)^3/(\tan kL - kL)$ .

$$\begin{aligned} \lim_{kL \rightarrow 0} \frac{(kL)^3}{\tan kL - kL} &= \lim_{kL \rightarrow 0} \frac{3(kL)^2}{\sec^2 kL - 1} = \lim_{kL \rightarrow 0} \frac{3(kL)^2 (1/\cos 2kL)}{1 - \cos 2kL} \\ &= \lim_{kL \rightarrow 0} \left[ \frac{6kL(1/\cos 2kL) - 6(kL)^2 \sin 2kL}{2 \sin 2kL} \right] \\ &= \lim_{kL \rightarrow 0} \left[ \frac{3(1/\cos 2kL) - 6kL \sin 2kL - 6kL \sin 2kL - 6(kL)^2 \cos 2kL}{2 \cos 2kL} \right] \\ &= 3 \end{aligned}$$

Substituting this value in Eq. 17, we may have the limiting value of  $P/T_h$  when  $kL$  approaches zero.

The values of  $P/T_h$  corresponding to specific values of  $kL$  with the angle  $\theta = 45^\circ$  are given in Table I, and the curves of  $P/T_h$  plotted against  $(2kL/\pi)^2$  shown in Fig. 3. For all the values of the coefficient  $\beta$  we find that

- |                 |                     |
|-----------------|---------------------|
| (a) $P/T_h > 1$ | when $kL < \pi/2$ . |
| (b) $P/T_h = 1$ | when $kL = \pi/2$ . |
| (c) $P/T_h < 1$ | when $kL > \pi/2$ . |

Table I

Computations of the ratio of concentrated load  $P$  to axial compressive force  $T_h$  with the different values of  $(2kL/\pi)^2$

		$\theta = 45^\circ$							
$kL$		0	$\pi/6$	$\pi/3$	$5\pi/12$	$\pi/2$	$7\pi/12$	$2\pi/3$	$5\pi/6$
$(2kL/\pi)^2$	0	0.111	0.444	0.695	1.000	1.361	1.778	2.778	
$\beta=0.10$	$P/T_h$	1.848	1.753	1.472	1.257	1.000	0.687	0.327	-0.588
$\beta=0.05$	$P/T_h$	1.424	1.376	1.238	1.130	1.000	0.844	0.663	0.206
$\beta=0.01$	$P/T_h$	1.085	1.073	1.046	1.023	1.000	0.970	0.933	0.842
$\beta=0.005$	$P/T_h$	1.042	1.033	1.022	1.013	1.000	0.986	0.968	0.921
$\beta=0.001$	$P/T_h$	1.008	1.005	1.002	1.001	1.000	0.998	0.994	0.984
$kL$		$\pi$	$7\pi/6$	$5\pi/4$	$4\pi/3$	$25\pi/18$	$17\pi/12$		
$(2kL/\pi)^2$		4.000	5.444	6.250	7.111	7.716	8.028		
$\beta=0.05$	$P/T_h$	-0.396	--	--	--	--	--		
$\beta=0.01$	$P/T_h$	0.721	0.550	0.414	0.154	-0.458	--		
$\beta=0.005$	$P/T_h$	0.861	0.771	0.706	0.576	0.270	--		
$\beta=0.001$	$P/T_h$	0.972	0.952	--	0.915	0.854	0.648		

The axial compressive force,  $T_h$ , increases as the ratio of  $P/T_h$  decreases.

#### 6. Relation between Concentrated Load $P/P_{cr}$ and Parameter $kL$

Substitution of Eq. 5 in 17 gives

$$P = EIk^2 \left( \frac{2\beta}{\sin \theta \sin 2\theta} - \frac{(kL)^3}{\tan kL - kL} - \cot \theta \right)$$

or, in the nondimensional form

$$P/P_{cr}^* = \frac{4L^2 P}{\pi^2 EI} = \left( \frac{2kL}{\pi} \right)^2 \left( \frac{2\beta}{\tan kL - kL} - \cot \theta \right) \quad (18)$$

Where

$$P_{cr}^* = 2EI/4L^2 \quad (h)$$

$P_{cr}$  is the critical or buckling load of a column with one end free and the other end built-in. The ratio of  $P/P_{cr}$ , for given values of  $\beta$  and  $\theta$ , varies with parameter  $kL$ . The value of  $P_{cr}$ , as defined, is a suitable and convenient non-dimensional measure for the various forces dealt with, such as the lateral load  $P$  and the axial compressive force  $T_h$ ; since the bar AB may be thought of as a beam-column of the type described.

It has been pointed out in Eq. 16 that for given values of  $\beta$  and  $\theta$  the parameter  $kL$  is essentially a measure of the deflection  $\delta/L$ . So that Eq. 18

\*  $P_{cr}$  should be  $P_{cr}$

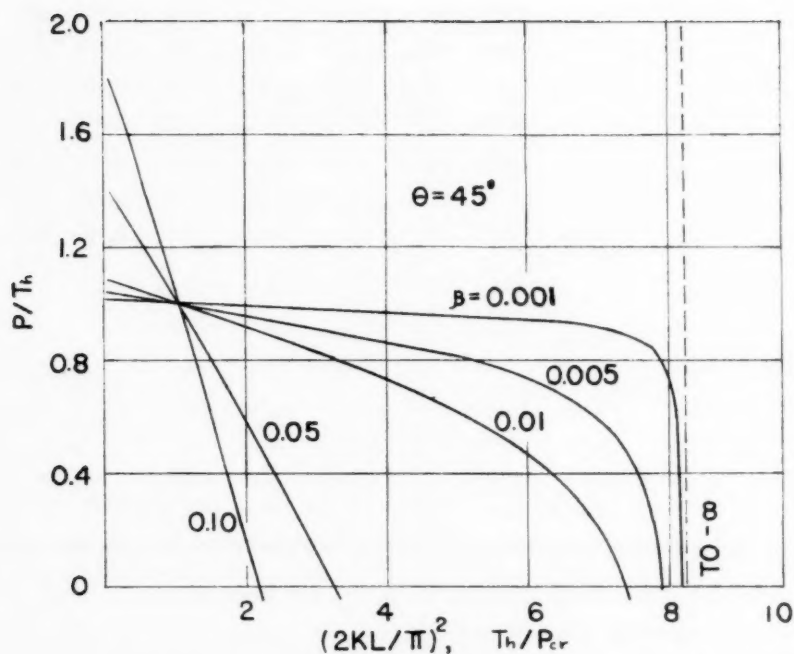


FIG.3 RELATION BETWEEN CONCENTRATED LOAD  $P/T_h$  AXIAL FORCE  $T_h/P_{cr}$  AND  $(2KL/\pi)^2$

Table II  
 Computations of the Concentrated Load  $P/Per$   
 with the different values of  $(2kL/\pi)^2$   
 $\theta = 45^\circ$

		$kL$	0	$\pi/6$	$\pi/4$	$\pi/3$	$5\pi/12$	$\pi/2$	$7\pi/12$	$2\pi/3$
		$(2kL/\pi)^2$	0	.111	.250	.444	.695	1.000	1.361	1.778
$\beta=1$	P/Per	0	0.933	1.848	2.556	2.516	1.000	-2.894	-10.2	
$\beta=0.5$	P/Per	0	0.529	1.049	1.500	1.604	1.000	-0.775	-4.210	
$\beta=0.1$	P/Per	0	0.195	0.410	0.655	0.874	1.000	0.935	0.581	
$\beta=0.05$	P/Per	0	0.153	0.330	0.550	0.785	1.000	1.148	1.180	
$\beta=0.01$	P/Per	0	0.120	0.266	0.465	0.712	1.000	1.318	1.658	
$\beta=0.005$	P/Per	0	0.115	0.258	0.455	0.705	1.000	1.341	1.720	
$\beta=0.001$	P/Per	0	0.112	0.252	0.446	0.687	1.000	1.356	1.765	
		$kL$	$5\pi/6$	$\pi$	$13\pi/12$	$7\pi/6$	$5\pi/4$	$4\pi/3$	$25\pi/18$	$17\pi/12$
		$(2kL/\pi)^2$	2.778	4.000	4.694	5.444	6.250	7.111	7.716	8.028
$\beta=1$	P/Per	--	--	--	--	--	--	--	--	--
$\beta=0.5$	P/Per	--	--	--	--	--	--	--	--	--
$\beta=0.1$	P/Per	-1.638	-7.168	--	--	--	--	--	--	--
$\beta=0.05$	P/Per	0.571	-1.584	--	-6.802	--	--	--	--	--
$\beta=0.01$	P/Per	2.340	2.884	3.022	2.995	2.585	1.095	-3.540	--	--
$\beta=0.005$	P/Per	2.559	3.442	--	4.200	4.420	4.104	2.081	-6.100	--
$\beta=0.001$	P/Per	2.732	3.888	--	5.190	5.880	6.508	6.590	5.210	--

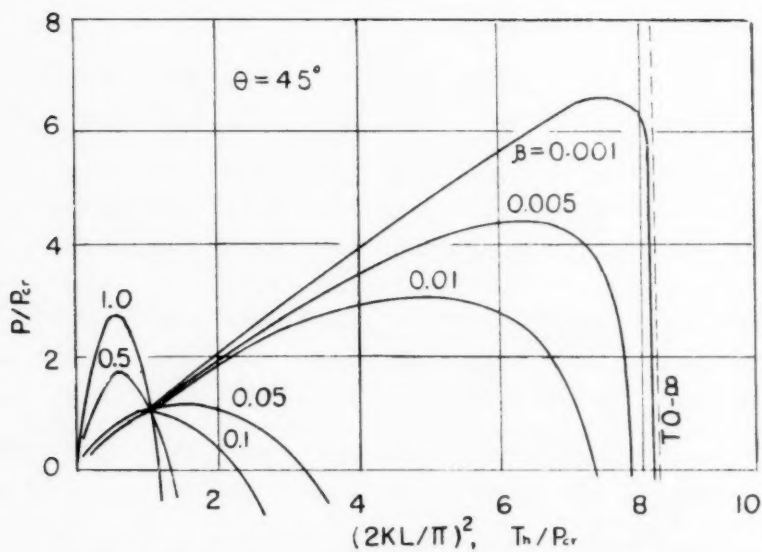


FIG. 4 RELATION BETWEEN CONCENTRATED  
LOAD  $P/P_{cr}$  AND  $(2KL/\pi)^2$

is implicitly to give the load-deflection relation of the concentrated loading condition.

The calculations of  $P/P_{cr}$  for various values of  $\beta$  and  $kL$ , with the angle  $\theta = 45^\circ$ , are given in Table II and the curves of  $P/P_{cr}$  plotted against  $(2kL/\pi)^2$  are shown in Fig. 4.

From Fig. 4, the following main points may be brought out

- a) All the curves pass through the point

$$P/P_{cr} = 1 \text{ at } kL = \pi/2$$

This may be realized by observing Eq. 18.

- b)  $\beta < 0.1$ , the value of  $(P/P_{cr})_{max}$  tends to shift to the right with larger  $(kL)$   
 c)  $\beta > 0.1$ , the value of  $(P/P_{cr})_{max}$  tends to shift to the left with smaller  $(kL)$ .

#### 7. Effects of the Cross-Sectional Area $A_1$ of the Wire and the Moment of Inertia $I$ of the Bar on Concentrated Load $P/P_{cr}$

Since the effect of the coefficient  $\beta = EI/E_1A_1L^2$ , is so great as shown in Fig. 4, it is felt that a further discussion of the influence of  $\beta$  is desirable. Now, let us consider the two particular cases by varying  $A_1$  and  $I$ :

1.  $\frac{EI}{E_1L^2} = \text{constant}$ .  $\beta \propto \frac{1}{A_1}$ ,  $A_1$  increases,  $\beta$  decreases,  $P/P_{cr}$  increases for  $\beta < 0.1$
2.  $\frac{E}{E_1A_1L^2} = \text{constant}$ .  $\beta \propto I$ ,  $I$  increases,  $\beta$  increases,  $P/P_{cr}$  increases for  $\beta > 0.1$

It can be concluded that when the materials of the structure are given and the length of the bar AB as well as of the wire AC, at a fixed angle  $\theta$ , is constant, the cross-sectional area  $A_1$  of the wire is the major factor controlling  $P/P_{cr}$  when  $\beta < 0.1$ ; and the moment of inertia  $I$  of the bar is the major factor controlling  $P/P_{cr}$  when  $\beta > 0.1$ . However, the effect of the cross-sectional area  $A_1$  is more powerful than that of the moment of inertia  $I$ , Fig. 4.

#### 8. Non-Linear Relation Between Concentrated Load $P/P_{cr}$ and Deflection $\delta/L$

With parameter  $kL$ , Eqs. 16 and 18 are the parametric form of the non-linear load-deflection relation of  $P/P_{cr}$  and  $\delta/L$  for the given values of  $\beta$  and  $\theta$ . The combination of these two equations yields:

$$\begin{cases} \frac{\delta}{L} = \frac{2\beta}{\sin \theta \sin 2\theta} (kL)^2 \\ \frac{P}{P_{cr}} = \left(\frac{2kL}{\pi}\right)^2 \frac{2\beta}{\sin \theta \sin 2\theta} \frac{(kL)^3}{\tan kL - kL} + \cot \theta \end{cases} \quad (19)$$

$$\frac{P}{P_{cr}} = \left(\frac{2kL}{\pi}\right)^2 \left( \frac{\delta}{L} \frac{kL}{\tan kL - kL} + \cot \theta \right)$$

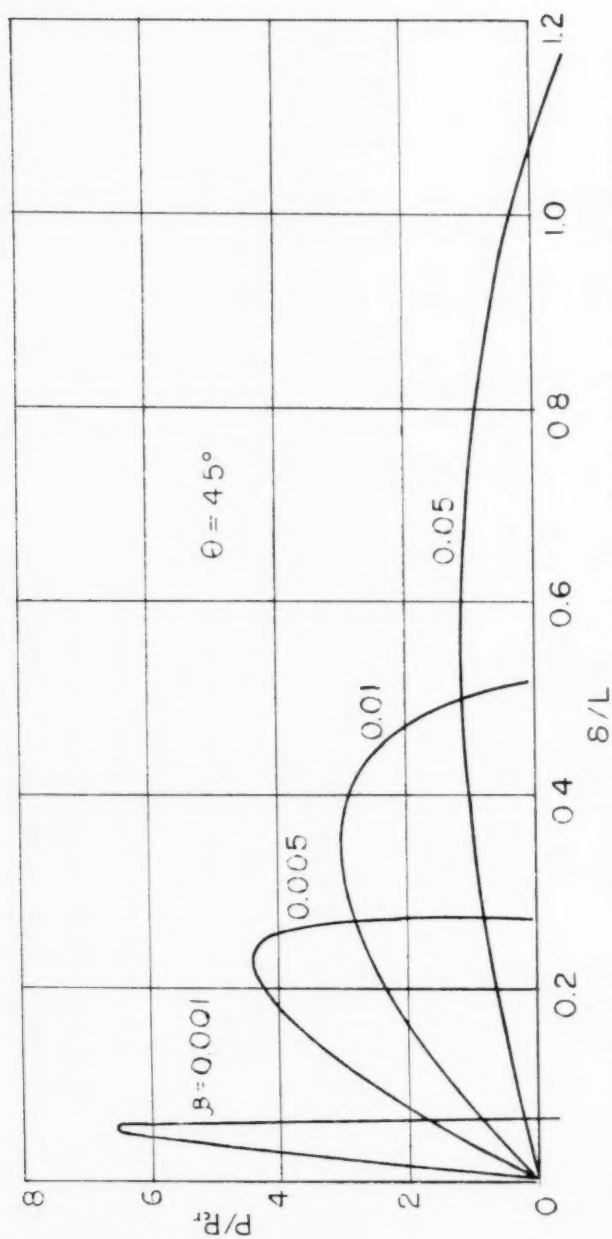
This defines the most essential characteristics of the structure.

Table III  
 Computations of the Concentrated Load P/Per and Deflection  $\delta/L$   
 with the different values of  $\beta$  and  $kL$

$\theta = 45^\circ$									
$\beta = 0.1$									
$kL$	0	$\pi/6$	$\pi/4$	$\pi/3$	$5\pi/12$	$\pi/2$	$7\pi/12$	$2\pi/3$	$5\pi/6$
P/Per	0	.195	.410	.655	.874	1.000	.935	.581	-1.638
$\delta/L$	0	.0775	.1742	.3100	.4844	.6980	.9492	1.240	1.938
$\beta = 0.05$									
$kL$	0	$\pi/6$	$\pi/4$	$\pi/3$	$5\pi/12$	$\pi/2$	$7\pi/12$	$2\pi/3$	$5\pi/6$
P/Per	0	.153	.330	.550	.785	1.000	1.140	1.180	.571
$\delta/L$	0	.0388	.0871	.1550	.2415	.3490	.4746	.6200	.9690
$\beta = 0.01$									
$kL$	0	$\pi/6$	$\pi/3$	$\pi/2$	$2\pi/3$	$5\pi/6$	$\pi$	$13\pi/12$	$7\pi/6$
P/Per	0	.120	.465	1.000	1.658	2.240	2.884	3.022	2.995
$\delta/L$	0	.0078	.0310	.0698	.1240	.1936	.2828	.3160	.3800
$\beta = 0.001$									
$kL$	$5\pi/4$	$4\pi/3$	$25\pi/18$						
P/Per	2.585	1.095	-3.540						
$\delta/L$	.4360	.4960	.5384						



$\beta=0.005$									
kL	0	$\pi/6$	$\pi/3$	$\pi/2$	$2\pi/3$	$5\pi/6$	$\pi$	$7\pi/6$	$5\pi/4$
P/Per	0	.115	.445	1.000	1.720	2.559	3.442	4.200	4.420
S/L	0	.0039	.0155	.0349	.0620	.0969	.1414	.1900	.2180
kL	$4\pi/3$	$25\pi/18$	$17\pi/12$						
P/Per	4.104	2.081	-6.100						
S/L	0.2480	.2691	.2800						
$\beta=1.001$									
kL	0	$\pi/6$	$\pi/3$	$\pi/2$	$2\pi/3$	$5\pi/6$	$\pi$	$7\pi/6$	$5\pi/4$
P/Per	0	.112	.446	1.000	1.765	2.732	3.888	5.190	5.880
S/L	0	.0008	.0031	.0070	.0124	.0194	.0283	.380	.0436
$\beta=0.001$									
kL	$4\pi/3$	$25\pi/18$	$17\pi/12$	$25\pi/180$					
P/Per	6.508	6.590	5.210	3.665					
S/L	.0496	.0538	.0560	.0565					

FIG. 5 RELATION BETWEEN CONCENTRATED LOAD  $P/P_{cr}$  AND DEFLECTION  $\delta/L$

The values for the non-linear load-deflection curves,  $P/P_{CR}$  plotted against  $\delta/L$  in Fig. 5, are taken from Table III. In the case of the angle  $\theta = 45^\circ$ , the effect of the coefficient  $\beta$  on the  $P/P_{CR}$  vs.  $\delta/L$  curves is very great. The maximum load,  $(P/P_{CR})_{max}$ , decreases rapidly with increasing  $\delta/L$  as  $\beta$  increases up to the value  $\beta = 0.1$ . If the value of  $\beta$  is further increased,  $(P/P_{CR})_{max}$  would then start to increase. In such case, however, the deflection at the outer end of the bar would be quite beyond the range of applicability of the basic assumptions on which this analysis is based.

## 9. Discussion on the Non-Linear Load-Deflection Curves

From the non-linear load-deflection curves of  $P/P_{CR}$  vs.  $\delta/L$ , Fig. 5, the criteria of stability of the structure can be visualized:

### a) Stable equilibrium

A positive slope (the tangent to the curve rising from left to right) indicates stable equilibrium. That is, an increase in the deflection  $\delta$  requires an increase in the lateral load  $P$ . But, the effective rigidity of the bar AB to sustain the lateral load is gradually reduced. In other words, the slope of the  $P/P_{CR}$  vs.  $\delta/L$  curve decreases with increasing deflection until the slope drops to zero. During the stage of stable equilibrium, the tendency of the structure is to return to its original configuration if there is any small disturbance on loading.

### b) Neutral equilibrium

Neutral equilibrium is reached when the positive slope  $P/P_{CR}$  vs.  $\delta/L$  curve becomes zero and the maximum lateral load,  $(P/P_{CR})_{max}$ , is reached.

### c) Unstable equilibrium

A negative slope (the tangent to the curve sloping downward from left to right) represents unstable equilibrium. The lateral load required to maintain the deflection decreases with increase in the value of  $\delta/L$ . This continues until the point at zero lateral load with finite deflection is past, and a negative lateral load is needed for balancing. It is noted that for the small values of  $\beta$  ( $\beta < 0.005$ ), this part of the  $P/P_{CR}$  vs.  $\delta/L$  curves is highly unstable. Therefore, it can be concluded that for the large cross-sectional area  $A_1$  of the wire and small deflection, as soon as the maximum lateral load is reached the structure would collapse immediately.

It is to be noted that these phenomena take place completely within the elastic range. Thus, a linear stress-strain relation for the element of the structure is accompanied by a non-linear load-deflection curve for the outer end of the bar. After the maximum load is reached, the lateral load,  $P/P_{CR}$ , required for equilibrium decreases with increasing deflection  $\delta/L$ . These essential characteristics are quite analogous to the buckling phenomena of thin shells and curved plates.

## 10. Effects of Varying Wire Inclination $\theta$ on Concentrated Load $P/P_{CR}$ and Deflection $\delta/L$

In order to study the effects of  $\theta$ , the angle of wire inclination, on the lateral load and deflection, curves of  $P/P_{CR}$  against  $(2kL/\pi)^2$  and  $\delta/L$  are plotted, from the data of Table IV, in Figs. 6 and 7 respectively. In these figures,  $\theta$  varies from  $30^\circ$  to  $75^\circ$  and the coefficient  $\beta$  is chosen as  $\beta = 0.01$ .

Table IV

Computations of the Concentrated P/Per and deflection  $\delta/L$ with the different values of  $\theta$  and  $(2kL/\pi)^2$  $\beta=0.01$ 

	kL	0	$\pi/6$	$\pi/4$	$\pi/3$	$5\pi/12$	$\pi/2$	$7\pi/2$	$2\pi/3$
	$(2kL/\pi)^2$	0	.111	.250	.444	.695	1.000	1.361	1.776
$\theta=30^\circ$	P/Per	0	.206	.459	.805	1.232	1.732	2.288	2.900
	$\delta/L$	0	.0127	.0285	.0507	.0792	.1140	.1556	.2028
$\theta=45^\circ$	P/Per	0	.120	.266	.465	.712	1.000	1.318	1.658
	$\delta/L$	0	.0078	.0174	.0310	.0483	.0698	.0948	.1240
$\theta=60^\circ$	P/Per	0	.073	--	.277	--	.577	--	.912
	$\delta/L$	0	.0074	--	.0266	--	.0658	--	.1121
$\theta=75^\circ$	P/Per	0	.029	.091	.150	.212	.268	.302	.304
	$\delta/L$	0	.0114	.0256	.0495	.0710	.1022	.1391	.1820
	kL	$5\pi/6$	$\pi$	$13\pi/12$	$7\pi/6$	$5\pi/4$	$4\pi/3$	$25\pi/18$	
	$(2kL/\pi)^2$	2.778	4.000	4.694	5.444	6.250	7.111	7.716	
$\theta=30^\circ$	P/Per	4.090	5.104	5.410	5.430	4.640	2.490	-4.780	
	$\delta/L$	.3170	.4559	.5356	.6210	.7136	.8125	.8810	
$\theta=45^\circ$	P/Per	2.340	2.884	3.022	2.995	2.585	1.095	-3.540	
	$\delta/L$	.1936	.2828	.3160	.3800	.4360	.4960	.5384	
$\theta=60^\circ$	P/Per	1.187	1.256	1.126	0.828	.163	-1.570	--	
	$\delta/L$	.1830	.2612	.3156	.3590	.4110	.4680	--	
$\theta=75^\circ$	P/Per	.097	-.548	--	-2.138	-3.700	--	--	
	$\delta/L$	.2841	.4087	--	.5560	.6390	--	--	

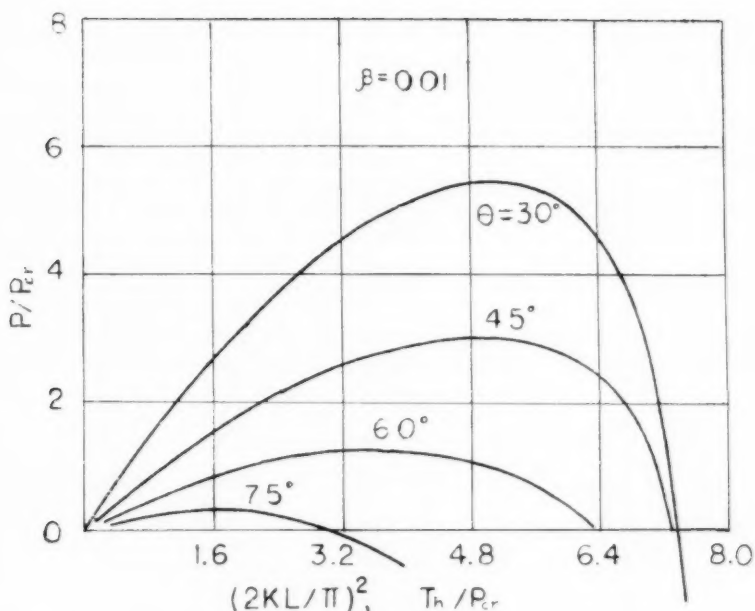


FIG. 6 EFFECT OF WIRE INCLINATION  $\theta$   
AND CONCENTRATED LOAD  $P/P_{cr}$   
AT  $\beta = 0.01$

These two figures show the same tendencies for the values of  $(P/P_{cr})_{max}$  decreasing and the peak of the curves becoming flatter and flatter with increasing  $\theta$ .

In Fig. 7, the deflection,  $\delta/L$ , at the maximum lateral load  $(P/P_{cr})_{max}$  decreases with increase in  $\theta$ , and the region, in which the deflection increases as the load decreases, becomes wider.

From Eqs. 17 and 18, the relation between the axial compressive force and the critical load of a column is obtained.

$$\frac{T_h}{P_{cr}} = \left( \frac{2kL}{\pi} \right)^2$$

It should be obvious that a curve of  $T_h/P_{cr}$  against  $\left( \frac{2kL}{\pi} \right)^2$  would plot as a straight line with a slope of unity. To correlate the value of  $P_{cr} = \pi^2 EI / 4L^2$ , the abscissas in Figs. 3, 4 and 6 are, therefore, shown simultaneously in terms of  $(2kL/\pi)^2$  and  $T_h/P_{cr}$ .

#### 11. Deflection Curves of the Bar

Now, it is desirable to find the shape of deflection curve of the bar AB. Let us rewrite Eq. 13 as

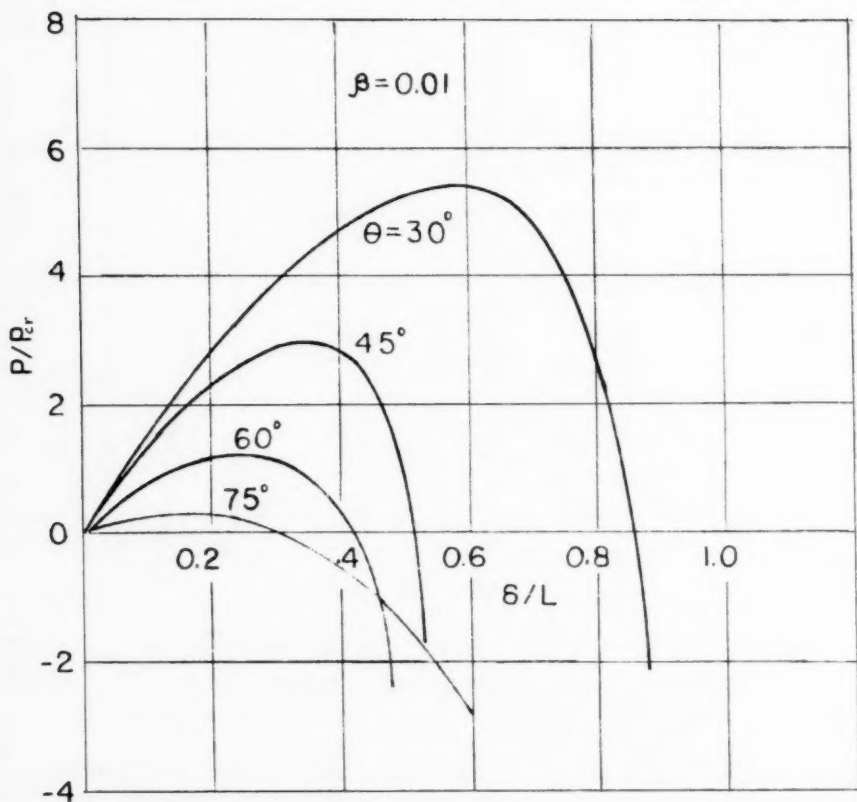


FIG.7 EFFECT OF WIRE INCLINATION  $\theta$  ON CONCENTRATED LOAD  $P/P_r$  AND DEFLECTION  $\delta/L$

$$\frac{P-T_y}{T_H} = \frac{\delta k \cos kL}{(\sin kL - kL \cos kL)}$$

Substitution of this expression in Eq. 11 gives

$$y = \delta \left\{ \frac{-\cos kL (kL \sin kL + \cos kL)}{(\sin kL - kL \cos kL) - \sin kL} \sin kx + \frac{kx \cos kL}{\sin kL - kL \cos kL} + 1 \right\} \quad (21)$$

$$\begin{aligned} \text{or } \frac{y}{\delta} &= 1 + \frac{1}{\sin kL - kL \cos kL} (kx \cos kL - \sin kx) \\ &= 1 + (kx \cos kL - \sin kx) \sec kL / (\tan kL - kL) \end{aligned}$$

It can be seen from this equation that the deflection ratio,  $y/\delta$ , increases

indefinitely when  $\tan kL - kL = 0$ , which happens at  $kL = 4.493$  (Fig. 2a). This corresponds to special case 2 of Eq. 17, where the concentrated load ratio,  $P/P_{cr}$ , also increases indefinitely. Such a result, obtained when  $\tan kL - kL$  approaches zero, is caused by using an approximate expression, Eq. 4, for the curvature i.e. the elementary beam theory has been employed instead of the exact expression for the deflection curve of the bar. Hence, if the exact expression of the deflection curve is taken into account, it may be shown that the deflection ratio  $y/\delta$  as well as  $P/P_{cr}$  will be always a finite value.<sup>(7)</sup> However, for a large value of deflection the basic assumptions of this analysis obviously no longer hold. The result, at  $\tan kL = kL$ , is therefore of interest only as a limit.

The deflection ratio,  $y/\delta$ , at any section  $x$  of the bar can be found for any given value of  $kL$  when  $kL < 4.493$ .

Deflection curves of the bar AB, based on the computations of Table V, are shown in Fig. 8. The value of  $kL$  used with each value of  $\beta$  is that corresponding to  $(P/P_{cr})_{max}$  approximately in Fig. 4.

Table V

Computations of the deflection curve of the beam-column,  $\theta = 45^\circ$

$\beta = 0.01 \quad kL = 10\pi/9 \quad T_h/P_{cr} = 4.938$							
x	0	L/6	L/3	L/2	2L/3	5L/6	L
y/ $\delta$	1	0.627	0.345	0.106	0.010	-0.010	0
$\beta = 0.005 \quad kL = 5\pi/4 \quad T_h/P_{cr} = 6.250$							
x	0	L/5	2L/5	3L/5	4L/5	11L/15	L
y/ $\delta$	1	0.394	-0.020	-0.145	-0.073	-0.012	0
$\beta = 0.001 \quad kL = 41\pi/31 \quad T_h/P_{cr} = 7.741$							
x	0	L/6	L/3	2L/5	L/2	2L/3	5L/6
y/ $\delta$	1	-0.131	-0.880	-1.020	-0.930	-0.727	-0.235

## 12. Bending Moments

By using Eqs. 16, 18 and 20, the fixed end moment,  $M_b$ , of the bar AB can be determined.

$$\begin{aligned}
 M_b &= (P - T_v)L + T_h \delta = T_h L \left( \frac{P - T_v}{T_h} \frac{\delta}{L} \right) = \frac{T_h}{P} \cdot PL \left( \frac{P}{T_h} - \cot \theta \right) \left( \frac{\tan kL - kL}{kL} \right) \quad (22) \\
 &= PL \left( 1 - \frac{T_h}{P} \cot \theta \right) \frac{\tan kL}{kL}
 \end{aligned}$$

Substituting this expression in Eq. 8, the bending moment at any section of the bar is

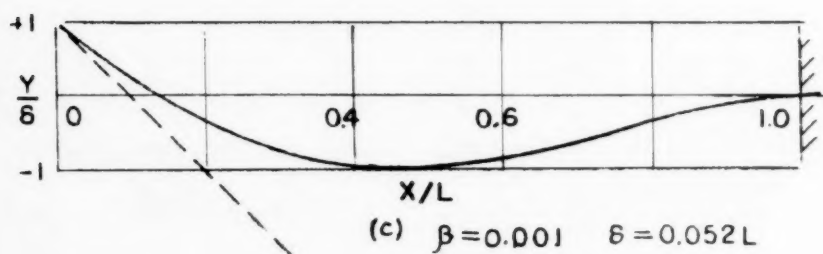
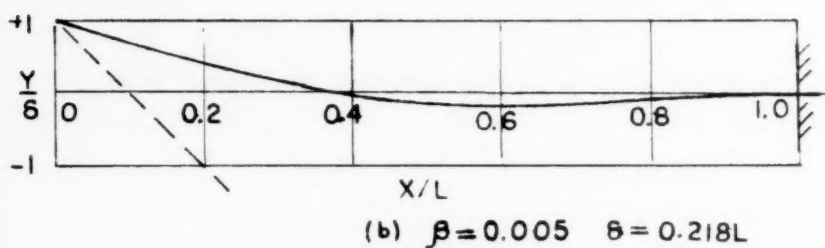
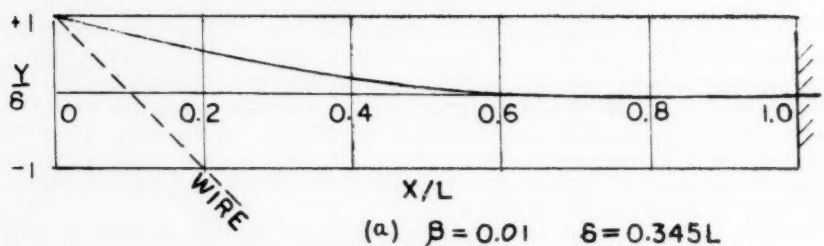


FIG. 8 VARIATION OF DEFLECTION CURVES OF THE BAR BY VARYING THE COEFFICIENT  $\beta$



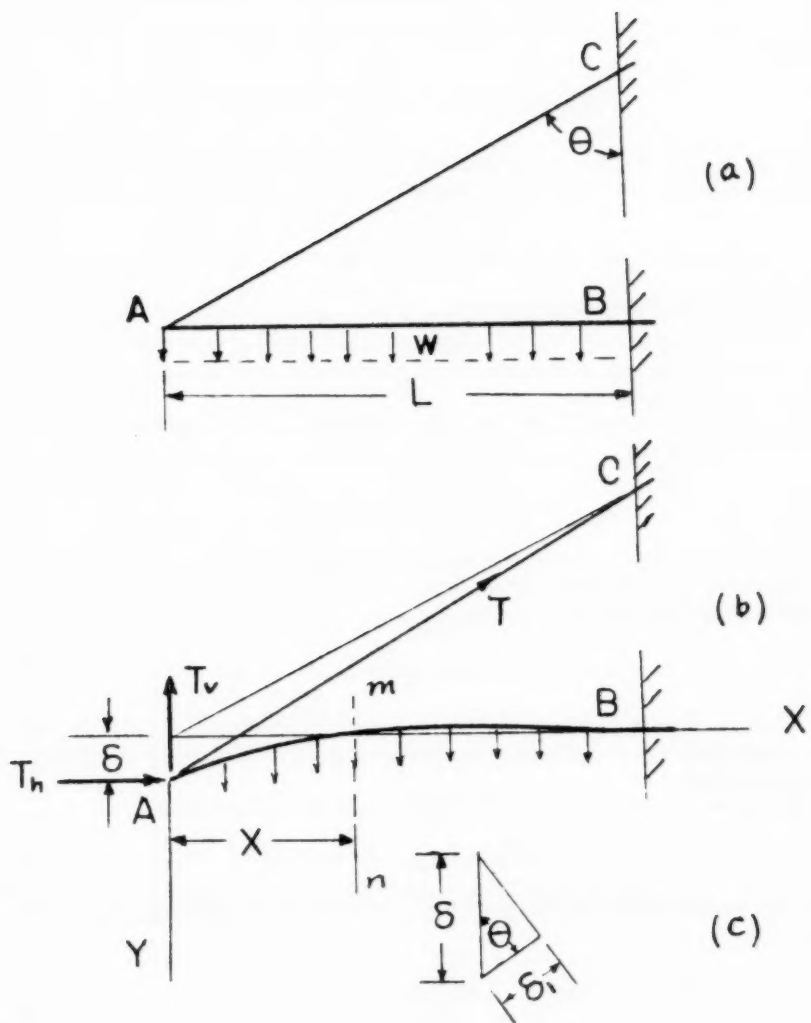


FIG. 9

$$M/PL = (1 - T_h \cot \theta/P) \sin kx/kL \cos kL \quad (23)$$

From Eqs. 9 and 22, we obtain the expression for the maximum moment of the bar

$$M_{\max}/PL = (1 - T_h \cot \theta/P) kL \sec kL \quad (24)$$

The location of the section of maximum moment should refer to Eq. b,  $x$  must be less than  $L$ . Otherwise there would be no maximum moment on the bar.

### Structure Subjected to Uniformly Distributed Load

#### 13. Derivation of Bending Moment

The truss, shown in Fig. 9, is the same structure as that of Fig. 1, except the concentrated load  $P$  is replaced by a uniformly distributed load over the whole span of the bar  $AB$ .

The bending moment at the section  $x$  from the outer end of the bar  $AB$ , Fig. 9b, is given by

$$M = T_h (\delta - Y) - T_v x + wx^2/2 \quad (25)$$

Where  $w$  = the intensity of the uniformly distributed load per unit length. Differentiating twice with respect to  $x$ , using Eq. 5 and the usual assumptions of elementary beam theory, we obtain

$$d^2M/dx^2 + k^2M = w \quad (26)$$

in which the curvature caused by the shear of uniformly distributed load is also neglected. This equation differs from Eq. 6 for the case of the concentrated loading.

The general solution of this differential equation is given by

$$M = C_1 \sin kx + C_2 \cos kx + w/k^2 \quad (27)$$

The end conditions for determination of the integration constants  $C_1$  and  $C_2$  are

$$\begin{aligned} \text{at } x = 0 \quad M = 0, \quad C_2 &= -w/k^2 \\ \text{at } x = L \quad M = M_b, \quad C_1 &= [M_b - w(1 - \cos kL)/k^2] / \sin kL \end{aligned} \quad (i)$$

Substitution of these expressions in Eq. 27 gives the general equation for the bending moment of the bar  $AB$

$$M = [M_b - w(1 - \cos kL)/k^2] \sin kx / \sin kL + w(1 - \cos kx)/k^2 \quad (28)$$

Where  $M_b$  = the bending moment at the fixed end of the bar  $AB$ , as defined before.

The location of the section of maximum moment can be found by differentiating Eq. 27 with respect to  $x$  and equating the first derivative to zero.

$$\begin{aligned} dM/dx &= C_1 k \cos kx - C_2 k \sin kx = 0 \\ \text{and } \tan kx &= C_1/C_2 = (1 - \cos kL - M_b k^2/w)/\sin kL \end{aligned} \quad (29)$$

Substituting this expression in Eq. 27, the maximum moment of the bar is

$$M_{\max} = wL^2(1 - \sec kx)/(kL)^2 \quad (30)$$

The value of  $kx$  as well as  $\sec kx$  may be determined from Eq. 29 and the maximum moment, therefore, determined from Eq. 30. It is necessary that  $x$  should be less than  $L$ , otherwise, the greatest moment which is equal to  $M_b$  is at  $x = L$ .

#### 14. Derivation of Load-Deflection Relation

From Eqs. 4 and 25, one of the most essential expressions for the relation between the lateral load and deflection can be obtained.

$$\begin{aligned} EI \, d^2y/dx^2 &= wx^2/2 + T_h(\delta - y) - T_v x \\ \text{or } y'' + k^2 y &= k^2 \delta + wx^2/2EI - T_v x/EI \end{aligned} \quad (31)$$

The general solution of this differential equation is given by

$$y = A \sin kx + B \cos kx + \delta + wx/2T_h - x \cot \theta \quad (32)$$

Where  $T_v/T_h = \cot \theta$  (Eq. 1)

The first derivative of this equation with respect to  $x$  is

$$y' = Ak \cos kx - Bk \sin kx + \frac{w}{T_h} - \cot \theta \quad (33)$$

Where  $A$  and  $B$  are the integration constants that must be determined from the fixed end conditions of the bar:

$$\text{at } x = L \quad y = 0$$

$$A \sin kL + B \cos kL + \delta + wL^2/2T_h - L \cot \theta = 0 \quad (j)$$

$$\text{at } x = L, \quad y' = 0$$

$$Ak \cos kL - Bk \sin kL + wL/T_h - \cot \theta = 0 \quad (k)$$

Substituting  $B$  of this expression in  $j$  gives

$$A = -\frac{1}{k} \left( \frac{wL}{T_h} \left( \frac{kL}{2} \sin kL + \cos kL \right) - (kL \sin kL + \cos kL) \cot \theta + \delta k \sin kL \right) \quad (l)$$

$$B = -\frac{1}{k \sin KL} \left\{ \left[ \frac{WL}{T_h} \left( \frac{KL}{2} \sin KL + \cos KL \right) - (KL \sin KL + \cos KL) \cot \theta \right] \cos KL + \frac{WL}{T_h} - \cot \theta \right\} - \delta \cos KL \quad (m)$$

Substituting l and m in Eqs. 32 and 33, the equations for the deflection and slope of the bar are

$$y = \frac{1}{k} \left[ (KL \sin KL + \cos KL) \cot \theta - \frac{WL}{T_h} \left( \frac{KL}{2} \sin KL + \cos KL \right) - \delta k \sin KL \right] \sin kx + \frac{1}{k \sin KL} \left\{ \left[ (KL \sin KL + \cos KL) \cot \theta - \frac{WL}{T_h} \left( \frac{KL}{2} \sin KL + \cos KL \right) - \delta k \sin KL \right] \cos kx - \frac{WL}{T_h} + \cot \theta \right\} \cos kx + \frac{wx^2}{2T_h} - x \cot \theta + \delta \quad (34)$$

$$y' = (KL \sin KL + \cos KL) \cot \theta - \frac{WL}{T_h} \left( \frac{KL}{2} \sin KL + \cos KL \right) - \delta k \sin KL \cos kx + \frac{1}{\sin KL} \left\{ \left[ \frac{WL}{T_h} \left( \frac{KL}{2} \sin KL + \cos KL \right) - (KL \sin KL + \cos KL) \cot \theta - \delta k \sin KL \right] \cos kx - \frac{WL}{T_h} + \cot \theta \right\} \sin kx + \frac{wx}{T_h} - \cot \theta \quad (35)$$

Applying the end condition,  $y = \delta$  at  $x = 0$ , to Eqs. 34 and 35, the deflection and slope at the outer end of the bar are

$$S/L = \left[ WL(\sin KL - KL \cos KL/2)/T_h - (\sin KL - KL \cos KL) \cot \theta \right] / KL \cos KL \quad (36)$$

$$y'_{x=0} = \left[ (1 - \cos KL) \cot \theta - \frac{WL}{T_h} \right] / \cos KL \quad (37)$$

#### 15. Relations Between Uniformly Distributed Load $W$ and Axial Compressive Force $T_h$

From Eqs. 16 and 36, we have

$$\begin{aligned} \delta \frac{2(KL)^2}{\sin \theta \sin 2\theta} &= \frac{WL}{T_h} \left( \frac{\tan KL}{KL} - \frac{1}{2} \right) - \left( \frac{\tan KL}{KL} - 1 \right) \cot \theta \\ \text{or } \frac{W}{T_h} &= \frac{2\delta}{\sin \theta \sin 2\theta} \frac{(KL)^3}{\tan KL - \frac{1}{2} KL} + \frac{\tan KL - KL}{\tan KL - \frac{1}{2} KL} \cot \theta \end{aligned} \quad (38)$$

Where  $W = wL$  = the total uniformly distributed load over the whole span of the bar AB.

It should be noted that Eq. 38 is different from 17 which defines the relations between the concentrated lateral load  $P$  and the axial compressive force  $T_h$  with the parameter  $kL$ . The main points of the difference are

$$1. \frac{W}{T_h} = \infty \quad \text{when} \quad \tan KL = 1/2 \quad kL = 0.$$

This happens when  $kL = 4.276 \approx \frac{49\pi}{36}$  (see Fig. 2b)

$$2. \frac{W}{T_h} = 0 \quad \text{when } kL = 0$$

Since the limit of the terms  $\frac{(kL)^3}{\tan kL = 1/2kL}$  and  $\frac{\tan kL - kL}{\tan kL = 1/2kL}$

can be shown to approach zero as  $kL$  approaches zero.

However, there is one relation which remains the same as in the case of the concentrated loading. i.e.

$$\frac{W}{T_h} = 1, \text{ when } kL = \frac{\pi}{2} \text{ and } \theta = 45^\circ$$

Curves of  $\frac{W}{T_h}$  vs  $\left(\frac{2kL}{\pi}\right)^2$  are given in Fig. 10, which is quite different from Fig. 3 of the  $P/T_h$  vs.  $(2kL/\pi)^2$  curves. The ordinates in Fig. 10 are computed in Table VI.

Table VI

Computations of the ratio of uniformly distributed load  $W (=wL)$  to axial compressive force  $T_h$  with the different values of  $(2kL/\pi)^2$

	$kL$	0	$\pi/6$	$\pi/3$	$5\pi/12$	$\pi/2$	$7\pi/12$	$2\pi/3$
	$(2kL/\pi)^2$	0	0.111	0.444	0.695	1.000	1.361	1.778
$\beta = 0.1$	$W/T_h$	0	0.299	0.836	0.993	1.000	0.885	0.443
$\beta = 0.05$	$W/T_h$	0	0.234	0.702	0.840	1.000	1.042	0.911
$\beta = 0.01$	$W/T_h$	0	0.183	0.594	0.808	1.000	1.168	1.285
$\beta = 0.005$	$W/T_h$	0	0.176	0.581	0.797	1.000	1.183	1.331
$\beta = 0.001$	$W/T_h$	0	0.171	0.570	0.789	1.000	1.202	1.369
	$kL$	$5\pi/6$	$\pi$	$7\pi/6$	$5\pi/4$	$4\pi/3$	$121\pi/90$	
	$(2kL/\pi)^2$	2.778	4.000	5.444	6.250	7.111	7.230	
$\beta = 0.1$	$W/T_h$	-0.997	-3.584	--	--	--	--	
$\beta = 0.05$	$W/T_h$	0.348	-0.792	--	--	--	--	
$\beta = 0.01$	$W/T_h$	1.424	1.442	1.352	1.260	1.028	0.920	
$\beta = 0.005$	$W/T_h$	1.558	1.721	1.906	--	3.898	--	
$\beta = 0.001$	$W/T_h$	1.624	2.350	6.194	--	--	--	

#### 16. Relation Between Uniformly Distributed Load $W/P_{cr}$ and Parameter $kL$

Substituting Eq. 5 in 38 and dividing by the critical load  $P_{cr}$ , we obtain

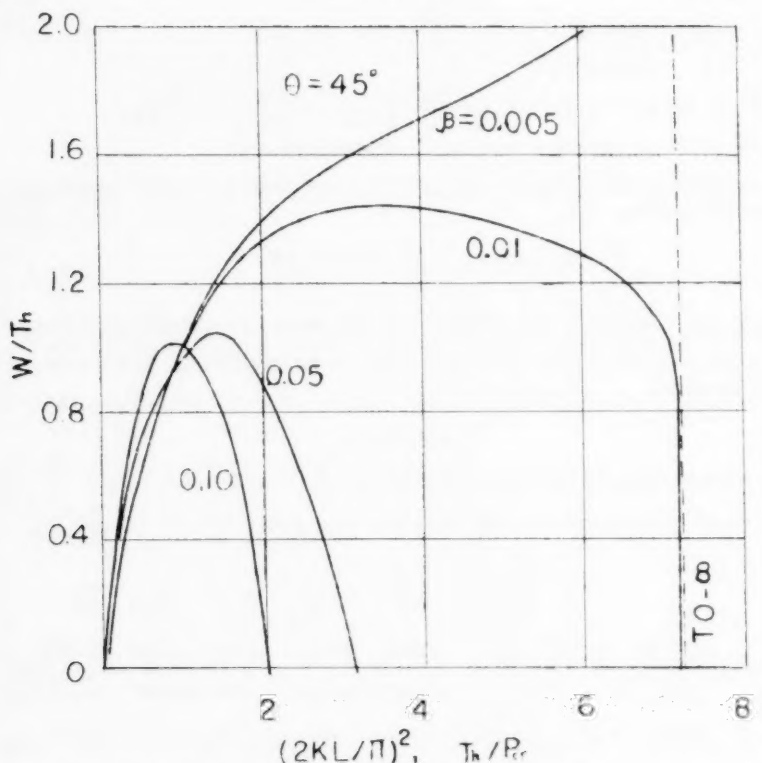


FIG.10 RELATION BETWEEN UNIFORMLY DISTRIBUTED LOAD  $W(=wL)$  AND AXIAL FORCE  $T_h$  WITH  $(2kL/\pi)^2$

$$\begin{aligned}
 W/P_{cr} &= (2kL/\pi)^2 \left\{ \frac{2\beta/\sin \theta \sin 2\theta \cdot (kL)^3 / (\tan kL - \frac{1}{2}kL) + (\tan kL - kL)(\tan kL - \frac{1}{2}kL) \cot \theta}{\sin \theta \sin 2\theta} \right\} \\
 &= (2kL/n)^2 \left\{ \frac{2\beta}{\sin \theta \sin 2\theta} \frac{(kL)^3}{\tan kL - \frac{1}{2}kL} + \frac{1 - kL/\tan kL}{1 - kL/2 \tan kL} \cot \theta \right\}
 \end{aligned} \quad (39)$$

Since the parameter  $kL$  is essentially a measure of the deflection  $\delta$ , this shows implicitly the similar load-deflection relation as that of the concentrated loading condition, Eq. 18.

The values of  $W/P_{cr}$  and  $(2kL/\pi)^2$ , taken from Table VII, are plotted in Fig. 11. It is seen that the effect of the coefficient  $\beta$  on  $W/P_{cr}$  is similar to that shown in Fig. 4, but  $W/P_{cr}$  increases much more rapidly when  $\beta < 0.01$ .

#### 17. Non-Linear Relation Between Uniformly Distributed Load $W/P_{cr}$ and Deflection $\delta/L$

For the given values of  $\theta$  and  $\beta$ , the combination of Eqs. 16 and 39 also

defines the parametric form of the non-linear load-deflection relation for the uniformly distributed load

$$w/p_{cr} = (2kL/\pi)^2 \left( \frac{\delta}{L} \frac{kL}{\tan kL - \frac{1}{2}kL} \neq \frac{\tan kL - kL}{\tan kL - \frac{1}{2}kL} \cot \theta \right) \quad (40)$$

The non-linear load-deflection curves,  $W/P_{cr}$  plotted against  $\delta/L$ , are given in Fig. 12 with the angle  $\theta = 45^\circ$  (Table VII). The essential characteristics of these curves are similar to those of the structure subjected to the concentrated load  $P/P_{cr}$ , Fig. 5, but the magnitude of  $(W/P_{cr})_{max}$  increases very greatly when  $\beta < 0.005$ .

The criteria of stability for this type of the non-linear load-deflection curves have been discussed previously. (see page 17)

#### 18. Effects of Varying Wire Inclination $\theta$ on Uniformly Distributed Load $W/P_{cr}$ and Deflection $\delta/L$

The effects of inclination of the wire AC, from  $\theta = 30^\circ$  to  $75^\circ$  on the lateral load and deflection are shown in Fig. 13 (from Table VIII), the characteristics of these curves are similar to those of Fig. 7. The values of  $(W/P_{cr})_{max}$  decreases with an increase in  $\theta$  and the peak of these curves becomes flatter and flatter.

#### 19. Deflection Curve and Bending Moments of the Bar

Substituting Eq. 36 in 34, the expression for the deflection curve of the bar AB can be simplified. It yields

$$y = 1/k \left\{ (kL \sin kL \neq \cos kL) \cot \theta - wL/T_h (kL/2 \sin kL \neq \cos kL) \right. \\ \left. - Sk \sin kL \right\} \sin kx \neq wx^2/2T_h - x \cot \theta \neq \delta \quad (41)$$

which satisfies the end conditions:

$$y/\delta = 1 \text{ at } x = 0$$

$$y/\delta = 0 \text{ at } x = L.$$

The fixed end moment,  $M_b$ , of the bar AB is given by

$$M_b = (wL/2 - T_v) L \neq T_h \delta = T_h L (w/2T_h - \cot \theta \neq \delta/L) \\ = T_h/w \cdot wL (\delta/L - \cot \theta) \neq wL/2 \quad (42)$$

Substitution of this equation in 28 gives the bending moment at any section of the bar AB

$$M = \left[ T_h/w (\delta/L - \cot \theta) wL \neq wL/2 - wL(1 - \cos kL)/(kL)^2 \right] \sin kx/\sin kL \\ \neq wL(1 - \cos kx)/(kL)^2 \quad (43)$$

or, in the nondimensional form

Computations of the uniformly distributed load  $W/Per$   
and deflection  $S/L$  with the different values of  $(2kL/\pi)^2$

$$\theta = 45^\circ$$

	kL	0	$\pi/6$	$\pi/3$	$5\pi/12$	$\pi/2$	$7\pi/12$	$2\pi/3$
	$(2kL/\pi)^2$	0	.111	.444	.695	1.000	1.361	1.778
$\beta=1.0$	W/Per	0	.162	1.451	1.917	1.000	-2.640	-11.35
$\beta=.5$	W/Per	0	.090	.851	1.261	1.000	-.505	-5.860
$\beta=.10$	W/Per	0	.033	.372	.690	1.000	1.204	.786
	S/L	0	.0775	.3100	.1844	.6980	.9492	1.240
$\beta=.05$	W/Per	0	.026	.312	.618	1.000	1.420	1.620
	S/L	0	.0388	.1550	.2422	.3490	.4746	.6200
$\beta=.01$	W/Per	0	.0203	.264	.561	1.000	1.590	2.282
	S/L	0	.0078	.0310	.0484	.0698	.0949	.1240
$\beta=.005$	W/Per	0	.0196	.258	.554	1.000	1.610	2.366
	S/L	0	.0039	.0155	.0242	.0349	.0475	.0620
$\beta=.001$	W/Per	0	.0190	.253	.548	1.000	1.640	2.432
	S/L	0	.00078	.00310	.00485	.00698	.00948	.01240
	kL	$5\pi/6$	$\pi$	$7\pi/6$	$5\pi/4$	$4\pi/3$	$121\pi/90$	
	$(2kL/\pi)^2$	2.778	4.000	5.444	6.250	7.111	7.230	
$\beta=.1$	W/Per	-2.768	--	--	--	--	--	
	S/L	1.938	--	--	--	--	--	
$\beta=.05$	W/Per	0.966	-3.168	--	--	--	--	
	S/L	.9690	1.414	--	--	--	--	
$\beta=.01$	W/Per	3.972	5.766	7.350	7.880	7.310	6.650	
	S/L	.1938	.2828	.3800	.4360	.4960	.5045	
$\beta=.005$	W/Per	4.324	6.884	10.37	13.44	27.65	--	
	S/L	.0969	.1414	.1900	.2180	.2480	--	
$\beta=.001$	W/Per	4.624	7.776	12.80	--	44.11	--	
	S/L	.01938	.02828	.03800	--	.0490	--	



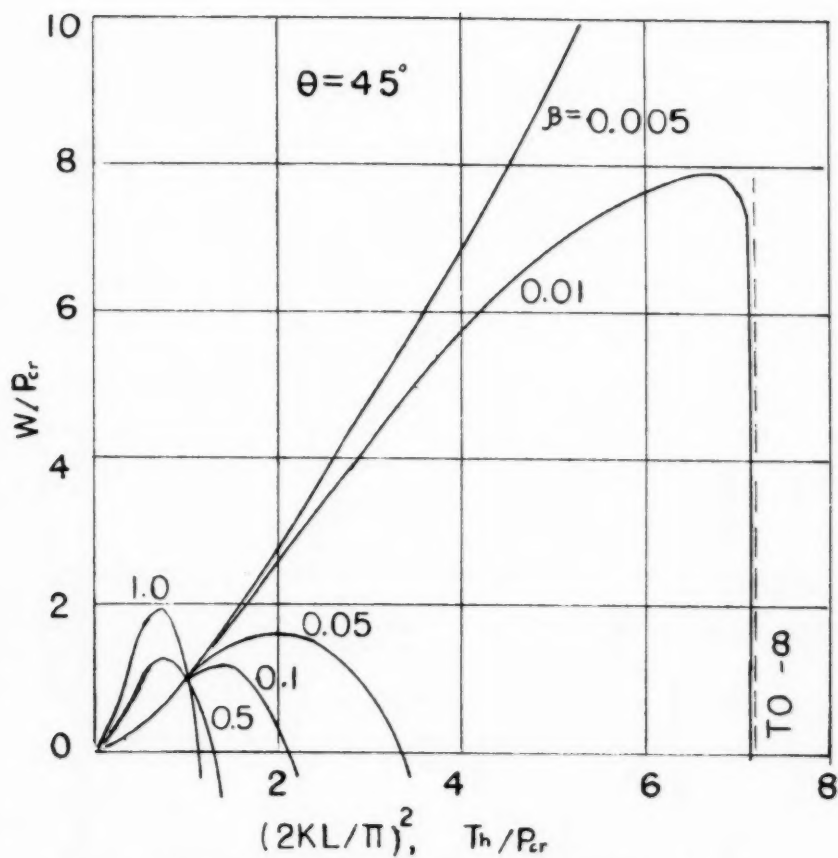


FIG. II RELATION BETWEEN UNIFORMLY  
DISTRIBUTED LOAD  $W/P_{cr}$  AND  
 $(2KL/\pi)^2$

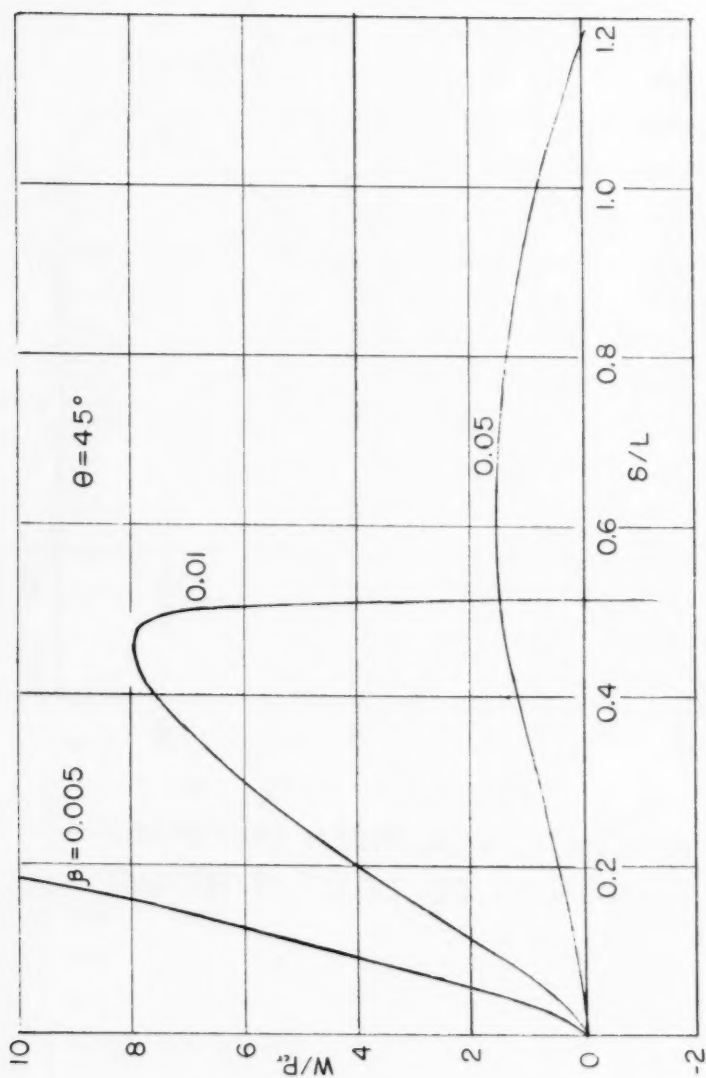


FIG.12 RELATION BETWEEN UNIFORMLY DISTRIBUTED LOAD  $W/R_r$  AND DEFLECTION  $s/L$

Table VIII

Computation of the uniformly distributed load  $W/Pcr$  and deflection $\delta/L$  with the different values of  $\theta$  and  $(2kL/\pi)^2$   $\beta = 0.01$ 

	$kL$	0	$\pi/6$	$\pi/3$	$5\pi/12$	$\pi/2$	$7\pi/12$	$2\pi/3$
	$(2kL/\pi)^2$	0	.111	.444	.695	1.000	1.361	1.778
$\theta=30^\circ$ {	$W/Pcr$	0	.035	.456	.970	1.732	2.756	3.968
	$\delta/L$	0	.0127	.0507	.0792	.1140	.1556	.2028
$\theta=45^\circ$ {	$W/Pcr$	0	.0203	.264	.561	1.000	1.590	2.282
	$\delta/L$	0	.0078	.0310	.0485	.0698	.0948	.1240
$\theta=60^\circ$ {	$W/Pcr$	0	.0122	.157	.328	.577	.901	1.257
	$\delta/L$	0	.0074	.0266	.0456	.0658	.0895	.1121
$\theta=75^\circ$ {	$W/Pcr$	0	.0072	.0851	.167	.268	0.374	.412
	$\delta/L$	0	.0114	.0495	.0710	.1022	.1391	.1820
	$kL$	$5\pi/6$	$\pi$	$13\pi/12$	$7\pi/6$	$5\pi/4$	$4\pi/3$	$121\pi/90$
	$(2kL/\pi)^2$	2.778	4.000	4.694	5.444	6.250	7.111	7.230
$\theta=30^\circ$ {	$W/Pcr$	6.930	10.12	--	13.30	--	--	--
	$\delta/L$	.3170	.4559	--	.6210	--	--	--
$\theta=45^\circ$ {	$W/Pcr$	3.972	5.766	--	7.350	7.880	7.310	6.650
	$\delta/L$	.1938	.2828	--	.3800	.4360	.4960	.5045
$\theta=60^\circ$ {	$W/Pcr$	2.014	2.514	2.505	2.020	0.481	-10.63	--
	$\delta/L$	.1830	.2612	.3156	.3590	.4110	.4680	---
$\theta=75^\circ$ {	$W/Pcr$	.167	-1.124	-5.240	-5.240	--	--	--
	$\delta/L$	.2841	.4087	--	.5560	--	--	--

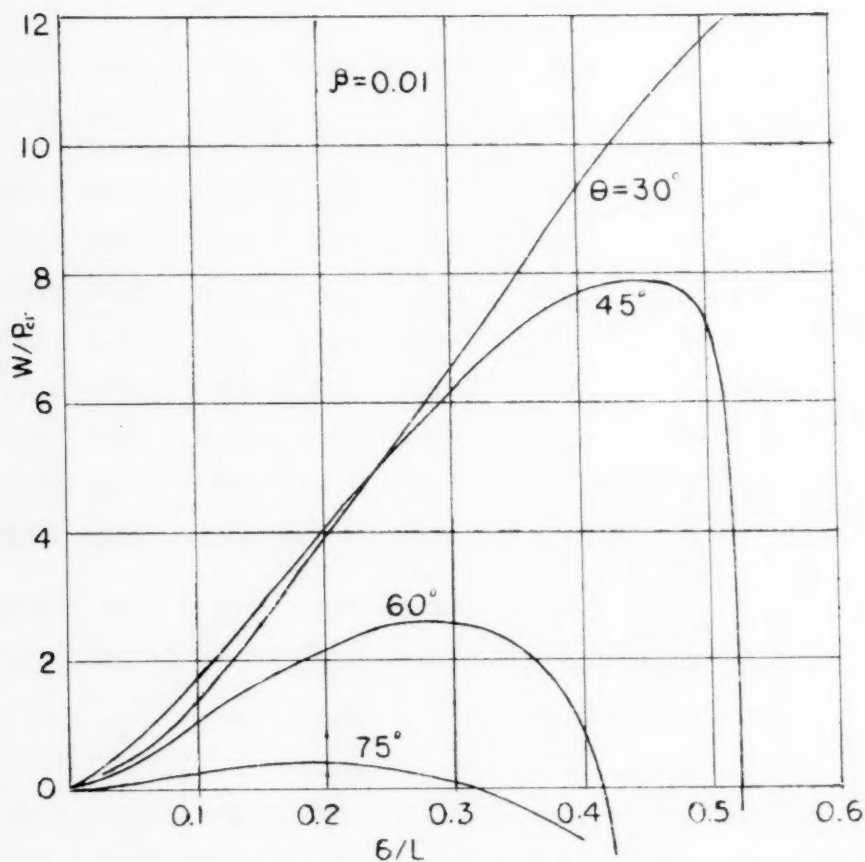


FIG.13 EFFECT OF WIRE INCLINATION  $\theta$  ON UNIFORMLY DISTRIBUTED LOAD  $W/P_{cr}$  AND DEFLECTION  $\delta/L$

$$M/WL = \left[ T_h/W (\delta/L - \cot \theta) \sqrt{\frac{1}{2} - (1 - \cos kL)(kL)^2} \right] \sin kx / \sin kL \quad (43)$$

$$\sqrt{(1 - \cos kx)/(kL)^2}$$

Substituting Eq. 42 into 29, the location of the section of maximum moment may be determined from the expression

$$\tan kx = \left[ 1 - \cos kL - T_h/W \cdot (\delta/L - \cot \theta) (kL)^2 - \frac{1}{2}(kL)^2 \right] / \sin kL \quad (44)$$

Where  $x$  should be less than  $L$ .

## 20. Comparison of the Effects of Concentrated Load and Uniformly Distributed Load

The essential characteristics of the structure subjected to the concentrated load  $P$  at the outer end and the uniformly distributed load  $w$  over the whole span of the bar  $AB$  are generally similar.

1. The maximum lateral load increases with decrease in  $\beta$  so long as  $\beta < 0.01$  (Figs. 4, 11).  $W/P_{Cr}$  increases very rapidly when  $\beta < 0.005$ .
2. The load-deflection curves are non-linear. (Figs. 5, 12) The values of  $W/P_{Cr}$  are much greater than that of  $P/P_{Cr}$  when  $\beta < 0.005$ .
3. The values of  $(P/P_{Cr})_{\max}$ ,  $(W/P_{Cr})_{\max}$  and  $\delta/L$  at  $(P/P_{Cr})_{\max}$  and  $(W/P_{Cr})_{\max}$  decrease with increase in the angle  $\theta$ . (Figs. 7, 13).

However, the variation of the ratio  $P/T_h$  with the parameter  $kL$  is very different from that of the ratio  $W/T_h$ , as can be seen from Figs. 3 and 10. In general, this structure can carry the uniformly distributed load  $W/P_{Cr}$  more than the concentrated one,  $P/P_{Cr}$ .

Quantitative study shows that the effect of varying the coefficient  $\beta$  on the maximum lateral load,  $(W/P_{Cr})_{\max}$ , is much greater than its effect on  $(P/P_{Cr})_{\max}$ . This difference can be seen from Figs. 4, 5, 11, and 12. Therefore, it may be concluded that the influence of the cross-sectional area  $A_1$  of the wire is much more powerful in the uniformly distributed loading condition than in the concentrated one.

## Discussion on the Range of Deflection

The general assumptions for the problem of the simple structure have been given previously that, in agreement with the elementary beam theory, the deflection at the outer end of the bar is small, the shortening of the bar and the change of the wire inclination are negligible. Based on these assumptions and the principle of consistent deformations we obtain, for both the concentrated and the uniformly distributed loading conditions, the deflection at the outer end of the bar, Eq. 16.

$$\delta/L = \beta 2(KL)^2 / \sin \theta \sin 2\theta$$

It is seen that the deflection,  $\delta/L$ , depends directly on the coefficient  $\beta$ , angle  $\theta$  and the parameter  $kL$ . For a given value of  $\theta$ ,  $\delta/L$  will increase with  $\beta$  and  $(kL)^2$ .

The influences of the variation of  $\beta$  on the non-linear load-deflection

curves are shown in Figs. 5 and 12. For small values of  $\beta$ , say  $\beta$  0.01,  $\delta/L$  is small. However, as  $\beta$  increases,  $\delta/L$  would fall in the range of large deflections. Then, the elementary beam theory would not be satisfactory. The larger the deflection is, the greater would be the error involved. It seems to be desirable that the values of  $\beta$  should be below 0.01. Remember that the small value of  $\beta$  means a large cross-sectional area  $A_1$  of the wire. Therefore, for the given angle  $\theta$  a stronger wire will give a small deflection in agreement with the elementary beam theory.

The shortening of the bar AB due to the bending moment and the axial compression is given by (see Appendix),

$$\epsilon/L = \pi^2/16 (E/L)^2 \neq \alpha (kL)^2 \quad (n)$$

Where  $\epsilon$  = the total shortening of the bar AB.

$$\alpha = I/AL^2 = \text{a non-dimensional coefficient.}$$

On the right side of  $n$  the first term represents the shortening due to the bending moment and the second that due to the axial compression. It should be noted that the coefficient  $\alpha$  will be a very small quantity when the bar AB is relatively long. Take, for instance,  $L = 100$  in.,

$$\alpha = 0.0001, \delta/L = 0.01 \text{ and } kL = \pi/2. \text{ From } n, \text{ we have}$$

$$\epsilon/L = (0.062 \neq 0.247) 10^{-3} = 0.31 \times 10^{-3}$$

$$\text{or } \epsilon = 0.031 \text{ in.}$$

Which is very small compared to the deflection  $\delta/L$  or  $\delta$  ( $\delta = 1.0$  in.), and justifies the given assumption that the shortening of the bar AB is negligible.

The last of the basic assumptions is that for small deflection the change of the angle  $\theta$  is negligible which agrees with the elementary beam theory. Actually, the change tends to decrease the angle  $\theta$  and, in turn, to increase the maximum lateral load to which the structure can be subjected (Figs. 7 and 13). Therefore, such a change in  $\theta$ , will cause the elementary theory developed here to give conservative results for the critical load in a practical application.

## CONCLUSION

The essential characteristics of this simple structure in practical use, which parallel the buckling phenomena of thin shells and curved plates, have been brought out by application of only elementary theory. No resort was made to large deflection theory nor to the complementary energy method; so that there was no difficulty in its mathematical expression. The process of solving this problem is also simple in comparison with the device of using an energy method to deal with the buckling of a column with non-linear lateral support.

One of the most essential characteristics of this structure is that: the linear stress-strain relation results in a non-linear load-deflection curve involving a region where the load decreases with increase in deflection, Figs. 5 and 12. This shows a superficial similarity to the behavior of a short column in plastic instability failure<sup>(8)</sup> resulting from plastic flow. However, in our problem the behavior is entirely within the elastic range.

The effects of varying the wire inclination  $\theta$  on the maximum lateral load, Figs. 7 and 13, seem to be an interesting discovery. The maximum lateral load decreases and the peak of the curves of the maximum lateral load flattens with increase in the angle  $\theta$ . This is due to the decrease in the vertical component,  $T_v$ , and increase in the horizontal component,  $T_h$ , of the tensile force of the wire as the wire inclination becomes smaller and smaller. Therefore, the characteristics which simulate a column with non-linear lateral spring support<sup>(1)</sup> diminish when the angle  $\theta$  increases.

All these essential characteristics of this simple structure, as analysed in this paper, are parallel to that of a column with non-linear lateral support as well as the buckling phenomena of thin shells and curved plates.

#### ACKNOWLEDGMENT

The writer wishes to take this opportunity to express his deep appreciation to Professors J. N. Goodier and A. N. Niles of Stanford University for their invaluable help in selecting the title and in discussing the analysis when this work was undertaken. The encouragement and cooperation which the writer received from his colleagues and the Department of Mechanical Engineering at South Dakota State College in preparing the manuscript are also greatly appreciated.

#### NOTATION

A	= the cross-sectional area of the bar
A <sub>1</sub>	= the cross-sectional area of the wire
E	= the modulus of elasticity of the bar
E <sub>1</sub>	= the modulus of elasticity of the wire.
I	= the moment of inertia of the bar
I <sub>1</sub>	= the moment of inertia of the wire
k	= $\sqrt{T_h/EI}$
L	= the length of the bar
L <sub>1</sub>	= the length of the wire
M	= the bending moment
M <sub>b</sub>	= the bending moment at the fixed end B
P	= the concentrated load
P <sub>cr</sub>	= $\pi EI/4L^2$ = the critical load
T	= the tensile force of the wire
T <sub>v</sub>	= the vertical component of the tensile force T
T <sub>h</sub>	= the horizontal component of the tensile force T
w	= the intensity of the uniformly distributed load
W	= $wL$ = the total uniformly distributed load
x	= the distance between the outer end A and any cross section of the bar.
y	= the deflection at any cross section of the bar
$\delta$	= the deflection at the end of the bar
$\delta_1$	= the deflection at any cross section of the bar
$\alpha$	= $I/AL^2$ = a nondimensional coefficient
$\beta$	= $EI/E_1A_1L^2$ = a nondimensional coefficient
$\epsilon$	= the total shortening of the bar

## APPENDIX

The shortening of the bar AB due to the bending moment and the axial compression may be obtained as follows:

## 1. The shortening due to bending moment.

We assume that the bar AB is deflected by the bending moment only and let

$ds$  = the length of an element of the deflected bar.

$dx$  = the length of an element of the corresponding chord of the bar.

Then, the difference between these two elements is equal to

$$ds - dx = dx \sqrt{1 + (dy/dx)^2} - dx \approx \frac{1}{2} (dy/dx)^2 dx$$

and shortening of the bar may be represented by the well-known expression

$$\epsilon = \frac{1}{2} \int_0^L (dy/dx)^2 dx \quad (A1)$$

Where  $\epsilon$  = the shortening of the bar due to the bending moment. Now let

$$y = \delta (1 - \sin \pi x / 2L) \quad (A2)$$

$$\text{at } x = 0 \quad y = \delta; \quad \text{at } x = L \quad y = 0, \quad (A3)$$

(A2) satisfies the end conditions of the deflected bar. Differentiating (A2) with respect to  $x$  and substituting it in (A1), we have

$$\epsilon_1 = \frac{1}{2} \delta^2 \pi^2 / 4L^2 \int_0^L \cos^2 \frac{\pi x}{2L} dx = \frac{\pi^2}{16} \frac{\delta^2}{L} \quad (A4)$$

$$\text{or } \frac{\epsilon_1}{L} = \frac{\pi^2}{16} \left( \frac{\delta}{L} \right)^2 \quad (A4)$$

## 2. The shortening due to axial compression.

The shortening of the bar due to the axial compression  $T_h$  is equal to

$$\frac{\epsilon_2}{L} = \frac{T_h}{AE} = \frac{EI k^2}{AE} = \frac{I}{AL^2} (kL)^2 = \alpha (kL)^2 \quad (A5)$$

Where  $\alpha = I/AL^2$  = a non-dimensional coefficient.

$\epsilon_2$  = the shortening of the bar due to the axial compression.

Adding (A4) and (A5), we obtain

$$\frac{\epsilon}{L} = \frac{\epsilon_1}{L} + \frac{\epsilon_2}{L} = \frac{\pi^2}{16} \left( \frac{\delta}{L} \right)^2 + \alpha (kL)^2 \quad (A6)$$

Where  $\epsilon$  = the total shortening of the bar due to the bending moment and the axial compression.



## REFERENCES

1. Von Karman, Th., Dunn, L. G., and Tsien, H. S., The Influence of Curvature on the Buckling Characteristics of Structures, Journal of the Aeronautical Sciences, Vol. 7, Pp. 269-288, May, 1940.
2. Von Karman, Th., and Tsien, H. S., The Buckling of Spherical Shells by External Pressure, Journal of the Aeronautical Sciences, Vol. 7, Pp. 43-50, Dec. 1939.
3. Von Karman, Th., and Tsien, H. S., The Buckling of Thin Cylindrical Shells under Axial Compression, Journal of the Aeronautical Sciences, Vol. 8, Pp. 303-312, June, 1941.
4. Cox, H. L., Stress Analysis of Thin Metal Construction, Journal of the Royal Aeronautical Society, Vol. 44, Pp. 231-282, March, 1940.
5. Von Karman, Th., Encyklopadie der Mathematischen Wissenschaften, Vol. IV, P. 349, 1910.
6. Westergaard, H. M., On the Method of Complementary Energy, Proceedings ASCE, Vol. 67, 1941, Pp. 199-227.
7. Timoshenko, S. Theory of Elastic Stability, Pp. 69-74 and Pp. 89-90, McGraw-Hill, New York, 1936.
8. Niles, A. S., and Newell, J. S., Airplane Structures, Vol. I. Pp. 268-269, John Wiley & Sons, 3rd Edition, 1943.



---

Journal of the  
STRUCTURAL DIVISION  
Proceedings of the American Society of Civil Engineers

---

CONTENTS

DISCUSSION  
(Proc. Paper 1442)

	Page
Simplified Analysis of Rigid Frames, by Robert M. Barnoff. (Proc. Paper 1106, November, 1956. Prior discussion: 1192, 1259. Discussion closed.)	
by Robert M. Barnoff (closure) . . . . .	1442-3
Confirmation of Inelastic Stress Distribution in Concrete, by Eivind Hognestad. (Proc. Paper 1189, March, 1957. Prior discussion: none. Discussion closed.)	
by Anthony M. DiGioia . . . . .	1442-5
Analysis of Multi-Story Frames, by T. F. Hickerson. (Proc. Paper 1233, May, 1957. Prior discussion: none. Discussion closed.)	
by John E. Goldberg . . . . .	1442-7
by Kenneth H. Lenzen . . . . .	1442-7
by R. A. Williamson . . . . .	1442-8
by Zdenek Sobotka . . . . .	1442-11
by E. Neil W. Lane . . . . .	1442-16
Beam Deflection in Bridges Designed for Continuity, by Guillermo Villena. (Proc. Paper 1234, May, 1957. Prior dis- cussion: none. Discussion closed.)	
by Zdenek Sobotka . . . . .	1442-19
The Behavior of Reinforced Concrete Shear Walls, by Jack R. Benjamin and Harry A. Williams. (Proc. Paper 1254, May, 1957. Prior discussion: none. Discussion closed.)	
by DeForest A. Matteson, Jr . . . . .	1442-27
Lateral Load Distribution Test on I-Beam Bridge, by Ardis White and William B. Purnell. (Proc. Paper 1255, May, 1957. Prior discussion: none. Discussion closed.)	
by Masso Naruoka . . . . .	1442-31
by Benjamin C. F. Wei . . . . .	1442-31

(Over)

Note: Paper 1442 is part of the copyrighted Journal of the Structural Division of the American Society of Civil Engineers, Vol. 83, ST 6, November, 1957.

Distribution of Loads on Bridge Decks, by A. M. Lount. (Proc. Paper 1303, July, 1957. Prior discussion: none. Discussion open until December 1, 1957.)

by Masso Naruoka . . . . . 1442-39

Synopsis of First Progress Report of Committee on Factors of Safety, by Oliver G. Julian. (Proc. Paper 1316, July, 1957. Prior discussion: none. Discussion open until December 1, 1957.)

by T. Au . . . . . 1442-41

Vibration Susceptibilities of Various Highway Bridge Types, by LeRoy T. Oehler. (Proc. Paper 1318, July, 1957. Prior discussion: none. Discussion open until December 1, 1957.)

by Masso Naruoka . . . . . 1442-45

SIMPLIFIED ANALYSIS OF RIGID FRAMES<sup>a</sup>

---

Closure by Robert M. Barnoff

---

ROBERT M. BARNOFF,<sup>1</sup> J.M. ASCE.—The author wishes to thank Messrs. Wah and Chang for their careful review of his paper.

Both Mr. Wah and Mr. Chang presented alternate solutions to the rigid-frame problem, but neither have simplified the problem to the same extent as the original paper. The original paper was written with the intention of providing designers with a useful tool for solving this problem in a minimum length of time.

The author agrees with Mr. Wah that the structural engineering profession does seem to be overburdened with charts and tables. But it is the duty of the structural designer to use the charts and tables, when practicable, to provide his clients with accurate designs at a reasonable cost. In actual practice, only a small portion of the designers time is spent in analyzing a structure. Most of the designers time is spent designing members and working out details; so when the designer is called upon to use moment distribution he usually finds that all of the short cut methods he learned as a student have long since been forgotten. The methods presented by Messrs. Wah and Chang seem to fall into this category.

---

a. Proc. Paper 1106, November, 1956, by Robert M. Barnoff.

1. Asst. Prof. of Civ. Eng., Pennsylvania State Univ., University Park, Pa.

100

101

102

103

104

105

106

107

108

109

110

111

112

113

114

115

116

117

118

119

120

121

122

123

124

125

126

127

128

129

130

131

132

133

134

135

136

137

138

139

140

141

142

143

144

145

146

147

148

149

150

151

152

153

154

155

156

157

158

159

160

161

162

163

164

165

166

167

168

169

170

171

172

173

174

175

176

177

178

179

180

181

182

183

184

185

186

187

188

189

190

191

192

193

194

195

196

197

198

199

200

## CONFIRMATION OF INELASTIC STRESS DISTRIBUTION IN CONCRETE<sup>a</sup>

Discussion by Anthony M. DiGioia

ANTHONY M. DIGIOIA,<sup>1</sup> J.M. ASCE.—Mr. Hognestad has done a fine job of reporting studies in the literature regarding inelastic stress distribution in flexural reinforced concrete members. The results of his investigation show that the values of  $K_1$ ,  $K_2$ ,  $K_3$ , and  $E_u$  recommended by the Joint ASCE-ACI Committee on Ultimate Strength Design are in good agreement with values determined experimentally by men such as Jensen, Whitney, and others. His review substantiates the validity and reality of the fundamental concepts of plasticity involved in ultimate strength design theories.

The writer believes that Mr. Hognestad and his associates, N. W. Hanson and D. McHenry, have devised an unique testing method for plain concrete specimens which permits the flexural compressive stress distribution to be measured accurately and directly. The results of these tests "show that the inelastic concrete stress distribution consists of a raising curve from zero to the maximum stress and a descending curve beyond the maximum stress." The test results confirm the inelastic stress concepts used by the Joint Committee both quantitatively and qualitatively.

The work of the Joint Committee is definitely a step in the right direction. The Committee has developed practical design procedures which enable the engineer to design a reinforced concrete flexural member by reasonably simple routine calculations. Of course, every precaution must be taken so that the design of members by the Ultimate Strength Procedure does not become too routine, i.e., that a point is never reached wherein the designer loses sight of the basic principles of statics and continuity which underly his work. If this loss of insight becomes a reality then this would be a step in the wrong direction.

It is believed that the Joint Committee was aware of this impending danger of "routineness" for the Committee did not feel that the time had come to standardize a single diagram to represent the stress distribution in compression. "A rectangle, trapezoid, parabola, or any other shape which results in reasonable agreement with tests" may be assumed.

At present, some engineers believe that the rectangular stress block is the form best adapted to design and that it is the simplest form. But with an assumed linear strain distribution across a section, does a rectangular stress distribution logically follow? Is continuity preserved? Of course the answers to these inquiries are in the negative. Then, should the rectangular stress block be used because of its simplicity when the risk of loss of reality is present? The writer feels that in order to avoid this loss, the rectangular stress distribution should not be used. The rectangular stress block is

a. Proc. Paper 1189, March, 1957, by Eivind Hognestad.

1. Graduate Student, Carnegie Inst. of Technology, Pittsburgh, Pa.

definitely simple, but are the trapezoidal or parabolic stress blocks anymore difficult to handle? It is believed that these latter stress blocks are not only as simple as the former stress block, but also have the added advantage of preserving continuity and reality. In time, it is felt, that a balance of simplicity, reasonableness, and practicality will be attained through the efforts of organizations such as ASCE and ACI.

#### REFERENCES

1. "Report of ASCE-ACI Joint Committee on Ultimate Strength Design," Proceedings ASCE, Vol. 81, Paper No. 809, Oct. 1955, 68 pp.
2. "Building Code Requirements for Reinforced Concrete (ACI 318-56)," ACI Journal, May, 1956, Proceedings Vol. 52, pp. 913-986.
3. Hognestad, E.; Hanson, N.W.; and McHenry, D: "Concrete Stress Distribution in Ultimate Strength Design," ACI Journal, Dec. 1955, Proceedings Vol. 52, pp. 455-479.
4. Ferguson, P. H.; "Simplification of Design by Ultimate Strength Procedures, Proceedings ASCE, Vol. 82, Paper No. 1022, July 1956.



ANALYSIS OF MULTI-STORY FRAMES<sup>a</sup>

Discussion by John E. Goldberg, Kenneth H. Lenzen, R. A. Williamson  
Zdenek Sobotka, and E. Neil W. Lane

JOHN E. GOLDBERG,<sup>1</sup> M. ASCE.—This paper is a source of a certain measure of gratification to the present writer because of previous and current interest in the topic of wind stress analysis of tall buildings. It is a source of gratification to the writer to learn that Mr. Hickerson has read a portion of the writer's earlier paper<sup>2</sup> and has re-stated the assumptions made in that paper by the writer.

These assumptions were made for the purpose of obtaining a simplified but, of course, approximate set of slope deflection equations which have application in the iterative solution of the wind stress problem and, except for minor changes in notation, the essential equations first presented by this writer are identical with those given by Mr. Hickerson. These equations form the basis of a method of solution previously presented<sup>3</sup> by this writer which also seems to be about the same as that suggested by Mr. Hickerson. Of the equations previously presented by the writer, one may see that Equations (7), (12), (6), (11) and (11c) are the same as Mr. Hickerson's Equations (1), (2), (9), (10) and (15), respectively; the writer's Equations (11), (11a) and (11b) include Mr. Hickerson's Equation (10). It appears that the writer's Equations (10a) and (10b) are the first approximate equations which take direct account of the classical limiting cases of column base fixity in the wind stress problem. Mr. Hickerson's Equation (27) is identical with the writer's Equation (10b). The iterative procedure previously presented by the writer, in common with other "relaxation" methods, gives the engineer a considerable latitude in its application. The procedure which Mr. Hickerson suggests, since it is based upon equations identical with those previously presented by the writer, naturally is essentially the same as the procedure previously outlined by the writer.

Mr. Hickerson has reawakened interest in this problem by confirming the equations and procedure previously presented by the writer.

KENNETH H. LENZEN,<sup>4</sup> A.M. ASCE.—Mr. Hickerson is to be commended for restating this method of analysis of multi-story building frames based on the slope-deflection theorem. Indeed, Goldberg's<sup>5</sup> method, which preceded

- a. Proc. Paper 1233, May, 1957, by T. F. Hickerson.
1. Prof. of Structural Eng., Purdue Univ., Lafayette, Ind.
2. "Wind Stresses by Slope Deflection and Converging Approximations," Trans. ASCE, Vol. 99 (1934), p. 962.
3. Ibid. See also Analysis of Statically Indeterminate Structures by J. I. Parcel and R. B. B. Moorman, 1955, John Wiley and Sons, New York, pp. 391-397.
4. Associate Prof., Dept. of Applied Mechanics, Univ. of Kansas, Lawrence, Kans.
5. "Wind Stresses by Slope Deflection and Converging Approximations" ASCE Trans., Paper No. 1878, p. 962, Vol. 99, 1934.

and is identical with the method proposed by Mr. Hickerson, is simple, rapid, workable and accurate. In most cases, a third convergence is unnecessary. Quoting from Professor G. A. Maney's discussion of Goldberg's original paper in 1934, "The writer wishes to commend Mr. Goldberg on having produced what is, in his estimation, the most expeditious convergence scheme yet applied to a frame under wind loads."

In addition, the slope deflection equations and bent equations lend themselves to direct solution in the matrix form by modern computing machinery. A great saving in manpower and time can be realized by using the computing devices.

It is well to have a procedure of this type restated, and Mr. Hickerson is to be thanked for his presentation and example problems.

R. A. WILLIAMSON,<sup>1</sup> A.M. ASCE.—The author's paper presents a method of effectively utilizing slope-deflection relations for determining wind moments in multi-story, multi-bay building frames. Several previous methods based on slope-deflection considerations are also available. Probably the best known of these is the one developed by Professor John E. Goldberg<sup>(1)</sup> over twenty years ago. This method was thoroughly discussed in subsequent literature.<sup>(2,3,4,5)</sup> It is the purpose of this discussion to compare the author's method with that of Mr. Goldberg, and to offer some general comments concerning other solutions.

Since both methods start with slope-deflection equations and both use successive corrections, it seems reasonable to suppose that there should be marked similarity between the two. The author has acknowledged his use of Mr. Goldberg's starting assumptions that the joint rotations in any floor are initially considered to be equal to those of the adjacent floors above and below. In addition to this, allowing for changes in notation, many of the equations derived by the author appear to be identical to those of Mr. Goldberg. The following list indicates some of these identities:

<u>Hickerson</u>		<u>Goldberg</u>
Eq 1	=	Eq 7
2	=	12
9	=	6
10	=	(11,11a,11b)
15,16,17	=	11c
24	=	10
27	=	10b

Goldberg also presented an additional, approximate equation accounting for a hinged condition at the base of the columns.

The principal differences between the two methods exist in the convergence technique. As previously mentioned both utilize the same assumptions and the same formulas for the starting values of the joint rotations and sideways ratios. Because of this, the author's preliminary values of  $\theta$  and  $x$  are identical to those of Goldberg, as shown by the foregoing tabulation. Beyond

1. Structural Engr., Holmes & Narver, Inc., Los Angeles, Calif.

this point, most of the values of  $\theta$  and  $x$  obtained by the two methods at various stages in the solutions are not identical, due to differences in the two convergence techniques.

To determine whether the author's method might have advantages in accuracy and rate of convergence, the writer has solved Example 1 by the Goldberg method, carried through the same number of cycles.

The following table lists the author's exact end moments, his convergence values, and those obtained using the Goldberg method.

End Moments						
	E	H	G	E	H	G
	Joint 2			Joint 2'		
Girder	-30.87	-27.12*	-30.2*	-36.91	-34.28*	-36.2*
Col. below	30.87	31.23	30.8	36.91	36.48	37.2
	Joint 1			Joint 1'		
Girder	-95.24	-93.39*	-94.8*	-108.02	-105.11*	-107.4*
Col. above	21.25	20.95	21.1	10.98	11.33	11.2
Col. below	73.99	73.11	74.0	97.04	99.34	97.6
	Joint 0			Joint 0'		
Col.	101.49	100.34	101.4	177.50	177.23	177.6

E = exact value

G = Goldberg value

H = author's value

\* = Computed using girder end rotations

The following table compares the relative joint rotations and sidesway ratios. The exact values have been computed from the author's exact moments using moment-area principles.

Relative Joint Rotations						Relative Sidesway Ratios		
E	H	G	E	H	G	E	H	G
Joint 2			Joint 2'			Upper Story		
2.07	1.67	2.03	3.53	3.45	3.50	8.82	8.585	8.75
Joint 1			Joint 1'			Lower Story		
6.88	6.81	6.85	10.06	9.74	10.00	10.77	10.630	10.73

The author approximates rotations at successive joints in each story, whereas Goldberg determines rotations by separating the joints throughout the frame into two groups, approximating rotations in the first group, and then using these results in approximating rotations in the second group. In the case of Example 1, this approach seems to give slightly faster convergence, as shown by the foregoing comparative tabulations of moments, rotations, and sidesway ratios. However, the difference is not great, and it seems likely that, in general, both methods will yield essentially the same moments with about the same amount of work.

Adapting this type of analysis to available sheet sizes is sometimes not the trivial matter it may seem. For frames with many bays or stories, the use of drawing size sheets is customary, and well suited to the Goldberg method, which places the entire calculated data on the frame diagram.

For lesser frames it is often desirable to use standard letter size calculation sheets. Unfortunately, the detail computations which determine the successive values of  $\theta$  and  $x$  are difficult to place on a frame diagram drawn in the limited space available on a sheet of this size. The author's separation of the major part of the computation from the frame diagrams brings the advantage of making it possible to analyze frames of fairly large extent on letter size sheets.

A majority of engineers prefer methods based on the moment distribution approach. Example 1 is readily solved by a straightforward application of moment distribution using sidesway corrections. Calculation of moments in the frame of Example 2 can be considerably simplified by using cantilever moment distribution in the upper three stories.<sup>(6)</sup> If desired, convergence can also be materially aided by adding rotation moments in the girders of the lower two stories.<sup>(7)</sup> A simple solution of Example 3 by balancing K values has been presented by Grinter.<sup>(8)</sup>

It is concluded that the author's method differs from that of Goldberg mainly in the convergence technique and in the details of recording the computed data. Results by either method, and the work involved, are nearly identical. It is questionable whether the author's method is preferable to those involving variations of conventional moment distribution procedures.

#### REFERENCES

1. Wind Stresses by Slope Deflection and Converging Approximations, John E. Goldberg, Paper 1878, Transactions ASCE, Number 99, 1934, Page 962.
2. Fifth Progress Report of the ASCE Wind-Bracing Committee Proceedings, March 1936.
3. Statically Indeterminate Stresses, J. I. Parcel and G. A. Maney, John Wiley and Sons, New York, Page 240.
4. Analysis of Statically Indeterminate Structures, J. I. Parcel and R. B. B. Moorman, John Wiley and Sons, New York, Page 391.
5. Tests and Design of Steel Wind Bents for Tall Buildings, Ohio State Engineering Experiment Station, Bulletin No. 93, Vol 5, No. 5, September 1936, Pages 35-37.
6. Joint Translation by Cantilever Moment Distribution, L. E. Grinter and CH. H. Tsao, Paper 2718, Transactions, ASCE, Vol 119, 1954, Page 1195.
7. Continuous Frames of Reinforced Concrete, H. Cross and N. D. Morgan, John Wiley and Sons, New York, 1932, Page 229.
8. Wind Stress Analysis Simplified, L. E. Grinter, Paper 1870, Transactions, ASCE, Number 99, 1934, Page 610.

ZDENEK SOBOTKA.<sup>1</sup>—The solution of the equations of the slope-deflection method presented in the excellent paper by Mr. Hickerson is extremely valuable and speeds up the analysis of complicated multi-story frames.

This method, based on certain transformations of the joint and story equations (1) and (9), is valid for the quite general case of a multi-story frame loaded not only by horizontal loads as shown in the paper but also by vertical loads. The effect of both types of loadings may be resolved simultaneously.

In that case equation (1) on page 1233-2 has the form

$$2K_1 (2\theta_1 + \theta_0 - 3x_1) + 2K_2 (2\theta_1 + \theta_2 - 3x_2) + 2K_{G1} (2\theta_1 + \theta_1') + M_{F11}' = 0, \quad (1)$$

where  $M_{F11}'$  is the fixed-end moment produced by the vertical loading at joint 1 on the beam 11'

From (1), we get

$$\begin{aligned} \theta_1 = & 3 \left[ \left( \frac{K_1}{2 \sum K_J} \right) x_1 + \left( \frac{K_2}{2 \sum K_J} \right) x_2 \right] - \\ & - \left( \frac{K_1}{2 \sum K_J} \right) \theta_0 - \left( \frac{K_2}{2 \sum K_J} \right) \theta_2 - \left( \frac{K_{G1}}{2 \sum K_J} \right) \theta_1' - \\ & - \frac{M_{F11}'}{4 \sum K_J} \end{aligned} \quad (2)$$

in place of Eq. (2) on page 1233-2. This equation is valid for the vertically loaded frames with joint displacement.

If the horizontal loading is not present, the preliminary value of the rotation is given by the formula

$$\theta_1 = - \frac{M_{F11}'}{4 \sum K_J}, \quad (3)$$

which yields from Eq. (2), instead by Eq. (24) on page 1233-7.

The subsequent calculation is similar to that used by the author for the horizontal loading.

In special cases of frame structures however, the joint and story rotations may be computed directly, as shown later.

#### Vertically Loaded Symmetrical Multi-Story Frames with One or Two Spans

Because of the symmetry of the structure and its loading and in absence of horizontal loads, there are only joint rotations and no story rotations in the

1. Docent of Theory of Elasticity and Strength of Materials, Technical University, Prague, Czechoslovakia.

symmetrical frames shown on Fig. 1.

Further, the joint rotations  $\theta_J$  and  $\theta'_J$  on the left and right sides of the same story have equal values and inverse sign, i.e.  $\theta_J = -\theta'_J$  and the rotations of the middle joints  $\theta''_J$  in the symmetrical 3-column frame on Fig. 1b are equal to zero.

Thus, applying the condition  $M=0$  at any joint of the 2-column frame on Fig. 1a, we have, by the slope-deflection theorem, the following system of equations for the unknown joint rotations

$$\begin{aligned}(2K_1 + 2K_2 + K_{G1})\theta_1 + K_2\theta_2 &= -M_{F1} \\ K_2\theta_1 + (2K_2 + 2K_3 + K_{G2})\theta_2 + K_3\theta_3 &= -M_{F2} \\ K_3\theta_3 + (2K_3 + 2K_4 + K_{G3})\theta_4 + K_4\theta_4 &= -M_{F3} \quad (4) \\ \text{etc.}\end{aligned}$$

The values of fixed-end moments on the right side of these equations are given in the case of uniform loading by

$$M_{FJ} = \frac{-1}{12} q_J l^2.$$

For the 3-column frame on Fig. 1b quite an analogous system of equations may be written, where only the term of beam-stiffness  $K_{GJ}$  is doubled. These equations are of the form

$$K_J\theta_{J-1} + 2(K_J + K_{J+1} + K_{GJ})\theta_J + K_{J+1}\theta_{J+1} = -M_{FJ}. \quad (5)$$

After dividing each equation by the factor  $K_{J+1}$  with  $j = 1, 2, \dots, 5$ , the systems of the three-member equations (4) and (5) may be reduced to the form

$$\begin{aligned}u_1\theta_1 + \theta_2 &= R_1 \\ v_1\theta_1 + u_2\theta_2 + \theta_3 &= R_2 \\ v_2\theta_2 + u_3\theta_3 + \theta_4 &= R_3 \\ v_3\theta_3 + u_4\theta_4 + \theta_5 &= R_4 \\ v_4\theta_4 + u_5\theta_5 + \theta_6 &= R_5 \\ v_5\theta_5 + u_6\theta_6 &= R_6, \quad (6)\end{aligned}$$

where

$$u_1 = \frac{2K_1 + 2K_2 + K_{G1}}{K_2} , \quad (7)$$

$$u_J = \frac{2K_J + 2K_{J+1} + K_{GJ}}{K_{J+1}} ,$$

or

$$u_1 = \frac{2(K_1 + K_2 + K_{G1})}{K_2}$$

and

$$u_J = \frac{2(K_J + K_{J+1} + K_{GJ})}{K_{J+1}}$$

respectively; also

$$v_J = \frac{K_J}{K_{J+1}} \quad (8)$$

and

$$R_J = \frac{-M_{FJ}}{K_{J+1}} . \quad (9)$$

The unknown joint rotation  $\theta_1$  may be expressed as the ratio of two determinants

$$\theta_1 = \frac{D_{R1}}{D_1} . \quad (10)$$

The determinant of the system

$$D_1 = \begin{vmatrix} u_1 & 1 & 0 & 0 & 0 & 0 \\ v_1 & u_2 & 1 & 0 & 0 & 0 \\ 0 & v_2 & u_3 & 1 & 0 & 0 \\ 0 & 0 & v_3 & u_4 & 1 & 0 \\ 0 & 0 & 0 & v_4 & u_5 & 1 \\ 0 & 0 & 0 & 0 & v_5 & u_6 \end{vmatrix} \quad (11)$$

may be in this case very easily computed from the minors beginning from the right lower corner by the following recurrent procedure

$$D_7 = 1 ;$$

$$D_6 = u_6 ;$$

$$D_5 = u_5 u_6 - v_5 \times 1 = u_5 D_6 - v_5 D_7 ;$$

$$D_4 = u_4 D_5 - v_4 D_6 ;$$

$$\begin{aligned}
 D_3 &= u_3 D_4 - v_3 D_5 ; \\
 D_2 &= u_2 D_3 - v_2 D_4 ; \\
 D_1 &= u_1 D_2 - v_1 D_3 .
 \end{aligned}
 \tag{12}$$

The value of the determinant in the numerator

$$D_{R1} = \begin{vmatrix} R_1 & 1 & 0 & 0 & 0 & 0 \\ R_2 & u_2 & 1 & 0 & 0 & 0 \\ R_3 & v_2 & u_3 & 1 & 0 & 0 \\ R_4 & 0 & v_3 & u_4 & 1 & 0 \\ R_5 & 0 & 0 & v_4 & u_5 & 1 \\ R_6 & 0 & 0 & 0 & v_5 & u_6 \end{vmatrix}
 \tag{13}$$

may be computed from the formula

$$\begin{aligned}
 D_{R1} &= R_1 D_2 - R_2 D_3 + R_3 D_4 - R_4 D_5 + R_5 D_6 = \\
 &= \sum_{k=1}^6 (-1)^k R_{k-1} D_k .
 \end{aligned}
 \tag{14}$$

The rotation  $\theta_1$ , determined from Eq. (10), may be substituted in the first equation of the system (6) from which there is obtained  $\theta_2$  and after substituting the values of  $\theta_1$  and  $\theta_2$  in the second equation, we get  $\theta_3$ , etc.

#### Two-Column Symmetrical Frames with Horizontal Loads

In the case of a 2-column symmetrical multi-story frame, Eq. (10) on the page 1233-4 for the story rotation becomes

$$x = R \varphi = \frac{\theta_U + \theta_L}{2} = \frac{M}{12EK_C} + \frac{\theta_U + \theta_L}{2}
 \tag{15}$$

and coincides with the approximative formula (15) on page 1233-6.

Here,  $M = S x h = \text{Shear} / x / \text{Story height}$  and  $K_C$  the column stiffness.

Applying the Eq. (15) for the rotation of each story and substituting it in the joint equations of the type

$$\begin{aligned}
 &K_J (2\theta_J + \theta_{J-1} - 3x_J) + K_{J+1} (2\theta_J + \theta_{J+1} - \\
 &- 3x_{J+1}) + 3K_{GJ} \theta_J = 0 ,
 \end{aligned}
 \tag{16}$$



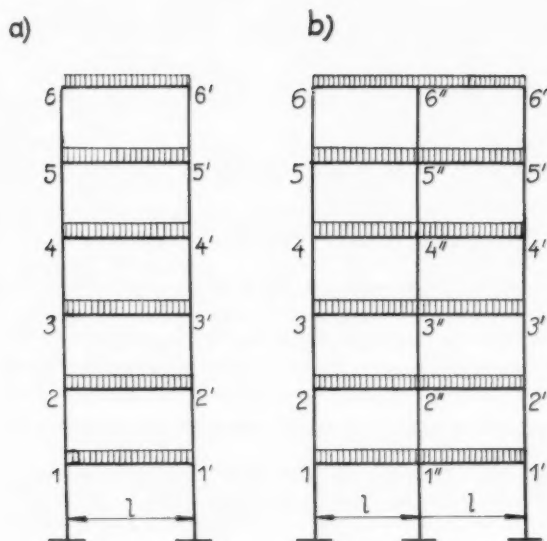


FIG. 1

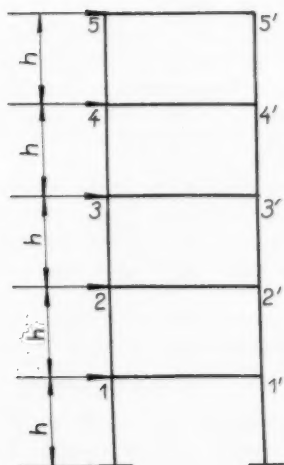


FIG. 2

where  $\theta_J = \theta'_J$ ,

leads, after adding and rearranging the terms, to the following system of three-member equations

$$\begin{aligned}
 (K_1 + K_2 + 6K_{G1})\theta_1 - K_2\theta_2 &= \frac{1}{4}(M_1 + M_2) \\
 -K_2\theta_1 + (K_2 + K_3 + 6K_{G2})\theta_2 - K_3\theta_3 &= \frac{1}{4}(M_2 + M_3) \\
 -K_3\theta_2 + (K_3 + K_4 + 6K_{G3})\theta_3 - K_4\theta_4 &= \frac{1}{4}(M_3 + M_4) \\
 -K_4\theta_3 + (K_4 + K_5 + 6K_{G4})\theta_4 - K_5\theta_5 &= \frac{1}{4}(M_4 + M_5) \\
 -K_5\theta_4 + (K_5 + 6K_{G5})\theta_5 &= \frac{M_5}{4} \quad (17)
 \end{aligned}$$

which may be resolved in quite a similar way as it was shown in the case of vertically loaded frame.

A similar procedure of the analysis of special multi-story frames with the use of determinants is described by I. Toth (see Ref.).

#### REFERENCE

1. I. Toth: Solution pour les portiques a étages sans résolution des équations (in French). La Technique des Travaux, Mars-Avril 1957, 33<sup>e</sup> année - No. 3-4.

E. NEIL W. LANE,<sup>1</sup> A.M. ASCE.—A few comments and an illustration regarding a comparison of the author's abbreviated slope-deflection analysis with the popular moment-and-shear distribution procedure of Hardy Cross appears in order. Similar comparisons with Grinter's slope distribution, Mitchell's elastic traverse, etc. would also be interesting and of value. This discussion, however, will confine itself with the abbreviated and regular methods of moment distribution.

Remarks concerning the extension of Hickerson's method to the solution of rigid-frame structures with sloping or offset members having variable moment of inertia, and the use of superficial or false ties for the simplification of analysis, also the handling of compound members should prove to be worth attention.

Deflection of single member dog-leg girders due to transverse loads and translation of the offsets in the span relative to the supports give rise to the additional factor of  $\frac{\Delta y}{l}$  to be accounted for in addition to the author's sidesway ratio  $x$ , or in other words a vertical shear correction to be applied in addition to the usual seismic or wind shears. This same effect can be found to an appreciable extent in mid-story framing for balconies, ramps and stairs where there is considerable difference in the floor plan of the adjacent

1. Structural Engineer, 611 Carlo Court, Lodi, Calif.

stories, thus necessitating offset column loads carried by heavy shear slabs with high torsional resistance. This is not done often, nor is it usually economical, but some times it is necessary. This additional

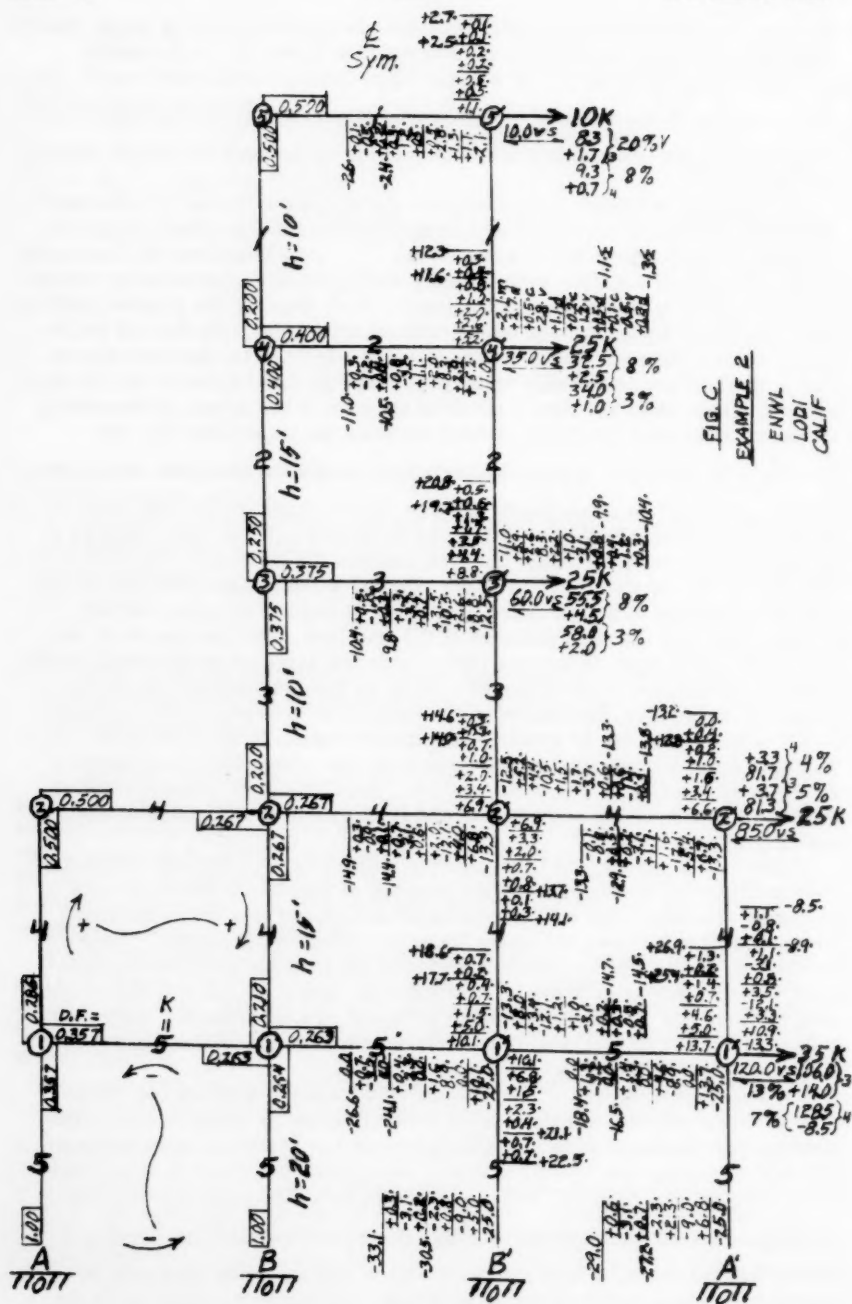
$\frac{\Delta y}{l}$  factor in the vertical direction also takes care of the vertical component of the translations at the two levels of the ends of straight sloping members.

The addition of haunches to prismatic members (or the use of otherwise variable moment of inertia) causes simple changes in the general formulas (3) and (10), and affects their derivatives. This also lengthens the application of Mr. Hickerson's method considerably when applied to low building frames of special shapes or for special purposes. As in most of the popular methods, however, this additional work mainly affects the preparation for and not the actual convergence procedure where the main merit of the process occurs. The product of the actual carryover factor and the true stiffness for the near end of the individual member divided by the sum of the actual stiffnesses of the near ends of the members of the joint must be substituted for the

$\left( \frac{K}{2 \sum K} \right)$  factors. Where the variations in section along the members are not great and an approximate answer only is required, it often pays to start the analysis with the prismatic formulae and use two convergences of  $\theta$  and  $X$  until the percentage changes indicate the approach of accuracy to that of the ratio of the products of the carryover factor and stiffness for the true as compared to an estimated equivalent prismatic member, before following through the final portions of the analysis. This procedure is also desirable where there is a large variation in the sections of individual members, or stiffnesses of members of a joint, or combinations of one frame connected to another, and appreciable accuracy in the end result is desired. In this way a trend can be quickly established leading to the average or convergence point for the start of the coup de grace. Often the approximation can be worked on by an assistant while the more exacting portions receive the best attention of the designer for the final selection of moments, shears and forces.

False ties or struts, the imaginary members of zero bending stiffness, used temporarily in analysis for the purpose of adapting a real structure to an easier solution, work well where there are offsets in a beam for dual levels of adjacent floors, or where there are compound columns. Their conception serves for the standardization of the process and their replacement with an equivalent force is most often an easy correction to the original computation. Mr. Cross has developed the use of equivalent for compound members in his original text, is quite complete with his method, and it is easily adapted for the writers method.

The accompanying Fig. C for the writer's Example 2 shows the Cross solution in its original standard form with convergence comparisons in the last two distributions. It is interesting to note the relatively slow contraction at the footings and top of the tower, but on the other hand it is perhaps more compact and complete with a direct answer. The abbreviated Cross procedure is a practical parallel to Mr. Hickerson's use of the  $\left( \frac{K}{2 \sum K} \right)$  factors and for some, a very practical way of making quick approximate analyses for preliminary designs requiring a more exacting final analysis.



BEAM DEFLECTION IN BRIDGES DESIGNED FOR CONTINUITY<sup>a</sup>

Discussion by Zdenek Sobotka

ZDENEK SOBOTKA.<sup>1</sup>—This paper has presented an extremely valuable and very time-saving simple procedure for the calculation of the deflection of uniformly loaded continuous beams with constant moment of inertia. The arrangement of the deflection formula and the use of the table of auxiliary coefficients speeds up the solution of this frequent problem.

## The Maximum Deflection

In many cases, a more precise determination of the maximum deflection and its position is of considerable practical importance, especially in the first or last span of continuous beams, where the point of maximum deflection is more remote from the midspan.

Substituting in Eq. (1)

$$\Delta_X = \Delta_X^S - \Delta_X^F$$

on page 1234-2 the formulae for the both parts of the deflection

$$\Delta_X^S = \frac{M_S L^2}{3EI} (C - 2C^3 + C^4)$$

and

$$\Delta_X^F = \frac{M_L L^2}{2EI} (C - C^2) + \frac{M_E L^2}{6EI} (C - C^3),$$

leads to

$$\Delta_X = \frac{M_S L^2}{3EI} (C - 2C^3 + C^4) - \frac{M_L L^2}{2EI} (C - C^2) - \frac{M_E L^2}{6EI} (C - C^3). \quad (1)$$

The position of the point of the maximum deflection is given by its distance from the left support of the span

$$X_0 = C_0 L. \quad (2)$$

Letting the first derivative  $\frac{d\Delta_X}{dC}$  equal to zero and putting  $C = C_0$

leads to

a. Proc. Paper 1234, May, 1957, by Guillermo Villena.

1. Docent of Theory of Elasticity and Strength of Materials, Technical University, Prague, Czechoslovakia.

$$\frac{d \Delta}{d C} = \frac{M_S L^2}{3EI} (1 - 6C_0^2 + 4C_0^3) - \frac{M_L L^2}{2EI} (1 - 2C_0) - \frac{M_E L^2}{6EI} (1 - 3C_0^2) = 0, \quad (3)$$

from which the cubic equation follows with the unknown coefficient  $C_0$  determining the point of the maximum deflection in an inner span of the continuous beam

$$C_0^3 - \frac{3}{2} \left(1 - \frac{M_E}{4M_S}\right) C_0^2 + \frac{3M_L}{4M_S} C_0 + \frac{1}{4} - \frac{3M_L + M_E}{8M_S} = 0. \quad (4)$$

In the first span with simple of articulated first support  $M_L = 0$  and  $M_E = M_R$ . Eq. (4) becomes then

$$C_0^3 - \frac{3}{2} \left(1 - \frac{M_R}{4M_S}\right) C_0^2 + \frac{1}{4} - \frac{M_R}{8M_S} = 0, \quad (5)$$

or, after transformation

$$C_0^3 - (3C_0^2 - 1)K - \frac{1}{4} = 0, \quad (6)$$

where

$$K = \frac{1}{2} \left(1 - \frac{M_R}{4M_S}\right). \quad (7)$$

Eq. (6) may be written in the form

$$K = \frac{C_0^3 - \frac{1}{4}}{3C_0^2 - 1} = \frac{\frac{1}{4} - C_0^3}{1 - 3C_0^2}. \quad (8)$$

According to the formula (8) the following table is calculated which gives the relation between  $K$  and  $C_0$  and which can speed up the computing of the position of the maximum deflection in the first span.

The value of  $C_0$  from Eq. (4) or from the table 1 once determined, the maximum deflection follows from the author's table on page 1234-7 and 1234-8.

#### The Continuous Beam with Variable Cross-Section

However, it is much more complicated to determine the deflections of a continuous beam with variable cross-section. As an example of such a case, the continuous beam with uniformly reinforced flanges at the supports may be presented (Fig. 1a).

TABLE 1.

$C_0$	$K$	$\frac{M_R}{M_S}$
.39	.3506	1.1952
.40	.3577	1.1284
.41	.3653	1.0776
.42	.3736	1.0112
.43	.3829	.9368
.44	.3932	.8544
.450	.4048	.7616
.455	.4122	.7024
.460	.4180	.6560
.465	.4254	.5968
.470	.4334	.5328
.475	.4420	.4640
.480	.4511	.3912
.485	.4618	.3056
.490	.4732	.2144
.495	.4850	.1200
.500	0	0

The moment of inertia at the left support is  $I_L$  and that at the right support  $I_R$ .

The deflection in a span of that continuous beam may be expressed as the bending moment of a simple beam loaded by an ideal pressure solid whose height in any point is determined by the bending moment and whose width is given by the reciprocal value of the flexural stiffness  $\frac{1}{EI}$ , as suggested by Mr. O. Ondra (see Ref. 1). For an easy visualization of the problem, this pressure solid is divided into two portions (Fig. 1b and 1c).

The deflection  $\Delta_{X1}$  of the ideal beam with constant moment of inertia  $I$ , as determined by the Eqs. (8) and (9) on page 1234-4, is diminished by the rise of the moment of inertia in the reinforced parts at the supports.

The two parts of the decrease of the reaction of the diminished pressure solid are

$$\begin{aligned} \Delta^F_{RL} = & \frac{M_L X_1}{2LE(I_L - I)} (2L - X_1) + \frac{M_E X_1^2}{6L^2 E(I_L - I)} (3L - 2X_1) + \\ & + \frac{M_L}{2LE(I_R - I)} (L - X_2)^2 + \frac{M_E}{2LE(I_R - I)} (L - X_2)^2 - \\ & - \frac{M_E}{3L^2 E(I_R - I)} (L - X_2)^3, \end{aligned} \quad (9)$$

as follows from Fig. 1b and

$$\begin{aligned} \Delta^S_{RL} = & \frac{w}{2LE(I_L - I)} \int_0^{X_1} x(L - x)^2 dx + \frac{w}{2LE(I_R - I)} \int_{X_2}^L x(L - x)^2 dx = \\ = & \frac{w}{24LE(I_L - I)} (6L^2 X_1^2 - 8LX_1^3 + 3X_1^4) + \\ & + \frac{w}{24LE(I_R - I)} (L^4 - 6L^2 X_2^2 + 8LX_2^3 - 3X_2^4), \end{aligned} \quad (10)$$

as may be seen from Fig. 1c.

After introducing a new variable  $t$  in the interval  $(0; X_1)$ , the farther part of the decrease of the deflection in the middle part of a span may be found from

$$\begin{aligned} \Delta_0 = & \frac{w}{2E(I_L - I)} \int_0^{X_1} t(L - t)(X - t) dt = \\ = & \frac{w}{24E(I_L - I)} (6L X_1^2 X - 4X_1^3 X - 4LX_1^3 + 3X_1^4). \end{aligned} \quad (11)$$



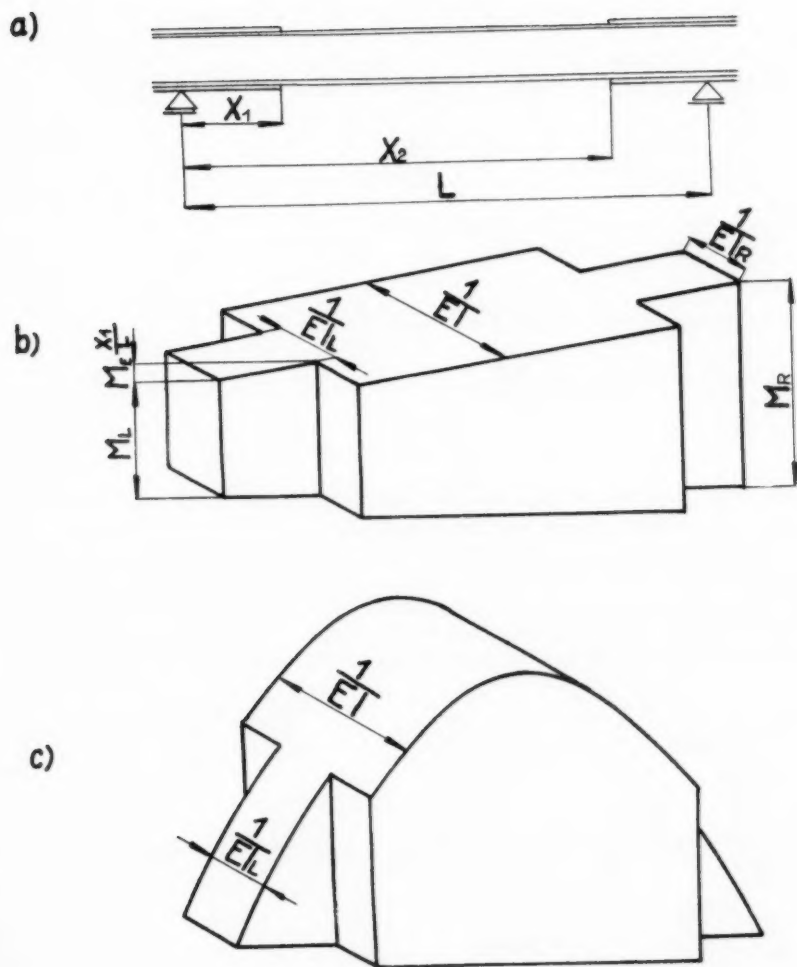


FIG. 1

The total deflection in the middle part of a span of the continuous beam with the reinforced parts at the supports is hence after addition and rearrangement of terms

$$\begin{aligned}
 \Delta_X &= \Delta_{X1} - \Delta_{R_L}^F \cdot X - \Delta_{R_L}^S X - \Delta_0 = \\
 &= \Delta_{X1} - \frac{M_L X_1 X}{2LE(I_L - I)} (2L - X_1) - \frac{M_E X_1^2 X}{6L^2 E(I_L - I)} (3L - 2X_1) - \\
 &- \frac{M_R X}{2LE(I_R - I)} (L - X_2)^2 - \frac{M_E X}{2LE(I_R - I)} (L - X_2)^2 + \\
 &+ \frac{M_E X}{3L^2 E(I_R - I)} (L - X_2)^3 - \\
 &- \frac{W}{24LE(I_L - I)} (12L^2 X_1^2 X - 12LX_1^3 - 4L^2 X_1^3 + \\
 &+ 3LX_1^4 + 3X_1^4 X) - \frac{WX}{24LE(I_R - I)} (L^4 - 6L^2 X_2^2 + 8LX_2^3 - 3X_2^4).
 \end{aligned} \quad (12)$$

The value  $\Delta_{X1}$  the deflection of the ideal continuous beam with constant moment of inertia  $I$ , which may be determined from the author's table.

A similar formula may be used also for the approximate calculating of the deflection in the more complicated case with continuously varying moment of inertia as shown on Fig. 2a. After segmenting the part with variable cross-section (Fig. 2b and c) and assuming the moment of inertia of each segment constant, the deflection may be computed from the approximate formula

$$\begin{aligned}
 \Delta_X &= \Delta_{X1} - \sum_{k=1}^n \frac{M_L X_{1k} X}{2L \Delta I_{Lk}} (2L - X_{1k}) - \sum_{k=1}^n \frac{M_E X_{1k}^2 X}{6L^2 E \Delta I_{Lk}} (3L - 2X_{1k}) - \\
 &- \sum_{k=1}^n \frac{M_R X}{2LE \Delta I_{Rk}} (L - X_{2k})^2 - \sum_{k=1}^n \frac{M_E X}{2LE \Delta I_{Rk}} (L - X_{2k})^2 + \\
 &+ \sum_{k=1}^n \frac{M_E X}{3L^2 E \Delta I_{Rk}} (L - X_{2k})^3 - \\
 &- \sum_{k=1}^n \frac{W}{24LE \Delta I_{Lk}} (12L^2 X_{1k}^2 X - 12LX_{1k}^3 X - 4L^2 X_{1k}^3 + 3LX_{1k}^4 + \\
 &+ 3X_{1k}^4 X) - \sum_{k=1}^n \frac{WX}{24LE \Delta I_{Rk}} (L^4 - 6L^2 X_{2k}^2 + 8LX_{2k}^3 - 3X_{2k}^4),
 \end{aligned} \quad (13)$$

where  $n$  is the number of segments in each part.

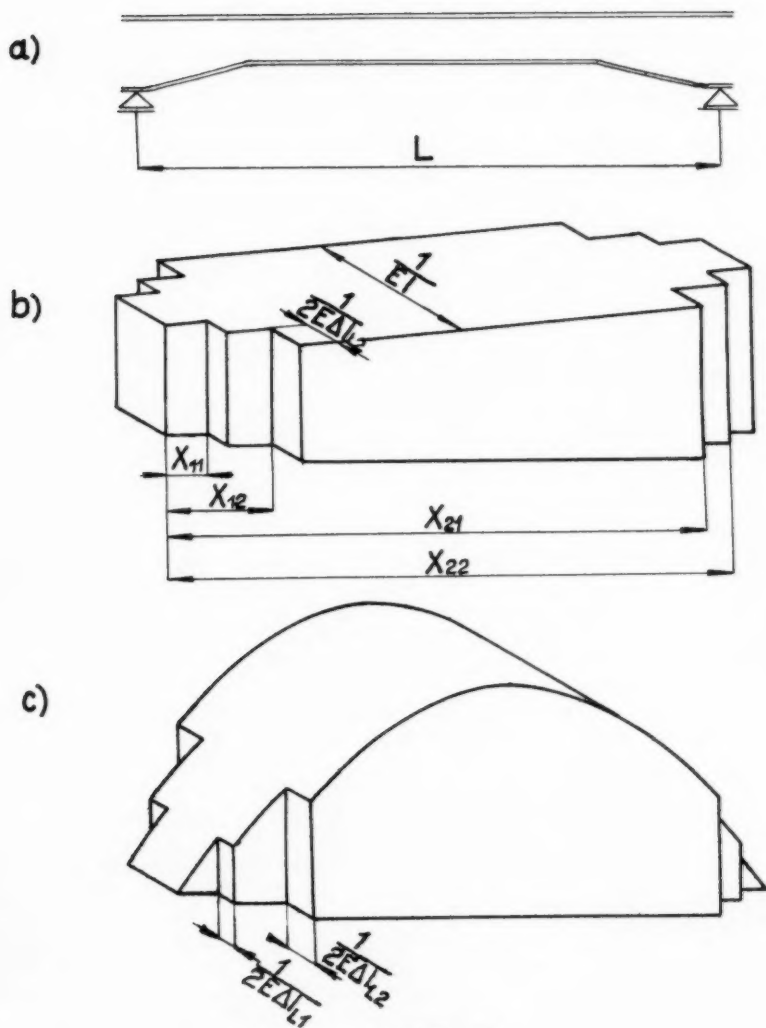


FIG. 2

## REFERENCES

1. Otakar Ondra: "Moment Distribution Constants from Models." Paper 1058, Journal of the Structural Division, Proceedings of the American Society of Civil Engineers, Vol. 82, ST 5, September, 1956.
2. John C. Murphy, Thomas D.Y. Fok: "Discussion of Moment Distribution Constants from Models." Paper 1192, Journal of the Structural Division, Proceedings of the ASCE, Vol. 83, ST 2, March, 1957.

## THE BEHAVIOR OF ONE-STORY REINFORCED CONCRETE SHEAR WALLS<sup>a</sup>

Discussion by DeForest A. Matteson, Jr.

DeFOREST A. MATTESON, JR.<sup>1</sup>—Despite a lack of conclusive strain-gage data, it seems worthwhile to try to interpret the authors' results in terms of principal-stress patterns.

The authors state that "Cracks are not only a product of stress but of the ability to form and propagate as well. Thus cracks are not observed necessarily in the most highly stressed regions but at locations where it is easier for cracks to form and propagate." This assertion needs clarification: Cracks in reinforced concrete lie parallel to the principal compressive stresses, and they occur where there is an insufficient component of steel in the direction of the principal tensile stress to prevent cracking. Hence, "the ability to form and propagate" may be described entirely in terms of stress resistance, and one should not infer that it is anything else. If the most highly-stressed regions are heavily reinforced in the proper direction, must not the first cracks then occur in a region carrying a lower stress, that stress being the highest principal tensile stress not properly resisted by steel? The direction and order of occurrence of these cracks are determined by the principal tensile stresses, the arrangement of the steel, and the geometry of the structure.

A few simple illustrations occur in the paper, the most obvious being the effect that variation in column reinforcement exerts on the crack pattern.

It is the writer's understanding that as the column reinforcement was increased the steel in the distributing beam also was increased. As the columns are made increasingly stiff, the bending resistance of the web tends to become relatively negligible. A theoretical condition must therefore be approached wherein shear stresses are constant across the web, including the shear stress at the juncture of web and column. Also, as the distributing beam is stiffened, the distribution of shear between it and the web becomes increasingly uniform over its length. The limit is a web panel in pure shear, the shear stresses being constant in both the horizontal and vertical directions; which means that when the columns are highly reinforced the principal stresses in the panel lie at about 45° to the boundaries and are approximately constant throughout the panel, principal tension being numerically equal to principal compression. As a result, whereas the specimens with lightly reinforced columns will fail first near the base of the tension column, increasing the column reinforcing theoretically increases the tendency for the first crack to appear in the web. With heavily reinforced columns and a large  $L/h$ -ratio, the probability of its appearing in any particular part of the web decreases—all parts of the web tend to become indiscriminately susceptible.

a. Proc. Paper 1254, May, 1957, by Jack R. Benjamin and Harry A. Williams.

1. Engineer-Editor, Douglas Fir Plywood Association, Tacoma.

The foregoing elementary hypothesis is borne out by many of the authors' illustrations in which crack patterns are shown.

From this it is further reasoned that web reinforcing is of little value if the columns are not heavily reinforced, but that it becomes increasingly desirable as the column reinforcing is increased. Also, it appears that since the principal stresses tend to lie diagonal to the web, diagonal reinforcing would be best where columns are well-reinforced. However, the authors found diagonal reinforcing less effective than rectangular reinforcing.

A possible explanation is suggested, as follows: When principal stresses are equal but of opposite sign and lie at  $45^\circ$  (an idealized situation), all bars in a rectangular reinforcement pattern participate as components in resisting diagonal tension and cracking. If the bars remain at  $90^\circ$  to each other but the grid is turned so that the bars lie at  $45^\circ$ , only half of them act in resisting cracking. Now, if the angle between these bars is gradually changed from  $90^\circ$  to  $0^\circ$  in such a way as to reduce the angle that all the bars make with the horizontal, the component of tension resistance in the vertical direction approaches the tensile strength of plain concrete. Similarly, the authors' diagonal reinforcement is stronger horizontally than vertically. It would seem that such an unbalanced pattern must certainly be more susceptible to diagonal-tension cracking than either the  $45^\circ$  pattern or the rectangular one. If specimen R-5 were to have its web reinforcement rotated further toward the horizontal, its  $p$ -value would approach that of VRR-2; the fact that the two specimens have about the same ultimate load and load at first crack may be significant in this regard.

Panel VRR-2 probably had a little less resistance to bending than VRR-3 or VRR-6, but it appears to have been tenacious, absorbing a great amount of mechanical work before failure. Specimen VRR-3 probably was stiffer and stronger against bending than VRR-2, but its failure was more sudden and the authors do not indicate that its resistance to shear was clearly superior. It is noted that VRR-6 had about the same ultimate load as R-1 (but perhaps greater stiffness after first crack); R-1 was more lightly reinforced vertically but had horizontal bars too. These observations suggest that direction of panel reinforcing influences stiffness and suddenness of failure.

The authors make little mention of energy-absorption capacity, although this is probably a criterion for design of reinforced concrete shear walls under seismic loading. The greater the wall's ability to continue carrying overload when badly deformed and the less brittle its mode of failure, the more valuable it will often be during an earthquake. To attain this end, the authors' results seem to indicate that heavy column reinforcing is helped by adding panel reinforcement parallel to load.

In specimens having heavy column steel, there was a tendency for the column to crack (subsequent to the first crack) at sections of low bending stress rather than of maximum bending stress. Frequently, these cracks seem not to have been perpendicular to the steel, as those at the bases of the lightly-reinforced columns were, but rather at a slight slope (Fig. 8). This seems reasonable; for in areas where shear stress predominates over bending stress, the principal tensile stress lies at some angle to the load other than perpendicular. Since the column steel was not bent at this angle also, the specimen was incompletely reinforced against the principal tensile stress in this area and it was merely necessary to increase the load to a certain magnitude for this principal tension to crack the concrete, even though the base of this column (where bending stress predominated) may not yet have cracked.

The foregoing comments are interpretive in intent. The writer does not refute the authors' statements, but trusts that his elementary explanations have clarified misleading assertion in the paper regarding the occurrence and propagation of cracks.

In the formula for linear deflection it is not clear why  $I$  does not include the column steel, since this steel will have an effect on the deflection in the linear range. Further, it would seem reasonable not to include the web cross-section in computing  $I$  because the expression  $\frac{VH}{AG}$  may be derived by assuming the shear constant over the width of the web, which implies an assumed absence of bending resistance in the web.

The authors' use of elementary procedures to compute deflection will be reassuring to the designer who is concerned about the probable seismic deflection of a shear wall under design load. Use of more involved methods to gain precision for such a purpose might be wasted, because shear-wall deflection is increased by rotation and slip at the base, which depend on the design and construction of the wall's anchorage to its foundation and upon other possible factors. All these factors involve assumptions and approximations conducive to conservative design, but not necessarily to exactness.





LATERAL LOAD DISTRIBUTION TEST ON I-BEAM BRIDGE<sup>a</sup>

Discussion by Masso Naruoka and Benjamin C. F. Wei

MASAO NARUOKA.<sup>1</sup>—The authors described that full and complete composite action was obtained in the region of positive moment in continuous beams. The shear connector used in the test bridge consists of a #7 bar bent as shown in Fig. 2 and welded at 2' 4" centers to the center of the upper flange of the beam. This connector is the so called flexible shear connector, and on the other hand, the rigid shear connector is used in Germany and Japan. The writer thinks that full and complete composite action can be achieved by the rigid connector, not by the flexible connector, but could be observed in authors' test because the test load was small.

The shear connector used in the test bridge may rather be called the slab connector. The writer has experimented the behavior of the incomplete composite I-beam with slab connectors up to the rupture and observed the following experimental facts:

- 1) The beam behaved as a complete composite beam so long as the test load was small,
- 2) The beam behaved gradually as a incomplete composite beam as the test load became larger,
- 3) At rupture, the upper one third of the slab behaved as being able to resist compression as a part of the composite member.

From these reasons, the author's conclusion (1) is a hasty one.

The writer agrees with the author's conclusion (5), and the grillage girder bridges recently erected in Japan have an outside beam stronger than the inside beams, and even in the girder bridge designed by conventional methods, the outside beam has been designed as having the moment of inertia about ten percent larger than that of the inside beam necessary by the usual method.

BENJAMIN C. F. WEI,<sup>2</sup> J.M. ASCE.—An interesting test on a full size continuous I-beam bridge was presented in this paper. The I-beam bridges, representing one of the most common types of highway structures, are widely used here in United States for their simplicity and ease of construction. Up to now bridge designers are still guided by many empirical rules set up by the AASHTO in the design of this type of bridge. Numerous analytical and test programs have been conducted<sup>(1)</sup> in search for a more rational design criteria of this simple I-beam bridge with a concrete roadway slab. The authors and the Public Works Department of the City of Houston are to be commended for setting up the test program of this full-size bridge as a step

- a. Proc. Paper 1255, May, 1957, by Ardis White and William B. Purnell.
1. Prof., Kyoto Univ., Kyoto, Japan.
2. Prin. Designing Engr. on Structures, Hydrocarbon Research Inc., New York, N. Y.

furthering the understanding of these complex problems of the composite action and the effectiveness of diaphragms in I-beam bridges.

While extensive laboratory tests on shear connectors have been made on I-beam bridges,<sup>(2,3)</sup> few tests have been recorded for the primary purpose of studying the behavior of diaphragms in such structures. An analytical study on the effects of diaphragms in I-beam bridges<sup>(4)</sup> has been made for a total of 85 different structures; the bridge considered were simple span right bridges, consisting of a continuous concrete slab supported by five uniformly-spaced identical I-beams running in the direction of the traffic. Several variables were studied, including (1) relative stiffness of diaphragm to that of each beam; (2) the position of diaphragms in the structure; (3) relative stiffness of beam to that of slab; (4) relative dimensions of the bridge; and (5) the type and position of loading. The analyses were based on the simplifying assumptions that the torsional restraint offered by I-beam is neglected, that the connection of the diaphragms to the beams are fully effective, and that the top of the diaphragm does not touch the bottom of slab under any loading condition.

It must be noted that the diaphragms at Station A in the test bridge are composed of a built-up section with two channels and a plate as top flange and two angles as bottom flange, and are placed directly underneath the roadway slab. This arrangement differs with a common layout of diaphragms for relatively short span I-beam bridges, where the diaphragm may be composed of a single channel or WF or simple angle cross-frame, placed sufficiently below the slab so that they do not touch the bottom of roadway slab under any loading condition.

From the data in the analytical study,<sup>(4)</sup> the influence lines for midspan moments in beams for a load moving across the bridge at midspan for a bridge with proportion  $b/a = 0.1$ ,  $H = 5$  and diaphragm at midspan may be plotted as shown in Fig. 1 (a), (b) and (c). The cases for  $r = 0$ , corresponding to bridge without diaphragms, and  $r = 0.40$  are included. The symbols are defined as follows:

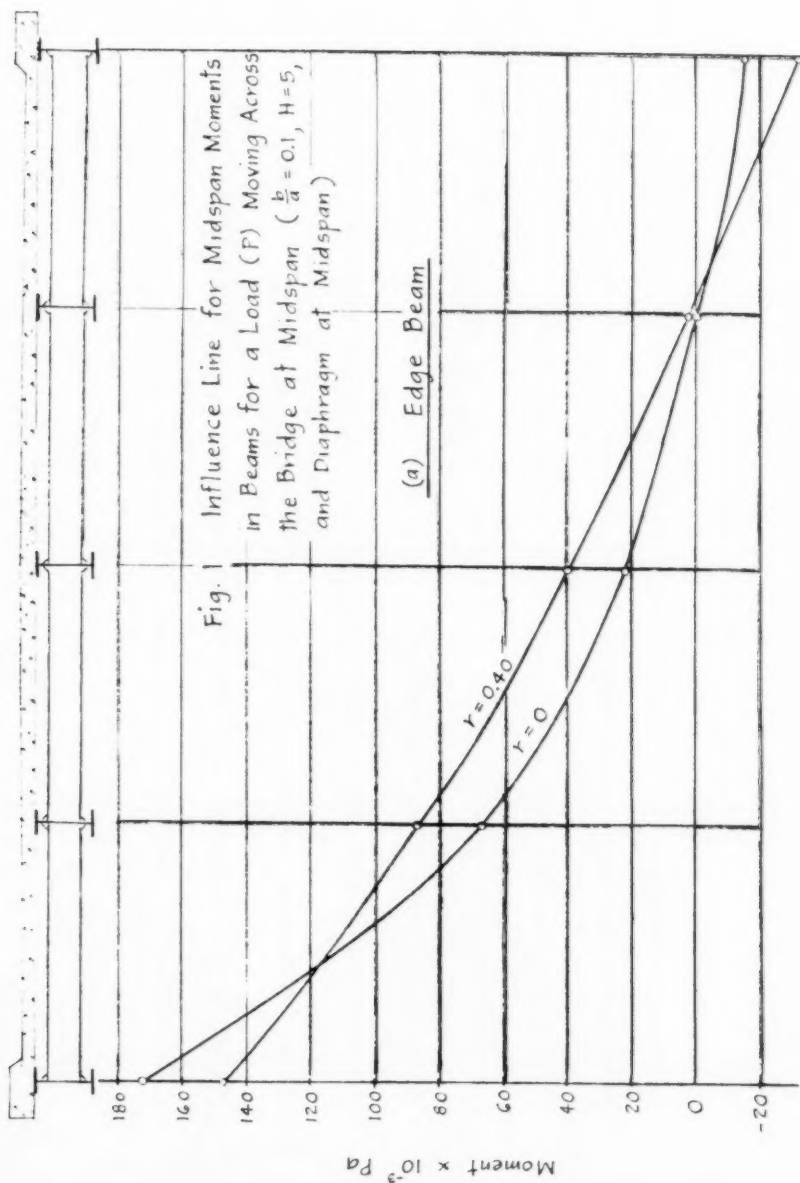
$a$  = span of simply-supported bridge, center to center of supports.

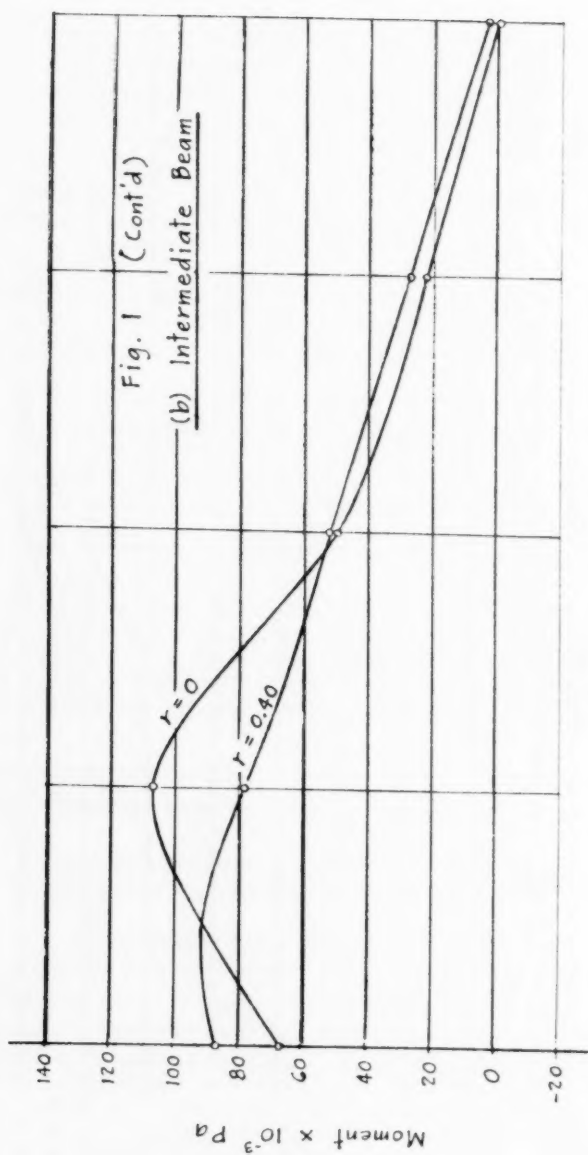
$b$  = transverse spacing of beams.

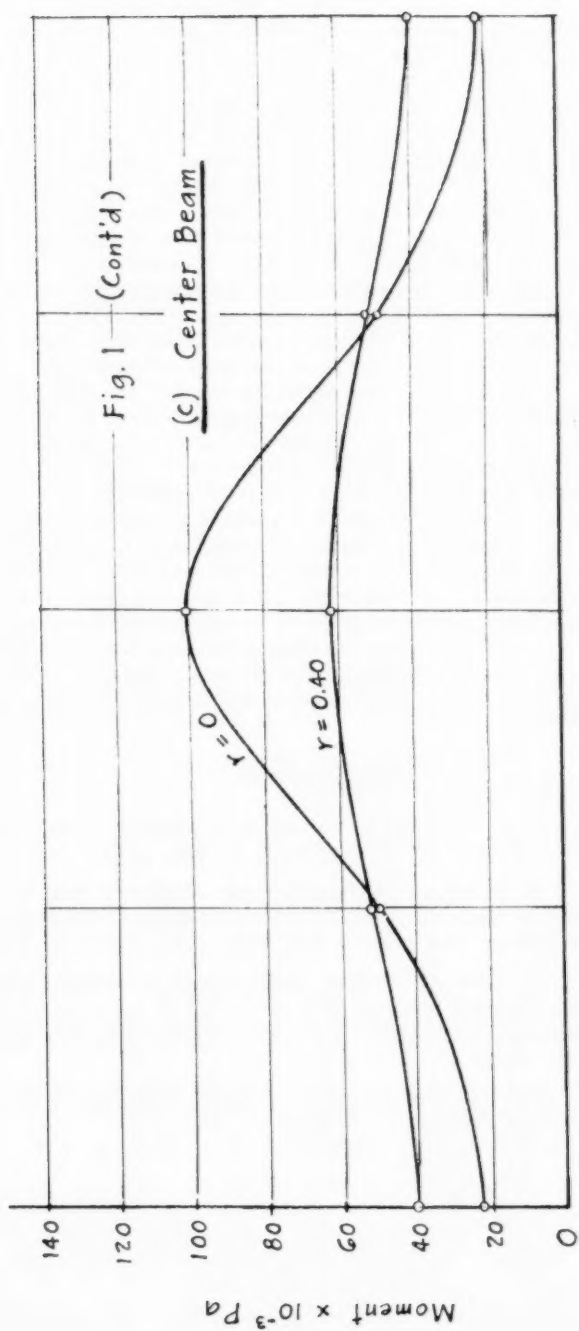
$H = \frac{E_b I_b}{a E_c I_c}$  = a dimensionless coefficient which is a measure of the stiffness of a beam relative to that of the slab.

$r = \frac{E_d I_d}{E_b I_b}$  = a dimensionless coefficient which is a measure of the stiffness of a diaphragm relative to that of a beam.

The bridge described above would correspond roughly to the center span of the test bridge in the paper, where the positive moment section of the center span is taken as the simple span length and the stiffness of diaphragm is calculated without the concrete slab. From Fig. 1, it may be noted that as the unit load moves from one beam to the other, the maximum moment in the beam under load decreases with the addition of the diaphragm. The decrease is more significant in the center beam than those in the edge and the intermediate beams. In general the action of the diaphragm under a moving load tends to flatten the moment curve by relieving the load in the beam directly under the load and distributing this relieved portion of the load to the adjacent beams.







By loading the beams in this analytical bridge with the same loadings I and II as designated in the paper, it is possible to draw the curves of the percentages of total moment taken by each beam. These figures are shown in Fig. 2 (a) and (b). For purpose of comparison, the curves for beams 1 and 2 at Station A as shown in Fig. 8 in the paper are superposed. Also, the curves for the bridge without the diaphragms are shown to serve as a limiting case where the load distribution is entirely due to concrete slab.

A close observation of Fig. 2 indicates that there is a reasonably good agreement between the theoretical and test results. It is apparent from the figure that, with the addition of diaphragm, the total reduction of moment in the center beam under loading II is much more than that in the edge beam under loading I. However, by comparing the percentage distribution of the total moment in beams for bridge with diaphragm versus the same one without diaphragm, one can calculate the percentage of the lateral transfer of total moment, as contributed by the action of the diaphragm. For the bridge illustrated, these percentages are, approximately, 22% for loading I on edge beams, and 19% for loading II on the center beam. Therefore, theoretical analyses seem to indicate the same result as concluded in the paper that, for the test bridge, approximately 80% of the lateral distribution of load is being transferred by the roadway slab and 20% by the diaphragm.

In closing this discussion, the writer wishes to caution the readers against the fact that the test was performed on this particular bridge on Houston Memorial Drive, which is designed with a specific physical proportion and a definite size and arrangement of the shear connectors and diaphragms. Hence, the conclusions given by the authors must be viewed with limitations. It is hoped that more full-size structures similar to this bridge would be tested in future to permit generalization on this subject of lateral load distribution for the most practical range of I-beam bridges in use.

#### REFERENCES

1. N. M. Newmark and C. P. Siess, 'Research on Highway Bridge Floors,' Reprint Series No. 52, Univ. of Ill. Eng. Exp. Sta., (1954).
2. C. P. Siess, I. M. Viest, and N. M. Newmark, 'Studies of Slab and Beam Highway Bridges: Part III - Small Scale Tests of Shear Connectors and Composite T-Beams,' Bulletin No. 396, Univ. of Ill. Eng. Exp. Sta., (1952).
3. I. M. Viest, C. P. Siess, J. H. Appleton, and N. M. Newmark, 'Studies of Slab and Beam Highway Bridges: Part IV - Full-Scale Tests of Channel Shear Connectors and Composite T-Beams,' Bulletin No. 405, Univ. of Ill. Eng. Exp. Sta., (1952).
4. B. C. F. Wei, 'Effects of Diaphragms in I-Beam Bridges,' Ph. D. Thesis, Dept. of Civil Eng., Univ. of Ill., (1951).

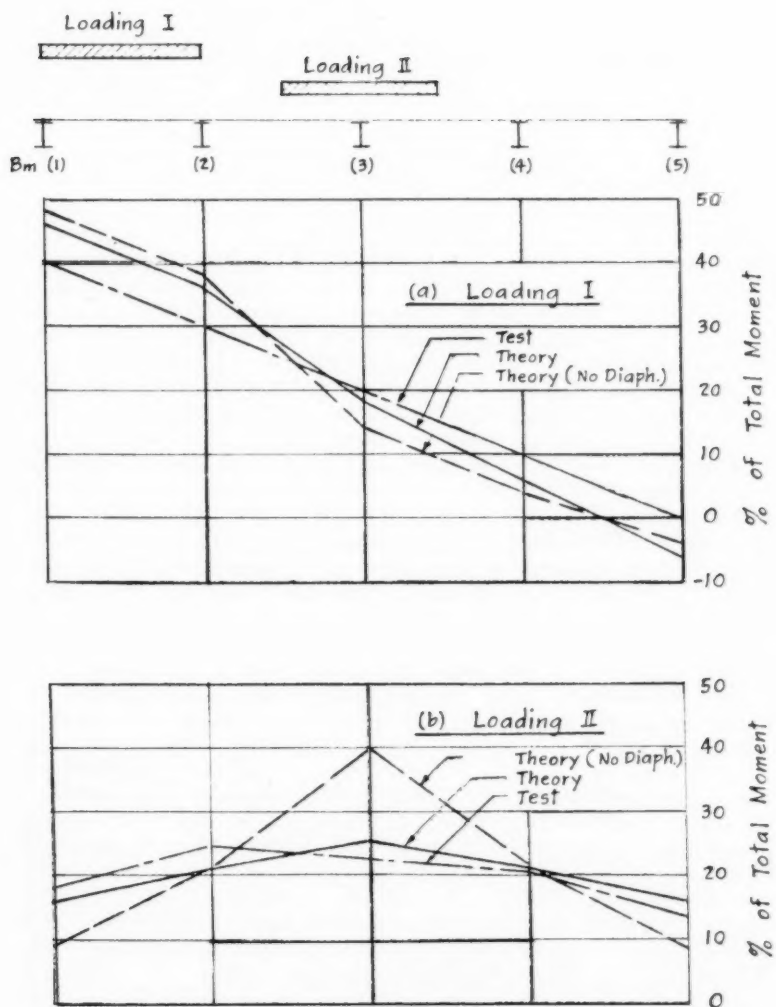
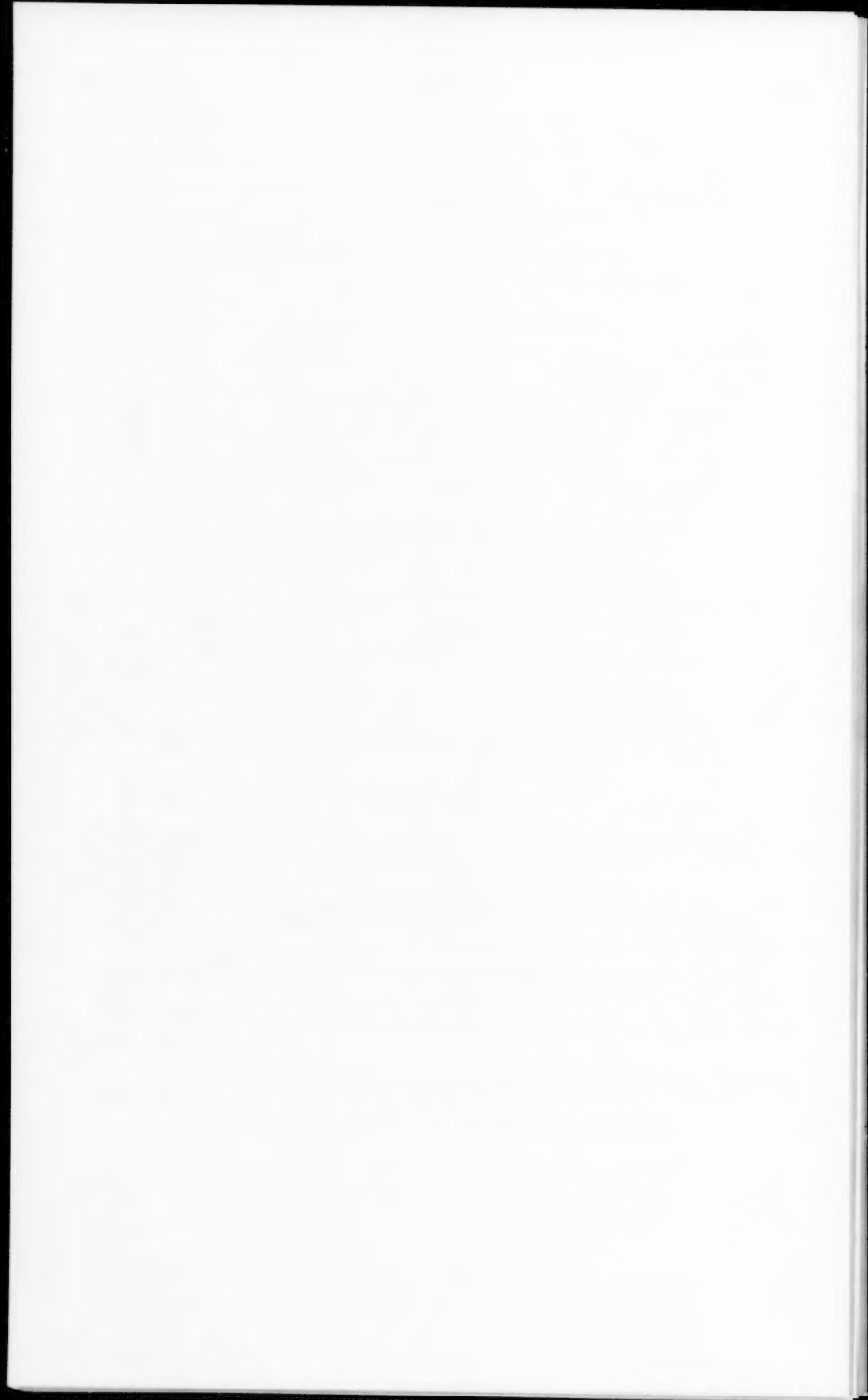


Fig. 2 Theoretical & Test Results of Distribution of Total Moment to Beams





DISTRIBUTION OF LOADS ON BRIDGE DECKS<sup>a</sup>

Discussion by Masao Naruoka

MASAO NARUOKA.<sup>1</sup>—The writer agrees in almost all of the points of the author's conclusions, but in the one point that the addition of diaphragms to bridge structures reduces hazards from fatigue loading, the writer is in doubt since nothing like this appears in previous investigations.

The writer understands the diaphragm to be the load distributing cross beam, not the lateral and sway bracing used generally in girder bridges. The author described that experience has shown that often an appreciable saving may be achieved, especially in structures with high live load to dead load ratios. However, for the case of the load specified by Japan Specification for Highway Steel Bridge which consists of line and uniform loads (similar to AASHO load), if the number of main girders is equal or less than four, the saving may not be achieved. If the bridge width is equal or larger than the span, the weight of the cross beam becomes heavier and the total weight of the cross and main beams which is designed by the load-distribution theory is often larger than the total weight of the main beams and various bracings calculated by the conventional theory, and the saving may not be achieved for such a case. The writer thinks that the appreciable saving may be achieved when the bridge has a suitable width compared with the span and especially for the live load such as DIN load, and that the highway live load specified in U.S.A. and Japan may not be suitable to design calculation by load distributing theory.

Is the value of  $\alpha$  used in Massonnet's formula for the Niagara River Bridge (PC bridge) shown in Fig. 8? Massonnet calculated the value of  $\alpha$  by means of the torsional rigidity of the shape of the main and cross beam. This is applicable to the case when the steel girder bridge has small torsional rigidity, but is not applicable to the case when the prestressed and reinforced concrete beam bridge has high transverse stiffness. For such a case, the torsional rigidity corresponding to the additional torque caused when the whole section rotates around the torsion center must be added to the torsional rigidity calculated by the shape of individual section of main and cross beam. If the value of  $\alpha$  modified as above is used, the distribution coefficient calculated by Massonnet's formula may approach the actual distribution coefficient.

a. Proc. Paper 1303, July, 1957, by A. M. Lount.

1. Dr. Eng. Prof. of Kyoto University, Kyoto, Japan.



## SYNOPSIS OF FIRST PROGRESS REPORT OF COMMITTEE ON FACTORS OF SAFETY<sup>a</sup>

---

Discussion by T. Au

---

T. AU,<sup>1</sup> A.M. ASCE.—The synopsis has convincingly indicated the necessity of redefining factors of safety and related quantities. The application of probability and statistical methods to safety analysis is essential in bringing out the real meaning of the term. The author has indeed taken a big step in this direction although he concedes that a considerable educational effort is required within the profession before such a concept of safety will be widely accepted by structural engineers.

In view of the wide range of variables that may be involved in structural design, one must agree with the synopsis that "a great deal of work remains to be done before it will be possible to determine factors of safety and related quantities on scientific and economic bases." For practical purposes, however, it seems possible to treat the problem in several stages and to approach the ultimate objective piecemeal. While admittedly such consideration may, at the beginning, neglect some significant points of the original intent, it will permit the introduction of the concepts of probability and statistical methods into the design specifications at the earliest possible date. Instead of dealing with the limiting standard load for which the entire structure is designed with the specified probability of either failure or unserviceability, the load-carrying capacity of individual members of the structure may be determined. It is realized, of course, that in statically indeterminate structures, the limiting load of the entire structure may be considerably greater than the load-carrying capacity of one member because of redistribution. Nevertheless, structural design based on the ultimate strength of individual members, as distinguished from limit design of the entire structure, represents at least a step moving toward the direction of uniform factors of safety for all members.

There are several phases of work in a rational procedure of structural design which can, at present, be treated separately and incorporated in the design specifications. The writer suggests the following items for consideration:

### 1. Properties of Materials

The response of the idealized material to load at various service conditions, either on a single application or after sustained or repeated applications, can be determined from the random variations of the strength and deformational properties of real material. The strength can be assumed to fall into some pattern of the normal or Gauss-Laplace distribution. The

a. Proc. Paper 1316, July, 1957, by Oliver G. Julian.

1. Univ. of Detroit; now Visiting Associate Prof. of Civ. Eng., Carnegie Inst. of Technology, Pittsburgh, Pa.

histograms and probability curves of strengths of concrete and structural steel given in the synopsis are fine examples of this type. Since discrepancies in sampling, fabrication and testing of control specimens may indicate variations in strength which do not exist in member of a structure, the test results of control specimens must be correlated to the load carrying capacity of the member by tests made with full-size structural members. The synopsis shows, as an example, that the average yield strength of structural steel determined by coupon tests should be reduced by 25% in order to correlate to the material under service conditions.

Great progress has been made in this direction, perhaps far more significantly than one realizes. Take, for instance, the building code requirements for test of concrete. In the ACI Building Code of 1951,<sup>(1)</sup> the average strength of laboratory control cylinders for any portion of the structure and the average strength of cylinders cured on the job were used as criteria of the compressive strength required by the design. Neither the range of variation nor the standard deviation was indicated by the provision. In the 1956 version,<sup>(2)</sup> however, the code was improved to include that "not more than one strength test in ten shall have an average value less than 90 percent of the specified strength." The improvement reflects no doubt the statistical approach for the evaluation of compression test results recommended in a report by ACI Committee 214<sup>(3)</sup> which has been adopted recently as a standard of ACI.<sup>(4)</sup> Although the concept of probability must have long been applied to maintain quality control of structural steel, it is nowhere reflected in the design specifications. With enough data from mill test reports, criteria for assessing results of strength tests of structural steel can be established.

## 2. Design Loads

Following the definition of Freudenthal,<sup>(5)</sup> the "standard load" defines a load pattern which is sufficiently characteristic of real load patterns to make the structural action equivalent or comparable. The conversion of real load patterns into standard loads may be quite elaborate or almost impossible in some cases if the criterion of equivalence is based on failure or unserviceability of the structure. However, a rational procedure can be developed for selecting the design load without necessarily considering the load effects.

The study of live-load frequencies on highway bridges serves as an example. Added to the list of literature already mentioned in the synopsis is a recent paper by Stephenson<sup>(6)</sup> which presents a method for estimating the frequencies of various intensities of random vehicle loadings. His paper contends that "the probability of vehicle groups of unspecified types occurring within specified lengths of time or distance can be estimated mathematically by use of Poisson's law," and shows how the loadings may be related to their stress-producing characteristics within specified interval of time or specified span length of the bridge. Similar procedures may be developed along this line for load patterns in other types of structures.

Possible changes in the loading conditions in future operations must be considered. The standard load based on existing operating conditions should be adjusted to reflect the anticipated future increase.

## 3. Load Factors

By suggesting the use of load factors, it is implied that the design is based on ultimate strength of members if not the limiting load of the structure. In

reinforced concrete, the ultimate-strength method has been adopted as an alternate procedure of design in the ACI Building Code,<sup>(2)</sup> but the load factors selected are based on the consideration that the members of multi-story buildings thus designed should have dimensions not too much different from those obtained by the straight-line method. A rational procedure of establishing these load factors may be developed by assuming logarithmic-normal distribution as illustrated in the synopsis. If the ultimate-strength method is to be introduced in steel-design specifications as well, the present synopsis can serve as a guide in selecting load factors.

In conclusion, the writer may add that, even with very limited objectives as listed above, the amount of work is enormous. The Committee on Factors of Safety has done an excellent job in pointing out the way by which the ultimate objective can be realized. If the concepts expressed in the synopsis are put into application a little at a time, there is no reason to doubt that the structural engineers will, in time, acquire the necessary competence to deal with the problem.

#### REFERENCES

1. "Building Code Requirements for Reinforced Concrete (ACI 318-51)," ACI Journal, Proc. v. 47, April 1951, p. 589.
2. "Building Code Requirements for Reinforced Concrete (ACI 318-56)," ACI Journal, Proc. v. 52, May 1956, p. 913.
3. "Evaluation of Compressive Test Results of Field Concrete," ACI Journal, Proc. v. 52, November 1955, p. 241.
4. "Recommended Practice for Evaluation of Compressive Test Results of Field Concrete (ACI 214-57)," ACI Journal, Proc. v. 54, July 1957, p. 1.
5. A. M. Freudenthal: "Safety and the Probability of Structural Failure," Transactions ASCE, v. 121, 1956, p. 1337.
6. H. K. Stephenson: "Highway Bridge Live Loads Based on Laws of Chance," Proceedings ASCE, v. 83, No. ST 4, Paper No. 1314.



## VIBRATION SUSCEPTIBILITIES OF VARIOUS HIGHWAY BRIDGE TYPES<sup>a</sup>

---

Discussion by Masao Naruoka

---

MASAO NARUOKA.<sup>1</sup>—With the development of electrical resistance wire strain gages, stress-analysis research of existing highway and railway bridges has become intensified in Japan. The writer has some experiences and wishes to discuss the deflection and natural frequency of vibration of simple-span bridges.

### a) Deflection

The author described that the ratio of observed to theoretical deflection (briefly called "deflection ratio") for the composite span varied from 24% to 40%, with an average of 32%, as shown in Table 1. The writer thinks that the author's theoretical deflection was calculated for the loaded girder by the conventional beam theory. The load-distribution theory for the bridge deck slab or the grid (orthogonal anisotropic slab) has recently become of practical use. According to these theories, the theoretical deflections become smaller than the author's values, and the deflection ratios become about from 70% to 80% for loaded and unloaded beams, and the variation of the deflection ratio of each girder becomes not considerable. The writer thinks that the most reasonable deflection ratio is from 70% to 80%, whereas the stress ratio is from 60% to 70%. The stress ratio obtained by K. Kloppel is 70% for the highway composite grillage girder bridge. The writer wishes that the author would calculate the reasonable deflection by considering the load-distributing action of the bridge deck slab, sway bracing, or load distributing cross beam.

### b) Natural Frequency of Vibration

The writer thinks that the theoretical values obtained by author were calculated by the simple beam theory. According to the writer's research, the observed natural frequency of the simply supported girder bridge coincides with the theoretical value calculated by the simple beam theory when the ratio of the bridge width (or the distance from edge beam to edge beam) to the span is small, but the former is considerably different from the latter when the bridge width is equal or larger compared with the span. The example obtained by the writer is shown in the following:

---

a. Proc. Paper 1318, July, 1957, by LeRoy T. Oehler.  
1. Prof., Kyoto University, Kyoto, Japan.

bridges	measured value (sec)	calculated value theory of orthotropic plate	by beam theory	width		remarks
				span	6.0	
The Sagorhi Bridge	0.136	0.127 ( A, C, $\alpha=0$ )	0.147	6.0		Composite grillage girder Bridge
		0.112 ( A, C, $\alpha=1$ )		15.0		
		0.134 ( B, C, $\alpha=0$ )				
		0.116 ( B, C, $\alpha=1$ )				
The Shigita Bridge	0.127	0.123 ( A, C, $\alpha=0$ )	0.189	22.0 20.0		Same with above
		0.105 ( A, C, $\alpha=1$ )				
		0.153 ( B, C, $\alpha=0$ )				
		0.132 ( B, C, $\alpha=1$ )				
		0.150 ( A, D, $\alpha=0$ )				
		0.112 ( A, D, $\alpha=1$ )				
The Kugsumma Bridge	0.040 0.065	0.059 ( B, D, $\alpha=1$ )	0.105	12.0 9.0		RC T beam bridge
The Shohel Bridge	0.063	0.071 ( B, D, $\alpha=1$ )	0.185	11.0 12.0		RC T Beam bridge

Note A ( B ) means that the formula

$$B_x = EJ/a, B_y = nEJ/l, \{ B_y = N = Eh^3/12(1-\nu^2) \}$$

is used in the calculation of the flexural rigidity of the orthotropic plate.

C means that the orthotropic plate is supported by the edge girders at the two sides.

D means that the orthotropic plate is free at the two sides.

$$\alpha = H/(B_x B_y)^{1/2}$$



The observed natural periods of vibration of the three bridges except the Sagoshi bridge coincide with the theoretical values calculated by the theory of orthotropic plate, and the former differs considerably from the latter calculated by the simple beam theory. That is, the natural frequency of the simply supported girder bridge is a function of the variables of the ratio of bridge width to span ( $b/l$ ), the ratio of the flexural rigidity in the bridge axis to that perpendicular to the bridge axis ( $E_x/E_y$ ), and etc.

The author does not show the bridge width. Does the author's observed value coincide with the theoretical value calculated by beam theory for the various values of ( $b/l$ ), ( $E_x/E_y$ ) and etc.?



# PROCEEDINGS PAPERS

The technical papers published in the past year are identified by number below. Technical-division sponsorship is indicated by an abbreviation at the end of each Paper Number, the symbols referring to: Air Transport (AT), City Planning (CP), Construction (CO), Engineering Mechanics (EM), Highway (HW), Hydraulics (HY), Irrigation and Drainage (IR), Pipeline (PL), Power (PO), Sanitary Engineering (SA), Soil Mechanics and Foundations (SM), Structural (ST), Surveying and Mapping (SU), and Waterways and Harbors (WW), divisions. Papers sponsored by the Board of Direction are identified by the symbols (BD). For titles and order coupons, refer to the appropriate issue of "Civil Engineering." Beginning with Volume 82 (January 1956) papers were published in Journals of the various Technical Divisions. To locate papers in the Journals, the symbols after the paper numbers are followed by a numeral designating the issue of a particular Journal in which the paper appeared. For example, Paper 1113 is identified as 1113 (HY6) which indicates that the paper is contained in the sixth issue of the Journal of the Hydraulics Division during 1956.

## VOLUME 82 (1956)

NOVEMBER: 1096(ST6), 1097(ST6), 1098(ST6), 1099(ST6), 1100(ST6), 1101(ST6), 1102(IR3), 1103 (IR3), 1104(IR3), 1105(IR3), 1106(ST6), 1107(ST6), 1108(ST6), 1109(AT3), 1110(AT3)<sup>c</sup>, 1111(IR3)<sup>c</sup>, 1112(ST6)<sup>c</sup>.

DECEMBER: 1113(HY6), 1114(HY6), 1115(SA6), 1116(SA6), 1117(SU3), 1118(SU3), 1119(WW5), 1120(WW5), 1121(WW5), 1122(WW5), 1123(WW5), 1124(WW5)<sup>c</sup>, 1125(BD1)<sup>c</sup>, 1126(SA6), 1127 (SA6), 1128(WW5), 1129(SA6)<sup>c</sup>, 1130(PO6)<sup>c</sup>, 1131(HY6)<sup>c</sup>, 1132(PO6), 1133(PO6), 1134(PO6), 1135(BD1).

## VOLUME 83 (1957)

JANUARY: 1136(CP1), 1137(CP1), 1138(EM1), 1139(EM1), 1140(EM1), 1141(EM1), 1142(SM1), 1143(SM1), 1144(SM1), 1145(SM1), 1146(ST1), 1147(ST1), 1148(ST1), 1149(ST1), 1150(ST1), 1151(ST1), 1152(CP1)<sup>c</sup>, 1153(HW1), 1154(EM1)<sup>c</sup>, 1155(SM1)<sup>c</sup>, 1156(ST1)<sup>c</sup>, 1157(EM1), 1158 (EM1), 1159(SM1), 1160(SM1), 1161(SM1).

FEBRUARY: 1162(HY1), 1163(HY1), 1164(HY1), 1165(HY1), 1166(HY1), 1167(HY1), 1168(SA1), 1169(SA1), 1170(SA1), 1171(SA1), 1172(SA1), 1173(SA1), 1174(SA1), 1175(SA1), 1176(SA1), 1177(HY1)<sup>c</sup>, 1178(SA1), 1179(SA1), 1180(SA1), 1181(SA1), 1182(PO1), 1183(PO1), 1184(PO1), 1185(PO1)<sup>c</sup>.

MARCH: 1186(ST2), 1187(ST2), 1188(ST2), 1189(ST2), 1190(ST2), 1191(ST2), 1192(ST2)<sup>c</sup>, 1193 (PL1), 1194(PL1), 1195(PL1).

APRIL: 1196(EM2), 1197(HY2), 1198(HY2), 1199(HY2), 1200(HY2), 1201(HY2), 1202(HY2), 1203 (SA2), 1204(SM2), 1205(SM2), 1206(SM2), 1207(SM2), 1208(WW1), 1209(WW1), 1210(WW1), 1211(WW1), 1212(EM2), 1213(EM2), 1214(EM2), 1215(PO2), 1216(PO2), 1217(PO2), 1218 (SA2), 1219(SA2), 1220(SA2), 1221(SA2), 1222(SA2), 1223(SA2), 1224(SA2), 1225(PO)<sup>c</sup>, 1226 (WW1)<sup>c</sup>, 1227(SA2)<sup>c</sup>, 1228(SM2)<sup>c</sup>, 1229(EM2)<sup>c</sup>, 1230(HY2)<sup>c</sup>.

MAY: 1231(ST3), 1232(ST3), 1233(ST3), 1234(ST3), 1235(IR1), 1236(IR1), 1237(WW2), 1238(WW2), 1239(WW2), 1240(WW2), 1241(WW2), 1242(WW2), 1243(WW2), 1244(HW2), 1245(HW2), 1246 (HW2), 1247(HW2), 1248(WW2), 1249(HW2), 1250(HW2), 1251(WW2), 1252(WW2), 1253(IR1), 1254(ST3), 1255(ST3), 1256(HW2), 1257(IR1)<sup>c</sup>, 1258(HW2)<sup>c</sup>, 1259(ST3)<sup>c</sup>.

JUNE: 1260(HY3), 1261(HY3), 1262(HY3), 1263(HY3), 1264(HY3), 1265(HY3), 1266(HY3), 1267 (PO3), 1268(PO3), 1269(SA3), 1270(SA3), 1271(SA3), 1272(SA3), 1273(SA3), 1274(SA3), 1275 (SA3), 1276(SA3), 1277(HY3), 1278(HY3), 1279(PL2), 1280(PL2), 1281(PL2), 1282(SA3), 1283 (HY3)<sup>c</sup>, 1284(PO3), 1285(PO3), 1286(PO3), 1287(PO3)<sup>c</sup>, 1288(SA3)<sup>c</sup>.

JULY: 1289(SM3), 1290(EM3), 1291(EM3), 1292(EM3), 1293(EM3), 1294(HW3), 1295(HW3), 1296(HW3), 1297(HW3), 1298(HW3), 1299(SM3), 1300(SM3), 1301(SM3), 1302(ST4), 1303 (ST4), 1304(ST4), 1305(SU1), 1306(SU1), 1307(SU1), 1308(ST4), 1309(SM3), 1310(SU1)<sup>c</sup>, 1311(EM3)<sup>c</sup>, 1312 (ST4), 1313(ST4), 1314(ST4), 1315(ST4), 1316(ST4), 1317(ST4), 1318 (ST4), 1319(SM3)<sup>c</sup>, 1320(ST4), 1321(ST4), 1322(EM3), 1323(AT1), 1324(AT1), 1325(AT1), 1326(AT1), 1327(AT1), 1328(AT1)<sup>c</sup>, 1329(ST4)<sup>c</sup>.

AUGUST: 1330(HY4), 1331(HY4), 1332(HY4), 1333(SA4), 1334(SA4), 1335(SA4), 1336(SA4), 1337(SA4), 1338(SA4), 1339(CO1), 1340(CO1), 1341(CO1), 1342(CO1), 1343(CO1), 1344(PO4), 1345(HY4), 1346(PO4)<sup>c</sup>, 1347(BD1), 1348(HY4)<sup>c</sup>, 1349(SA4)<sup>c</sup>, 1350(PO4), 1351(PO4).

SEPTEMBER: 1352(IR2), 1353(ST5), 1354(ST5), 1355(ST5), 1356(ST5), 1357(ST5), 1358(ST5), 1359(IR2), 1360(IR2), 1361(ST5), 1362(IR2), 1363(IR2), 1364(IR2), 1365(WW3), 1366(WW3), 1367(WW3), 1368(WW3), 1369(WW3), 1370(WW3), 1371(HW4), 1372(HW4), 1373(HW4), 1374(HW4), 1375(PL3), 1376(PL3), 1377(IR2)<sup>c</sup>, 1378(HW4)<sup>c</sup>, 1379(IR2), 1380(HW4), 1381(WW3)<sup>c</sup>, 1382(ST5)<sup>c</sup>, 1383(PL3)<sup>c</sup>, 1384(IR2), 1385(HW4), 1386(HW4).

OCTOBER: 1387(CP2), 1388(CP2), 1389(EM4), 1390(EM4), 1391(HY5), 1392(HY5), 1393(HY5), 1394(HY5), 1395(HY5), 1396(PO5), 1397(PO5), 1398(PO5), 1399(EM4), 1400(SA5), 1401(HY5), 1402(HY5), 1403(HY5), 1404(HY5), 1405(HY5), 1406(HY5), 1407(SA5), 1408(SA5), 1409(SA5), 1410(SA5), 1411(SA5), 1412(EM4), 1413(EM4), 1414(PO5), 1415(EM4)<sup>c</sup>, 1416(PO5)<sup>c</sup>, 1417 (HY5)<sup>c</sup>, 1418(EM4), 1419(PO5), 1420(PO5), 1421(PO5), 1422(SA5)<sup>c</sup>, 1423(SA5), 1424(EM4), 1425(CP2).

NOVEMBER: 1426(SM4), 1427(SM4), 1428(SM4), 1429(SM4), 1430(SM4)<sup>c</sup>, 1431(ST6), 1432 (ST6), 1433(ST6), 1434(ST6), 1435(ST6), 1436(ST6), 1437(ST6), 1438(SM4), 1439(SM4), 1440(ST6), 1441(ST6), 1442(ST6)<sup>c</sup>, 1443(SU2), 1444(SU2), 1445(SU2), 1446(SU2), 1447 (SU2), 1448(SU2)<sup>c</sup>.

c. Discussion of several papers, grouped by Divisions.

# AMERICAN SOCIETY OF CIVIL ENGINEERS

## OFFICERS FOR 1958

### PRESIDENT

LOUIS R. HOWSON

### VICE-PRESIDENTS

*Term expires October, 1958:*

FRANCIS S. FRIEL  
NORMAN R. MOORE

*Term expires October, 1959:*

WALDO G. BOWMAN  
SAMUEL B. MORRIS

### DIRECTORS

*Term expires October, 1958:*

JOHN P. RILEY  
CAREY H. BROWN  
MASON C. PRICHARD  
ROBERT H. SHERLOCK  
R. ROBINSON ROWE  
LOUIS E. RYDELL  
CLARENCE L. ECKEL

*Term expires October, 1959:*

CLINTON D. HANOVER, Jr.  
E. LELAND DURKEE  
HOWARD F. PECKWORTH  
FINLEY B. LAVERTY  
WILLIAM J. HEDLEY  
RANDLE B. ALEXANDER

*Term expires October, 1960:*

PHILIP C. RUTLEDGE  
WESTON S. EVANS  
TILTON E. SHELBURNE  
CRAIG P. HAZELET  
DONALD H. MATTERN  
JOHN E. RINNE

### PAST PRESIDENTS

*Members of the Board*

ENOCH R. NEEDLES

MASON G. LOCKWOOD

---

### EXECUTIVE SECRETARY

WILLIAM H. WISELY

### TREASURER

CHARLES E. TROUT

### ASSISTANT SECRETARY

E. LAWRENCE CHANDLER

### ASSISTANT TREASURER

CARLTON S. PROCTOR

---

## PROCEEDINGS OF THE SOCIETY

HAROLD T. LARSEN

*Manager of Technical Publications*

PAUL A. PARISI

*Editor of Technical Publications*

FRANCIS J. SCHNELLER, JR.

*Assistant Editor of Technical Publications*

---

### COMMITTEE ON PUBLICATIONS

HOWARD F. PECKWORTH, *Chairman*

PHILIP C. RUTLEDGE, *Vice-Chairman*

E. LELAND DURKEE

R. ROBINSON ROWE

TILTON E. SHELBURNE

LOUIS E. RYDELL

1957 - 20  
DIVISION  
ACTIVITIES

VOLUME 83 NO. ST6  
NOVEMBER 1957  
PART 2

# **JOURNAL of the**

## ***Structural Division***

---

**PROCEEDINGS OF THE**



**AMERICAN SOCIETY  
OF CIVIL ENGINEERS**



---

## DIVISION ACTIVITIES

### STRUCTURAL DIVISION

---

#### Proceedings of the American Society of Civil Engineers

---

#### NEWS

November, 1957

Another new committee has been formed in the Structural Division.

Letters of invitation were sent out to 24 representatives of state highway departments, universities, consultants and industry to serve on the Committee on Electronic Computation. The committee expects to investigate all applications of electronic computers to structural engineering. Its field of interest will range from the evaluation of methods most suitable for machine computation to the actual coding for particular computers. The committee expects to acquaint the structural engineer with this new tool and report on progress made.

To handle this large assignment task committees will be formed. A suggested list of such committees was outlined in a letter from Prof. N. M. Newmark, chairman, and further comments invited. The areas of the task committees will be defined after this first canvas is completed. An early meeting is planned to complete arrangements and to start off the committee's work. Extensive productive work is anticipated to start within a few months.

Structural designers will want to follow this activity. Comments and suggestions should be addressed to:

Dr. N. M. Newmark  
111 Talbot Laboratory  
Urbana, Illinois

OF GREAT BRITAIN AND IRELAND

THE JOURNAL OF THE

ROYAL ANTHROPOLOGICAL INSTITUTE

OF GREAT BRITAIN AND IRELAND

OF GREAT BRITAIN AND IRELAND

OF GREAT BRITAIN AND IRELAND

OF GREAT BRITAIN AND IRELAND

OF GREAT BRITAIN AND IRELAND

OF GREAT BRITAIN AND IRELAND

OF GREAT BRITAIN AND IRELAND

OF GREAT BRITAIN AND IRELAND

OF GREAT BRITAIN AND IRELAND

OF GREAT BRITAIN AND IRELAND

OF GREAT BRITAIN AND IRELAND

OF GREAT BRITAIN AND IRELAND

OF GREAT BRITAIN AND IRELAND

OF GREAT BRITAIN AND IRELAND

OF GREAT BRITAIN AND IRELAND

OF GREAT BRITAIN AND IRELAND

OF GREAT BRITAIN AND IRELAND

OF GREAT BRITAIN AND IRELAND

OF GREAT BRITAIN AND IRELAND

OF GREAT BRITAIN AND IRELAND

OF GREAT BRITAIN AND IRELAND

OF GREAT BRITAIN AND IRELAND

OF GREAT BRITAIN AND IRELAND

OF GREAT BRITAIN AND IRELAND

OF GREAT BRITAIN AND IRELAND

OF GREAT BRITAIN AND IRELAND